NANOSCALE CHARACTERISATION OF ARTERIAL STIFFENING

Thesis submitted in accordance with the requirements of the University of Liverpool for the degree of Doctor of Philosophy by

Zhuo Chang

May 2018

Acknowledgements

Firstly, and foremost, I would like to convey my gratitude to my primary supervisor Dr Riaz Akhtar for all his continuous support and encouragement through my PhD. Your trust and guidance in my research gave me confidence and helped me to become an eligible researcher. I also thank my supervisor Professor Po-Yu Chen. I am so appreciative of your help and guidance during my research in Taiwan. I would like to think my supervisor Dr Paolo Paoletti for his AFM knowledge in my studies.

My appreciation goes to my collaborators in Denmark. Professor Lars Melholt Rasmussen, Professor Hans Christian Beck and Dr Maria Lyck Hansen in University of Southern Denmark. I am grateful for the opportunity to benefit from your expertise in artery and biochemistry. I also thank Professor Yung-Jen Chuang in National Tsing Hua University for his contribution and support with zebrafish.

I also acknowledge Dr Eva Caamaño-Gutiérrez, Dr Ya Hua Chim and Dr Steve Barrett for their assistance and expertise in the statistics and image analysis. My sincere gratitude to Mr Dave Atkinson, Dr Tim Joyce and Dr Rui Chen for their kind support and assistance for my research in Liverpool.

I would also like to thank the University of Liverpool and the National Tsing Hua University for sponsoring this dual PhD programme.

Next, I thank all my friends. Thank you for the memorable times and your support and I am always grateful to have you in my life.

I thank my parents for their relentless support and love. I am deeply grateful for your trust and encouragement.

A special dedication to my wife Liuying Li for her love, support and sacrifice throughout this journey to success.

Nanoscale characterisation of arterial stiffening

Author: Zhuo Chang

Abstract

Arterial stiffening as part of the natural ageing process is strongly linked to cardiovascular risk. Although arterial stiffening is routinely measured *in vivo*, little is known about how localised changes in artery structure and biomechanics contribute to *in vivo* arterial stiffening. This is mainly due to the limitation of the conventional mechanical testing methods.

To circumvent this challenge, a novel nano-scale structural and mechanical characterisation technique, known as PeakForce Quantitative Nanomechanical Mapping (QNM) technique, was developed in a zebrafish model. Using the zebrafish vertebral column, the utility of the PeakForce QNM for probing small-scale biological samples and structures was validated, which paved the way to probe human artery and investigate the localised alterations in artery structure *in vitro* with arterial stiffening.

Human internal mammary artery (IMA) was used as a model vessel for understanding the development of arterial stiffening in this thesis. This thesis focuses on the role of the tunica media and the outmost layer, the tunica adventitia, in arterial stiffening. Using the PeakFoce QNM, the hydrated and dehydrated arterial sections were tested that provided data on nano-scale changes in collagen fibril structure and mechanical properties in the hydrated media, dehydrated media and adventitia and showed how they related to *in vivo* stiffness measurements in the vascular system. The indentation depth for AFM measurement on the IMA tissues of 5 μm thickness were controlled at 20 nm and 5 nm in liquid and ambient conditions respectively and thus the indentation depth/tissue thickness ratio was 0.4% and 0.1%

for the hydrated and dehydrated samples respectively. Furthermore, integrating the findings in this thesis with the proteome analysis data, the localised alterations in the collagen and ultrastructure were explained, and the *in vivo* arterial stiffening, nanomechanical and structural changes in artery biopsy samples were linked. This approach could be used to develop new diagnostic methods for vascular disease.

List of Publications

Peer reviewed publications

Zhuo Chang, Po-Yu Chen, Yung-Jen Chuang, Riaz Akhtar, 'Zebrafish as a model to study bone maturation: nanoscale structural and mechanical characterization of age-related changes in the zebrafish vertebral column', Journal of the Mechanical Behavior of Biomedical Materials, Vol. 84, August 2017, pp. 54-63, DOI: 10.1016/j.jmbbm.2018.05.004.

Zhuo Chang, Paolo Paoletti, Steve D. Barrett, Ya Hua Chim, Eva Caamaño-Gutiérrez, Maria Lyck Hansen, Hans Christian Beck, Lars Melholt Rasmussen, Riaz Akhtar, 'Nanomechanics and ultrastructure of the internal mammary artery adventitia in patients with low and high pulse wave velocity', Acta Biomaterialia, DOI: 10.1016/j.actbio.2018.04.036.

Zhaoliang Zheng, **Zhuo Chang**, Guang-Kui Xu, Fiona McBride, Alexandra Ho, Zhuola, Marios Michailidis, Wei Li, Rasmita Raval, Riaz Akhtar, Dmitry Shchukin, 'Microencapsulated Phase Change Materials in Solar-Thermal Conversion Systems: Understanding Geometry-Dependent Heating Efficiency and System Reliability', ACS Nano, Vol. 11, Issue 1, 2017, pp. 721-729, DOI: 10.1021/acsnano.6b07126.

Homayemem K. Weli, Riaz Akhtar**, Zhuo Chang**, Wen-Wu Li, Jason Cooper, Ying Yang, 'Advanced glycation products' levels and mechanical properties of vaginal tissue in pregnancy', European journal of obstetrics, gynecology, and reproductive biology, Vol. 214, pp. 78-85, DOI: 10.1016/j.ejogrb.2017.04.037.

Conferences

Z. Chang, M.L. Hansen, L.M. Rasmussen, PY. Chen. P. Paoletti and R. Akhtar, 'Nanoscale characterisation of human internal mammary artery with high pulse wave velocity', The Italian Chapter of the European Society of Biomechanics (ESB-ITA), 2017, Roma, Italy.

Z. Chang, M.L. Hansen, L.M. Rasmussen, PY. Chen. P. Paoletti and R. Akhtar, 'Altered adventitial collagen fibril mechanics and morphology with high pulse wave velocity', ARTERY17, 2017, Pisa, Italy. 'Highly Commended Poster' award.

Z. Chang, L.M. Rasmussen, P. Paoletti, PY. Chen and R. Akhtar, 'Localized Nanomechanical Characterization of Arterial Stiffening In Human Arteries with the PeakForce Quantitative Nanomechanical Mapping Technique', TMS2017, 2017, San Diego, California, USA.

Z. Chang, M.L. Hansen, L.M. Rasmussen, PY. Chen and R. Akhtar, 'Quantitative measurement of the mechanical properties of vascular tissue with PeakForce QNM atomic force microscopy', 5th International Conference of Bionic Engineering (ICBE'16), 2016, Ningbo, China.

Z. Chang, M.L. Hansen, L.M. Rasmussen and R. Akhtar, 'Nanomechanical alterations in the adventitial layer of the internal mammary artery of patients with high PWV', ARTERY15, 2015, Krakow, Poland. 'Best Poster' award.

Structure of Thesis

This thesis consists of seven chapters:

- **Chapter 1** highlights the research motivation, aims and objectives of this thesis. The layout of this thesis and author's publications are summarised.
- **Chapter 2** provides an overview of arterial structure**,** and stiffening-related changes in the arterial wall. The diverse techniques and methods used for characterising arterial biomechanics are introduced, with a focus on nanoscale techniques.
- **Chapter 3** demonstrates the utility of the AFM PeakForce QNM (which is explained in detail in Chapter 2 Section 2.6) as a tool for characterising the properties of small-scale biological samples. This chapter focusses on zebrafish vertebral bone samples and explores the relationship between elastic modulus values obtained via PeakForce QNM and the features of bone tissue ultrastructure.
- **Chapter 4** describes the ultrastructural properties in the adventitia of the human IMA in patients with low and high arterial stiffness. The mechanical and morphological alterations in adventitial collagen fibrils that dominant in the IMA adventitia are integrated with the SLRPs expression for assessing the correlation between ultrastructural changes and arterial stiffening.
- **Chapter 5** describes how the changes in the ultrastructure of the IMA tunica media in hydrated and dehydrated conditions in patients with severe arterial stiffening. This chapter also develops the nanoscale assessment in the fluid environment and compares the nanomechanical mapping of hydrated media to previous measurements in dehydrated samples.

- **Chapter 6** discusses and compares our experimental results to the similar studies. Limitations of the work and suggestions for continuing the current studies presented in this thesis are also discussed and outlined in this chapter.
- **Chapter 7** concludes the overall key findings and contributions of the research work in this thesis.

Clinical parameters and histological images for each patient are summarised in Appendix A and C respectively. The elastin content of the IMAs assessed and conducted by Prof. Rasmussen is presented in Appendix D. The calibration procedure for the PeakForce QNM mechanical mapping is described in Appendix B. AFM images with adventitial and medial collagen fibrils for measurements are presented in Appendix E and G respectively. The custom-made macro for assessing adventitial collagen fibrils are presented in Appendix F.

Contribution of Authors

Authors contributing to this thesis include: Mr Zhuo Chang (ZC), Dr Riaz Akhtar (RA), Dr Paolo Paoletti (PP), Dr Steve Barrett (SB), Dr Ya Hua Chim (YHC) and Dr Eva Caamaño-Gutiérrez (ECG) in University of Liverpool (UoL), UK; Prof Po-Yu Chen (PYC) and Prof Yung-Jen Chuang (YJC) in National Tsing Hua University (NTHU), Taiwan; Prof Lars Melholt Rasmussen (LMR), Prof Hans Christian Beck (HCB) and Dr Maria Lyck Hansen (MLH) in University of Southern Denmark (SDU), Denmark.

The work in Chapter 3 was conducted in NTHU and collaborated with YJC and PYC in NTHU.

The work in Chapter 5 and Chapter 6 was conducted in UoL collaborated with PP, DB, YHC and ECG in UoL and LMR, HCB and MLH in SDU.

Contents

Chapter 1. Introduction

Chapter 2. Literature review

Chapter 4. Nanomechanics and ultrastructure of the IMA adventitia in patients with low and high PWV

Chapter 5. Characterisation of ultrastructural changes in the medial layer of the IMA in patients with arterial stiffening

Chapter 6. Discussion and Limitations

Chapter 7. Conclusions and Future work

List of Figures

Chapter 2

Chapter 3

Chapter 4

Chapter 5

Chapter 6

List of Tables

Chapter 2

Chapter 3

Chapter 4

Chapter 5

Abbreviation

AFM	Atomic force microscopy
BMI	Body mass index
CABG	Coronary artery bypass grafting
CVD	Cardiovascular diseases
ECs	Endothelial cells
ECM	Extracellular matrix
EDX	Energy-dispersive X-ray spectroscopy
EEL	External elastic lamina
EL	Elastic lamellae
GAG	Glycosaminoglycans
IEL	Internal elastic lamina
IMA	Internal mammary artery
MLU	Medial lamellar units
MMPs	Matrix metalloproteinases
NS	Not significant
OI	Osteogenesis imperfecta
PCA	Principal component analysis

PeakForce QNM	PeakForce Quantitative Nanomechanical Mapping
PDMS	Polydimethylsiloxane
PWV	Pulse wave velocity
PS1	Photostress coating 1
SD	Standard deviation
SEM	Standard error mean
SEM	Scanning electron microscope
SLRPs	Small leucine-rich proteoglycans
SMCs	Smooth muscle cells
TEM	Transmission electron microscopy
TGF-β1	Transforming growth factor

Chapter 1

Introduction

This chapter introduces the motivation of this research. The aims and objectives of this thesis are described. All of the relevant publications are summarised in the end.

1.1 Motivation

Arterial stiffening is closely associated with the progression of cardiovascular diseases (CVDs) which is the leading cause of mortality in the UK, Europe and worldwide. The British Heart Foundation reported the total number of CVD associated mortality was 152, 465 (accounting for 25.5% of overall deaths) in the UK in 2016 (Cardiovascular Disease Statistics 2018, British Heart Foundation). CVD has also caused more than 4 million deaths from 2013 to 2016, corresponding to 45% of total deaths in Europe. A significant increase in CVD related deaths worldwide that from 12.3, 15.6 to 17.3 million happened from 1990, 2010 to 2013. Moreover, CVD represents a serve economic burden all over the world that it caused approximately US$863 billion in direct healthcare cost and the cost is estimated to reach an astonishing US$20 trillion by the year 2030 (Bloom *et al*., 2012).

Because of resolution limitation of conventional mechanical testing techniques, arterial stiffening studies are mostly focused on the whole vessel level and alterations in the vessel overall. However, recent evidence suggests that greater insight can be obtained in understanding disease and ageing by focussing on alterations in the extracellular matrix (ECM) architecture and also specific structural components at the micro- and the nano-scale (Kohn *et al*., 2015, Akhtar *et al*., 2011). Hence, given that the architectural constructions and constitutions of each layer vary, it is important to probe the nanostructure and mechanical properties of individual layers within the artery to understand the mechanisms driving arterial stiffening.

Hence, this thesis is motivated by the urgent need to develop a systematic nanoscale approach to characterise the localised ultrastructure changes at the nanoscale. To circumvent the problems described above, the work in this thesis has utilised an atomic force microscopy (AFM) based PeakForce Quantitative Nanomechanical Mapping (QNM) technique which has

recently been developed (Young *et al*., 2011) and increasingly being used for biological studies (Berquand, 2011, Sweers *et al*., 2011, Pretorius *et al*., 2014, Eghiaian *et al*., 2015). Firstly, to validate the utility of this technique and model the stiffening process, a suitable alternative to mammalian animal models is needed to comply with the '3Rs' (reduce, refine and replace) approach of animal use for scientific studies (Vliegenthart *et al*., 2014). Secondly, although the microscale mechanical variations and disease-related changes have been assessed and associated with the elastic lamellae in the aorta (Akhtar *et al*., 2014), information on how the mechanical alterations in the other key tissue components are limited. Given the gap in the understanding between the pathology and the mechanisms driving arterial stiffening, this study seeks to a good target in the arterial wall to reflect the development of arterial stiffening and even other diseases and ageing. Finally, the majority of studies have focused on the characterising the alterations in intimal and media layers with arterial stiffening (Wolinsky and Glagov, 1964). However, the adventitia has received less attention, although it is dominant during high-pressure loading and plays an important role in several vascular processes and ageing process (Majesky *et al*., 2012). Hence, this study aims to locally characterise the arterial stiffening driven alterations across the arterial wall, especially the changes in tunica adventitia.

1.2 Aims and Objectives

The overall aim of this study is to characterise changes in the ultrastructural and nanomechanical properties of the human internal mammary artery (IMA) in patients with a high degree of arterial stiffening. This aim will be achieved through the following objectives:

- The first objective of this thesis is to explore the utility of the AFM PeakForce QNM for probing localised nanomechanical and structural properties of small biological samples using a zebrafish model.
- The second objective is to experimentally determine the ultrastructural and nanomechanical changes in the adventitia of the human IMA in patients with low and high arterial stiffening.
- The third objective is to characterise the structural and mechanical alterations in the medial ultrastructure of the human IMA in patients with normal and high degree of arterial stiffness.
- The fourth objective is the development of nanomechanical mapping of hydrated biological tissues in a fluid environment using the human IMAs and compares with the measurements in air condition.
- The final objective is to link ultrastructural changes across the human IMA with the expression of extracellular matrix proteins that have associated with high degree of arterial stiffness.

References

AKHTAR, R., CRUICKSHANK, J., ZHAO, X., WALTON, L., GARDINER, N., BARRETT, S., GRAHAM, H., DERBY, B. & SHERRATT, M. 2014. Localized micro-and nano-scale remodelling in the diabetic aorta. *Acta biomaterialia,* 10**,** 4843-4851.

AKHTAR, R., SHERRATT, M. J., CRUICKSHANK, J. K. & DERBY, B. 2011. Characterizing the elastic properties of tissues. *Materials Today,* 14**,** 96-105.

BERQUAND, A. 2011. Quantitative imaging of living biological samples by PeakForce QNM atomic force microscopy. *Bruker Application Note,* 135**,** 1-10.

BLOOM, D. E., CAFIERO, E., JANé-LLOPIS, E., ABRAHAMS-GESSEL, S., BLOOM, L. R., FATHIMA, S., FEIGL, A. B., GAZIANO, T., HAMANDI, A. & MOWAFI, M. 2012. The global economic burden of noncommunicable diseases. Program on the Global Demography of Aging.

EGHIAIAN, F., RIGATO, A. & SCHEURING, S. 2015. Structural, mechanical, and dynamical variability of the actin cortex in living cells. *Biophysical journal,* 108**,** 1330-1340.

KOHN, J. C., LAMPI, M. C. & REINHART-KING, C. A. 2015. Age-related vascular stiffening: causes and consequences. *Frontiers in genetics,* 6**,** 112.

MAJESKY, M. W., DONG, X. R., HOGLUND, V., DAUM, G. & MAHONEY JR, W. M. 2012. The adventitia: a progenitor cell niche for the vessel wall. *Cells Tissues Organs,* 195**,** 73-81.

PRETORIUS, E., SWANEPOEL, A. C., BUYS, A. V., VERMEULEN, N., DUIM, W. & KELL, D. B. 2014. Eryptosis as a marker of Parkinson's disease. *Aging (Albany NY),* 6**,** 788.

SWEERS, K., VAN DER WERF, K., BENNINK, M. & SUBRAMANIAM, V. 2011. Nanomechanical properties of α-synuclein amyloid fibrils: a comparative study by nanoindentation, harmonic force microscopy, and Peakforce QNM. *Nanoscale research letters*, 6**,** 270.

VLIEGENTHART, A., TUCKER, C. S., DEL POZO, J. & DEAR, J. W. 2014. Zebrafish as model organisms for studying drug-induced liver injury. *British journal of clinical pharmacology*, 78**,** 1217-1227.

WOLINSKY, H. & GLAGOV, S. 1964. Structural basis for the static mechanical properties of the aortic media. *Circulation research,* 14**,** 400-413.

YOUNG, T., MONCLUS, M., BURNETT, T., BROUGHTON, W., OGIN, S. & SMITH, P. 2011. The use of the PeakForceTM quantitative nanomechanical mapping AFM-based method for high-resolution Young's modulus measurement of polymers. *Measurement Science and Technology*, 22**,** 125703.

Chapter 2

Literature review

The literature review provides comprehensive background information on all of the involved topics within this thesis. Section 2.1 briefly introduces the CVDs and the burden of CVD within the UK, Europe and worldwide. Section 2.2 presents arterial stiffening and the clinical method for assessing arterial stiffness (pulse wave velocity (PWV)). In Section 2.3, arterial structure and its key tissue components, and classification of human arteries are described. Section 2.4 elaborates how the current mechanical testing methods characterise biomechanics of arterial wall from the macro- to the nano-scale. Changes in different tissue components with arterial stiffening are summarised in Section 2.5. Finally, Section 2.6 emphasises the main techniques employed in this thesis, the AFM and PeakForce QNM method.

2.1 CVDs

2.1.1 Background

With industrialisation, the health status and physical conditions of humans have been closely linked to the level of their economic and social development. Nowadays, the major causes of death and disability in our societies has shifted from nutritional malnutrition and infectious diseases to a variety of chronic and noncommunicable diseases, such as CVDs, cancer and diabetes. Noncommunicable diseases are major global public health challenges of the 21st century among which CVDs have become the leading causes of mortality globally, especially in developing countries. (Mendis and Chestnov, 2014) CVD is a class of diseases that involve the heart and circulation, also known as blood vessels, and there are 4 main types of CVD associated with varying diseases (Figure 2.1) (Mendis *et al*., 2011). For example, coronary heart disease occurs with reduced blood supply to the heart muscle and leads to angina, heart attacks and heart failure. Stroke happens when the blood supply to the brain is interrupted; it may cause brain damage and even brain death. With blockage in the arteries from the heart to the limbs and at aorta, the peripheral arteries and aorta can become weakened and over-expanded, causing what are known as peripheral arterial and aortic diseases, respectively. The underlying risk factors of CVDs are various factors involving hypertension (Sowers *et al*., 2001), smoking (Ambrose and Barua, 2004), age (North and Sinclair, 2012) and diabetes (Sowers *et al*., 2001).

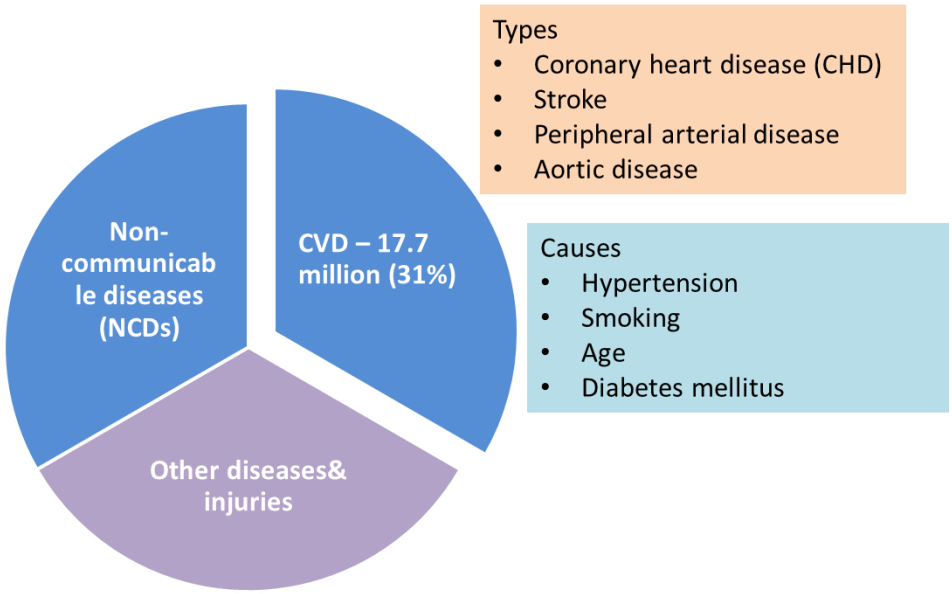

Figure 2.1 Global mortality in 2017 and major types and causes of CVDs. CVDs, as the leading cause of death in non-communicable diseases, took the lives of 17.3 million people (31%) in 2017. Data from World Health Organization.

2.1.2 CVD in the UK, Europe and worldwide

Diseases of the heart and circulatory system are the leading causes of mortality in the UK, Europe and all over the world. The British Heart Foundation reported that CVD was one of the two leading causes of death in the UK in 2016, accounting for 25.5% of overall deaths (Cardiovascular Disease Statistics 2018, British Heart Foundation). Another primary cause of death in the UK is cancer that accounts for 28.5% of the overall mortality. However, CVD still caused a larger number of deaths in Europe and was responsible for more than 4 million deaths from 2013 to 2016, corresponding to 45% of total deaths (Figure 2.2A). Overall, CVD is estimated to cost the EU economy US$260 billion a year. Globally, a series of up-to-date studies of Global Burden of Disease from 1990, 2010 to 2013 reported a profound increase in CVD related deaths that range from 12.3, 15.6 to 17.3 million deaths worldwide, accounting for 25.9%, 29.6% to 31.5%, respectively of all deaths worldwide (Figure 2.2B)

(Nichols *et al*., 2014, Townsend *et al*., 2016). In 2010 alone, CVD caused approximately US$863 billion in direct healthcare cost, which is estimated to reach an astonishing US$20 trillion by the year 2030 (Bloom *et al*., 2012). Although notable efforts have been made to tackle CVD, there is still a lack of a comprehensive programme for early detection, prevention and treatment. Mortality and morbidity from CVD remain the chief causes of death all over the world, especially in low- and middle-income countries, where about 80% of the cardiovascular burden is borne (Mendis and Chestnov, 2014). Therefore, CVDs are not solely public health issues, but more importantly a significant economic burden to the sustainable development of many countries.

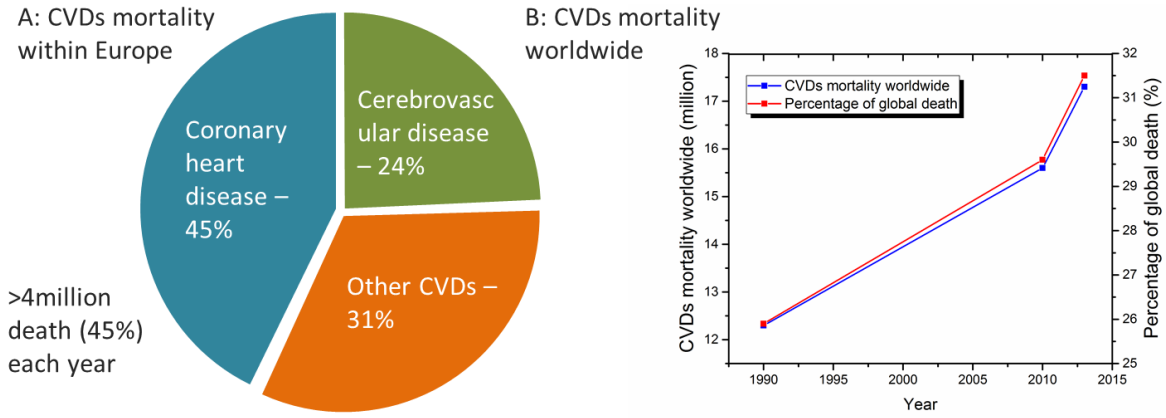

Figure 2.2 Proportion and number of CVDs causing death within (A) Europe and (B) all over the world. (A) Major CVDs and their proportion (Townsend *et al*., 2016). (B) Total mortality and proportion of global death from 1990 (Abubakar *et al*., 2015), 2010 (Townsend *et al*., 2015) to 2013 (Townsend *et al*., 2016).

2.2 Arterial stiffening

2.2.1 Background

Arterial stiffness refers to the reduced capability of an artery to expand (vasodilatation) and contract (vasoconstriction) in response to altered pressures, which can be described by parameters involving compliance (C) and distensibility (D). Generally, arterial wall stiffens with age, accompanied by luminal enlargement and wall thickening (remodelling) and a reduction of elastic properties (stiffening) namely arteriosclerosis (Izzo Jr and Shykoff, 2001). In recent years, there has been a dramatic resurgence of interest in the process of arterial stiffening and its biochemical and biomechanical changes. The structural changes or extracellular matrix modifications with ageing within the intima, media and adventitial layers include elevated collagen deposition, reduction in elastin and advanced glycation end-products (AGEs) accumulation (Kohn *et al*., 2015, Fonck *et al*., 2009, Sell and Monnier, 2012, Sherratt, 2009)

2.2.2 Relationship between arterial stiffening and CVD

Arterial stiffening as a hallmark of normal ageing is recognised as an independent predictor of cardiovascular mortality (Cecelja and Chowienczyk, 2012). Increasing numbers of studies have evidenced that stiffening in the larger central arterial wall is positively associated with CVDs, including coronary artery disease and atherosclerosis (Cecelja and Chowienczyk, 2012).

2.2.3 Assessment of arterial stiffening with PWV

PWV is an *in vivo* technique used routinely in a clinical setting to assess arterial stiffening and to predict CVDs. A PWV value is determined from the time difference of a pulse between two separate areas of the body, usually the carotid and femoral arteries (Figure 2.3).

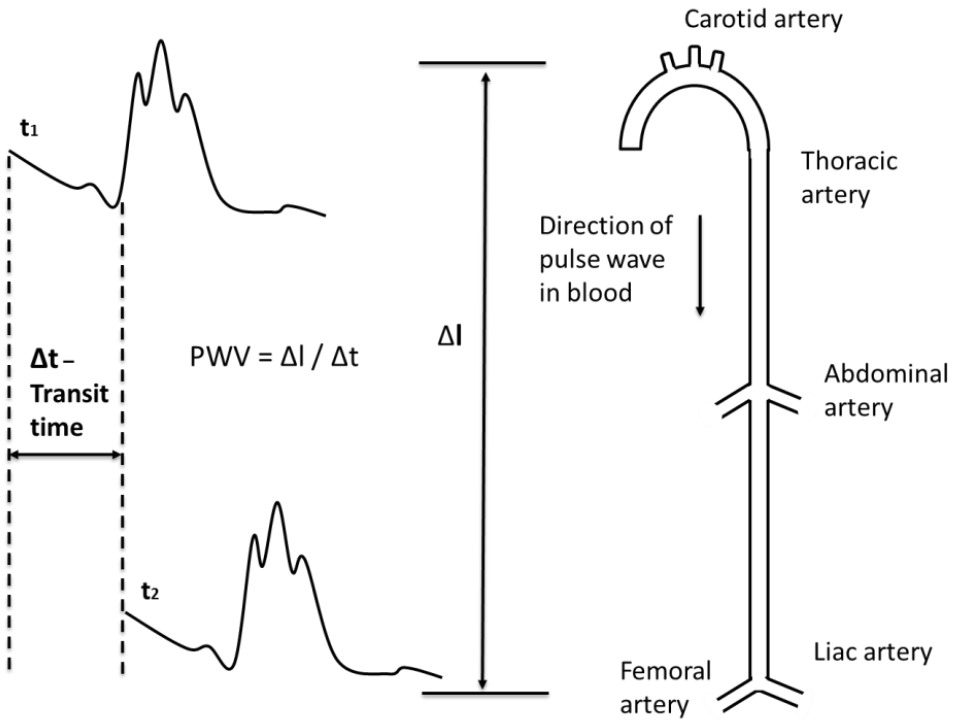

Figure 2.3 Schematic diagram demonstrating basis of PWV. The distance between the carotid and femoral sites can be measured using body surface landmarks for most accurate estimation of the arterial path length and accurate PWV calculation. As the pulse wave passes through the artery, the time taken of the two wave points is recorded.

The physical distance between these two distinct points is measured on the surface of the body; thereby the pulse wave velocity can be determined as the ratio of distance travelled to elapsed time (Laurent *et al*., 2006). Aortic PWV is a powerful predictor of risk of morbidity and mortality including for patients with diabetes (Cruickshank *et al*., 2002) and hypertension (Blacher *et al*., 1999). More importantly, the measurement of PWV is often referred to as a gold standard in aortic stiffness assessment to cardiovascular risk estimation, and it exhibits

profound positive correlation with aortic PWV (Podolec *et al*., 2007). Based on the Moens-Korteweg equation (Newman and Greenwald, 1978), the PWV value is directly related to the incremental elastic modulus of the arterial wall, which takes into account the vessel radius, vessel wall thickness and blood density. The Moens-Korteweg equation demonstrates the relationship between the PWV and the arterial stiffness, which can be simplified as

$$PWV = \sqrt{\frac{E_a h}{2pr}} \quad (1)$$

where *r* and *p* are the lumen radius and the blood density, respectively. E_a and h give the mean Young's modulus and thickness of the arterial wall.

PWV value is inversely correlated with artery distensibility and compliance (Cecelja and Chowienczyk, 2012). However, the measurement of PWV does not take into account the progressive loss of the cushioning function from the ascending aorta (elastic artery) to the less elastic peripheral arteries and muscular arteries (Laurent *et al*., 2006). Reference and normal values of PWV in healthy individuals at different ages have been well documented (Collaboration, 2010, Reusz *et al*., 2010).

2.3 Arterial structure and classification

2.3.1 Arterial structure

2.3.1.1 Tunica intima

The intimal layer is defined as the innermost layer of the arterial wall and consists of two layers: (a) the luminal layer, known as the basal membrane, is comprised of a thin basement membrane with a proteoglycan-rich matrix and few collagen (Figure 2.4A) (Gasser *et al*.,

2006). There is normally a single layer of endothelial cells (ECs) attached at the luminal layer where these ECs partly regulate the vascular homeostasis. (b) The second intimal layer known as the sub-endothelial layer consists of elastin and collagen fibres, which anchor the EC layer to the internal elastic lamina. (Stary *et al*., 1992) The intimal collagen fibres, primarily of type I and III, are dispersed, while the intimal elastin forms the three-dimensional network of elastic fibres (Shekhonin *et al*., 1985, Gasser *et al*., 2006).

Although the mechanical properties of the intima are not well studied due to its relatively thin thickness compared to the dominant media and adventitia in the arterial wall, tunica intima is vital in atherosclerosis and restenosis (Stary *et al*., 1992). Recent evidence has shown that ECs are mechanosensitive to matrix stiffness and lead to intimal stiffening and endothelial dysfunction, implying that the biomechanics of the intima may associate with CVDs (Huynh *et al*., 2011, Califano and Reinhart-King, 2010). Histopathologic examination of the tunic intima has shown that the ECs play a key role in mediating the mechanical and chemical response by secreting various vasoactive molecule and growth factors (Isenberg and Wong, 2006). Interestingly, a recent study has shown that ECs are mechanosensitive to the stiffening of intimal ECM through increased cell permeability, which results in the disruption of endothelial monolayer and atherosclerosis pathogenesis (Huynh *et al*., 2011).

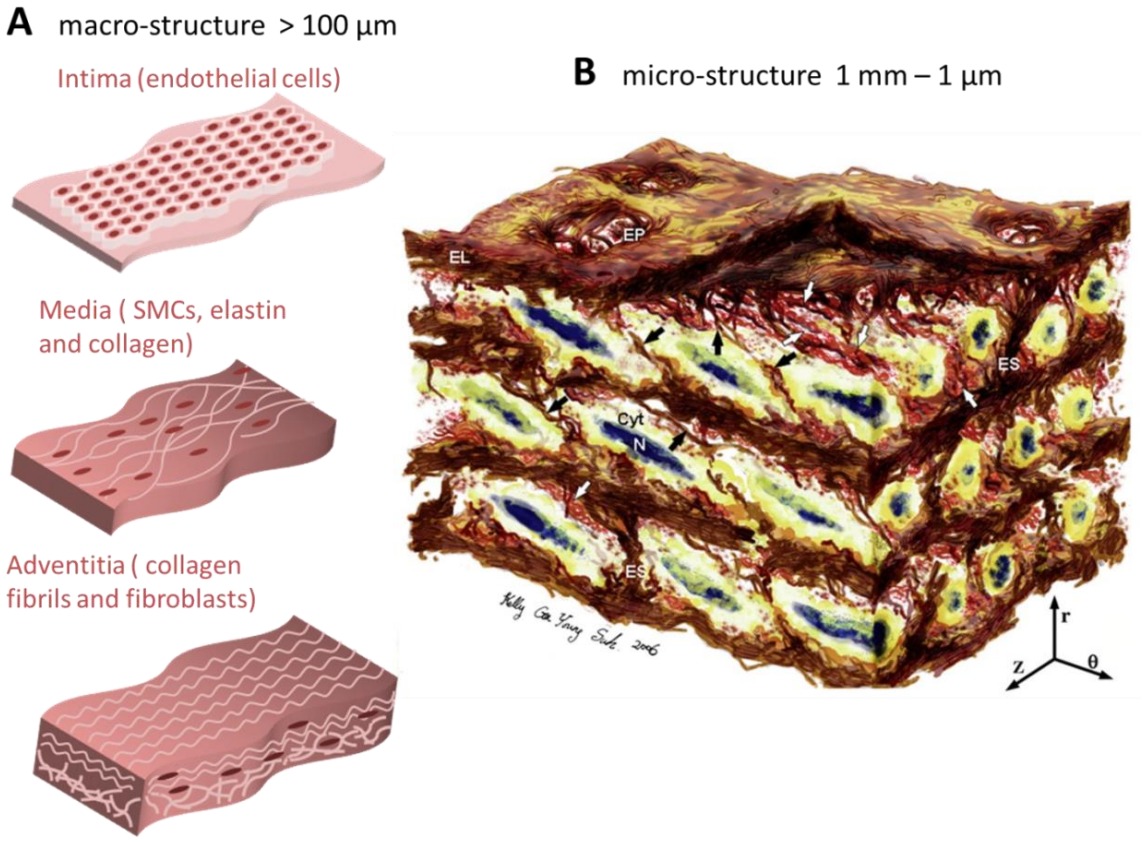

Figure 2.4 Schematic representation of the hierarchical structure of the mammalian aorta from macro-, micro- to nano-scale. (A) The arterial wall is divided into three distinct layers with different components at the macroscale. (B) At the microscale, medial aortic microstructure was studied by O'Connell *et al.* (O'Connell *et al.*, 2008). Image dimensions (θ × Z × r) are 80µm × 60µm × 45µm, with the lumen surface at the top (r represents radial direction, z axial, and θ circumferential).

2.3.1.2 Tunica media

The tunica media is separated from the intima and adventitia by the internal elastic lamina (IEL) and external elastic lamina (EEL), respectively (Wagenseil and Mecham, 2009). The medial layer is composed of repeating medial lamellar units (MLU) which are the structural and functional units of arteries (Akhtar *et al.*, 2011). In Connell and Murthy's MLU model (O'Connell *et al.*, 2008), the MLU is comprised of approximately 47% collagen, 29% elastin and 24% SMCs, which together constitute the framework of the MLU. Each MLU is composed of parallel layer-by-layer elastic lamellae by thick elastic fibres between which are

sandwiched and reinforced by a dense network of finer inter-lamellar elastin fibres and elastin struts, as well as SMCs. The number of concentric lamellae layers in the media remains constant with age (Wolinsky and Glagov, 1967). Hence, the tunica media responds to the mechanical stress as a homogeneous material, though it is histologically heterogeneous. Specific collagen types have been identified by using polarised light microscopy, indicating that there have two major types of collagen (type I: 30% and type III: 70%) in the tunica media (O'Connell *et al*., 2008). These collagen fibres are dispersed in the interstices and are arranged circumferentially (Figure 2.4B). The SMCs are circumferentially oriented and coherently aligned in the media among the fine elastin and collagen fibres, and connect to the latter (O'Connell *et al*., 2008, Wagenseil and Mecham, 2009). Since the majority of the arterial wall is comprised of the characteristic medial lamellae, tunica media is recognised as playing a dominant role in arterial mechanical behaviour (Holzapfel *et al*., 2005). The tunica media is mainly responsible for the elastic recoil to maintain the blood pressure during diastole. The specialised structural arrangement drives the tunica media to resist high loads in the circumferential direction. More importantly, the characteristic lamellae of the media play a vital role in the arterial wall bulk and attribute to the mechanical properties of the artery to withstand blood pressure. Therefore, the number of lamellar units is closely related to the tension that the arteries need to withstand, which means that the higher wall tension the arterial walls experience, the more elastic layers and larger diameter they have (Shadwick, 1999, Holzapfel *et al*., 2005). At physiological pressures, the medial mechanical property is dominated by elastin within the medial lamella (Greenwald *et al*., 1997). Under axial stretch and non-axisymmetric deformation, the media is profoundly less compliant than the adventitia (Pandit *et al*., 2005, Yu *et al*., 1993). Under circumferential and longitudinal tensions, the media bears approximately 60% and 25% of the load respectively *(*Holzapfel *et al*., 2005, Pandit *et al*., 2005). When the artery is subjected to a pressure, the elastin fibres

exhibit high recoil properties and initially stretched (low strain), and then at higher load and tension, the stiffer collagen fibres are recruited (Samila and Carter, 1981).

2.3.1.3 Tunica adventitia

The tunica adventitia is the outmost layer of arterial wall and mainly consists of fibroblasts and circumferentially oriented, thick wavy bundles of collagen fibres with a reinforced and support component of longitudinal fibrils (Figure 2.4A) (Fleenor *et al*., 2010). These collagen fibrils, primarily of type I, are intermixed with elastin to form typical fibrous tissue, with some dispersed fibroblasts and are surrounded by loose connective tissue. The orientation of the collagen fibres is dispersed where the inner adventitial collagen fibres are thin and highly oriented, and interwoven with elastin allowing for arterial distension and protection against rupture, while the outer adventitial collagen fibres are thick and less tightly packed and are likely to be more load bearing (Figure 2.4A) (Rezakhaniha *et al*., 2012, Finlay *et al*., 1998).

Adventitial mechanics is mainly attributed to the collagen organisation, and these collagen fibres ensure the adventitia to be much less stiff at low pressure or the stress-free configuration, by which the collagen fibres are embedded with crimped morphology in the soft ground-matrix (Zoumi *et al*., 2004). Under circumferential and longitudinal tensions, the adventitia bears approximately 40% and 75% of the load, respectively (Holzapfel *et al*., 2005, Pandit *et al*., 2005). At high pressure and strain of the arterial wall, these collagen fibres can be stretched to reach their straightened lengths that give them the ability to prevent the artery from overstretch and rupture to the adventitia (Berillis, 2013).

2.3.1.4 Collagen

In arterial wall, collagen is the ubiquitous central load-bearing element which forms the fundamental arterial structure. The structural arrangement of collagen not only contributes to

the anisotropic mechanical behaviour of the arterial wall but also allows for cellular attachment. To date, there are 28 different types of collagen and collagen-like proteins and they are grouped into 8 sub-families, among which fibrillar collagen, including type I, II, III, V, XI, draws the most attention because of its biomechanical properties and characterised repeating banding pattern known as D-period (Fratzl, 2008). Within the collagen fibril, collagen molecules with a length of 300 nm and width of 1.5 nm are staggered parallel aligned to form the gap and overlap regions of the D-period (Figure 2.5A) (Kadler *et al*., 1996). As two of the significant collagens in an artery, type I collagen comprises approximately 2/3 of the total collagen and is the most predominant in all layers of the artery, whereas type III collagen is more prominent in the media than in the other layers (Shekhonin *et al*., 1985) (Figure 2.5A).

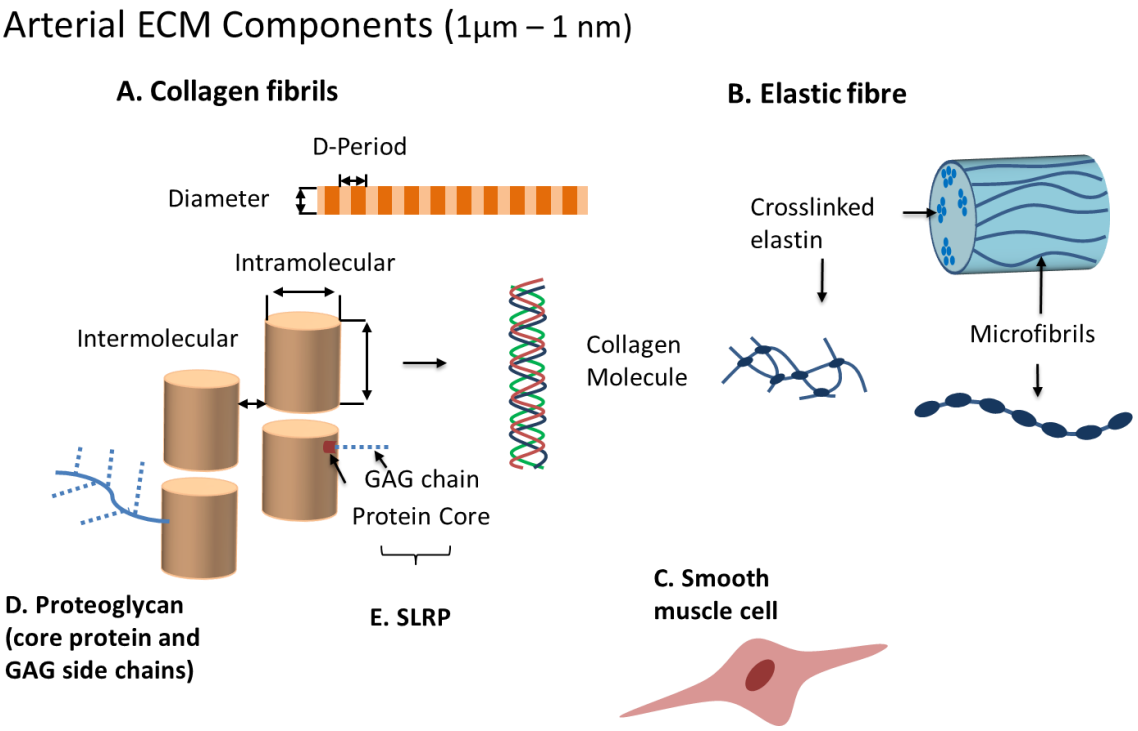

Figure 2.5 Structures of major arterial ECM components, including collagen, elastin, SMC and proteoglycans, are demonstrated at the nanoscale. (A) Collagen fibrils exhibit a characteristic gap and overlap regions known as the D-period (~ 67 nm) which is formed by staggered parallel aligned collagen molecules (length = 300nm; diameter = 1.5 nm). A collagen molecule is composed of three polypeptide strands with a left-handed helix, named alpha chain. (B) An elastic fibre (thickness = 2 - 3 µm) consists of the outer microfibrillar mantle with characteristic repeating structures and inner amorphous crosslink elastin. (C) SMCs. (D) and (E) Proteoglycans.

The collagen molecular packing of collagen fibril has been extensively studied. As defined by the Hodge-Petruska model (Petruska and Hodge, 1964) and Orgel *et al*. (Orgel *et al*., 2006), within a collagen fibril, collagen molecules are parallelly aligned giving a repeating gap/overlap pattern, resulting in the characteristic collagen D-period. Fang *et al*. (Fang *et al*., 2012) recently demonstrated two collagen fibril bundle formation, which is still an open question and a poorly understood phenomenon in fibrillogenic models.

Collagen D-period was characterised by electron microscopy (Schmitt *et al*., 1942), X-ray scattering studies (Parry, 1988) and AFM (Fang *et al*., 2012, Wallace *et al*., 2011) that the D-period is around 67 nm. Collagen size (diameter) varies widely in different tissues ranging

from above a micron in the tendon to below 40 nm in the cornea. Collagen fibrils are initially formed as short fibril intermediates, and then they are matured through linear and lateral growth. Christiansen *et al*. (Christiansen *et al*., 2000) studied the collagen fibril assembly in which fibril subunits, called sub-fibrils, are critical for collagen fibril growth via affecting the lateral or linear aggregation and fusion, as well as the cross-link. The small leucine-rich repeat proteoglycans (SLRPs) interact with the fibril surface via forming a composite structure and are involved in the regulation of the later stages in fibril growth and fibril packing (Figure 2.5E).

Next in the hierarchical level of collagen in ECM is the organisation of collagen fibrils into collagen bundles at micrometre to millimetre scale, which is a group of parallel fibrils linked with each other via interfibrillar cross-links (Eyre and Wu, 2005).

2.3.1.5 Elastin

Elastic fibres are a major insoluble ECM component of the arterial wall with both structural and biological signalling functions. The mature elastic fibres consist of an outer microfibrillar mantle and an inner core of amorphous crosslinked elastin (Figure 2.5B). They are incredibly stable and have a slow turnover rate, lasting the entire lifespan (Mecham and Birk, 2013). In an arterial wall, elastic fibres possess remarkable longevity lasting for over 70 years and maintain the ability to recoil 3×10^9 times (Sherratt, 2009). Arterial elastin is synthesised and secreted by SMCs in the medial layer during late foetal and early postnatal development. Following post-translational modification and cross-linking, in the tunica media, elastic fibres form concentric fenestrated lamellar separated by SMC layers, which endows the arterial wall with elasticity and resilience (O'Connell *et al*., 2008). The number of elastic lamellar decreases from 40 - 70 in conducting arteries such as the aorta, to fewer than ten in the smaller resistance arteries. The elastic lamella has a predominant role in arterial

biomechanics which is to absorb the hemodynamic stress of cardiac systole and release this energy to maintain the sustained blood pressure during diastole (Brooke *et al*., 2003).

Elastin is essential during vascular morphogenesis and functions to maintain the homeostasis of the mature vessel wall. Researchers have unravelled the biological roles of elastin in arterial tissues. For example, elastin has been proved to be critical in arterial morphogenesis, stabilising the arterial structure and regulating SMC proliferation (Li *et al*., 1998). More importantly, elastin matrix is deposited in the arterial media and appears to negatively regulate SMC proliferation, migration, and differentiation within the arterial wall (Ito *et al*., 1998). Therefore, the disruption of elastin-SMC interactions is not only a stimulus for cellular activity during vascular occlusion but also an essential contributor to the pathogenesis of the human vascular disease, including hypertension, atherosclerosis and restenosis (Brooke *et al*., 2003).

2.3.1.6 SMCs

In an artery, SMCs (Figure 2.5C) play an important role in synthesising and organising specific ECM which is responsible for the mechanical properties of the arterial wall, though the SMC itself contributes little to the static mechanical properties of the wall in elastic arteries (Lacolley *et al*., 2017). Mechanical connection and signalling between SMCs and the ECM are likely to be responsible for the arterial mechanical properties (Qiu *et al*., 2010).

2.3.1.7 Proteoglycans and small leucine-rich proteoglycans (SLRPs)

Proteoglycans are a group of complex and diverse macromolecules that are functionally essential for arterial wall. They can be categorised into two classes by their relative sizes: large proteoglycans (such as aggrecan and versican) that form large aggregates by interaction

with hyaluronan and SLRPs (such as decorin, biglycan, lumican and mimican) (Figure 2.5D and 2.5E).

The SLRP is likely to bind ECM molecules such as collagen, tropoelastin, fibronectin, and fibrillin microfibrils (Reinboth *et al*., 2002) to regulate tissue structure and functions. SLRPs are a family of essential and ubiquitous biological active ECM components which have been identified to involve in the ECM assembly and cell-matrix interactions. In a blood vessel, SLRPs play a crucial role in arterial tissue integrity by regulating synthesis, construction and remodelling of ECM components like collagen, elastin and SMCs. SLRPs also show promise as novel biomarkers for CVDs for their specific roles in cell signalling like transforming growth factor beta 1 (TGF-β1) signalling (Dupuis and Kern, 2014). Layer-specific distribution of SLRPs has also been revealed in the arterial wall where biglycan can be found in both medial and adventitial layers while decorin, fibromulin and lumican can only be detected in the adventitia (Dupuis and Kern, 2014).

Studies have also evidenced the possible role of SLRPs in elastic fibre biology through forming complexes with elastin component or precursor of mature elastin, i.e. fibrillin-1, tropoelastin and microfibril-associated glycoprotein-1. Decorin can be involved in the synthesis of the elastic fibre component (fibrillin-1) in renal fibroblasts via various pathways (Schaefer *et al*., 2007). Biglycan is also capable of regulating the composition of the ECM of arterial wall through inhabiting elastin synthesis and assembly mainly due to its galactosamine-containing glycosaminoglycans (GAG) chains (Hwang *et al*., 2008).

2.3.2 Classification of arteries

The vascular system consists of a branched network of blood vessels classified into 5 types: the arteries, the arterioles, the capillaries, the venules and the veins. Arteries deliver blood at

high pressure to peripheral vascular beds and the arterial system and can be structurally as well as functionally classified into two major types: elastic arteries and muscular arteries (Figure 2.6A). Both types of the artery are structurally composed of three distinct layers. These arteries have a concentric layered structure, with each layer being distinct in its cell and ECM composition and conferring specific functional properties (Megens *et al*., 2007).

2.3.2.1 Elastic arteries

Elastic arteries contain the pulmonary arteries, the aorta and its branches. In the media of elastic arteries, SMCs are embedded between two layers of elastic lamellae and collagen fibres are arranged along the elastic lamellae. The elastic lamella is fenestrated, and its spaces are filled up with other ECM components (Figure 2.6C). Thus, the stiffness of the elastic arterial wall is associated with the stiffness of each ECM component (i.e. SMC, elastic lamellae and collagen fibre) and their geometrical and functional relationships *(*O'Connell *et al*., 2008). The elastic laminae dominate the tunica media of elastic arteries with few SMCs. Because the SMC is neglectable in the biomechanics of arterial wall, elastic arteries exhibit pronounced elastic behaviour, which permits the elastic arteries to distend and accommodate the considerable increase in blood volume during systole (Holzapfel *et al*., 2000, Megens *et al*., 2007).

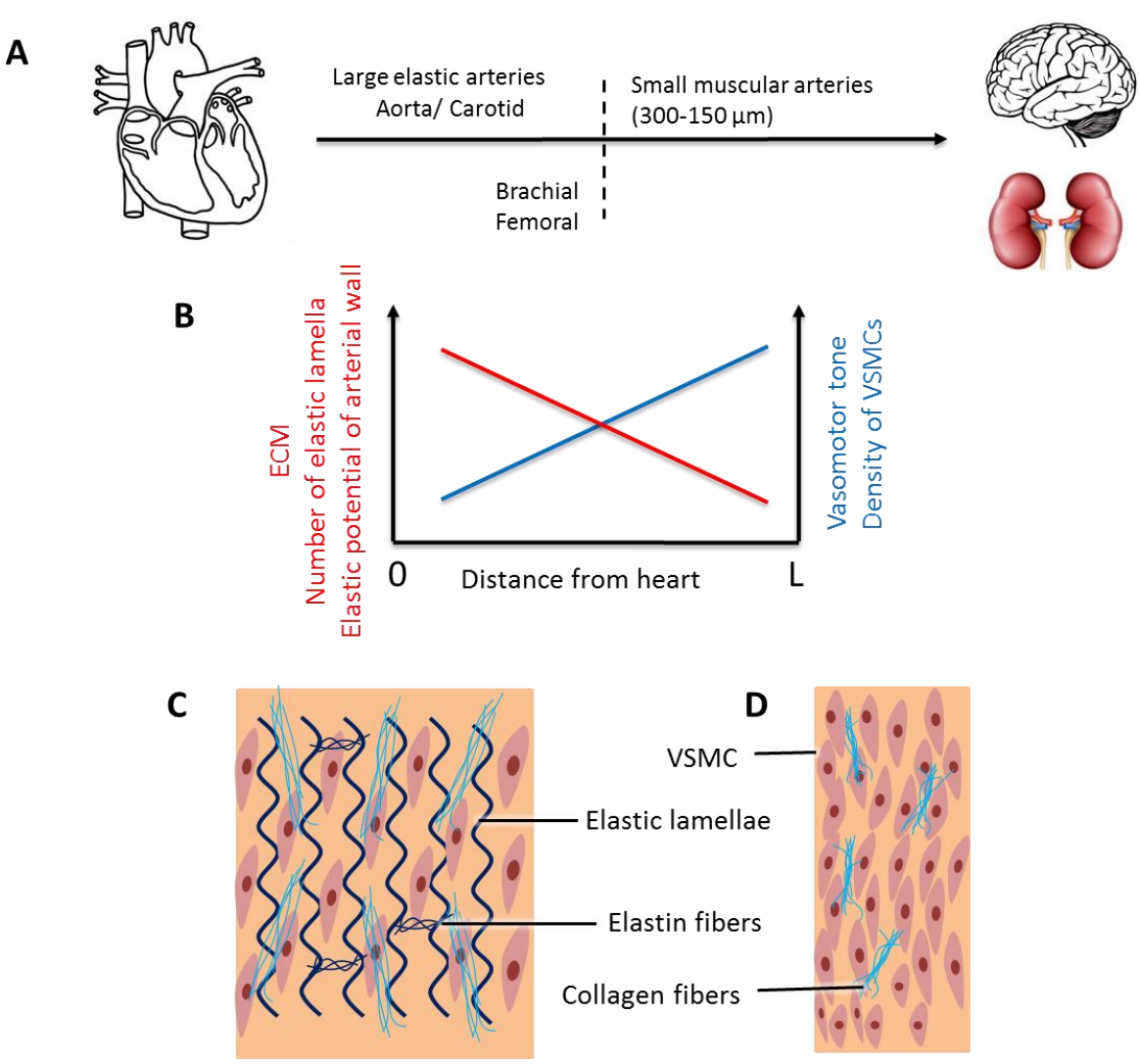

Figure 2.6 Structural and functional heterogeneity of the arterial tree. (A) Two major types of arteries. The elastic arteries close to the heart (proximal) with large sizes are capable of distending to accommodate the considerable increase in blood volume during systole, while the muscular arteries with smaller diameter drive constriction or dilation of the arteries to maintain tone and regulate blood flow to the peripheral regions (Lacolley *et al*., 2017). (B) As the distance increases from the heart, the elastic potential of the arterial wall decreases because of the reduction in the number of muscle-elastic complexes, ECM and number of elastic lamellae, while the vasomotor tone increases due to the increased density in SMCs, media structure in (C) elastic and (D) muscular arteries. In elastic media, SMCs are embedded between two layers of elastic lamellae and collagen fibres are arranged along the elastic lamellae. The elastic lamella is fenestrated, and its spaces are filled up with other ECM components. Thus, the stiffness of the elastic arterial wall is associated with the stiffness of each ECM component (i.e. SMC, elastic lamellae and collagen fibre) and their geometrical and functional relationships (O'Connell *et al*., 2008). There are few or no elastic lamellae and several layers of predominant SMCs with some collagen fibres which constitute the muscular medial layer.

2.3.2.2 Muscular arteries

Muscular arteries include the radial arteries and the splenic arteries. The significant differences between the elastic and muscular arteries are the medial structures and components in that the SMCs predominantly constitute a circumferentially continuous fibrous helix with fewer elastic laminae in muscular arteries (Figure 2.6D) (Holzapfel *et al*., 2000, Megens *et al*., 2007). Due to the structural differences, they play different roles in the arterial system in that the media SMCs in muscular arteries drive constriction or dilation of the arteries to maintain tone and regulate blood flow to the peripheral regions in the body (Figure 2.6B) (Shirwany and Zou, 2010). SMCs contribute profoundly to the mechanical behaviour of muscular arteries (Faury *et al*., 1999). Thus, muscular arteries show notable viscoelastic behaviour with hysteresis (Holzapfel *et al*., 2002, Bauer *et al*., 1982).

2.3.2.3 Transitional arteries

The IMA is considered a transitional artery. It can be either muscular or elastic (Borovic *et al*., 2010). It is found to supply the anterior chest wall and the breasts along the sternum (Figure 2.7). The IMA is most frequently used arterial graft in contemporary cardiac surgery due to its long-term and great patency after coronary artery bypass grafting (CABG) (Figure 2.7) (Canham *et al*., 1997, Calafiore *et al*., 2005). The outstanding suitability of IMA in CABG is proved to attribute to low-grade intimal hyperplasia and thickening in the native IMA (van Son *et al*., 1997).

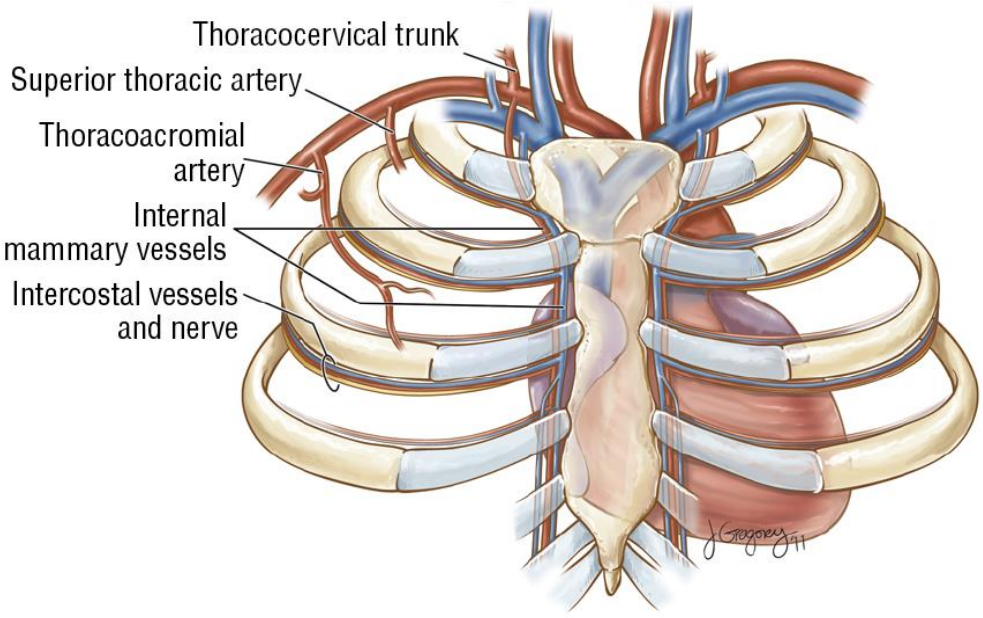

Figure 2.7 Schematic diagram of the vascular anatomy of the IMA and vein (Jacobson *et al.*, 2013).

2.4 Biomechanical properties of the artery wall

As conduits in the body, the primary role of blood vessels is to distribute and collect blood to and from various tissues and organs. The large arteries are capable of regulating the pulsatile ejection of blood from the ventricle, supplying less pulsatile and continuous blood flow to the smaller arteries and microcirculation. The mechanical properties of the arteries are largely derived by the quantity and structure of collagen, elastin and SMCs and their organisations. These specialised structures enable the large elastic arteries to store a portion of the stroke volume with each systole and discharging that volume with diastole, which is called the windkessel effect (Bauer *et al.*, 1982). Due to the composite structure and inhomogeneous nature, conduit arteries possess non-linear mechanical behaviour in that the arterial wall does not obey Hooke's Law of a perfectly elastic material and the modulus of the arterial wall

increases with increasing applied stress (Figure 2.8). Under physiological condition, the incremental elastic modulus of the arterial wall is less than that of collagen but much higher than that of elastin alone. The extensible elastin and the relatively stiffer collagen act as the compliant and reinforcing phase respectively, thereby endowing the arterial wall with a non-linear stress-strain pattern. At low degrees of stretch, the compliant elastin fibres dominate the mechanics, while helically oriented collagen fibres are recruited at higher load bearing, so that the higher the blood pressure, the smaller the change in the circumference for a given change in pressure.

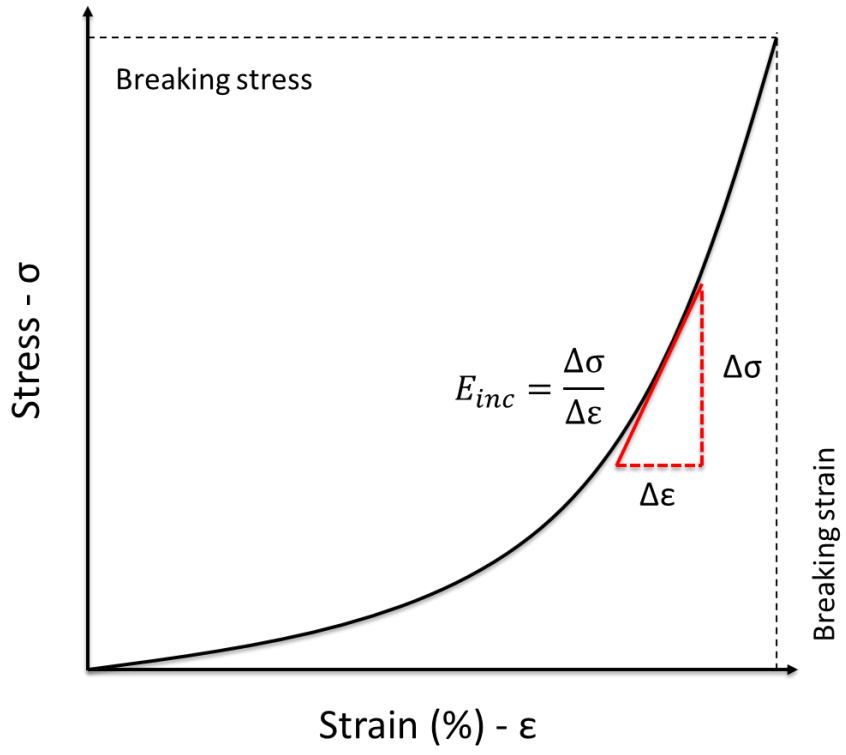

Figure 2.8 A typical non-linear stress-strain curve for the arterial wall with stress being applied in the circumferential direction. The incremental elastic modulus (E_{inc}) is the instantaneous ratio of the change in applied stress (Δσ) and the associated change in strain (Δε) (Derby and Akhtar, 2015).

As pressure increases, the elastic lamellas are circumferentially stretched accompanied by a progressive reduction in the inter-lamellar distances and alignment of the collagen fibres, which eventually results in increased elastic modulus of the arterial wall (Shadwick, 1999).

To evaluate arterial mechanics and understand how mechanical changes occur in arterial stiffening, it is essential to assess the mechanical behaviour of bulk arterial mechanics at the macroscopic level because of its clinical importance in cardiovascular events, including atherosclerosis (van Popele *et al*., 2001) and hypertension (Kaess *et al*., 2012). Given the multi-layered and inhomogeneous nature of the arterial wall, it is more important to investigate the mechanical properties at the microscopic level (within distinct arterial layers) and nanoscale (molecular or cellular level) (Akhtar *et al*., 2011). More importantly, the pathological alterations always start at the molecular level and progressively develop to the higher levels of the structure resulting in permanent and irreversible changes and dysfunction (Stolz *et al*., 2009). Hence, the micro- and nano-scale investigations in arterial biomechanics and structure are capable to not only fundamentally elucidate its macroscopic structure and function, but also promote a better understanding of changes in arterial tissue with ageing and diseases for early detection and improving clinical treatment.

However, due to the inhomogeneous properties of biological samples' overall length scales, the measured elastic modulus varies significantly by using different spatial testing methods. Macroscale tensile testing induces a macroscopic deformation that spans the bulk of tissue with the entire specimen stretched, whereas nanoindentation and AFM are likely to separately conduct an assessment of the mechanical behaviour of extracellular matrix and individual assemblies like collagen and elastin. Therefore, it is essential to understand the mechanical behaviour of inner compositions of biological tissues and how they contribute to the overall tissues.

2.4.1 Macroscale mechanical testing methods and tensile testing

2.4.1.1 Macroscale mechanical testing methods

Macroscopic mechanical properties of intact arteries have been well-documented and widely used to predict the cardiovascular risk (Blacher *et al*., 1999, Cecelja and Chowienczyk, 2012). To date, several macroscale techniques for assessing the mechanical properties of the entire arterial wall have been developed *in vitro* involving tensile testing, opening angle measurement and *in vivo*, like ultrasound testing measurements and PWV assessment.

2.4.1.2 Tensile testing

To determine the macroscopic biomechanical properties of an arterial wall, a rectangular artery specimen is cut from arterial tissue and its features are uniaxially (Duprey *et al*., 2010, Karimi *et al*., 2013) measured to yield a non-linear stress-strain curve (Figure 2.9). Although the biomechanical behaviour of human arterial tissue to uniaxial loading conditions has been primarily studied (Karimi *et al*., 2013, Holzapfel *et al*., 2005), it is significantly insufficient to characterise the multi-axial mechanical properties of arterial wall (Geest *et al*., 2004), because the uniaxial test treats the artery as an isotropic material instead of quantifying the anisotropic behaviour of the arterial wall thoroughly (Cowin and Humphrey, 2001).

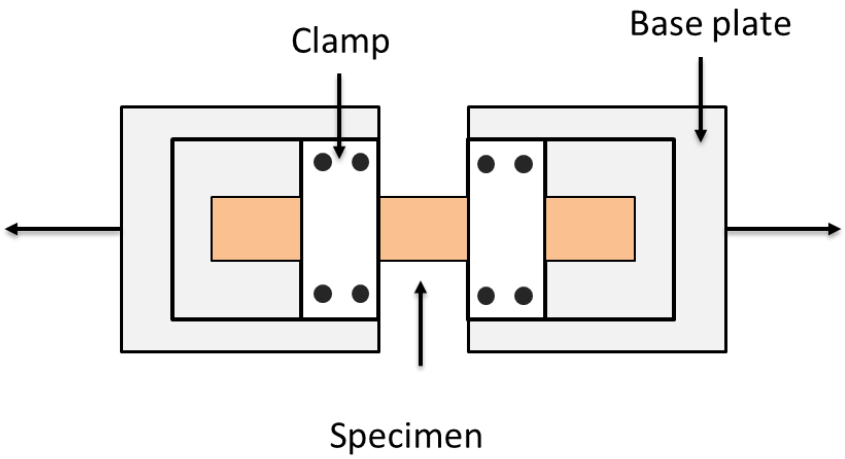

Figure 2.9 Schematic diagram showing the sample setup for uniaxial tensile test. The tissue is prepared to a rectangular section and clamped during the test (Akhtar, 2014).

The layer-specific mechanical properties of arteries have been reported by using tensile test (Holzapfel *et al*., 2005). Furthermore, the mechanical changes between health and human atherosclerotic arteries and age-related alterations in arterial wall are also evaluated by the tensile test (Karimi *et al*., 2013, Geest *et al*., 2004).

2.4.2 Microscale - nanoindentation

To date, even though macroscale biomechanics of artery have been profoundly addressed, understanding of changes in the mechanical behaviour of individual arterial layers, ECM and components within these layers is scant (Kohn *et al*., 2015). Characterisation on the cell-scale is seen as fundamental to illuminating the structure-function relationship and understanding the biomechanical changes in arteries with ageing or diseases. However, cell size is usually of the order of tens of microns which is impossible for macroscale measurements (Kohn *et al*., 2015). To elucidate fundamental changes in biomechanical properties of the arterial wall and address numerous questions that are relevant to the medical community, a variety of

techniques with high-spatial resolution have been developed for characterising microscale and layer-specific mechanical changes.

Nanoindentation is a depth-sensing indentation technique that is used to measure local mechanical properties, such as hardness and reduced modulus of material on the micron and submicron scale by recording the load and surface deformation, which allows the elucidation of structure-biomechanics relationships in the same tissue (Ebenstein and Pruitt, 2006). Due to its ability to characterise small and heterogeneous specimens from biopsy samples and small animal models, nanoindentation is used extensively for determining localised mechanical properties of various biological samples. Given the various geometries of the indenter tip, nanoindentation allows localised mechanical measurement from microscale to nanoscale, with a force range of 1 μN to 500 mN and a displacement range of 1 nm to 20 μm which significantly bridge the gap between nanoscale AFM measurements and macroscale testing (Fischer-Cripps, 2011, Ebenstein and Pruitt, 2006). Three analytical models are largely utilised to fit nanoindentation data to generate mechanical properties, including the Hertz model (Johnson, 1982), the Oliver-Pharr model (Oliver and Pharr, 2004, Oliver and Pharr, 1992) and the Johnson–Kendall–Roberts (JKR) adhesion model (Johnson *et al*., 1971).

To circumvent the challenges associated with testing of soft tissues like arteries, researchers utilise a larger radius tip with either flat or rounded ends (radius more than 100 μm) (Ebenstein and Pruitt, 2004). Using smaller tips (radius = 10 μm), differences in the local mechanical properties of distinct anatomical layers in the arterial wall have been well studied. Hemmasizadeh *et al*. (Hemmasizadeh *et al*., 2012) conducted nanoindentation testing on porcine aorta wall and revealed the difference in the instantaneous Young's modulus between the inner half and outer half layer, implying that the outer half was stiffer and showed less relaxation. They also found an increasing trend in the instantaneous Young's modulus from the inner towards the outer layers of the porcine aorta (Hemmasizadeh *et al*., 2015). Similarly,

in ferret aorta, the elastic modulus was found to progressively increase from the intima to the adventitia, and the mean elastic modulus for the medial layer is around 20 MPa (Akhtar *et al*., 2009). Although several studies have focused on the mechanical characterisation of the human atherosclerotic plaque tissue (Ebenstein *et al*., 2009, Akyildiz *et al*., 2014), there is still scant information in the literature on human arteries that has been obtained from nanoindentation testing.

It is noteworthy that the arterial stiffness data generated through nanoindentation are several orders of magnitude lower than the macroscale measurement of bulk arteries, which makes the nanoindentation data more comparable to AFM results (Section 2.6.3) and both techniques provide similar information. Nevertheless, for indenting tissue-level properties in soft tissues, a large indenter tip (> 50 μm) is necessary to ensure the contact area will be much greater than the dimensions of crucial tissue components and avoid damaging the sample (Ebenstein and Pruitt, 2006). Therefore, it is complicated and challenging to use nanoindentation for characterising tiny biological samples.

2.4.3 Nanoscale - AFM

AFM is a nanoscale technique that allows us to visualise and measure surface structure at the nano- or, in some cases, atomic scale (Young *et al*., 2011). This is mainly due to the ability of the technique to measure forces and distances at a very high resolution between the probe and surface, and to non-destructively explore various surfaces in ambient or fluid conditions. The vertical resolution is mainly determined by the AFM scanner sensitivity, and it can be as high as 0.01 nm (Young *et al*., 2011). In addition to characterising topography, surface mechanical properties can be measured by AFM-based force modulation semi-quantitative scanning techniques (Maivald *et al*., 1991) or force curve fitting based AFM (Burnham and Colton, 1989). Compared with other high-resolution surface characterisation techniques (SEM and

TEM), AFM measurement is relatively simple with minimal sample preparation and available for measuring in air and fluid environments without extreme conditions like vacuum and dehydration. In recent years, AFM has been used for probing the ultrastructure of aorta ECM (Raspanti *et al*., 2006, Graham *et al*., 2010) and mapping the mechanical properties of tunica adventitia (Grant and Twigg, 2012), atherosclerotic plaque *(*Tracqui *et al., 2011,* Hayenga *et al*., 2011), and the altered SMC stiffness with ageing (Qiu *et al*., 2010) and hypertension (Nakamura *et al*., 2010). Details about AFM are discussed in Section 2.6.

2.5 Alterations in arterial composition and biomechanics with age-related arterial stiffening

2.5.1 Alterations in collagen

In the arterial wall, increased collagen concentration in all three arterial layers (Kohn *et al*., 2015) and redistribution of collagen around the lamellar units in media (Schlatmann and Becker, 1977) have been found with age (Figure 2.10). A study in mice showed *ex vivo* increases in carotid artery stiffness was associated with TGF-β1 increases in type I and III collagen deposition. Increases in PWV have been related to downregulation of the collagen marker carboxyterminal propeptide for type I procollagen (PICP) (Rajzer *et al*., 2003) indicating elevated collagen synthesis and content. Furthermore, age-related arterial stiffening has been associated with increased TGF-β1 expression, which, in turn, stimulates the deposition of adventitial collagen and changes in fibroblasts (Fleenor *et al*., 2010).

In concert with increased collagen concentration, non-enzymatic glycation driven collagen crosslinking is also associated with arterial stiffening with age (Figure 2.10) (Schleicher *et al*., 1997). In the body, glycation process can stiffen tissues via producing deleterious end

products, known as advanced glycation end products (AGEs) which accumulated through Maillard reaction. Several clinical and experimental studies have shown that AGEs have a critical role in the pathogenesis of CVDs by contributing to its development and progression. However, it is still under debate as to whether AGEs can serve as clinical biomarkers for CVD due to the limited studies (Prasad *et al*., 2012).

2.5.2 Alterations in elastin

Due to the longevity and extremely low turnover rate, the age-related fragmentation, calcification, and matrix metalloproteinases (MMP) degradation in elastin can be accumulated and thereby shift load bearing to collagen fibrils, which significantly contribute to arterial stiffening (Figure 2.10) (Schlatmann and Becker, 1977). To be specific, elastin fragmentation can be caused by fatigue failure from pulsatile wall stress (Greenwald, 2007). Elastin fibres can also be calcified through binding to calcium ions in the arterial wall with ageing (Otto *et al*., 1999), which facilitate medial elastin fragmentation and arterial stiffening (Elliott and McGrath, 1994, Gaillard *et al*., 2005). Elastin degradation as an enzyme-driven process is mediated by MMPs. In the tissues, ECM is continually remodelled and mediated primarily by these zine-dependent endopeptidases and their inhibitors (tissue inhibitors of MMPs, or TIMPs) (Ergul *et al*., 2004, Bonnema *et al*., 2007). There are so far eight MMPs that have been proved to degrade elastic fibre into soluble fragments, including MMP-2, -7, -9, -10, -12 and -14, and to catabolize fibrillin microfibrils and peptides by MMP-2, -3, -9, -12, and -13 (Sherratt, 2009, Tsuruga *et al*., 2007). The dysregulation of MMPs, especially MMP-2, MMP-9, is highly correlated with aneurysms (Thompson and Baxter, 1999), cardiovascular pathologies, hypertension and arterial stiffness (Wallace *et al*., 2005). Upregulated ECM protease expression is associated with atherosclerosis (Robert *et al*., 2008) and ageing (McNulty *et al*., 2005) in the arterial wall. Although the absolute elastin content in

the aorta is stable with age, a substantial decrease in elastin concentration and increased collagen concentration are observed (Fonck *et al*., 2009).

2.5.3 Alterations in SMCs

SMCs have been proved to be involved in atherosclerosis and the restenosis change of arteries through migrating into the intima, proliferating and synthesising a variety of ECMs, including collagen, elastin and proteoglycans in the thickened intima (Figure 2.10) (Raines, 2000). SMC dysfunction results in impaired vasodilation, increased vasoconstriction, increased proliferation and migration, which likely contribute to the overall impairments in blood pressure regulation and arterial stiffness. The arterial stiffening is attributed not only to fundamental changes in SMCs but also to SMCs related signalling and structural events in ECM (Qiu *et al*., 2010). Therefore, SMCs, being highly related to extracellular signalling and structural changes, significantly contribute to arterial stiffening.

2.5.4 Alterations in proteoglycans and SLRPs

Although proteoglycans are a minor component of arterial tissue (2% ~ 5% by dry weight) (Wight, 1989), a number of studies have shown that these macromolecules, especially SLRPs, are highly associated with arteriogenesis (Kampmann *et al*., 2009), atherosclerosis (Talusan *et al*., 2005) and extracellular matrix remodelling (Barallobre-Barreiro *et al*., 2012). To be specific, versican and aggrecan are major components of the intimal ECM and predominant proteoglycans in human intimal hyperplasia, which are highly related to the formation of atherosclerosis (Figure 2.10) (Talusan *et al*., 2005).

2.5.4.1 Influences on collagen formation and organisation

Collagen fibril as a vital component of arterial ECM can be structurally and functionally regulated through binding to SLRPs, including collagen fibrillogenesis process, collagen formation and fibril organisation (Kalamajski and Oldberg, 2010). Hence, disordered SLRPs expression can trigger irregular collagen fibril formation and organisation, altered ECM assembly and dysfunctional ECM, thus further influencing the structural and functional integrity of the tissue (Figure 2.10). For instance, decorin was indicated to associate with collagen assembly and structural organisation of collagen matrix, thereby maintaining the sufficient mechanical properties and normal functions of collagenous tissues (Iozzo, 1998).. Through interaction with protofibrils in the ECM, SLRPs play an essential part in the discontinuity of the ECM during tissue growth and functionality of collagen fibrils. With tissue maturation, mechanical properties of the connective tissue are promoted through fibril maturation such as collagen growth and organisation, as well as covalent crosslinking. Larger diameter collagen fibrils are known to associate with lateral fibril growth and fuse laterally in mature tissues. In the absence of decorin and biglycan, collagen fibrils experience an uncontrolled lateral fusion and enlarged thickness with advanced weakened mechanical strength in the mouse. These structural abnormalities can further arouse skin laxity and fragility and osteopenia (Danielson *et al*., 1997).

2.5.4.2 Influence on elastin formation and organisation

Studies have also evidenced the possible role of SLRPs in elastic fibre biology through forming complexes with elastin component or precursor of mature elastin, i.e. fibrillin-1, tropoelastin and microfibril-associated glycoprotein-1. Decorin can be involved in the synthesis of the elastic fibre component (fibrillin-1) in renal fibroblasts via various pathways (Schaefer *et al.*, 2007). Biglycan is also capable of regulating the composition of the ECM of

arterial wall through inhabiting elastin synthesis and assembly mainly due to its galactosamine-containing glycosaminoglycans (GAG) chains (Hwang *et al*., 2008).

2.5.4.3 Influence on SMCs

SLRPs have been noticed to associate with intima thickening and be involved in regulation of SMCs and CVDs. For instance, accumulation of lumican has been prominently localised in the fibrous thickened intima and inner media and this protein was highly expressed in SMCs across the inner media and thickened intima in arteries from patients with atherosclerosis (Onda *et al*., 2002). Besides, lumican has also been discovered in the outer layer of medial SMCs and may be secreted to adventitia for maintaining adventitial mechanical property dominated by collagen fibres (Onda *et al*., 2002). Upregulated mimecan expression in human aortic SMCs was shown to suppress cell proliferation and accelerate cell migration and death, thereby modulating atherosclerosis (Zhang *et al*., 2015) and atherosclerotic plaques (Fernández *et al*., 2003).

Table 2.1 Functions of proteoglycans in different types of collagen, elastic fibre and SMCs and their effects on CVDs.

Proteoglycans	Collagen	Elastic fibre	VSMCs	CVDs
Large proteoglycans (Talusan *et al*., 2005)				
Aggrecan Versican				Intimal hyperplasia and atherosclerosis
SLRPs (Kalamajski and Oldberg, 2010, Chen and Birk, 2013)				
Class I				
Biglycan	Type I, II, III, VI, IX	Tropoelastin and glycoprotein-1	SMCs proliferation and migration	Atherosclerosis and vascular injury/lesion
Decorin	Type I, II, III, V, VI, XII	Fibrillin-1, tropoelastin and glycoprotein-1	SMCs calcification	Atherosclerosis lesions
Asporin	Type I			
Class II				
Lumican	Type I		SMCs proliferation and migration	Intima thickening and atherosclerosis
Prolargin				
Class III				
Mimecan			SMCs proliferation, migration and death	Atherosclerosis, atherosclerotic plaques and intima thickening
Class V				
Podocan	Type I		SMCs proliferation, migration	Arterial repair

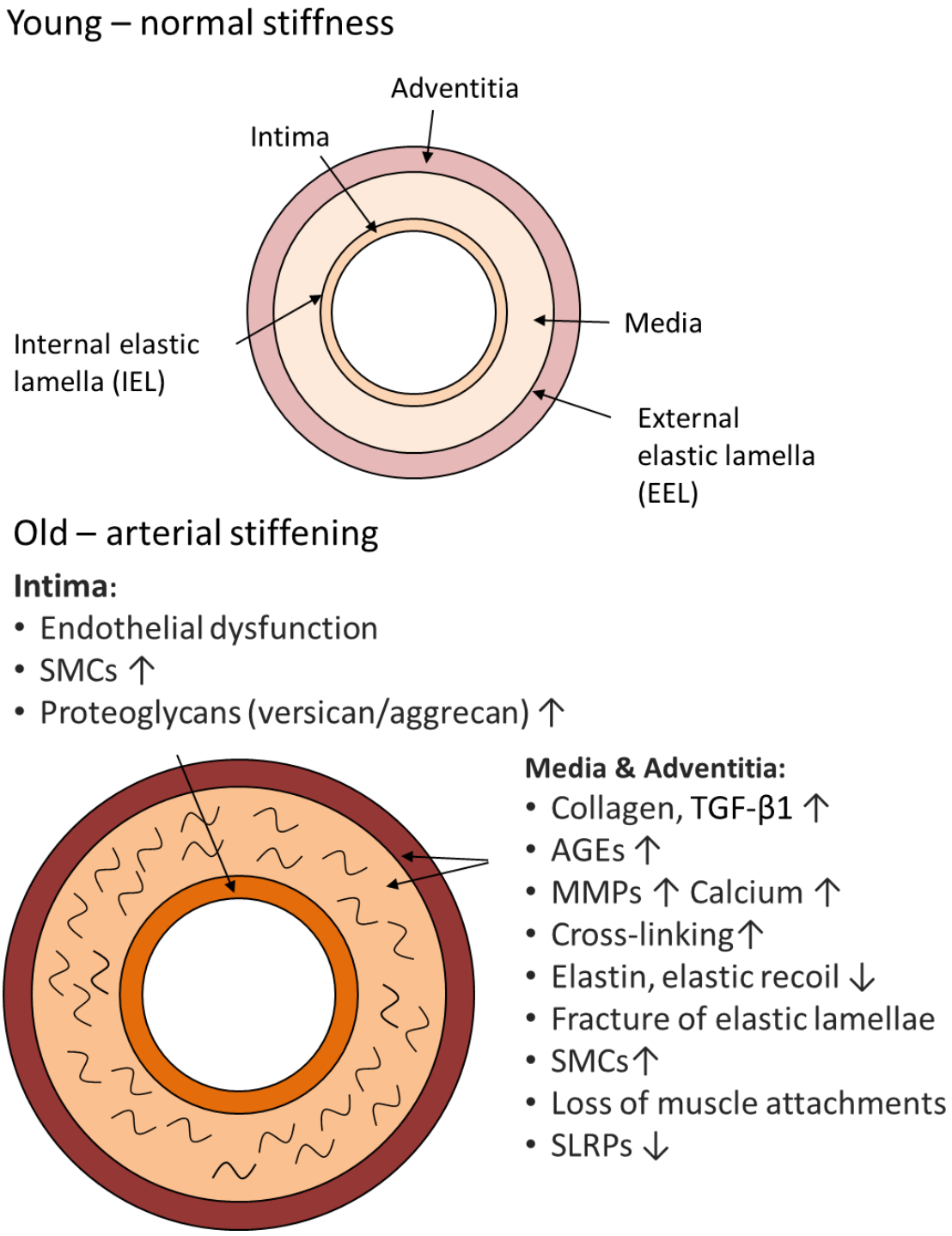

Figure 2.10 Schematic diagram of the arterial section in a young and an old human. In the young sample, each layer and IEL and EEL is labelled. In the aged artery, changes in the intima, media and adventitia are various and across the artery. The medial layer is disorganised due to fraying, and fracture of the elastic lamellae and loss of muscular attachment, together with increased collagen fibres can be seen. Multiple causes are also associated with arterial stiffening across the arterial wall, such as changes in SMCs, proteoglycans, AGEs and TGF-*β*1 (Akhtar, 2014, Sherratt, 2013, Sawabe, 2010, Kohn *et al.*, 2015).

2.6 AFM

2.6.1 Biological application of AFM

AFM has gained vital importance in the recent years for studying biological samples at nano- and sub-nanoscale. Except for characterising surface topography as its high sensitivity, AFM is being widely used to study surface adhesion and stiffness properties for a range of biological tissues from cells (Sokolov *et al*., 2013), tissues such as aorta (Mao *et al*., 2009), cartilage (Stolz *et al*., 2004), tissue ECM components like collagen (Grant *et al*., 2012) and also for hard tissues such as bone (Wallace, 2012), which enable the generation of a three-dimensional surface topography with height profile and localised mechanical properties. Moreover, AFM measurement can be conducted in physiological buffers or natural aqueous environments at 37℃ to monitor biological reactions and even observe them in real time without any complicated sample preparation or under extreme conditions (Graham *et al*., 2010). Compared with other high-resolution surface characterisation techniques (SEM and TEM), AFM measurement is relatively simple with minimal sample preparation and available for measuring in ambient and fluid environments without extreme conditions like vacuum and dehydration.

AFM has also been used in small animal models to study complex biochemical process and human diseases (Mahamid *et al*., 2008, Mao *et al*., 2009). For example, researchers have proved the utility of the zebrafish vertebral column for characterising collagen fibrils and biomineralisation (Ge *et al*., 2007, Ge *et al*., 2006).

2.6.2 Principles of AFM

2.6.2.1 AFM instrumentation

AFM mainly consists of the microscope stage itself, control electronics and control system with a computer, which is shown in Figure 2.11. The most critical component, the microscope stage, involves a scanner, sample holder and a force sensor (cantilever system). Due to the similar length scales, AFM is often combined with an optical microscope or fluorescence microscope, and the integration allows the measurements to be correctly localised, especially in biological samples.

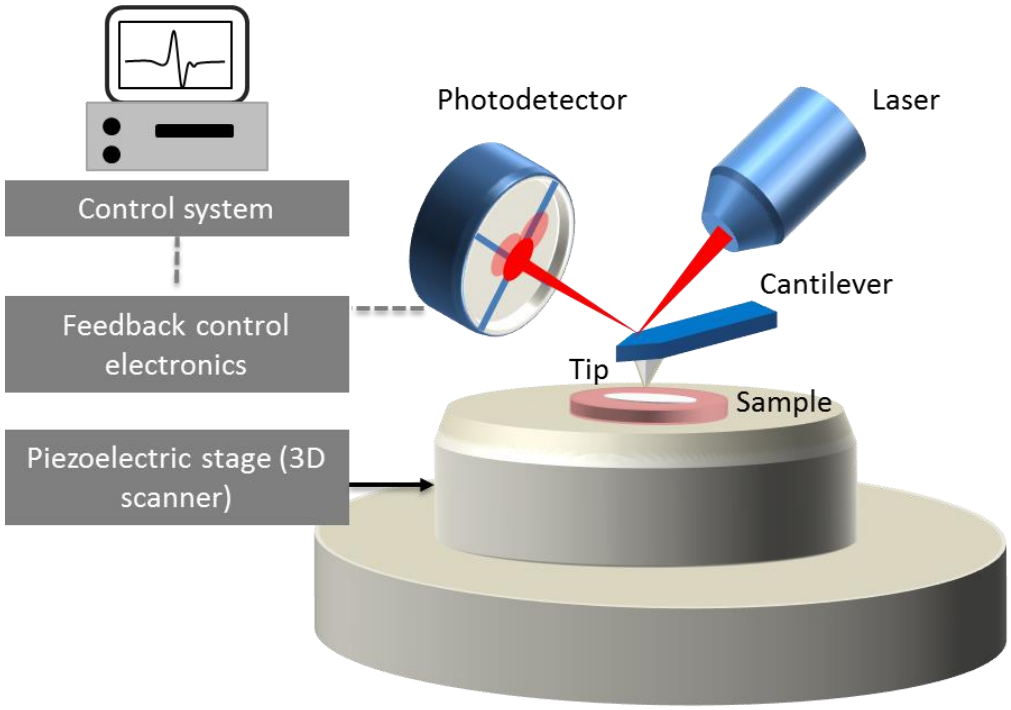

Figure 2. 11 Schematic diagram for the AFM setup, involving control system with computer, feedback control electronics and microscope stage (3D scanner, sample holder and force sensor) (Kaemmer, 2011).

The spring constant of the force sensor (cantilever) should be adequately selected according to the sample measurement, allowing for small sensitivity to the force. The laser beam

reflecting off the back surface of the cantilever detects the deflections of the cantilever and can be registered by the deflection detector (four-quadrant photodetector). The feedback control electronics connected to the microscope stage and the control system is used to generate signals to drive the scanner and other motorised components in the microscope stage, as well as digitise the obtained signals for display and analysis by the computer. The stage is usually supported by a vibration isolation platform which reduces environmental noise.

In AFM measurement, the probe is brought into proximity to the sample, and the probe/sample are subsequently moved relative to each other that interactions between the tip and sample surface are measured by monitoring the displacement of the free end of the attached cantilever at each locations (pixels). During operation the interaction force is controlled by a closed-loop feedback system. The setpoint value generally represents the imaging force in conventional AFM and determines the magnitude of the tip-sample interaction. The resulting error signal (or difference between the setpoint and actual value) is processed by a Proportional-Integral-Differential (PID) feedback controller that adjusts the z-piezo to move the probe up and down and minimise the error signal, thereby realising the desired setpoint. Thus, the resulting z-piezo movements provide the height information to create the surface topography (Kaemmer, 2011)..

2.6.2.2 Working modes

The contact mode AFM was the first and simplest working mode developed for AFM by which the deflection of the cantilever leads directly to the topography of the sample. The cantilever is adjusted on the sample and the probe are in contact and deflection is read directly on the four-quadrant, force is drive by Hooke's law. It is notable that in contact mode measurement, both the tip of the probe and the sample surface are in touch with each other, which results in the following problems: (a) the repulsive force between the tip and the

sample may damage or change the surface and the sharp tip during scanning; (b) as the tip moves along the sample surface, lateral forces can get generated in addition to the normal force between them; (c) the generated data is profoundly affected by the nature of the sample surface, which implicates the stability and sensitivity of the technique (Eaton and West, 2010, Kaemmer, 2011).

In the dynamic mode, the cantilever is oscillated, typically at its resonant frequency and the vibration amplitude (amplitude modulation) or the shift of the resonance frequency (frequency modulation) of the cantilever is measured to estimate the deflection of the cantilever. When the oscillating probe approaches the sample surface, the oscillation changes as per the interaction between the probe and the sample. Also, changes in amplitude and frequency enable the feedback control of tip-sample interaction during measurement.

In non-contact mode, the tip is brought extremely close to the surface at a constant distance and is oscillated by the system at or near its resonance frequency without contacting the sample surface. Thus, unlike the contact mode, the non-contact mode is capable of imaging very soft samples using small oscillation amplitudes with minute interacting forces, which gives better and more consistent results.

In tapping mode, the probe is vibrated close to its resonance frequency like the non-contact mode and contacts the surface for a short time, which enables probing a wide range of samples with negligible lateral forces (Figure 2.12). Therefore, this mode has several advantages: (a) lateral forces vanish as there is only a perpendicular movement of the tip on the surface; (b) the contamination layer effect can be eliminated; (c) tip-sample contact is capable of gaining some other sample properties (Kaemmer, 2011, Eaton and West, 2010).

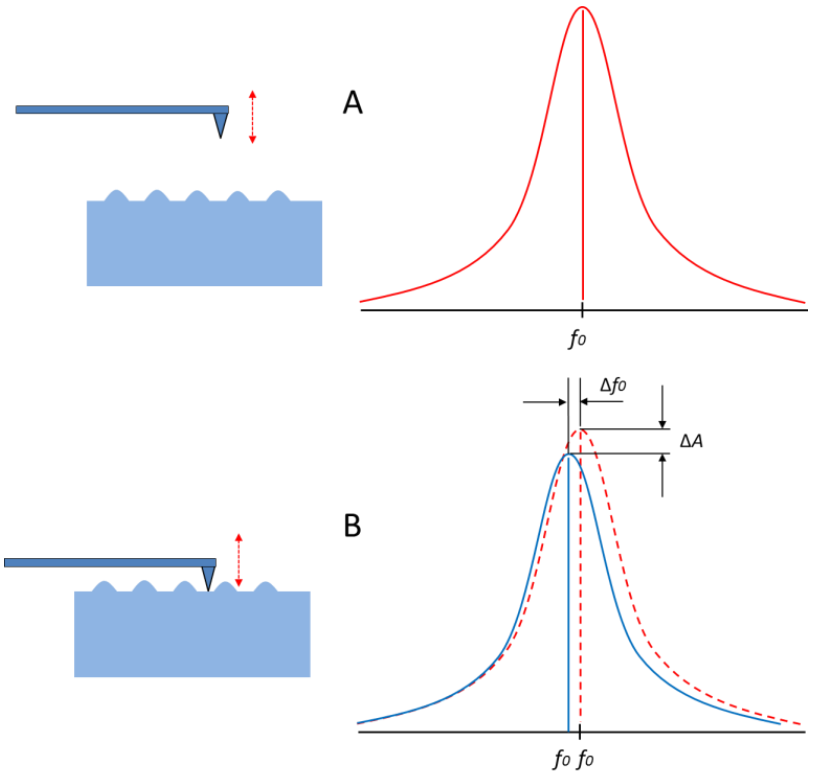

Figure 2.12 Resonance curve of a Tapping mode cantilever (A) above and (B) close to the surface. After contact with the surface, there is a resonance shift to a lower frequency (Δf0) and a reduction in amplitude (ΔA) (Kaemmer, 2011).

2.6.3 Characterisation of mechanical properties with AFM

2.6.3.1 Force curves

By maintaining the x-y position of the AFM probe and ramping it in the z-axis, the deflection can be measured during the time the probe approaches and retracts from the sample surface that generates the force-distance curves between them. This mode can measure the force between the contacting atoms or molecules at the end of the probe and the sample surface that allows for single-molecule interaction studies.

2.6.3.2 Contact models

2.6.3.2.1 Hertz model

The Hertz model (Johnson, 1982, Hertz, 1881) is extensively used to fit force versus indentation curves for Young's modulus calculation (Figure 2.14A). The Hertz model describes the elastic deformation of two perfectly homogeneous smooth bodies under load (Figure 2.13A). When using the Hertz model, two critical assumptions need to be considered: (a) the indenter must have a parabolic shape or a spherical tip radius that is much bigger than the indentation depth; (b) the indented sample is much thicker in comparison to the indentation depth (Mahaffy *et al*., 2000). Given the sphere tip with the radius *R*, the force on the cantilever *F* is given by:

$$F = \frac{4}{3} \frac{E}{(1-\nu^2)} \sqrt{R}\delta^{3/2} \quad (7)$$

where *E, v, R* and δ refer to the Young's modulus, Poisson's ratio, tip radius, and indentation depth, respectively (Adamcik and Mezzenga, 2012).

Although the Hertz model has been shown to accurately describe the contact area between elastic spheres without considering adhesion between the indenter and surface, for soft biological samples, adhesion resulting from attractive forces between tip and sample surface is critical to characterising contact mechanics. The Hertz mechanics considered the deformation of two elastic spheres initially and only described the elastic deformation of a spherical tip on poorly deformable samples (contact radius << tip radius), which can lead to the unphysical prediction that contact radius is more significant than tip radius. Therefore, there are several difficulties in applying the Hertz model for describing biological samples, which are mainly due to the soft and rough surface and inherent inhomogeneity of biological samples (Carpick *et al*., 1999).

2.6.3.2.2 Sneddon mode

Considering the elastic deformation of surface and tip in measurement on very soft samples (e.g. cells, tissues, biomolecules), the Sneddon model is developed (Sneddon, 1965). When measuring very soft samples, e.g. cells, tissues and biomolecules, elastic deformation of both the AFM tip and the sample can cause a finite contact area which cannot be ignored (Berquand, 2011). When the sharp tips (small tip radius) or soft samples (highly deformed surfaces) are involved, it is more appropriate to use the Sneddon model (Equation 8) (Figure 2.13B) which considers the tip as an infinite conical indenter and describes the corresponding elastic deformation of the initially flat surface without limitation on contact radius/tip radius (Calzado-Martín *et al*., 2016).

$$F = \frac{2}{\pi}\frac{E}{(1-\nu^2)}\tan(\alpha)\,\delta^2 \qquad (8)$$

where F is the force, E is the apparent Young's modulus, ν is the Poisson's ratio of the sample, α is the half angle of the AFM tip and δ is the indentation depth.

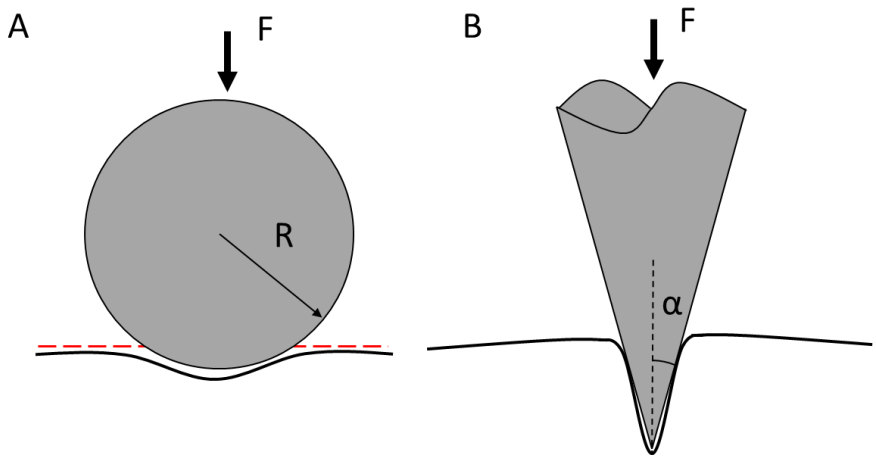

Figure 2.13 Contact mechanics of Hertz and Sneddon in AFM. (A) Hertz mode is well-adapted to poorly deformable samples and spherical tip (tip radius >> contact radius). (B) Sneddon mode considers the sharp tip as an infinite conical indenter, which is appropriate to describe soft and deformable samples.

2.6.3.2.3 Other models with adhesion

After considering adhesion, more advanced theories were developed, such as JKR (Johnson *et al*., 1971) and Derjaguin-Muller-Toporov (DMT) (Derjaguin *et al*., 1975) models. The JKR model involved strong short-range adhesion forces within the contact area (Figure 2.14B), and the DMT model considered weak long-range adhesion forces outside the contact area (Figure 2.14C) (Adamcik and Mezzenga, 2012).

2.6.3.2.3.1 JKR mode

To incorporate the adhesion of the indenter to the Hertz model, Johnson, Kendal and Roberts (Johnson *et al*., 1971) modified the theory to develop a more advanced model for contact mechanics (Mahaffy *et al*., 2004). When the contacts are characterised by relatively low stiffness, high adhesion forces and large tip radii, they can be described by the JKR model (Johnson *et al*., 1971). The JKR model characterises short range adhesion within the contact zone and applies to modelling reaction between a very soft tip and samples where the adhesion is strong enough to overcome the stiffness of the sample and cause the substrate to be drawn toward the tip. Conversely, in rigid systems (stiff materials) with low adhesion forces and small tip radius, the DMT model is likely to be the more appropriate model to characterise the interaction by considering the long-range surface force and the adhesion forces outside the contact surface (Nakajima *et al*., 2014, Garcıa and Perez, 2002)

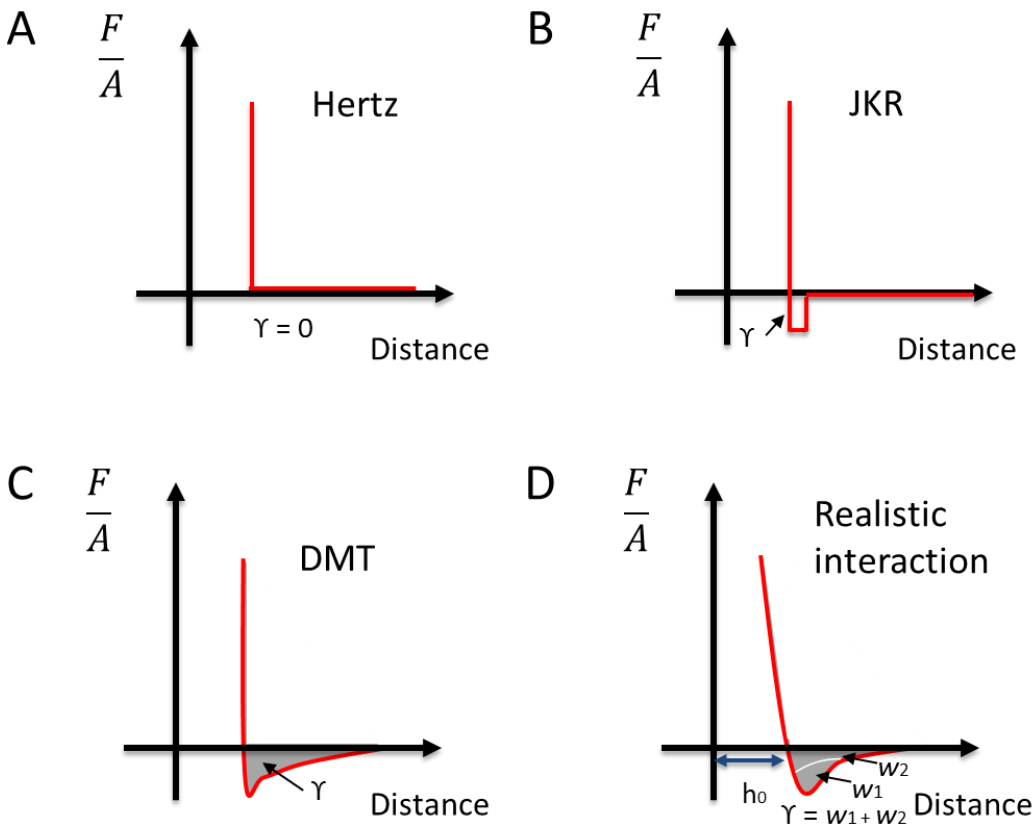

Figure 2.14 Contact models. Typical force (F) per unit area (A) displacement curve for (A) Hertz, (B) JKR, (C) DMT models, and (D) realistic interaction. The shaded areas reflect the work of adhesion ϒ. (A) Attractive forces (adhesion) are not considered in the Hertz model. However, adhesion is included (B) as a delta function in the JKR model and (C) as a long-range part in the DMT model (Schwarz, 2003).

2.6.3.2.3.2 DMT model

The DMT model (Derjaguin *et al*., 1975) modifies the Hertz model by adding the adhesive forces between the tip and the surface:

$$F - F_{adh} = \frac{4}{3} E^* \sqrt{R(d - d_0)^3} \qquad (5)$$

where $F - F_{adh}$ is force on the cantilever relative to the adhesion force, R is the tip end radius which can be calibrated prior to measurement, and $d - d_0$ is the deformation of the sample. We can get the reduced modulus E^* and calculate the Young's modulus (elastic

modulus) of the sample (E_s) if the Poisson's ratio is known. The relationship between the sample modulus and reduced modulus is described by the equation

$$E^* = \left[\frac{1-v_s^2}{E_s} + \frac{1-v_{tip}^2}{E_{tip}}\right]^{-1} \quad (6)$$

The tip modulus (E_{tip}) is assumed to be infinite when we calculate Young's modulus of the sample (E_s). The Poisson's ratio ranges from 0.2 to 0.5, giving a variation in the reduced modulus of the sample between 4% and 25%; however, this ratio is mostly not accurately known (Pittenger *et al*., 2010).

2.6.3.3 PeakForce QNM

2.6.3.3.1 Principles of PeakForce QNM

To accelerate the measuring rate and correlate it with the mechanical and topographic information, PeakForce QNM technique was developed based on Tapping mode and PeakForce mode that allow direct measurement of interaction force by the cantilever deflection (Young *et al*., 2011). The PeakForce QNM technique precisely controls the maximum peak force on the probe during measurement, enabling mechanical characterisation of different samples (Pittenger *et al*., 2014).

The working principle of PeakForce QNM is demonstrated as shown in Figure 2.15A. During PeakForce QNM measurement, when the tip is far from the surface (i), there is almost no force on the tip. The probe subsequently approaches the surface by attractive forces (negative force), including van der Walls, electrostatic, or capillary forces. At (ii), the tip reaches the surface and progressively indents into the surface as the force increases. After the Z position of the modulation reaches its bottom-most position (iii), we also obtain the peak force that is kept constant by the AFM system feedback during the interaction period. Then the probe

withdraws, and the force decreases until the minimum value (iv) where the tip comes off the surface and maximum adhesion occurs. Once the tip has separated from the surface, there are only long-range forces which are negligible for the probe (v). It is noteworthy that the feedback of the AFM system maintains the point (iii) instantaneous force (known as peak force) as a constant value by adjusting the extension of the Z piezo as the tip scans the sample surface (Pittenger *et al*., 2010, Pittenger *et al*., 2014).

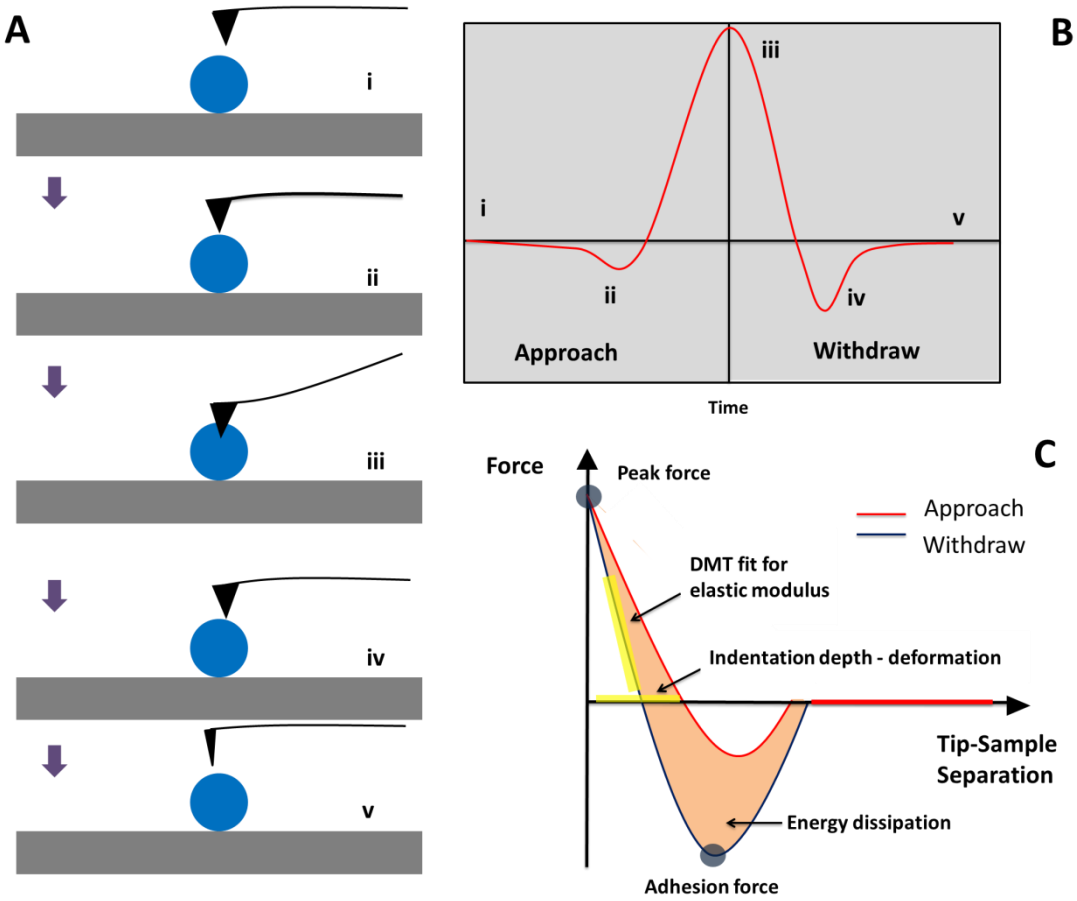

Figure 2.15 Working principle of PeakForce QNM. (A) Schematic diagram of the oscillating probe and (B) the corresponding force-time curve during an approach-retract cycle: (i) The probe is far from the surface the sample surface before measurement; (ii) At the beginning, the probe approaches the surface and attracted by the capillary, Van der Waals and electrostatic forces; (iii) After this, the tip on the top of probe is pulled to the surface by those forces and start indenting until the maximum Z-position (nm). At this point, the peak force values are obtained for feedback control; (iv) The probe withdraws and gets the maximum adhesion point before departing from the sample surface; and (v) Finally, the probe retracts and goes back to its original position where there is no more force. (C) Illustrates the typical force curve (force-z position curve) which is used to determine mechanical information of the sample, including adhesion, deformation, elastic modulus and energy dissipation.

Due to the control of the Z position and measurement of the cantilever deflection as a function of time (Figure 2.15B), the force is plotted as a function of the distance (force-Z-position curve) that can be converted to a force-separation plot for further analysis (Figure 2.15C). As shown in Figure 2.15C, mechanical information can be obtained by fitting different regions of the tip-separation curve, such as elastic modulus, tip-sample adhesion, energy dissipation and maximum deformation. In PeakForce QNM, elastic modulus (Young's modulus) is typically calculated by using the DMT model (Derjaguin *et al*., 1975)

PeakForce QNM utilises PeakForce Tapping technology for system feedback to deliver a number of important benefits, especially in the mechanical measurements. Unlike tapping mode, PeakForce Tapping oscillates, but far below the cantilever resonant frequency (i.e. non-resonant mode), thus avoids the filtering effect and dynamics of a resonating system. Because PeakForce Tapping does not resonate the cantilever, cantilever tuning is not required, which is particularly advantageous in fluids. Moreover, PeakForce Tapping provides direct control of the maximum normal force (and thus the deformation depth) of the sample, while eliminating lateral forces. This preserve both the tip and sample. Therefore, PeakForce Tapping has an oscillating system that combines the benefits of contact and tapping mode: direct force control and elimination of lateral forces. The key differences of PeakForce Tapping to the conventional force curve and the force volume measurement are that the z-position is modulated by a sine wave (as shown in Figure 2.16) instead of a triangular one, thus avoiding unwanted resonances at the turnaround points. Due to the sinusoidal ramping in PeakForce Tapping, the tip velocity during the indentation is close to zero and thus the effect of ramping speed on the mechanical mapping can be reduced or even eliminated (Pittenger *et al*., 2010, Pittenger *et al*., 2014).

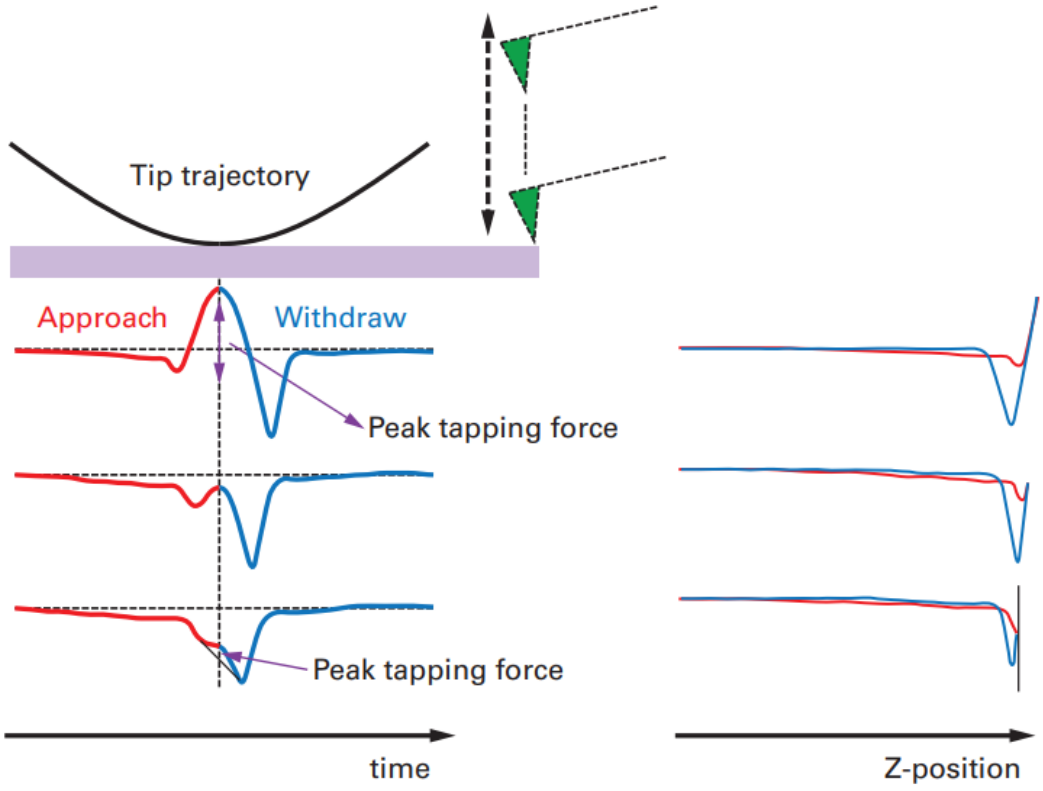

Figure 2.16 Experimental data of force curves for a cantilever during PeakForce Tapping. The cantilever ramps in a sinusoidal wave and the curves displayed as force versus time and force versus distance (Kaemmer, 2011).

2.6.3.3.2 Probe selection

Prior to the mechanical characterisation of PeakForce QNM, it is critical to choose a probe with an appropriate cantilever and a tip that produces sufficient sample deformation whilst still retaining high force sensitivity. The selection of the cantilever is highly dependent on the stiffness of the sample (Figure 2.17), i.e. the stiffness of the cantilever should be in the range of the sample stiffness.

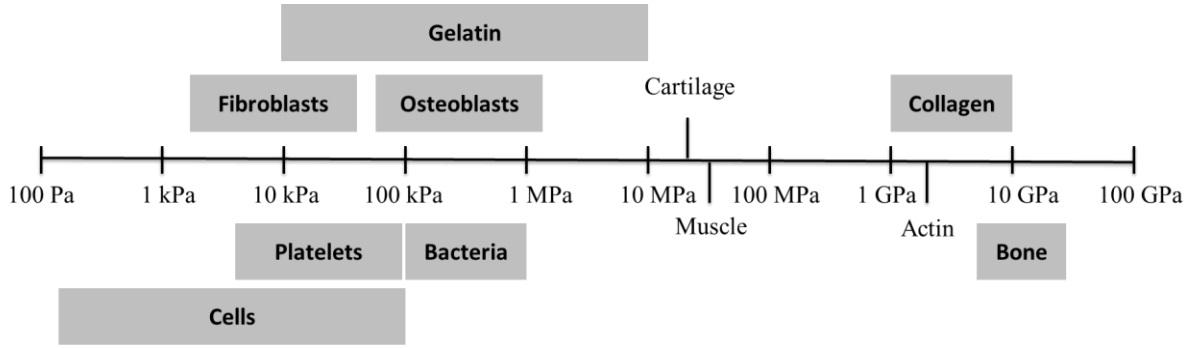

Figure 2.17 Overview of Young's modulus of different biological samples, from very stiff materials such as bone to very compliant materials, such as cells (Alonso and Goldmann, 2003, Docheva *et al*., 2008, Berquand, 2011).

Bruker (Nano Surfaces Division, Santa Barbara, USA) has provided a list of recommended probes for PeakForce QNM measurements for different ranges of expected elastic modulus values as shown in Table 2.2.

Table 2.2 Recommended probes for different ranges of expected elastic modulus.

Sample Modulus (E)	Probe	Nominal Spring Constant (k)
0.7 MPa < E < 20 MPa	SNL – A	0.5 N/m
5 MPa < E < 500 MPa	Tap150A	5 N/m
200 MPa < E < 2000 MPa	RTESPA	40 N/m
1 GPa < E < 20 GPa	Tap525A	200 N/m
10 GPa < E < 100 GPa	DNISP - HS	350 N/m

Therefore, PeakForce QNM provides quantitative modulus results over the range of 700kPa to 70 GPa once the appropriate probe is selected and calibrated (Pittenger *et al*., 2010).

In order to test small biological structure at high resolution (~nm), the appropriate AFM probes need to be selected. The mapping resolution highly depends on the size of tips that only the smaller tips resolve smaller topographic features without influence from

neighbouring structure. Thus, it is rational to use tips with nanometre radius for imaging various tissue ECM components (i.e., collagen and elastin), cells and even proteins. However, the sharp tips can cause excessive indentation or even penetrate the soft tissues, resulting in invalid measurement and sample/tip damage. In addition, the AFM mechanical measurement associates with the tip shape and the contact model (Hertz/DMT (spherical or Sneddon (conical)), see section 2.6.3.2) (Pittenger *et al*., 2014). Hence, the majority of AFM mechanical studies used blunt and spherical tips with Hertz model (see Chapter 5, Table 5.4). Although blunt probes can minimise the applied pressure on the sample and prevent the tip and sample from damage, the validity and resolution of mechanical mapping would be dramatically lost. In order to improve the valid resolution of mechanical mapping, PeakForce QNM permits ultra-low force control (pN ~ nN) of the applied force on the tip, resulting in the usage of sharp tips (Young *et al*., 2011). Moreover, PeakForce QNM equipped with the ScanaAsyst technique that automatically adjust all critical imaging parameters (i.e., gain, setpoint and scan speed), which optimises the high resolution nanomechanical mapping especially for soft biological samples testing. For PeakFocce QNM, Bruker also provides a list of recommended probes with different spring constants depending on the stiffness of the sample (Kaemmer, 2011).

2.6.3.3.3 Application of PeakForce QNM for biological samples

PeakForce QNM enables direct extraction of quantitative nanomechanical information from biological samples in real time, which is accomplished through controlling the force on the probe and generating force curves each time the AFM tip on the delicate biological samples and tissues in ambient or fluid environments. PeakForce QNM, unlike those conventional mechanical testing techniques, is a particularly appropriate method to determine the

mechanical properties of nanometre-sized biological structures due to the following advantages (Dokukin and Sokolov, 2012, Pittenger *et al*., 2010, Pittenger *et al*., 2014):

a. Analysis of force curves are done simultaneously with topographical mapping that PeakForce QNM provides multiple mechanical properties that have the same resolution as the height image (nanoscale);
b. As the force on the tip is controlled, the sample deformation depths are limited to a few nanometers, which avoids large tip-sample contact areas and profoundly increases the scanning resolution;
c. PeakForce QNM provides direct control or automatic adjustment of the maximum normal force of the sample and eliminates the lateral forces, which not only protect both the tip and sample but also ensure real-time scanning and optimising on soft samples;
d. Since the measurable range of mechanical properties is highly dependent on the properties of the probes, PeakForce QNM covers a comprehensive range of materials.

In recent years, PeakForce QNM, as a novel high spatial resolution and multifunctional research technique, has been extensively used to probe a variety of biological samples. PeakForce QNM has realised quantitative imaging of living biological specimens and cells under physiological conditions. For instance, nanomechanical imaging has been conducted on living diatoms (Pletikapić *et al*., 2012) and E. coli (Berquand, 2011) using PeakForce QNM. More importantly, this technology has also been utilised for monitoring cell dynamics involving the rearrangement of their cytoskeleton scaffold and spreading and migrating (Berquand *et al*., 2010). Also, the signalling pathways among cells and the corresponding changes in cell properties can be investigated for a better understanding of the cell deaths and the process of cancer (Berquand, 2011).

To date, some tissues and small-scale samples, in particular, and their disease-related changes have been quantitatively qualified using PeakForce QNM. For example, the mechanical property of human erythrocytes (red blood cells) has been proved to associate with Alzheimer (Bester *et al*., 2013) and Parkinson (Pretorius *et al*., 2014) diseases. Liu *et al*. explored the implication of hierarchical intrafibrillar mineralisation within a collagen fibril at the molecular and nanoscale levels (Liu *et al*., 2013). Anura *et al*. studied nanomechanical and structural changes in the oral mucosa under fibrotic pre-cancer conditions using PeakForce QNM and they indicated the relation between the sub-epithelial ECM stiffening and remodelling which can be the potential causes of oral pre-cancer progression (Anura *et al*., 2017). Furthermore, in recent years, PeakForce QNM is increasingly believed to be effective to explore structural changes and related mechanical attributes of various tissue components. For example, using PeakForce QNM, Papi *et al*. (Papi *et al*., 2014) studied the regional variations in the structural properties of porcine sclera and found a direct correlation between collagen fibril size and elastic modulus. Sweers *et al*. (Sweers *et al*., 2011) determined the nanomechanical properties of α-synuclein amyloid fibrils that is only approximately 10 nm diameter and lengths ranging from 100 nm to several microns. Eghiaian *et al*. (Eghiaian *et al*., 2015) investigated the fine structure of the actin cortex and characterised the actin dynamics in living fibroblasts.

2.6.3.3.4 Nanoscale imaging and mechanical characterisation and its application to biomedicine

AFM imaging directly observes biological specimens at work in buffer solution with excellent signal-to-noise ratio, providing a unique tool to understand the relationship between their structure and function. In addition, AFM enables the simultaneous probing of the structure and specific biological, chemical and physical properties of the cells and even

proteins. Therefore, over the past 10 years, the nanoscale structural and mechanical characterisation of AFM has been extensively used to biomedicine. For example, osteoarthritis, a type of common joint diseases among older people, has been found to occurs from the molecular level to the higher levels of the tissue architecture and leads to progressive degeneration and dysfunctions of articular cartilage. Stolz *et al*. (Stolz *et al*., 2009) have proved the utility of AFM for characterising the nanoscale morphological and biomechanical changes occurring in articular cartilage during ageing and osteoarthritis. Their study demonstrated the AFM as a simple nanodevice can be potentially used in clinic, allowing for direct arthroscopic inspection, quality control of the articular cartilage repair and early detection of ageing cartilage and osteoarthritis. Furthermore, AFM force spectroscopy has been shown as a promising tool of monitoring the changes in elasticity on incubation of the cells with drugs, such as the effects of various drugs on actin or microtubule networks that affects the elasticity of cells (Rotsch & Radmacher, 2000), as well as the nanomechanical analyses of cancer cells. Therefore, AFM driven nanometre level imaging and mechanical characterisation have opened new avenues for medical diagnostics and biomedicine.

2.7 Summary

In summary, the literature review, encompassing a wide range of disciplines, presents an overview of information that is relevant to this thesis. The author has introduced the importance of studying the arterial stiffening and summarised the current understanding in various changes with arterial stiffening. Importantly, the multiscale *in vitro* biomechanical testing methods have been highlighted to address the significance to develop the AFM for characterisation of biological tissues and structures. In particular, the author has described the principle and advantages of PeakForce QNM method for biological studies. Throughout the thesis, the author will utilise PeakForce QNM in probing small-scale biological structures and

for characterising alterations in arterial stiffening.

References

ABUBAKAR, I., TILLMANN, T. & BANERJEE, A. 2015. Global, regional, and national age-sex specific all-cause and cause-specific mortality for 240 causes of death, 1990-2013: a systematic analysis for the Global Burden of Disease Study 2013. *Lancet,* 385**,** 117-171.

ADAMCIK, J. & MEZZENGA, R. 2012. Study of amyloid fibrils via atomic force microscopy. *Current opinion in colloid & interface science,* 17**,** 369-376.

AKHTAR, R. 2014. In vitro characterisation of arterial stiffening: From the macro-to the nano-scale. *Artery Research,* 8**,** 1-8.

AKHTAR, R., SCHWARZER, N., SHERRATT, M., WATSON, R., GRAHAM, H., TRAFFORD, A., MUMMERY, P. & DERBY, B. 2009. Nanoindentation of histological specimens: mapping the elastic properties of soft tissues. *Journal of materials research*, 24, 638-646.

AKHTAR, R., SHERRATT, M. J., CRUICKSHANK, J. K. & DERBY, B. 2011. Characterizing the elastic properties of tissues. *Materials Today,* 14, 96-105.

AKYILDIZ, A. C., SPEELMAN, L. & GIJSEN, F. J. 2014. Mechanical properties of human atherosclerotic intima tissue. *Journal of biomechanics*, 47, 773-783.

ALONSO, J. L. & GOLDMANN, W. H. 2003. Feeling the forces: atomic force microscopy in cell biology. *Life sciences,* 72, 2553-2560.

AMBROSE, J. A. & BARUA, R. S. 2004. The pathophysiology of cigarette smoking and cardiovascular disease: an update. *Journal of the American college of cardiology,* 43**,** 1731-1737.

ANURA, A., DAS, D., PAL, M., PAUL, R. R., DAS, S. & CHATTERJEE, J. 2017. Nanomechanical signatures of oral submucous fibrosis in sub-epithelial connective tissue. *Journal of the mechanical behavior of biomedical materials,* 65**,** 705-715.

BARALLOBRE-BARREIRO, J., DIDANGELOS, A., SCHOENDUBE, F. A., DROZDOV, I., YIN, X., FERNáNDEZ-CAGGIANO, M., WILLEIT, P., PUNTMANN, V. O., ALDAMA-LóPEZ, G. & SHAH, A. M. 2012. Proteomics analysis of cardiac extracellular matrix remodeling in a porcine model of ischemia-reperfusion injury. *Circulation***,** CIRCULATIONAHA. 111.056952.

BAUER, R. D., BUSSE, R. & SCHABERT, A. 1982. Mechanical properties of arteries. *Biorheology,* 19**,** 409-424.

BERILLIS, P. 2013. The role of collagen in the aorta's structure. *The open circulation and vascular journal,* 6.

BERQUAND, A. 2011. Quantitative imaging of living biological samples by PeakForce QNM atomic force microscopy. *Bruker Application Note,* 135**,** 1-10.

BERQUAND, A., RODUIT, C., KASAS, S., HOLLOSCHI, A., PONCE, L. & HAFNER, M. 2010. Atomic force microscopy imaging of living cells. *Microscopy Today,* 18**,** 8-14.

BESTER, J., BUYS, A., LIPINSKI, B., KELL, D. B. & PRETORIUS, E. 2013. High ferritin levels have major effects on the morphology of erythrocytes in Alzheimer's disease. *Frontiers in aging neuroscience,* 5**,** 88.

BLACHER, J., ASMAR, R., DJANE, S., LONDON, G. M. & SAFAR, M. E. 1999. Aortic pulse wave velocity as a marker of cardiovascular risk in hypertensive patients. *Hypertension,* 33**,** 1111-1117.

BLOOM, D. E., CAFIERO, E., JANé-LLOPIS, E., ABRAHAMS-GESSEL, S., BLOOM, L. R., FATHIMA, S., FEIGL, A. B., GAZIANO, T., HAMANDI, A. & MOWAFI, M.

2012. The global economic burden of noncommunicable diseases. Program on the Global Demography of Aging.

BONNEMA, D. D., WEBB, C. S., PENNINGTON, W. R., STROUD, R. E., LEONARDI, A. E., CLARK, L. L., MCCLURE, C. D., FINKLEA, L., SPINALE, F. G. & ZILE, M. R. 2007. Effects of age on plasma matrix metalloproteinases (MMPs) and tissue inhibitor of metalloproteinases (TIMPs). *Journal of cardiac failure,* 13**,** 530-540.

BOROVIC, M. L., BOROVIC, S., PERIC, M., VUKOVIC, P., MARINKOVIC, J., TODOROVIC, V., RADAK, D. & LAČKOVIC, V. 2010. The internal thoracic artery as a transitional type of artery: a morphological and morphometric study. *Histology and histopathology,* 25**,** 561.

BROOKE, B. S., BAYES-GENIS, A. & LI, D. Y. 2003. New insights into elastin and vascular disease. *Trends in cardiovascular medicine,* 13**,** 176-181.

BURNHAM, N. A. & COLTON, R. J. 1989. Measuring the nanomechanical properties and surface forces of materials using an atomic force microscope. *Journal of Vacuum Science & Technology A: Vacuum, Surfaces, and Films,* 7**,** 2906-2913.

CALAFIORE, A., WELTERT, L., MAURO, M., ACTIS-DATO, G., IACò, A., CENTOFANTI, P., TORRE, M. & PATANè, F. 2005. Internal mammary artery. *Multimedia manual of cardiothoracic surgery: MMCTS,* 2005**,** mmcts. 2004.001008.

CALIFANO, J. P. & REINHART-KING, C. A. 2010. Exogenous and endogenous force regulation of endothelial cell behavior. *Journal of biomechanics,* 43**,** 79-86.

CALZADO-MARTíN, A., ENCINAR, M., TAMAYO, J., CALLEJA, M. & SAN PAULO, A. 2016. Effect of actin organization on the stiffness of living breast cancer cells revealed by peak-force modulation atomic force microscopy. *ACS nano,* 10**,** 3365-3374.

CANHAM, P. B., FINLAY, H. M. & BOUGHNER, D. R. 1997. Contrasting structure of the saphenous vein and internal mammary artery used as coronary bypass vessels. *Cardiovascular research,* 34**,** 557-567.

CARPICK, R. W., OGLETREE, D. F. & SALMERON, M. 1999. A general equation for fitting contact area and friction vs load measurements. *Journal of colloid and interface science,* 211**,** 395-400.

CECELJA, M. & CHOWIENCZYK, P. 2012. Role of arterial stiffness in cardiovascular disease. *JRSM cardiovascular disease,* 1**,** 1-10.

CHEN, S. & BIRK, D. E. 2013. The regulatory roles of small leucine-rich proteoglycans in extracellular matrix assembly. *The FEBS journal,* 280**,** 2120-2137.

CHRISTIANSEN, D. L., HUANG, E. K. & SILVER, F. H. 2000. Assembly of type I collagen: fusion of fibril subunits and the influence of fibril diameter on mechanical properties. *Matrix Biology,* 19**,** 409-420.

COLLABORATION, R. V. F. A. S. 2010. Determinants of pulse wave velocity in healthy people and in the presence of cardiovascular risk factors:'establishing normal and reference values'. *European heart journal,* 31**,** 2338-2350.

COWIN, S. C. & HUMPHREY, J. D. 2001. *Cardiovascular soft tissue mechanics*, Springer.

CRUICKSHANK, K., RISTE, L., ANDERSON, S. G., WRIGHT, J. S., DUNN, G. & GOSLING, R. G. 2002. Aortic pulse-wave velocity and its relationship to mortality in diabetes and glucose intolerance: an integrated index of vascular function? *Circulation,* 106**,** 2085-2090.

DANIELSON, K. G., BARIBAULT, H., HOLMES, D. F., GRAHAM, H., KADLER, K. E. & IOZZO, R. V. 1997. Targeted disruption of decorin leads to abnormal collagen fibril morphology and skin fragility. *The Journal of cell biology,* 136**,** 729-743.

DERBY, B. & AKHTAR, R. 2015. *Mechanical Properties of Aging Soft Tissues*, Springer.

DERJAGUIN, B. V., MULLER, V. M. & TOPOROV, Y. P. 1975. Effect of contact deformations on the adhesion of particles. *Journal of Colloid and interface science,* 53**,** 314-326.

DOCHEVA, D., PADULA, D., POPOV, C., MUTSCHLER, W., CLAUSEN-SCHAUMANN, H. & SCHIEKER, M. 2008. Researching into the cellular shape, volume and elasticity of mesenchymal stem cells, osteoblasts and osteosarcoma cells by atomic force microscopy. *Journal of cellular and molecular medicine,* 12**,** 537-552.

DOKUKIN, M. E. & SOKOLOV, I. 2012. Quantitative mapping of the elastic modulus of soft materials with HarmoniX and PeakForce QNM AFM modes. *Langmuir,* 28**,** 16060-16071.

DUPREY, A., KHANAFER, K., SCHLICHT, M., AVRIL, S., WILLIAMS, D. & BERGUER, R. 2010. In vitro characterisation of physiological and maximum elastic modulus of ascending thoracic aortic aneurysms using uniaxial tensile testing. *European Journal of Vascular and Endovascular Surgery,* 39**,** 700-707.

DUPUIS, L. E. & KERN, C. B. 2014. Small leucine-rich proteoglycans exhibit unique spatiotemporal expression profiles during cardiac valve development. *Developmental Dynamics,* 243**,** 601-611.

EATON, P. & WEST, P. 2010. *Atomic force microscopy*, Oxford University Press.

EBENSTEIN, D. & PRUITT, L. 2004. Nanoindentation of soft hydrated materials for application to vascular tissues. *Journal of Biomedical Materials Research Part A,* 69**,** 222-232.

EBENSTEIN, D. M., COUGHLIN, D., CHAPMAN, J., LI, C. & PRUITT, L. A. 2009. Nanomechanical properties of calcification, fibrous tissue, and hematoma from atherosclerotic plaques. *Journal of biomedical materials research Part A,* 91**,** 1028-1037.

EBENSTEIN, D. M. & PRUITT, L. A. 2006. Nanoindentation of biological materials. *Nano Today,* 1**,** 26-33.

EGHIAIAN, F., RIGATO, A. & SCHEURING, S. 2015. Structural, mechanical, and dynamical variability of the actin cortex in living cells. *Biophysical journal,* 108**,** 1330-1340.

ELLIOTT, R. & MCGRATH, L. 1994. Calcification of the human thoracic aorta during aging. *Calcified tissue international,* 54**,** 268-273.

ERGUL, A., PORTIK-DOBOS, V., HUTCHINSON, J., FRANCO, J. & ANSTADT, M. P. 2004. Downregulation of vascular matrix metalloproteinase inducer and activator proteins in hypertensive patients. *American Journal of Hypertension,* 17**,** 775-782.

EYRE, D. R. & WU, J.-J. 2005. Collagen cross-links. *Collagen.* Springer.

FANG, M., GOLDSTEIN, E. L., TURNER, A. S., LES, C. M., ORR, B. G., FISHER, G. J., WELCH, K. B., ROTHMAN, E. D. & BANASZAK HOLL, M. M. 2012. Type I collagen D-spacing in fibril bundles of dermis, tendon, and bone: bridging between nano-and micro-level tissue hierarchy. *ACS nano,* 6**,** 9503-9514.

FAURY, G., MAHER, G. M., LI, D. Y., KEATING, M. T., MECHAM, R. P. & BOYLE, W. A. 1999. Relation between outer and luminal diameter in cannulated arteries. *American Journal of Physiology-Heart and Circulatory Physiology,* 277**,** H1745-H1753.

FERNáNDEZ, B., KAMPMANN, A., PIPP, F., ZIMMERMANN, R. & SCHAPER, W. 2003. Osteoglycin expression and localization in rabbit tissues and atherosclerotic plaques. *Vascular Biochemistry.* Springer.

FINLAY, H. M., WHITTAKER, P. & CANHAM, P. B. 1998. Collagen organization in the branching region of human brain arteries. *Stroke,* 29**,** 1595-1601.

FISCHER-CRIPPS, A. C. 2011. Factors affecting nanoindentation test data. *Nanoindentation.* Springer.

FLEENOR, B. S., MARSHALL, K. D., DURRANT, J. R., LESNIEWSKI, L. A. & SEALS, D. R. 2010. Arterial stiffening with ageing is associated with transforming growth factor-β1-related changes in adventitial collagen: reversal by aerobic exercise. *The Journal of physiology,* 588**,** 3971-3982.

FONCK, E., FEIGL, G. G., FASEL, J., SAGE, D., UNSER, M., RüFENACHT, D. A. & STERGIOPULOS, N. 2009. Effect of aging on elastin functionality in human cerebral arteries. *Stroke,* 40**,** 2552-2556.

FRATZL, P. 2008. Collagen: structure and mechanics, an introduction. Collagen. Springer.

GAILLARD, V., CASELLAS, D., SEGUIN-DEVAUX, C., SCHOHN, H., DAUçA, M., ATKINSON, J. & LARTAUD, I. 2005. Pioglitazone improves aortic wall elasticity in a rat model of elastocalcinotic arteriosclerosis. *Hypertension,* 46**,** 372-379.

GARCıA, R. & PEREZ, R. 2002. Dynamic atomic force microscopy methods. *Surface science reports,* 47**,** 197-301.

GASSER, T. C., OGDEN, R. W. & HOLZAPFEL, G. A. 2006. Hyperelastic modelling of arterial layers with distributed collagen fibre orientations. *Journal of the royal society interface,* 3**,** 15-35.

GE, J., CUI, F.-Z., WANG, X. & WANG, Y. 2007. New evidence of surface mineralization of collagen fibrils in wild type zebrafish skeleton by AFM and TEM. *Materials Science and Engineering: C,* 27**,** 46-50.

GE, J., WANG, X. & CUI, F. 2006. Microstructural characteristics and nanomechanical properties across the thickness of the wild-type zebrafish skeletal bone. *Materials Science and Engineering: C,* 26**,** 710-715.

GEEST, J. P. V., SACKS, M. S. & VORP, D. A. 2004. Age dependency of the biaxial biomechanical behavior of human abdominal aorta. *Journal of biomechanical engineering,* 126**,** 815-822.

GRAHAM, H. K., HODSON, N. W., HOYLAND, J. A., MILLWARD-SADLER, S. J., GARROD, D., SCOTHERN, A., GRIFFITHS, C. E., WATSON, R. E., COX, T. R. & ERLER, J. T. 2010. Tissue section AFM: In situ ultrastructural imaging of native biomolecules. *Matrix Biology,* 29**,** 254-260.

GRANT, C. A., PHILLIPS, M. A. & THOMSON, N. H. 2012. Dynamic mechanical analysis of collagen fibrils at the nanoscale. *Journal of the mechanical behavior of biomedical materials,* 5**,** 165-170.

GRANT, C. A. & TWIGG, P. C. 2012. Pseudostatic and dynamic nanomechanics of the tunica adventitia in elastic arteries using atomic force microscopy. *ACS nano,* 7**,** 456-464.

GREENWALD, S. 2007. Ageing of the conduit arteries. *The Journal of pathology,* 211**,** 157-172.

GREENWALD, S., MOORE, J., RACHEV, A., KANE, T. & MEISTER, J.-J. 1997. Experimental investigation of the distribution of residual strains in the artery wall. *Journal of biomechanical engineering,* 119**,** 438-444.

HAYENGA, H., TRACHE, A., TRZECIAKOWSKI, J. & HUMPHREY, J. 2011. Regional atherosclerotic plaque properties in ApoE–/–mice quantified by atomic force, immunofluorescence, and light microscopy. *Journal of vascular research,* 48**,** 495-504.

HEMMASIZADEH, A., AUTIERI, M. & DARVISH, K. 2012. Multilayer material properties of aorta determined from nanoindentation tests. *Journal of the mechanical behavior of biomedical materials,* 15**,** 199-207.

HEMMASIZADEH, A., TSAMIS, A., CHEHELTANI, R., ASSARI, S., D'AMORE, A., AUTIERI, M., KIANI, M. F., PLESHKO, N., WAGNER, W. R. & WATKINS, S. C. 2015. Correlations between transmural mechanical and morphological properties in porcine thoracic descending aorta. *journal of the mechanical behavior of biomedical materials,* 47**,** 12-20.

HERTZ, H. 1881. On the contact of elastic solids. *Z. Reine Angew. Mathematik,* 92**,** 156-171.

HOLZAPFEL, G. A., GASSER, T. C. & OGDEN, R. W. 2000. A new constitutive framework for arterial wall mechanics and a comparative study of material models. *Journal of elasticity and the physical science of solids,* 61**,** 1-48.

HOLZAPFEL, G. A., GASSER, T. C. & STADLER, M. 2002. A structural model for the viscoelastic behavior of arterial walls: continuum formulation and finite element analysis. *European Journal of Mechanics-A/Solids,* 21**,** 441-463.

HOLZAPFEL, G. A., SOMMER, G., GASSER, C. T. & REGITNIG, P. 2005. Determination of layer-specific mechanical properties of human coronary arteries with nonatherosclerotic intimal thickening and related constitutive modeling. *American Journal of Physiology-Heart and Circulatory Physiology,* 289**,** H2048-H2058.

HUYNH, J., NISHIMURA, N., RANA, K., PELOQUIN, J. M., CALIFANO, J. P., MONTAGUE, C. R., KING, M. R., SCHAFFER, C. B. & REINHART-KING, C. A. 2011. Age-related intimal stiffening enhances endothelial permeability and leukocyte transmigration. *Science translational medicine,* 3**,** 112-122.

HWANG, J.-Y., JOHNSON, P. Y., BRAUN, K. R., HINEK, A., FISCHER, J. W., O'BRIEN, K. D., STARCHER, B., CLOWES, A. W., MERRILEES, M. J. & WIGHT, T. N. 2008. Retrovirally mediated overexpression of glycosaminoglycan-deficient biglycan in arterial smooth muscle cells induces tropoelastin synthesis and elastic fiber

formation in vitro and in neointimae after vascular injury. *The American journal of pathology,* 173**,** 1919-1928.

IOZZO, R. V. 1998. Matrix proteoglycans: from molecular design to cellular function. Annual Reviews 4139 El Camino Way, PO Box 10139, Palo Alto, CA 94303-0139, USA.

ISENBERG, B. C. & WONG, J. Y. 2006. Building structure into engineered tissues. *Materials Today,* 9**,** 54-60.

ITO, S., ISHIMARU, S. & WILSON, S. E. 1998. Effect of coacervated α-elastin on proliferation of vascular smooth muscle and endothelial cells. *Angiology,* 49**,** 289-297.

IZZO JR, J. L. & SHYKOFF, B. E. 2001. Arterial stiffness: clinical relevance, measurement, and treatment. *Rev Cardiovasc Med,* 2**,** 29-40.

JACOBSON, A. S., SMITH, M. & URKEN, M. L. 2013. Internal mammary artery and vein as recipient vessels in head and neck reconstruction. *JAMA Otolaryngology–Head & Neck Surgery,* 139**,** 623-628.

JOHNSON, K. 1982. One hundred years of Hertz contact. *Proceedings of the Institution of Mechanical Engineers,* 196**,** 363-378.

JOHNSON, K., KENDALL, K. & ROBERTS, A. Surface energy and the contact of elastic solids. Proc. R. Soc. Lond. A, 1971. The Royal Society, 301-313.

KADLER, K. E., HOLMES, D. F., TROTTER, J. A. & CHAPMAN, J. A. 1996. Collagen fibril formation. *Biochemical Journal,* 316**,** 1-11.

KAEMMER, S. 2011. Application Note 133: Introduction to Bruker's ScanAsyst and PeakForce Tapping AFM Technology. Bruker Nano Surfaces Division, Santa Barbara.

KAESS, B. M., RONG, J., LARSON, M. G., HAMBURG, N. M., VITA, J. A., LEVY, D., BENJAMIN, E. J., VASAN, R. S. & MITCHELL, G. F. 2012. Aortic stiffness, blood pressure progression, and incident hypertension. *Jama,* 308**,** 875-881.

KALAMAJSKI, S. & OLDBERG, Å. 2010. The role of small leucine-rich proteoglycans in collagen fibrillogenesis. *Matrix Biology,* 29**,** 248-253.

KAMPMANN, A., FERNáNDEZ, B., DEINDL, E., KUBIN, T., PIPP, F., EITENMüLLER, I., HOEFER, I. E., SCHAPER, W. & ZIMMERMANN, R. 2009. The proteoglycan osteoglycin/mimecan is correlated with arteriogenesis. *Molecular and cellular biochemistry,* 322**,** 15-23.

KARIMI, A., NAVIDBAKHSH, M., SHOJAEI, A. & FAGHIHI, S. 2013. Measurement of the uniaxial mechanical properties of healthy and atherosclerotic human coronary arteries. *Materials Science and Engineering: C,* 33**,** 2550-2554.

KOHN, J. C., LAMPI, M. C. & REINHART-KING, C. A. 2015. Age-related vascular stiffening: causes and consequences. *Frontiers in genetics,* 6**,** 112.

LACOLLEY, P., REGNAULT, V., SEGERS, P. & LAURENT, S. 2017. Vascular Smooth Muscle Cells and Arterial Stiffening: Relevance in Development, Aging, and Disease. *Physiological reviews,* 97**,** 1555-1617.

LAURENT, S., COCKCROFT, J., VAN BORTEL, L., BOUTOUYRIE, P., GIANNATTASIO, C., HAYOZ, D., PANNIER, B., VLACHOPOULOS, C., WILKINSON, I. & STRUIJKER-BOUDIER, H. 2006. Expert consensus document on arterial stiffness: methodological issues and clinical applications. *European heart journal,* 27**,** 2588-2605.

LI, D. Y., BROOKE, B., DAVIS, E. C., MECHAM, R. P., SORENSEN, L. K., BOAK, B. B., EICHWALD, E. & KEATING, M. T. 1998. Elastin is an essential determinant of arterial morphogenesis. *Nature,* 393**,** 276.

LIU, Y., LUO, D., KOU, X. X., WANG, X. D., TAY, F. R., SHA, Y. L., GAN, Y. H. & ZHOU, Y. H. 2013. Hierarchical intrafibrillar nanocarbonated apatite assembly

improves the nanomechanics and cytocompatibility of mineralized collagen. *Advanced Functional Materials,* 23**,** 1404-1411.

MAHAFFY, R., PARK, S., GERDE, E., KäS, J. & SHIH, C. 2004. Quantitative analysis of the viscoelastic properties of thin regions of fibroblasts using atomic force microscopy. *Biophysical journal,* 86**,** 1777-1793.

MAHAFFY, R., SHIH, C., MACKINTOSH, F. & KäS, J. 2000. Scanning probe-based frequency-dependent microrheology of polymer gels and biological cells. *Physical review letters,* 85**,** 880.

MAHAMID, J., SHARIR, A., ADDADI, L. & WEINER, S. 2008. Amorphous calcium phosphate is a major component of the forming fin bones of zebrafish: Indications for an amorphous precursor phase. *Proceedings of the National Academy of Sciences,* 105**,** 12748-12753.

MAIVALD, P., BUTT, H., GOULD, S., PRATER, C., DRAKE, B., GURLEY, J., ELINGS, V. & HANSMA, P. 1991. Using force modulation to image surface elasticities with the atomic force microscope. *Nanotechnology,* 2**,** 103.

MAO, Y., SUN, Q., WANG, X., OUYANG, Q., HAN, L., JIANG, L. & HAN, D. 2009. In vivo nanomechanical imaging of blood-vessel tissues directly in living mammals using atomic force microscopy. *Applied Physics Letters,* 95**,** 013704.

MCNULTY, M., SPIERS, P., MCGOVERN, E. & FEELY, J. 2005. Aging is associated with increased matrix metalloproteinase-2 activity in the human aorta. *American journal of hypertension,* 18**,** 504-509.

MECHAM, R. P. & BIRK, D. E. 2013. *Extracellular matrix assembly and structure*, Academic Press.

MEGENS, R., REITSMA, S., SCHIFFERS, P., HILGERS, R., DE MEY, J., SLAAF, D., OUDE EGBRINK, M. & VAN ZANDVOORT, M. 2007. Two-photon microscopy of vital murine elastic and muscular arteries. *Journal of vascular research,* 44**,** 87-98.

MENDIS, S. & CHESTNOV, O. 2014. The global burden of cardiovascular diseases: a challenge to improve. *Current cardiology reports,* 16**,** 486.

MENDIS, S., PUSKA, P., NORRVING, B. & ORGANIZATION, W. H. 2011. *Global atlas on cardiovascular disease prevention and control*, Geneva: World Health Organization.

NAKAJIMA, K., ITO, M., WANG, D., LIU, H., NGUYEN, H. K., LIANG, X., KUMAGAI, A. & FUJINAMI, S. 2014. Nano-palpation AFM and its quantitative mechanical property mapping. *Journal of Electron Microscopy,* 63**,** 193-208.

NAKAMURA, K., SHIMIZU, J., KATAOKA, N., HASHIMOTO, K., IKEDA, T., FUJIO, H., OHTA-OGO, K., OGAWA, A., MIURA, A. & MOHRI, S. 2010. Altered nano/micro-order elasticity of pulmonary artery smooth muscle cells of patients with idiopathic pulmonary arterial hypertension. *International journal of cardiology,* 140**,** 102-107.

NEWMAN, D. & GREENWALD, S. 1978. Validity of the Moens-Korteweg equation. *The Arterial System.* Springer.

NICHOLS, M., TOWNSEND, N., SCARBOROUGH, P. & RAYNER, M. 2014. Cardiovascular disease in Europe 2014: epidemiological update. *European heart journal,* 35**,** 2950-2959.

NORTH, B. J. & SINCLAIR, D. A. 2012. The intersection between aging and cardiovascular disease. *Circulation research,* 110**,** 1097-1108.

O'CONNELL, M. K., MURTHY, S., PHAN, S., XU, C., BUCHANAN, J., SPILKER, R., DALMAN, R. L., ZARINS, C. K., DENK, W. & TAYLOR, C. A. 2008. The three-

dimensional micro-and nanostructure of the aortic medial lamellar unit measured using 3D confocal and electron microscopy imaging. *Matrix Biology,* 27**,** 171-181.

OLIVER, W. C. & PHARR, G. M. 1992. An improved technique for determining hardness and elastic modulus using load and displacement sensing indentation experiments. *Journal of materials research,* 7**,** 1564-1583.

OLIVER, W. C. & PHARR, G. M. 2004. Measurement of hardness and elastic modulus by instrumented indentation: Advances in understanding and refinements to methodology. *Journal of materials research,* 19**,** 3-20.

ONDA, M., ISHIWATA, T., KAWAHARA, K., WANG, R., NAITO, Z. & SUGISAKI, Y. 2002. Expression of lumican in thickened intima and smooth muscle cells in human coronary atherosclerosis. *Experimental and molecular pathology,* 72**,** 142-149.

ORGEL, J. P., IRVING, T. C., MILLER, A. & WESS, T. J. 2006. Microfibrillar structure of type I collagen in situ. *Proceedings of the National Academy of Sciences,* 103**,** 9001-9005.

OTTO, C. M., LIND, B. K., KITZMAN, D. W., GERSH, B. J. & SISCOVICK, D. S. 1999. Association of aortic-valve sclerosis with cardiovascular mortality and morbidity in the elderly. *New England Journal of Medicine,* 341**,** 142-147.

PANDIT, A., LU, X., WANG, C. & KASSAB, G. S. 2005. Biaxial elastic material properties of porcine coronary media and adventitia. *American Journal of Physiology-Heart and Circulatory Physiology,* 288**,** H2581-H2587.

PAPI, M., PAOLETTI, P., GERAGHTY, B. & AKHTAR, R. 2014. Nanoscale characterization of the biomechanical properties of collagen fibrils in the sclera. *Applied Physics Letters,* 104**,** 103703.

PARRY, D. A. 1988. The molecular fibrillar structure of collagen and its relationship to the mechanical properties of connective tissue. *Biophysical chemistry,* 29**,** 195-209.

PETRUSKA, J. A. & HODGE, A. J. 1964. A subunit model for the tropocollagen macromolecule. *Proceedings of the National Academy of Sciences,* 51**,** 871-876.

PITTENGER, B., ERINA, N. & SU, C. 2010. Quantitative mechanical property mapping at the nanoscale with PeakForce QNM. *Application Note Veeco Instruments Inc***,** 1-12.

PITTENGER, B., ERINA, N. & SU, C. 2014. Mechanical property mapping at the nanoscale using PeakForce QNM scanning probe technique. *Nanomechanical analysis of high performance materials.* Springer.

PLETIKAPIĆ, G., BERQUAND, A., RADIĆ, T. M. & SVETLIČIĆ, V. 2012. Quantitative nanomechanical mapping of marine diatom in seawater using peak force tapping atomic force microscopy. *Journal of phycology,* 48**,** 174-185.

PODOLEC, P., KOPEĆ, G., PODOLEC, J., WILKOŁEK, P., KROCHIN, M., RUBIŚ, P., CWYNAR, M., GRODZICKI, T., ŻMUDKA, K. & TRACZ, W. 2007. Aortic pulse wave velocity and carotid-femoral pulse wave velocity: similarities and discrepancies. *Hypertension Research,* 30**,** 1151.

PRASAD, A., BEKKER, P. & TSIMIKAS, S. 2012. Advanced glycation end products and diabetic cardiovascular disease. *Cardiology in review,* 20**,** 177-183.

PRETORIUS, E., SWANEPOEL, A. C., BUYS, A. V., VERMEULEN, N., DUIM, W. & KELL, D. B. 2014. Eryptosis as a marker of Parkinson's disease. *Aging (Albany NY),* 6**,** 788.

QIU, H., ZHU, Y., SUN, Z., TRZECIAKOWSKI, J. P., GANSNER, M., DEPRE, C., RESUELLO, R. R., NATIVIDAD, F. F., HUNTER, W. C. & GENIN, G. M. 2010. Vascular smooth muscle cell stiffness as a mechanism for increased aortic stiffness with agingnovelty and significance. *Circulation research,* 107**,** 615-619.

RAINES, E. W. 2000. The extracellular matrix can regulate vascular cell migration, proliferation, and survival: relationships to vascular disease. *International journal of experimental pathology,* 81**,** 173-182.

RAJZER, M., KLOCEK, M. & KAWECKA-JASZCZ, K. 2003. Effect of amlodipine, quinapril, andlosartan on pulse wave velocity andplasma collagen markers in patients withmild-to-moderate arterial hypertension. *American journal of hypertension,* 16**,** 439-444.

RASPANTI, M., PROTASONI, M., MANELLI, A., GUIZZARDI, S., MANTOVANI, V. & SALA, A. 2006. The extracellular matrix of the human aortic wall: ultrastructural observations by FEG-SEM and by tapping-mode AFM. *Micron,* 37**,** 81-86.

REINBOTH, B., HANSSEN, E., CLEARY, E. G. & GIBSON, M. A. 2002. Molecular Interactions of Biglycan and Decorin with Elastic Fiber Components BIGLYCAN FORMS A TERNARY COMPLEX WITH TROPOELASTIN AND MICROFIBRIL-ASSOCIATED GLYCOPROTEIN 1. *Journal of Biological Chemistry,* 277**,** 3950-3957.

REUSZ, G. S., CSEPREKAL, O., TEMMAR, M., KIS, É., CHERIF, A. B., THALEB, A., FEKETE, A., SZABó, A. J., BENETOS, A. & SALVI, P. 2010. Reference values of pulse wave velocity in healthy children and teenagers. *Hypertension,* 56**,** 217-224.

REZAKHANIHA, R., AGIANNIOTIS, A., SCHRAUWEN, J. T. C., GRIFFA, A., SAGE, D., BOUTEN, C. V., VAN DE VOSSE, F., UNSER, M. & STERGIOPULOS, N. 2012. Experimental investigation of collagen waviness and orientation in the arterial adventitia using confocal laser scanning microscopy. *Biomechanics and modeling in mechanobiology,* 11**,** 461-473.

ROTSCH, C., & RADMACHER, M. 2000. Drug-induced changes of cytoskeletal structure and mechanics in fibroblasts: an atomic force microscopy study. Biophysical Journal, 78, 520-535.

ROBERT, L., ROBERT, A. & FüLöP, T. 2008. Rapid increase in human life expectancy: will it soon be limited by the aging of elastin, *Biogerontology*, 9, 119-133.

SAMILA, Z. J. & CARTER, S. A. 1981. The effect of age on the unfolding of elastin lamellae and collagen fibers with stretch in human carotid arteries. *Canadian journal of physiology and pharmacology,* 59**,** 1050-1057.

SAWABE, M. 2010. Vascular aging: from molecular mechanism to clinical significance. *Geriatrics & gerontology international,* 10.

SCHAEFER, L., TSALASTRA, W., BABELOVA, A., BALIOVA, M., MINNERUP, J., SOROKIN, L., GRöNE, H.-J., REINHARDT, D. P., PFEILSCHIFTER, J. & IOZZO, R. V. 2007. Decorin-mediated regulation of fibrillin-1 in the kidney involves the insulin-like growth factor-I receptor and Mammalian target of rapamycin. *The American journal of pathology,* 170**,** 301-315.

SCHLATMANN, T. J. & BECKER, A. E. 1977. Histologic changes in the normal aging aorta: implications for dissecting aortic aneurysm. *The American journal of cardiology,* 39**,** 13-20.

SCHLEICHER, E. D., WAGNER, E. & NERLICH, A. G. 1997. Increased accumulation of the glycoxidation product N (epsilon)-(carboxymethyl) lysine in human tissues in diabetes and aging. *The Journal of clinical investigation,* 99**,** 457-468.

SCHMITT, F. O., HALL, C. E. & JAKUS, M. A. 1942. Electron microscope investigations of the structure of collagen. *Journal of Cellular Physiology,* 20**,** 11-33.

SCHWARZ, U. D. 2003. A generalized analytical model for the elastic deformation of an adhesive contact between a sphere and a flat surface. *Journal of Colloid and Interface Science,* 261**,** 99-106.

SELL, D. R. & MONNIER, V. M. 2012. Molecular basis of arterial stiffening: role of glycation–a mini-review. Gerontology, 58, 227-237.

SHADWICK, R. E. 1999. Mechanical design in arteries. *Journal of Experimental Biology,* 202**,** 3305-3313.

SHEKHONIN, B. V., DOMOGATSKY, S. P., MUZYKANTOV, V. R., IDELSON, G. L. & RUKOSUEV, V. S. 1985. Distribution of type I, III, IV and V collagen in normal and atherosclerotic human arterial wall: immunomorphological characteristics. *Collagen and related research,* 5**,** 355-368.

SHERRATT, M. J. 2009. Tissue elasticity and the ageing elastic fibre. *Age,* 31**,** 305-325.

SHERRATT, M. J. 2013. Structural proteins and arterial ageing. *Artery Research,* 7**,** 15-21.

SHIRWANY, N. A. & ZOU, M.-H. 2010. Arterial stiffness: a brief review. *Acta Pharmacologica Sinica,* 31**,** 1267.

SNEDDON, I. N. 1965. The relation between load and penetration in the axisymmetric Boussinesq problem for a punch of arbitrary profile. *International journal of engineering science,* 3**,** 47-57.

SOKOLOV, I., DOKUKIN, M. E. & GUZ, N. V. 2013. Method for quantitative measurements of the elastic modulus of biological cells in AFM indentation experiments. *Methods,* 60**,** 202-213.

SOWERS, J. R., EPSTEIN, M. & FROHLICH, E. D. 2001. Diabetes, hypertension, and cardiovascular disease: an update. *Hypertension,* 37**,** 1053-1059.

STARY, H. C., BLANKENHORN, D. H., CHANDLER, A. B., GLAGOV, S., INSULL, W., RICHARDSON, M., ROSENFELD, M. E., SCHAFFER, S. A., SCHWARTZ, C. J. &

WAGNER, W. D. 1992. A definition of the intima of human arteries and of its atherosclerosis-prone regions. A report from the Committee on Vascular Lesions of the Council on Arteriosclerosis, American Heart Association. *Arteriosclerosis, Thrombosis, and Vascular Biology,* 12**,** 120-134.

STOLZ, M., GOTTARDI, R., RAITERI, R., MIOT, S., MARTIN, I., IMER, R., STAUFER, U., RADUCANU, A., DüGGELIN, M. & BASCHONG, W. 2009. Early detection of aging cartilage and osteoarthritis in mice and patient samples using atomic force microscopy. *Nature nanotechnology,* 4**,** 186.

STOLZ, M., RAITERI, R., DANIELS, A., VANLANDINGHAM, M. R., BASCHONG, W. & AEBI, U. 2004. Dynamic elastic modulus of porcine articular cartilage determined at two different levels of tissue organization by indentation-type atomic force microscopy. *Biophysical journal,* 86**,** 3269-3283.

SWEERS, K., VAN DER WERF, K., BENNINK, M. & SUBRAMANIAM, V. 2011. Nanomechanical properties of α-synuclein amyloid fibrils: a comparative study by nanoindentation, harmonic force microscopy, and Peakforce QNM. *Nanoscale research letters,* 6**,** 270.

TALUSAN, P., BEDRI, S., YANG, S., KATTAPURAM, T., SILVA, N., ROUGHLEY, P. J. & STONE, J. R. 2005. Analysis of intimal proteoglycans in atherosclerosis-prone and atherosclerosis-resistant human arteries by mass spectrometry. *Molecular & Cellular Proteomics,* 4**,** 1350-1357.

THOMPSON, R. W. & BAXTER, B. T. 1999. MMP inhibition in abdominal aortic aneurysms: rationale for a prospective randomized clinical trial. *Annals of the New York Academy of Sciences,* 878**,** 159-178.

TOWNSEND, N., NICHOLS, M., SCARBOROUGH, P. & RAYNER, M. 2015. Cardiovascular disease in Europe—epidemiological update 2015. *European heart journal,* 36**,** 2696-2705.

TOWNSEND, N., WILSON, L., BHATNAGAR, P., WICKRAMASINGHE, K., RAYNER, M. & NICHOLS, M. 2016. Cardiovascular disease in Europe: epidemiological update 2016. *European heart journal,* 37**,** 3232-3245.

TRACQUI, P., BROISAT, A., TOCZEK, J., MESNIER, N., OHAYON, J. & RIOU, L. 2011. Mapping elasticity moduli of atherosclerotic plaque in situ via atomic force microscopy. *Journal of structural biology,* 174**,** 115-123.

TSURUGA, E., IRIE, K. & YAJIMA, T. 2007. Fibrillin-2 degradation by matrix metalloproteinase-2 in periodontium. *Journal of dental research,* 86**,** 352-356.

VAN POPELE, N. M., GROBBEE, D. E., BOTS, M. L., ASMAR, R., TOPOUCHIAN, J., RENEMAN, R. S., HOEKS, A. P., VAN DER KUIP, D. A., HOFMAN, A. & WITTEMAN, J. C. 2001. Association between arterial stiffness and atherosclerosis: the Rotterdam Study. *Stroke,* 32**,** 454-460.

VAN SON, J. A., FALK, V., WALTHER, T., SMEDTS, F. M. & MOHR, F. W. 1997. Low-grade intimal hyperplasia in internal mammary and right gastroepiploic arteries as bypass grafts. *The Annals of thoracic surgery,* 63**,** 706-708.

WAGENSEIL, J. E. & MECHAM, R. P. 2009. Vascular extracellular matrix and arterial mechanics. *Physiological reviews,* 89**,** 957-989.

WALLACE, J. M. 2012. Applications of atomic force microscopy for the assessment of nanoscale morphological and mechanical properties of bone. *Bone,* 50**,** 420-427.

WALLACE, J. M., ORR, B. G., MARINI, J. C. & HOLL, M. M. B. 2011. Nanoscale morphology of Type I collagen is altered in the Brtl mouse model of Osteogenesis Imperfecta. *Journal of structural biology,* 173**,** 146-152.

WALLACE, S., MCENIERY, C. M., DAKHAM, Z., PUSALKAR, P., MAKI-PETAJA, K., ASHBY, M. J., COCKCROFT, J. R. & WILKINSON, I. B. 2005. Matrix metalloproteinase-9 (MMP-9), MMP-2, and serum elastase activity are associated with systolic hypertension and arterial stiffness. *Arteriosclerosis, thrombosis, and vascular biology,* 25**,** 372-378.

WIGHT, T. N. 1989. Cell biology of arterial proteoglycans. *Arteriosclerosis, Thrombosis, and Vascular Biology,* 9**,** 1-20.

WOLINSKY, H. & GLAGOV, S. 1967. A lamellar unit of aortic medial structure and function in mammals. *Circulation research,* 20**,** 99-111.

YOUNG, T., MONCLUS, M., BURNETT, T., BROUGHTON, W., OGIN, S. & SMITH, P. 2011. The use of the PeakForceTM quantitative nanomechanical mapping AFM-based method for high-resolution Young's modulus measurement of polymers. *Measurement Science and Technology,* 22**,** 125703.

YU, Q., ZHOU, J. & FUNG, Y. 1993. Neutral axis location in bending and Young's modulus of different layers of arterial wall. *American Journal of Physiology-Heart and Circulatory Physiology,* 265**,** H52-H60.

ZHANG, H. J., WANG, J., LIU, H. F., ZHANG, X. N., ZHAN, M. & CHEN, F. L. 2015. Overexpression of mimecan in human aortic smooth muscle cells inhibits cell proliferation and enhances apoptosis and migration. *Experimental and therapeutic medicine,* 10**,** 187-192.

ZOUMI, A., LU, X., KASSAB, G. S. & TROMBERG, B. J. 2004. Imaging coronary artery microstructure using second-harmonic and two-photon fluorescence microscopy. *Biophysical journal,* 87**,** 2778-2786.

Chapter 3

Technique development for nanoscale characterisation of biological samples in a zebrafish model

---

This chapter focusses on applying the PeakForce QNM technique to characterise tissue from the vertebral column of the zebrafish. The rationale for utilising the zebrafish model and for focussing on the vertebral column is outlined in the Introduction (Section 3.1.1.2). This chapter demonstrates the utility of using PeakForce QNM for small-scale biological structures. Sample preparation procedures for PeakForce QNM testing are developed in this chapter. Furthermore, calibration methods for nanomechanical testing are optimised, which are applied for the work on the IMA in later chapters.

Abstract

Zebrafish (*Danio rerio*) is a useful model for understanding biomedical properties of bone and are widely employed in developmental and genetics studies. Here, the development of zebrafish vertebral bone has been studied at the nanoscale from adolescence (6 months), early adulthood (10 months) to mid-life (14 months). Characterisation of the bone was conducted using energy-dispersive X-ray spectroscopy (EDX), SEM and PeakForce QNM AFM techniques. SEM and AFM revealed a lamellar structure with mineralised collagen fibrils. There was a significant increase in the wall thickness from 6 to 10 months (76%) and 10 months to 14 months (26 %), which is positively correlated with nanomechanical behaviour. An increase in the Ca/P ratio was found which was also positively correlated with nanomechanical properties. The change in mechanical properties and Ca/P are similar to those expected in humans when transitioning from adolescence to mid-life. This study suggests that zebrafish serve as a suitable model for further studies on age-related changes in bone ultrastructure.

3.1 Introduction

3.1.1 Zebrafish as a model for human diseases

3.1.1.1 The use of zebrafish in cardiovascular research

Over the last decade, the zebrafish (*Danio rerio*) has become an ideal vertebrate animal model for cardiovascular research because of diverse reasons. Zebrafish have a closed circulatory system and the structure of vasculature and process underlying vessel formation are extremely similar to those in humans (Isogai *et al*., 2001). The zebrafish aorta also shares the same tissue organisation and constitutions as mammalian aortae, including endothelial cells, SMC layers, and adventitial fibroblasts and collagen network (Miano *et al*., 2006). Importantly, given the optical transparency of their embryos and larvae and the high similarity in the genome compared to humans, zebrafish are amenable to conduct genetic manipulation and screens for identifying vascular developing- and disease-related mutations and genes (Gore *et al*., 2012). In the zebrafish embryo, the angiogenesis including the origins and growth of vessels (Childs *et al*., 2002), and the angiogenic network formation (Isogai *et al*., 2003) has been investigated. Zebrafish have also been used to study cardiac development, growth and function (Stainier *et al*., 1996, Stainier and Fishman, 1994, Tu and Chi, 2012). Moreover, zebrafish promise researchers a new model organism for modelling CVDs, such as thrombosis (Gregory *et al*., 2002, Jagadeeswaran *et al*., 2005), inflammation (Renshaw *et al*., 2006), cardiomyopathies (Gerull *et al*., 2002, Knöll *et al*., 2007) and congenital heart diseases (Tu and Chi, 2012, Lambrechts and Carmeliet, 2004).

3.1.1.2 Rationale for focussing on the zebrafish vertebral column

Initially, the dorsal aorta of zebrafish was designed as an artery model for developing nanoscale characterisation approach for probing structural changes in small-scale biological samples. However, it was impossible to dissect and isolate the aorta from the zebrafish. Since the dorsal aorta is conjoint with the fish spine, the cryosectioning procedure could not be used to section the hard vertebral column and soft aorta at the same time. Due to this difficulty, the dorsal aorta was always missing although the vertebral column could be properly sectioned. Hence, due to the experimental difficulties, it was decided that the work on the vertebral column instead of the dorsal aorta should be conducted. This allowed the author to make full use of the expertise available at the National Tsing Hua University, Taiwan. Although it is not soft tissue, given the size of the vertebral column (wall thickness < 50μm and lumen diameter < 200 μm) it is an appropriate tissue for use with PeakForce QNM technique due to its dimensions (which are close to that of the IMA) and also due to the presence of collagen fibrils. The work also allowed calibration and sample preparation methods to be established for application to the human IMA (Section 3.7). Hence, the zebrafish work not only allowed the author to setup and tune the technique that is going to use for IMA, but (as added bonus) also contributed to the knowledge of a tissue that is widely employed in developmental and genetic studies. The subsequent section provides an overview of the use of the zebrafish vertebral column as a model for the human bone.

3.1.2 Zebrafish as a model to study bone maturation: Nanoscale structural and mechanical characterisation of age-related changes in the zebrafish vertebral column

The zebrafish possess complex ossified skeleton that comprised of cartilage and bone, which show key similarities to humans (Lieschke and Currie, 2007). Although zebrafish have 'compact bone' but not 'cortical bone' i.e. compact bone that surrounds a bone marrow cavity (Geurtzen *et al*., 2017), and trabecular bone is only found in the skull (Weigele and Franz‐Odendaal, 2016) zebrafish share many key features of bone structure and remodeling with humans (Spoorendonk *et al*., 2010, Asharani *et al*., 2012, Brittijn *et al*., 2009, Shin and Fishman, 2002), which suggests they are a suitable model to understand age-related development of human bone, as well as human bone diseases. For example, a study has shown that although there is no complete Haversian system in the zebrafish bone, it does have a lamellar structure and a bio-mineralised microstructure with hierarchical organisation which is similar to human bone (Ge *et al*., 2006). In recent years, changes associated with skeletogenesis and osteogenesis (Weigele and Franz-Odendaal, 2016), osteogenesis imperfecta (OI) (Asharani *et al*., 2012) and bone regeneration (Knopf *et al*., 2011) have been modelled and assessed in the zebrafish system. Thus, these studies suggest that zebrafish have the potential to complement or even replace mammalian models in studies on skeletal disorders on mammals. Until now, there have been no studies that have explored age-related development and changes in zebrafish bone.

Age-related development and changes with advanced ageing in the skeleton system are known to associate with increased bone fragility and fracture (Ensrud, 2013). Although the mechanical properties and age-related bone development have been studied in humans, there

are still gaps in current understanding in relation to the structural and mechanical changes that occur in the bone matrix and microarchitecture during the ageing process (Legrand *et al*., 2000, Akkus *et al*., 2003). Furthermore, there is an urgent need to develop suitable alternatives to mammalian animal models for studying bone development, skeletal maturation and ageing to comply with the '3Rs' (reduce, refine and replace) approach of animal use for scientific studies. Zebrafish align with the 3Rs which covers replacement of higher-order animals such as rodents with lower-order zebrafish (Vliegenthart *et al*., 2014). Zebrafish models can also overcome limitations associated with human biopsy samples including concerns in relation to ethics, suitability of samples and costs (Grizzle *et al*., 2011, Barut and Zon, 2000).

To determine how zebrafish bone develops with age in terms of ultrastructure and biomechanical properties, this chapter studied the vertebral column of adolescence, early adulthood and mid-life fish. This work employed a number of high spatial resolution techniques to characterise the micro- and nano-scale structural features and mechanical properties of the zebrafish vertebral column. Specifically, SEM was utilised to observe bone microstructure. Calcium (Ca) and phosphate (P) levels were determined with SEM integrated EDX. AFM based PeakForce QNM was used to co-localise ultrastructural and nanomechanical properties in the bone. This study is the first to report how the ultrastructure and nanomechanical properties change as zebrafish bone ages.

3.2. Materials and methods

3.2.1 Sample information

All wild-type AB strain zebrafish (*Danio rerio*) were raised at The Taiwan Zebrafish Core Facility (TZCF) at National Tsing Hua University (NTHU). The fish were maintained under standard conditions (Westerfield, 1995), following the strict animal usage guidelines and complying with the humane endpoints that are stipulated at TZCF where zebrafish are maintained up to around 18 months on average (You *et al*., 2016).

In this study, zebrafish were euthanised in an ice bath and dissected to collect the front-end of the fish body at the following ages; 6 months, 10 months and 14 months. Three fish were collected for each age group. The three age groups were selected to represent 'adolescence' (6 months), 'early adulthood' (10 months) and 'mid-life' (14 months), loosely based on the classification of Gilbert *et al*. (Gilbert *et al*., 2014) and Armstrong (Armstrong, 2007). The average lifespan of zebrafish is approximately 36 months (Gerhard *et al*., 2002) hence these three age groups correspond to 17 %, 28 % and 39 % of the maximum zebrafish lifespan. Given that the average life expectancy is 79.2 for males and 82.9 for women (Office for National Statistics, UK: 2014-2016), the equivalent age groups for humans would be 14 years, 23 years and 32 years. Therefore, these are relevant for studying bone development because bone mass peaks at around 30 years of age (O'Flaherty, 2000).

Zebrafish use was approved by the Experimental Animal Care and Use Committee of NTHU (Approval number: 10048). The precaudal vertebrae were used for all experiments as detailed below.

3.2.2 Sample preparation

The zebrafish were collected immediately after sacrifice and subsequently embedded in optimum cutting temperature (OCT) compound (Tissue-Tek Sakura Finetek, Torrance, USA) along with a transverse plane of the fish trunk. They were immediately immersed into the pre-frozen isopentane (2-Methylbutane) (Sigma-Aldrich, Saint Louis, USA) with a liquid nitrogen bath for 2 minutes until the sample was totally frozen. The unfixed, frozen fish samples, which included the vertebral column from the precaudal regions of the zebrafish, were then cryo-sectioned to a nominal thickness of 10 µm along a transverse plane of the skeletal bone using a Leica CM1850 cryostat (Leica Microsystems, Heidelberger, Germany) and adhered onto glass coverslip for further experimentation (Figure 3.1). At least 10 sections were cut from each fish vertebral column. Due to the small size of the vertebral bodies, it was not possible to determine whether the sections were from the same or adjacent vertebral bodies. All the cryo-sections were stored in a -80 ℃ freezer until testing.

3.2.3 Hematoxylin and eosin staining

For histological characterisation, the sample sections were stained with Hematoxylin and Eosin (H&E). Cryo-sections were de-thawed at room temperature for 10 minutes and washed with distilled water for 10 minutes to remove any excess OCT compound. Following drying in air for 10 minutes, the H&E stained tissue section was characterised following standard histological procedures (Cardiff *et al*., 2014) and optical images were captured using an optical microscope (Olympus, Tokyo, Japan). 15 measurements of the wall thickness of the vertebral column were made in each group to assess its development with age.

3.2.4 Scanning electron microscopy (SEM)

For SEM observation, the sample sections were fixed on the coverslip with Karnovsky's fixative (2.5% glutaraldehyde (GA) in 0.2M phosphate) for 2 hours, and they were dipped in buffer solution (0.2M monobasic sodium phosphate and 0.2M dibasic sodium phosphate) for 15 hours. The sodium phosphate buffers used in the SEM sample preparation allow a constant pH to be maintained at a physiological level along with physiological osmolality and ion concentrations, thus preventing acidification during fixation (Schiff and Gennaro, 1979). Following this, the samples were dehydrated in graded ethanol concentrations (from 50%, 70%, 95% to 100%) for 15 minutes each. Finally, the samples were critical-point-dried (Samdri-795 Critical Point Dryer, Tousimis®, MD, USA) and stored in a desiccator for the SEM study. Prior to SEM characterisation, the sections were sputter-coated with gold and then imaged with an SEM (Hitachi SU8010, Chiyoda, Japan) at 15 kV.

3.2.5 Energy-dispersive X-ray spectroscopy (EDX) analysis

The SEM instrument (Hitachi SU8010, Chiyoda, Japan) was equipped with an EDX. EDX was employed to determine the elemental compositions of the zebrafish vertebral column for the different ages. EDX measurements were performed with an electron beam of accelerating voltage 15 kV. The weight proportion of each assessed element was obtained, involving carbon (C), nitrogen (N), oxygen (O), sulfur (S), phosphorous (P) and calcium (Ca). The Ca/P ratio was subsequently determined to evaluate bone properties. One measurement was made on the outer half of the vertebral column in each fish with a fixed size of $7\times7\ \mu m^2$.

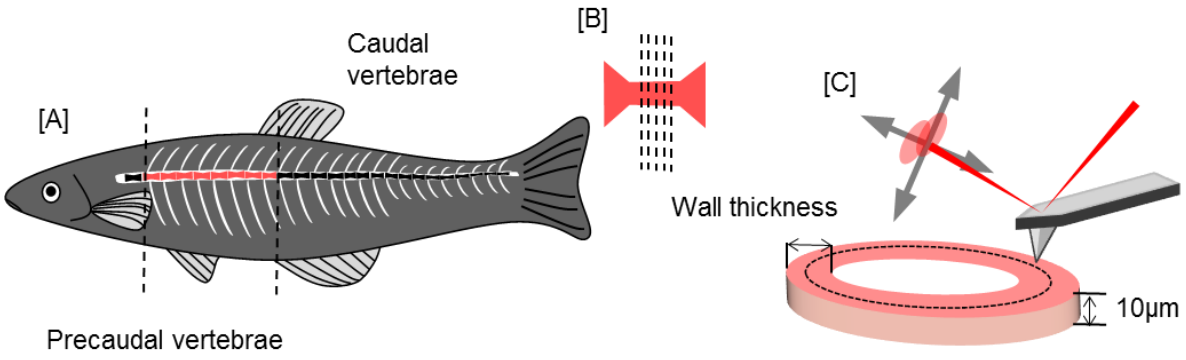

Figure 3.1 Schematic diagram of the experimental approach for PeakForce QNM and EDX measurements of the zebrafish vertebral column. (A) The front-end with the precaudal vertebra of the fish body was collected. (B) The vertebrae were sectioned to a nominal thickness of 10 µm. (C) The outer half of the vertebral column (posterior) was probed using PeakForce QNM to assess the localised nanomechanical properties, and EDX was solely conducted on another corresponding section to investigate chemical compositions.

3.2.6 PeakForce QNM AFM

All experiments were conducted using PeakForce QNM on a Bruker AFM (Bruker, ICON Dimension, MA, USA). Prior to AFM measurements, the tissue was de-thawed at room temperature for 10 minutes and washed with distilled water for 10 minutes to remove any excess OCT compound. Subsequently, the sample was dried at room temperature (21°C) for 30 minutes and the outer half layer of the vertebral column was imaged with AFM. An RTESPA-150A probe (Bruker, California, USA) was used for all of the experiments. The probe had a nominal spring constant of 5 N/m, tip radius of 8 nm and a resonant cantilever frequency of 150 kHz. To assess the nanoscale mechanical properties of the sample, the deflection sensitivity was calibrated, following which the spring constant of the cantilever was calibrated using the thermal tune method. The thermal tune method is based on linking the spring constant of the cantilever to its thermal (Brownian) motion. The included thermal tune module in NanoScope Analysis version 1.5 software (Bruker, Santa Barbara, CA, USA) directly supports the thermal tune method and automatically fits the resonance peak of the

obtained power spectral density plot of the cantilever in ambient conditions with the Lorentzian model to calculate the spring constant of the cantilever.

Finally, a photo-stress coating polymer reference sample (PS1, Vishay Precision Group, Heilbronn, Germany) with a known elastic modulus was used to calibrate the elastic modulus. The manufacturer states that the elastic modulus of PS1 is 2.5 GPa. The elastic modulus of PS1 was also determined independently via nanoindentation (Keysight Technologies, Nanoindenter G200 with a DCM Head) utilising a Berkovich tip with 25 indents conducted to a depth of 500 nm. The nanoindentation results yielded an average elastic modulus of 2.8 GPa ± 0.1 GPa, as shown in Figure 3.2. The mechanical mapping calibration procedure was described in Appendix A.

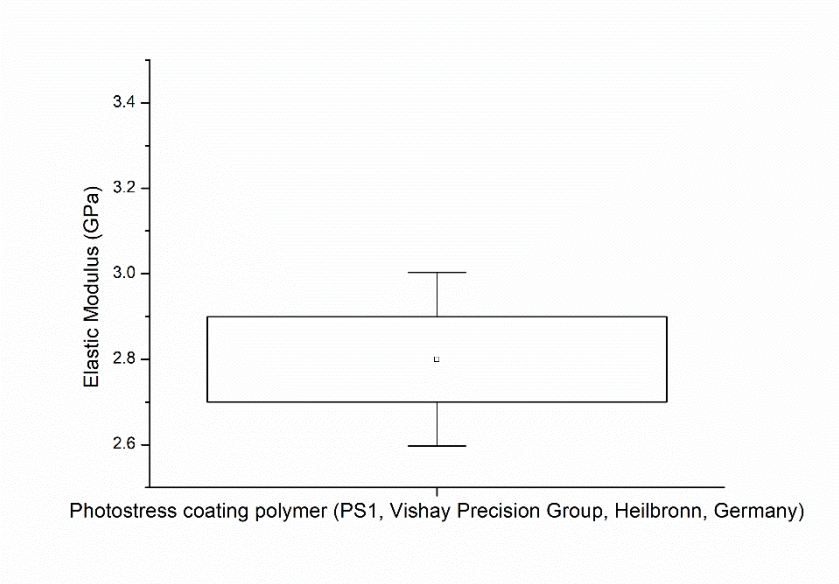

Figure 3.2 Box and whisker plot showing the elastic modulus of the photostress coating polymer (PS1, Vishay Precision Group, Heilbronn, Germany) determined with nanoindentation.

The AFM setup was integrated with an optical microscope which enabled the vertebral column to be identified and the probe was placed over it before testing. All testing was conducted with a scan rate of 0.9 Hz, a resolution of 256 pixels/line and a fixed scan size (2 ×

2 μm). The indentation depth of the AFM tip into the vertebral column tissue section for all the measurements performed in this study was controlled around 5 nm and thus the indentation depth/tissue thickness ratio was 0.05% for the zebrafish bone tissue section.

For each of the age groups (3 samples per group), 14 representative images were collected from the outer half region per sample. There were 65,536 (256 × 256 independent force curves) measurements for each image. The force curves were fitted using the DMT analytical model as outlined by Young *et al*. (Young *et al*., 2011). All AFM raw data files were analysed to yield the mean elastic modulus for each image with NanoScope Analysis version 1.5 (Bruker, Santa Barbara, CA, USA).

3.2.7 Statistical analysis

All statistical analysis was conducted in OriginPro version 9 (OriginLab, Northampton, MA, USA). All of the data are presented as mean ± standard deviation (SD). Firstly, as a quality control step, intra-group homogeneity was studied via the Kruskal-Wallis ANOVA test to determine if there were significant variations between measurements of wall thickness and also nanomechanical properties within each age group. Following this, group differences were assessed via suitable 2-sample independent tests selected after appraisal of data normality and homoscedasticity. Differences in vertebral column wall thickness, Ca/P ratio and nanomechanical properties were tested with the Kruskal-Wallis ANONA with Mann-Whitney post-hoc test. The adjusted p values in our results were calculated by applying the Benjamini and Hochberg false discovery rate correction to all raw p values (Benjamini and Hochberg, 1995). To assess for statistical significance between distributions of nanomechanical properties, Kolmogorov-Smirnov (K-S) tests were applied to the data. The elastic modulus-Ca/P ratio and elastic modulus-wall thickness relationships were obtained through Spearman's Rank Order Correlation, and a correlation test was used to test the

significance. A multivariate transformation called principal component analysis (PCA) was used for integrating the chemical and histological data with nanomechanical results.

3.3 Results

3.3.1 Histological analysis

Histology of the zebrafish was conducted on the fish trunk to identify the presence and structure of vertebral column (Figure 3.3). The locations of critical structures are labelled in Figure 3.3A including the spinal cord, muscular tissue, dorsal aorta and vertebral column. As shown in Figure 3.3, the vertebral column was visible in all samples as a dense, ring-like structure.

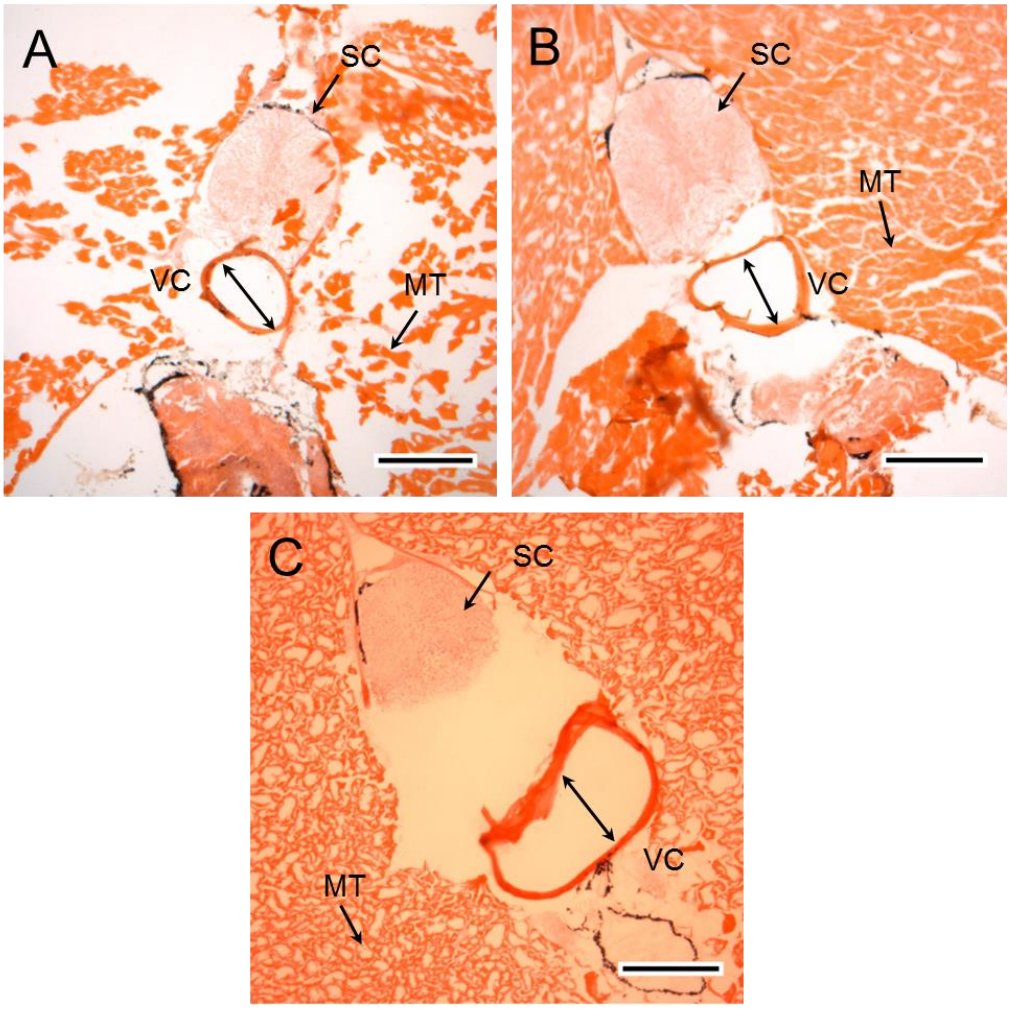

Figure 3.3 H&E stained histological sections for the zebrafish trunk at (A) 6 months (B) 10 months (C) 14 months. The circular structure above the vertebral column is the spinal cord (SC). The majority of the trunk section was loosely organised muscular tissue (MT) surrounding the spinal cord and vertebral column (VC). The scale bar represents 200 µm.

To assess the development of the vertebral column from adolescence (6 months) through to early adulthood (10 months) and mid-life (14 months), the thickness of vertebral column wall was measured via the histological images, as shown in Figure 3.4. Kruskal-Wallis test was performed for each group to test that no measurement within an age group was skewing the data. The test confirmed that there were non-significant differences between samples of the same group (Kruskal-Wallis ANOVA, $p>0.05$). Overall, the wall thickness was significantly increased as the zebrafish age increased through appositional growth (6 months = 8.4 ± 2.0

µm, 10 months = 14.8 ± 3.7 µm and 14 months = 18.6 ± 1.9 µm, Kruskal-Wallis ANOVA with Mann-Whitney post-hoc test, $p<0.000$, adjusted $p<0.0001$).

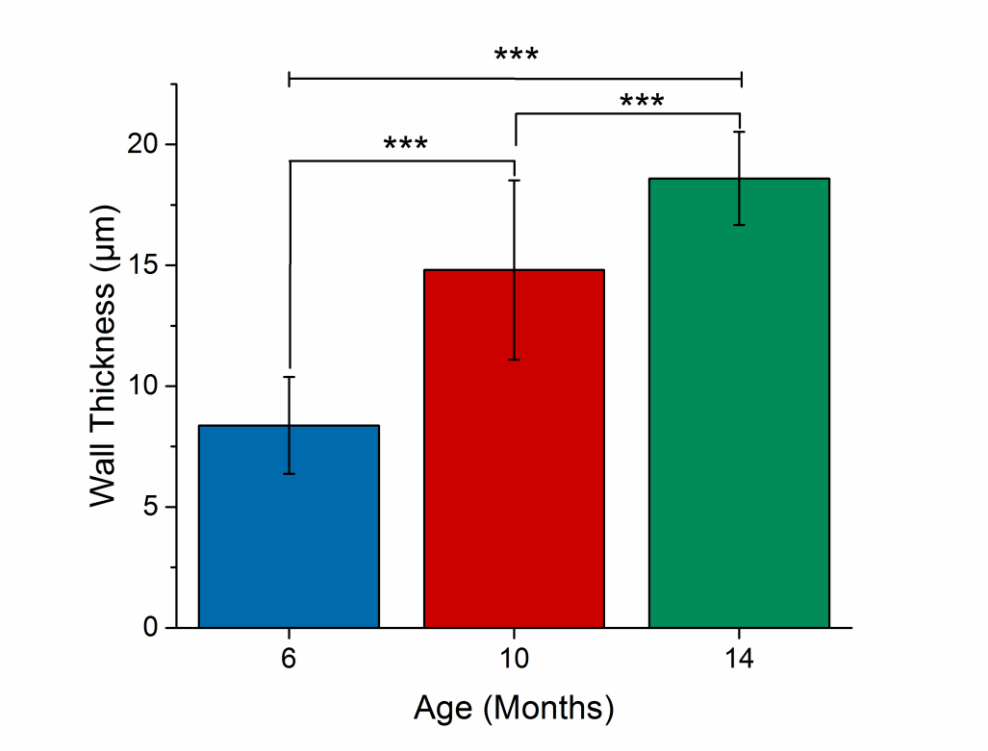

Figure 3.4 Zebrafish vertebral column wall thickness at 6 months, 10 month and 14 months. Bar graph shows the mean ± SD (n = 3 fish per group). There were 15 measurements in each group (n=3 fish/age group with 5 locations for each age group).

3.3.2 Bone ultrastructure

The ultrastructure of zebrafish vertebral column was characterised by SEM and AFM. As shown in Figure 3.5, a defined lamellar structure was visible in the bone with it being most pronounced at 14 months (Figure 3.5E and 3.5F).

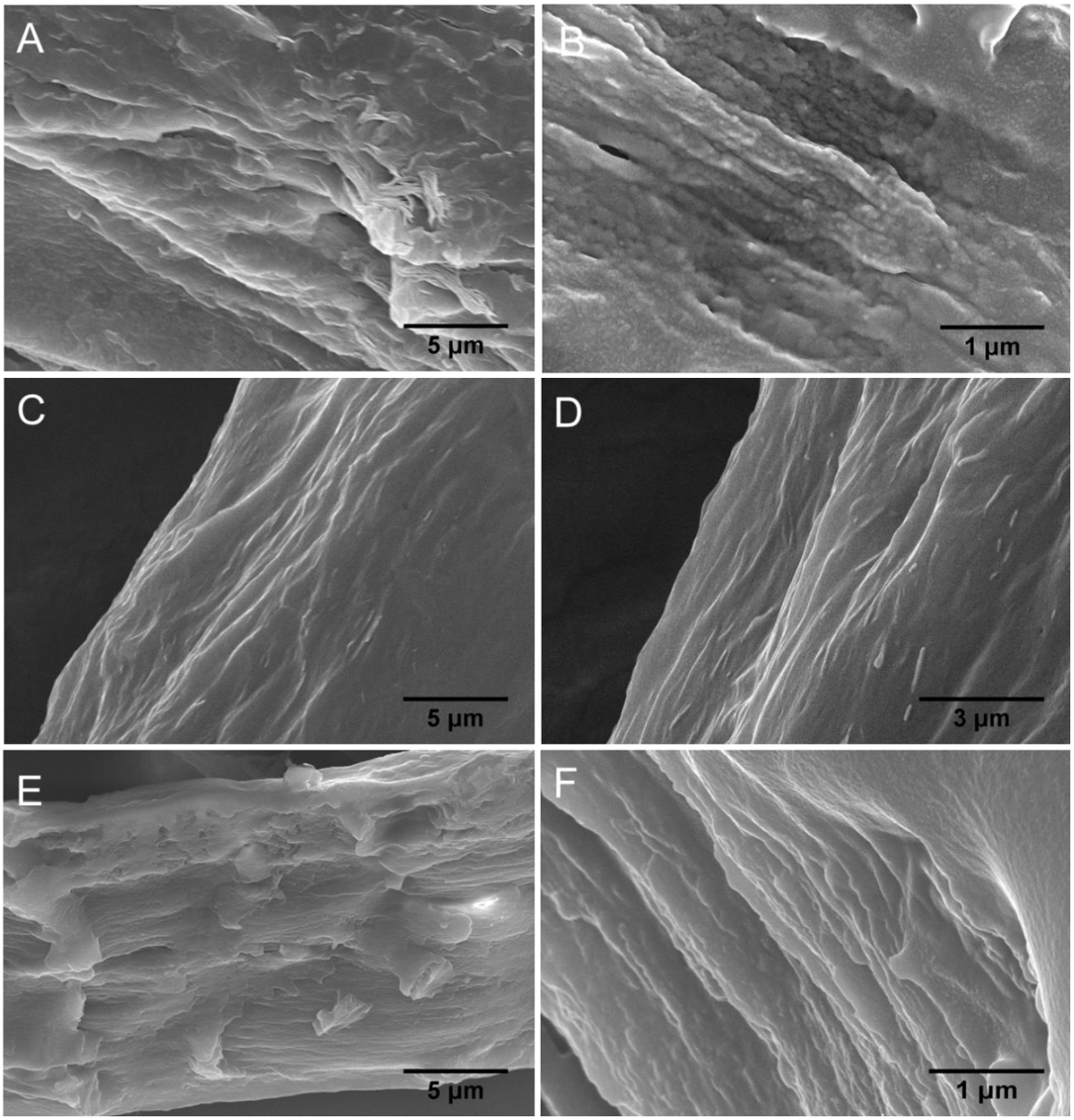

Figure 3. 5 SEM micrographs of the cross-section of the vertebral column in zebrafish at (A)&(B) 6 months, (C)&(D) 10 months and (E)&(F) 14 months. (A), (C) and (E) lamellar structure in all age groups. (D)&(F) high magnification of lamellar structure in 10 months and 14 months sample. (E) Mineralized collagen fibrils in 6 months sample. Images (A), (C) and (E) are at x5000 magnification, (D) at x10000 magnification and (B)&(F) at x25000 magnification.

Subsequently the ultrastructure of the vertebral column sections was probed using AFM and the major bone components were identified: mineral crystals and collagen fibrils (Figure 3.6). As shown in Figure 3.6A, 3.6C and 3.6E, the bone ultrastructure was highly mineralised in all of the groups. Furthermore, collagen fibrils were also observed in all of the samples (Figure

3.6B, 3.6D and 3.6F). These mineralised collagen fibrils appeared to be more randomly distributed in the samples at 6 months, while fibrils were highly organised and tightly packed along one direction in the samples at 10 months and 14 months. In some of the images, the 67 nm collagen D-period could be identified in the fibrils, which had typical diameters of around 100 - 150 nm (Figures 3.6G and 3.6H).

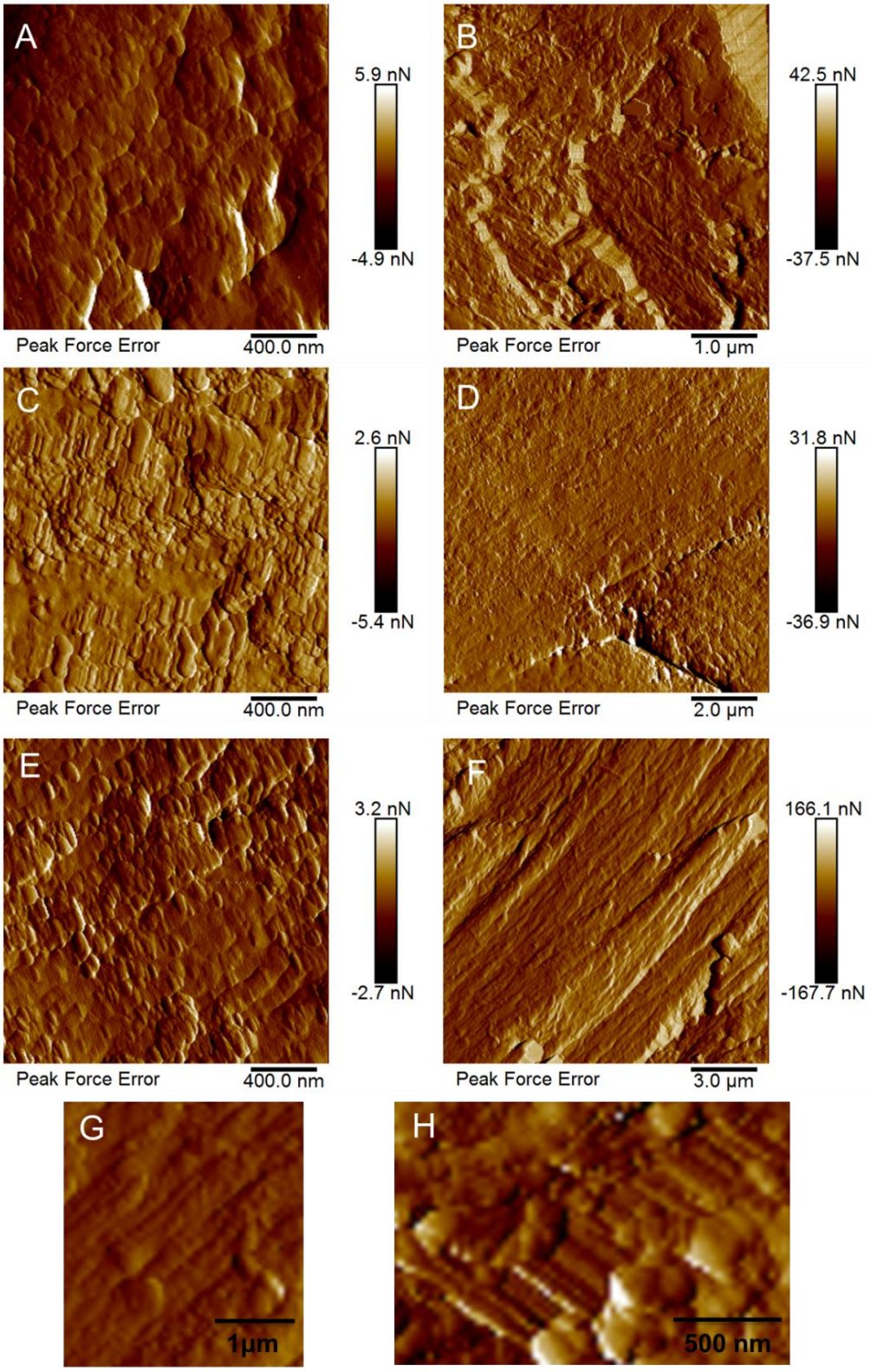

Figure 3. 6 Peak Force Error AFM images showing the ultrastructure of the zebrafish vertebral column at (A and B) 6 months, (C and D) 10 months and (E-H) 14 months (A), (C) and (E) are highly mineralized ultrastructure of zebrafish vertebral column at 6 months, 10 months and 14 months respectively. (B), (D) and (F) are mineralised collagen fibrils of zebrafish vertebral column at (B) 6 months, (D) 10 months and (F) 14 months respectively. (G) and (H) are zoomed in Peak Force Error images of collagen fibrils with distinct D-period.

3.3.3 Chemical compositions in the bone

EDX analysis was performed to determine the bone chemical composition at different ages. The vertebral column was mostly comprised of C, N, O, P and Ca elements. S appeared to be a minimal element, which was less than 1% in all groups (Table 3.1). Calcium and phosphorus were two of the most abundant elements in all samples, which were also the essential elements in bone tissue. The Ca/P ratio was evaluated for all the three groups as shown in Figure 3.7. Although no statistically significant difference was detected in the Ca/P ratio between the three age groups (Kruskal-Wallis ANONA, $p = 0.4$), the Ca/P ratio in the 10 months and 14 months groups was slightly higher than that in the 6 months group; 6 months = 1.74, 10 months = 1.97 and 14 months = 1.90). These data were related to nanomechanical properties (Section 3.3.4 and 3.3.5).

Table 3.1 EDX results (mean±SD) for the 6 months, 10 month and 14 months zebrafish vertebral column.

	6 months (weight %)	10 month (weight %)	14 months (weight %)
Ca	41.06 ± 2.51	42.61 ± 11.25	42.91 ± 1.72
P	23.63 ± 0.37	21.40 ± 2.02	22.54 ± 0.76
O	14.32 ± 0.48	8.04 ± 4.48	17.38 ± 1.67
C	14.02 ± 2.42	20.59 ± 6.36	11.76 ± 0.11
N	6.27± 0.69	6.54 ± 3.36	5.09 ± 0.91
S	0.69 ± 0.18	0.81 ± 0.08	0.32 ± 0.06

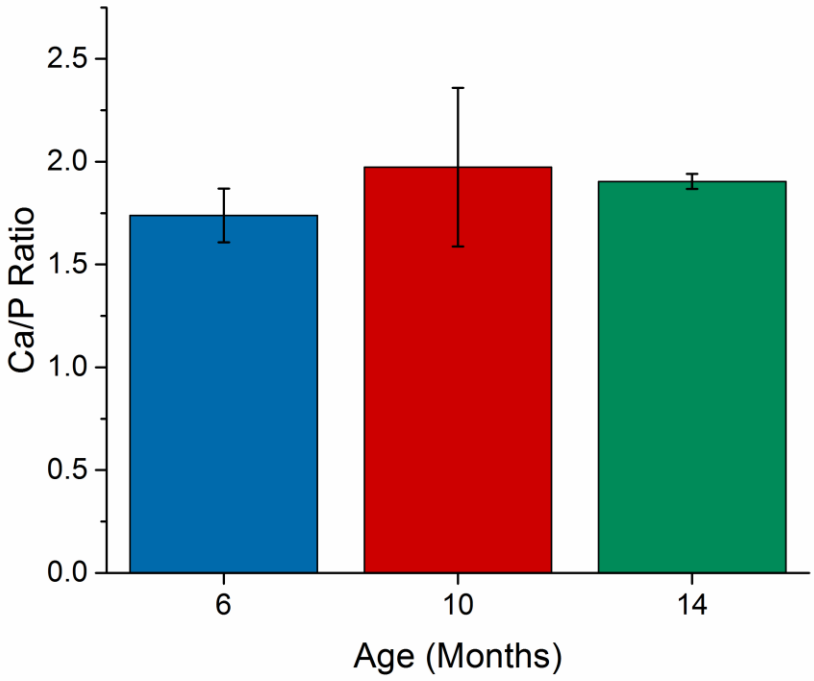

Figure 3.7 Ca/P ratio of zebrafish vertebral column at 6 months, 10 months and 14 months. Data are shown as mean±SD. There were 3 measurements in each age group (i.e. one EDX measurement/fish).

3.3.4 Nanoscale mechanical properties

PeakForce QNM was used to probe nanomechanical properties along with ultrastructural topography in the zebrafish vertebral column. Kruskal-Wallis ANOVA testing confirmed that there were no differences within each group ($p > 0.05$). As shown in Figure 3.8A, the mean elastic modulus was significantly higher in the 10 months and 14 months group as compared to the 6 months group; 6 months = 1703.6 ± 846.5 MPa, 10 months = 2056.1 ± 454.9 MPa and 14 months = 2301.5 ± 736.6 MPa (Kruskal-Wallis ANONA with Mann-Whitney post-hoc test, $p < 0.001$, adjusted $p < 0.001$). The median of the measured nanomechanical properties was 1563.5 MPa, 2015.2 MPa and 2127.4 MPa for the 6, 10 and 14 months groups respectively.

Furthermore, significant differences in the elastic modulus distribution were observed between the 6 months and 10 months groups (Kolmogorov–Smirnov test, $p < 0.0001$), as well as the 6 months and 14 months groups (Kolmogorov–Smirnov test, $p < 0.0001$) (Figure 3.8B). Subsequently, the 14 measurements of elastic modulus and the 5 measurements of wall thickness obtained for each fish were averaged and compared with the mean Ca/P ratio. Overall, a significant and positive correlation with Ca/P ratio and nanomechanical properties was found (Figure 3.8C). The relationship between the elastic modulus and wall thickness was also found to be positively correlated in all samples (Figure 3.8D).

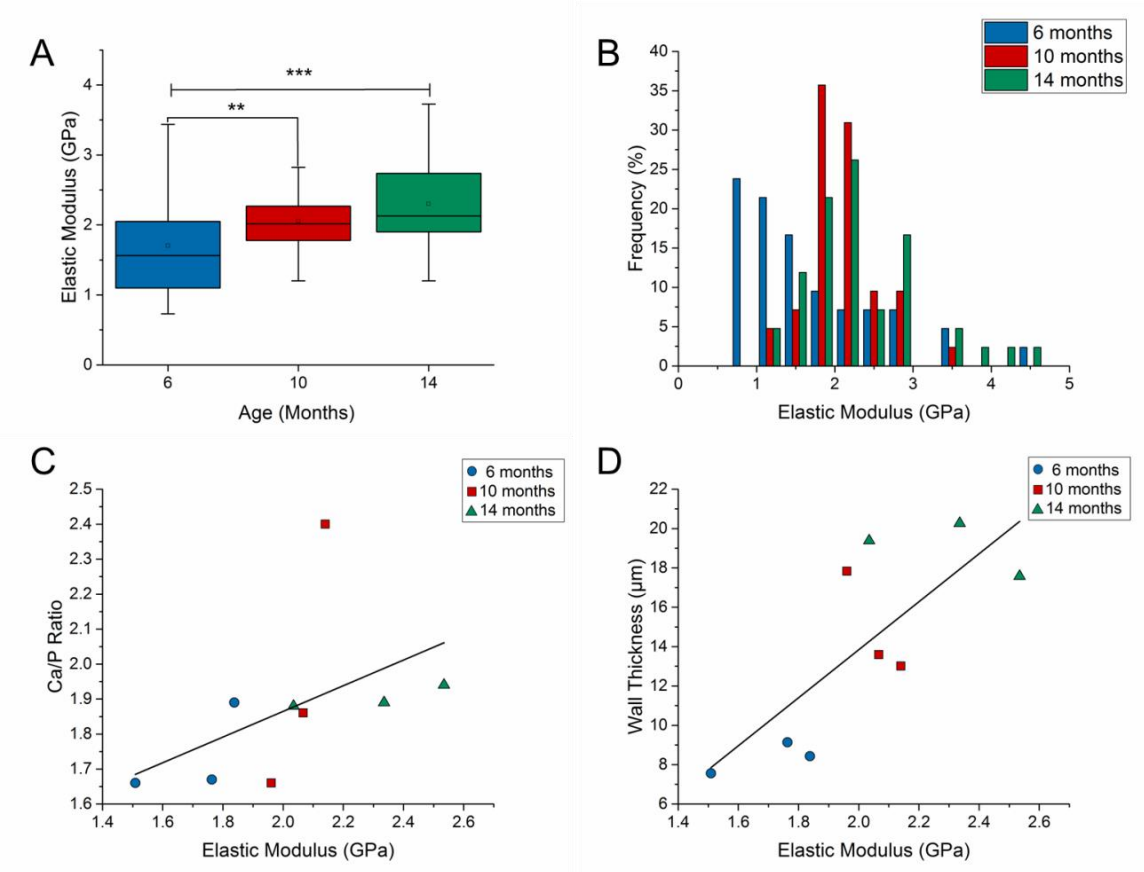

Figure 3.8 Nanomechanical properties of the zebrafish vertebral column for 6 months, 10 months and 14 months and its relationships with other parameters. (A) Elastic modulus of the vertebral column for each group (Kruskal-Wallis ANONA with Mann-Whitney post-hoc test, $p < 0.001$, There are 42 measurements per age group (n = 3 fish × 14 regions per group). (B) Frequency distribution of the elastic modulus (Kolmogorov–Smirnov test, $p < 0.0001$). The (C) Ca/P ratio-elastic modulus and (D) vertebral column wall thickness-elastic modulus relationship were found to be positively correlated (Spearman's Rank Order Correlation, Ca/P-elastic modulus: $r_S = 0.74$, $p = 0.022$; Wall thickness-elastic modulus: $r_S = 0.67$, $p = 0.049$). Plots (c) and (d) are based on the mean values for each fish.

3.3.5 Principle component analysis

PCA was utilised to study the relations between all of the variables measured in this study. The measurements of elastic modulus and wall thickness in each fish were averaged (n = 3 fish per age group) for the PCA. The projections that showed the best separation between the three ages studied corresponded to PC2 and PC3 (Figure 3.9A and 3.9B). The loading plot (Figure 3.9B) shows that whilst elastic modulus (E), wall thickness and S contribute the most to the separation of 14 months from 6 and 10 months, the variables Ca, P, C and O are the variables most responsible for the differences between 6 and 10 months from 14 months. Note that plots for PC1 and PC2 are provided in Figure 3.10.

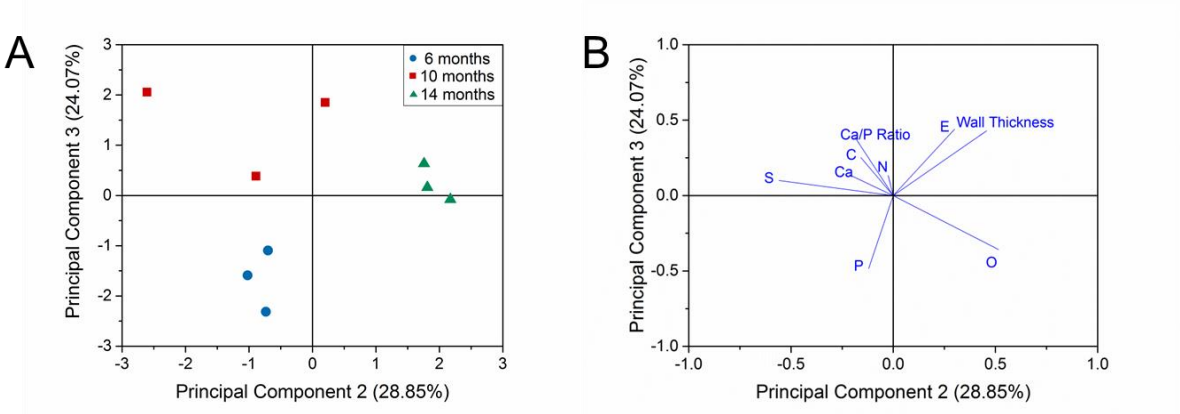

Figure 3.9 PCA for the variables measured in this study (A) Score plots of PC2 and PC3 indicated a distinct separation in all of the three age groups. (B) Loading plot showed the relationships of the original variables with respect to each principal component. Elastic modulus and wall thickness appear closely correlated and relatively anticorrelated to P. Similarly Ca, C, N and Ca/P are closely correlated and anticorrelated to O. Overall, this multivariate approach is suitable to assess the age-related differences at the three time points selected.

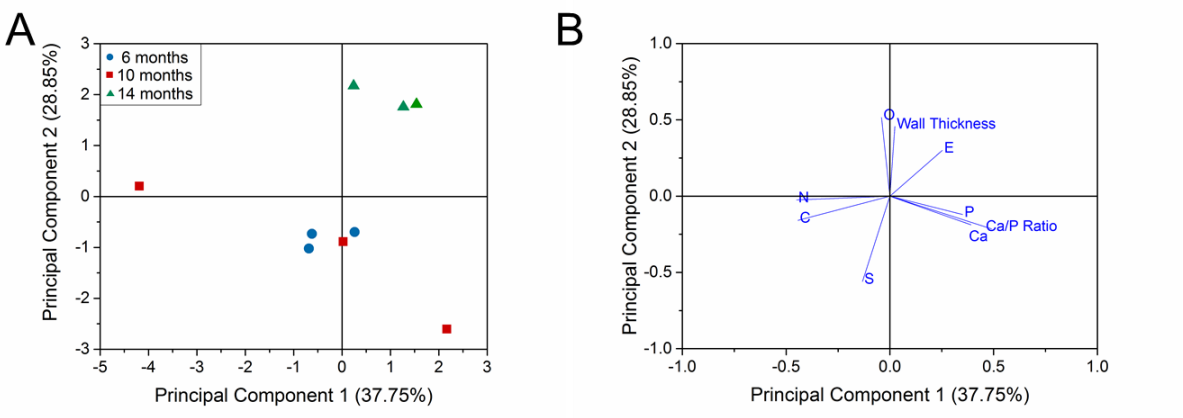

Figure 3.10 (A) Score plots of PC1 and PC2. (B) Corresponding loading plots. These plots show good separation between 14 months and the other 2 time points only. Hence, PC3 was incorporated in the analysis, as shown in Figure 3.9.

3.4 Discussion

In this study, the zebrafish as a model vertebrate was used to investigate age-related structural, chemical and biomechanical changes during skeletal maturation. Under laboratory conditions, zebrafish typically reach sexual maturity at 3 months, and their optimal reproduction age ranges from 6 months to 12 months (Kishi *et al*., 2003, Nasiadka and Clark, 2012). The average lifespan of zebrafish is approximately aged 36 months with a maximum lifespan of up to 66 months (Gerhard *et al*., 2002, Kishi *et al*., 2003). Here, the wild-type zebrafish at 6 months, 10 months and 14 months were used to explore age-dependent skeletal maturation and ageing process. The rationale for selecting these age groups was explained in Section 3.1.1.2, which correspond to adolescence, early adulthood and mid-life of the average human lifespan. This is particularly relevant because human bone density peaks at about 30 years of age (early adulthood) and hence in this zebrafish model the properties of bone with advancing age, and its relevance to humans were explored.

Given the small sample size and high spatial resolution demands, an approach combining different techniques at the micro- and nano-scales was developed to study the zebrafish vertebral column, where SEM and AFM were employed for observation of the bone matrix and ultrastructural features, whilst EDX and PeakForce QNM were applied to characterise the chemical and nanomechanical changes, respectively.

3.4.1 Zebrafish as a bone ageing model

Zebrafish have several advantages as a model system for ageing research. This is because they experience senescence, have a genome which has been evolutionarily conserved and can also be manipulated genetically (Gerhard, 2003, Gilbert *et al*., 2014, Lieschke and Currie, 2007). They have been found to be a suitable model for studying ageing and exercise (Gilbert *et al*., 2014), and also for bone research because their skeleton and mineralised tissues share many similarities with humans (Mackay *et al*., 2013). It is for this reason that zebrafish bone is hypothesised to be a suitable model for understanding changes in human bone with advancing age.

Most of the research on bone to date has focussed on bone disorders such as osteogenesis imperfecta because, as highlighted by Mackay *et al*. (2013), in such conditions there are genomic and phenotypic similarities between the zebrafish and human cases. This study addresses the gap in the literature with regard to normal ageing and bone development in wild-type zebrafish. The limitations of using zebrafish for such bone ageing studies are addressed in Section 3.5.

3.4.2 Wall thickness

The wall thickness measurements are a useful way of assessing the development of the fish skeleton with age. The ring-like structure in fish vertebrae serves as a way of determining age (Das, 1994). In this study, the wall thickness was assessed because it provides a good indication of the development of skeleton with age. Wall thickness measurements allow us to relate growth in the skeleton with mechanical properties and chemical composition. Although the relevance to the human skeleton may not be directly obvious, there may be some equivalence with cortical shell thickness, which plays an important role in the mechanical properties of the vertebral body (Eswaran *et al*., 2006). The PCA analysis (Figure 3.9) demonstrated that the wall thickness was most related to the elastic modulus.

3.4.3 Ultrastructural properties of zebrafish bone

A number of previous studies have used the zebrafish as a model vertebrate to explore the microstructure and mechanical properties of mineralised tissues. For example, zebrafish fin bony rays are proved to be a model for studying mineral formation process in skeletal bone (Mahamid *et al*., 2008). Ge *et al*. (Ge *et al*., 2006) first demonstrated the utility of zebrafish skeletal bone as a simple model to study bone mineralisation and human diseases using AFM and TEM. The same group have also used gene-mutated zebrafish models to explore changes in nanomechanical properties (Wang *et al*., 2002) and bone ultrastructure (Wang *et al*., 2003, Wang *et al*., 2004). In this study, the age-related structural and mechanical changes during skeletal maturation were linked in the zebrafish using the vertebral column as the target bone.

Similar to previous studies (Wang *et al*., 2004, Zhang *et al*., 2002), a lamellar structure was visible in the SEM images. The lamellar structure was more discernible in the 14 months specimens. However, the plywood-like structure reported by Wang *et al*. (2004) was not

clearly identifiable in this study. This is most likely because the cryosections were analysed and not fracture surfaces. The AFM images showed mineralised collagen fibrils with plate-like crystals evident. It should be noted that these tests were conducted without any chemical surface treatment, e.g. demineralisation, however, it was still feasible to detect some collagen fibrils with the distinct banding evident (Figure 3.6G and 3.6H).

3.4.4 Ca/P ratio

EDX analysis has been extensively documented as a useful quantitative method for the analysis of bone mineral status (Lochmüller *et al*., 2001), as well as the evaluation of mineralization by determining the Ca/P ratio (Mahamid *et al*., 2008) and assessing bone mineral changes (Åkesson *et al*., 1994). Although absolute measurements of Ca and P with EDX vary greatly, the Ca/P ratio exhibits good accuracy (Åkesson *et al*., 1994, Zaichick and Tzaphlidou, 2002). In bone, the relative content of Ca and P is essential for maintaining mineral balance and bone remodelling. Their co-dependence with the appropriate Ca/P ratio is also critical for bone mineralisation and development (Shapiro and Heaney, 2003). Bone Ca/P ratio is a good index of bone quality and can be used for diagnosing bone disorders. For example, reduced Ca/P ratio has been associated with osteogenesis imperfecta (OI) (Sarathchandra *et al*., 1999) and osteoporosis (Kourkoumelis *et al*., 2012). In OI bone, the Ca/P ratio is lower than healthy bone (Cassella *et al*., 1995). In a rabbit model of osteoporosis, a relationship was found between induced bone loss and a reduced Ca/P ratio (Kourkoumelis *et al*., 2012). Ca/P ratio for bone has also been reported for healthy rats (Kourkoumelis and Tzaphlidou, 2010) and rabbits (Kourkoumelis *et al*., 2012) with ranges from 1.8 to 2.0 and 1.9 to 2.2, respectively, which is relatively consistent with the data in this study. In the human skeleton, although Ca/P ratio is not significantly different with age, it appears to increase slightly from 15 to 40 years in males (Tzaphlidou and Zaichick, 2003) and 15 to 35 years in

females (Zaichick and Tzaphlidou, 2002) during skeletal maturation. This is also in good agreement with the findings in zebrafish bone in this study. Interestingly, the chemical composition measurements via the EDX analysis were the most useful to separate 6 and 10 months, as seen by PCA.

3.4.5 Elastic properties

Due to the small size of the zebrafish vertebral column, AFM and nanoindentation are suitable techniques for characterising the biomechanical properties of the bone. Previous studies have shown that for 3 months old wild-type zebrafish, the elastic modulus of the vertebral column varies across the bone cross-section, with a decrease in elastic modulus from the inner to the outer layers of the vertebral column (Zhang *et al*., 2002). A similar trend has also been reported for 6 months zebrafish (Ge *et al*., 2006). This variation in mechanical properties matches their ultrastructural characterisation of the bone in terms of the degree of mineralisation from the outer to the inner layer in the bone. In this study, the PeakForce QNM was used to characterise the mechanical properties of the outer half region of bone for the three age groups. The mean values were 1.7 ± 0.8 GPa in the 6 months group, 2.1 ± 0.4 GPa in the 10 months group and 2.3 ± 0.7 GPa in the 14 months group. The modulus values ranged from 0.7 - 4.3 GPa in the 6 months group, 1.2 - 3.4 GPa in the 10 months group and 1.2 - 4.5 GPa in the 14 months group. These values were lower than the range reported by Ge *et al*. (6.4 - 9.8 GPa) and Zhang *et al*. (1.1 - 8.4 GPa). However, the differences in values are likely to be related to the different spatial resolution, location, testing methods (nanoindentation vs AFM) and due to the embedding/preparation method. With regard to the latter point, both Ge *et al*. and Zhang *et al*. utilised PMMA-embedded samples which may have elevated the elastic modulus values (Bushby *et al*., 2004).

The trends in the mechanical properties from adolescence to mid-life in the zebrafish (an increase of 35 %) follow the expected trends for human bone, based on apparent-level mechanical tests. For example, in human tibial trabecular bone, the Young's modulus was found to increase by 27 % from young (16 to 39 years) to middle-age (40 to 59 years) (Ding *et al*., 1997). In human femoral cortical bone, the ultimate tensile strength of bone peaks at approximately 35 years and increases by 33% from adolescence (10 to 19 years) to mid-life (30 to 39 years) (Wall *et al*., 1979). It should be noted that the measurements with AFM are at the tissue-level and hence it cannot be compared directly with apparent-level modulus measurements. However, there have been no studies at the tissue-level on human bone which cover these age ranges. Rho *et al*. (Rho *et al*., 2002) used nanoindentation to show that there were no differences in the tissue modulus of human femoral bone with age, however their age range was from 35-95 years old. Similarly, Mirzaali *et al*. (Mirzaali *et al*., 2016) found that bone composition and the tissue-level modulus of human femoral bone (determined with microindentation) was independent of age, covering the age range 46 to 99. Given the scarcity of mechanical property data for younger human bones, the relevance of the zebrafish model here is clear. Although there is a gap in the literature regarding bone maturation and tissue-level modulus, other studies on mammals are consistent with the trends found in this study. Chittenden *et al*. (Chittenden *et al*., 2015) examined the elastic modulus and hardness of porcine cortical bone, with nanoindentation. They found an increase with age, from 1 to 48 months, as the bone develops. They found that mineral content also increased with age. In a study on murine cortical bone, Raghavan *et al*. (Raghavan *et al*., 2012) used linear regression analysis to show that there are patterns in the relationship between mechanical and compositional properties at the tissue scale when comparing skeletally mature young (4 or 5 months) and old (19 months) animals.

Further studies on zebrafish could be extended to include structural and biomechanical changes associated with old age. The combination of genomic editing and chemical screening studies with the approach in this study holds great potential to advance orthopaedic medicine in the future.

3.5 Limitations

In the present study, we demonstrated that the zebrafish vertebral column has the potential for studies on bone maturation and ageing studies. However, although there are numerous advantages of using zebrafish for bone research, a number of limitations must be considered, as summarised by Geurtzen *et al*. (2017) (Geurtzen *et al*., 2017). Strictly speaking (as stated in the Section 3.1.2), zebrafish have 'compact bone' but not 'cortical bone' and trabecular bone is only located in the skull (Weigele and Franz‐Odendaal, 2016). Furthermore, it has been reported that zebrafish bone is devoid of obvious Haversian systems (Cui *et al*., 2007, Wang *et al*., 2004). However, in a detailed histological study, Weigele and Franz - Odendaal (2016) have clearly identified osteons in zebrafish bone with central Haversian canals, although they reported that osteons were rarely detected. This finding leads on to one major difference between zebrafish and mammalian bone; in zebrafish acellular bone (devoid of osteocytes) is found as well as mononucleated osteoclasts. In contrast, mammalian bone is exclusively cellular with multinucleated osteoclasts (Laizé *et al*., 2014). These acellular regions may explain why Cui *et al*. have not found complete Haversian systems. Despite these differences, the zebrafish skeleton does have a lamellar structure and exhibits a hierarchical organisation which is a characteristic of human long bones (Cui *et al*., 2007). Overall, the biomineralisation process and microstructure of zebrafish bone has also been found to be similar to that of human Haversian bone (Ge *et al*., 2006). In terms of cellular

activity and remodelling, there are a number of similarities between zebrafish and human mammalian bone including endochondral bone formation and ossification, bone formation by osteoblasts and bone resorption by osteoclasts (Laizé *et al*., 2014). Zebrafish osteoblast differentiation is also similar to that in mammals (Witten *et al*., 2001, Weigele and Franz‐Odendaal, 2016). Differences arise in remodelling due to the presence of both mono- and multinucleated osteoclasts in the zebrafish. Nonlacunar bone resorption by mononucleated cells is an important remodelling process in zebrafish (Witten *et al*., 2001). Overall, zebrafish share many essential features in terms of bone formation and remodelling with vertebrates including mammals (Geurtzen *et al*., 2017).

Similar to mammals, teleost skeletal tissue adaptively remodels to their loading environment (Fiaz *et al*., 2012), and have even been used as a model for human exercise and ageing (Gilbert *et al*., 2014). However, one limitation that should also be considered is that the loading environment on the zebrafish skeletal system is different from that of mammals.

There are some limitations with the experimental approach that should also be addressed. Firstly, our study focused on the outer half layer (posterior) of the precaudal vertebral column. In future, it may be useful to examine the entire vertebral column to assess age-related, regional variations in the bone especially given the variation across the vertebral column that has been reported by Ge *et al*. (2006) (Ge *et al*., 2006). Secondly, future work could be conducted to determine apparent-level mechanical properties through tension and compression rather than focusing only on localised, tissue-level mechanical properties. PeakForce QNM AFM provides topographical and elastic modulus information at the nano-scale. However, to fully understand the biomechanical properties of zebrafish bone it would be useful to determine its fracture resistance, strength and toughness. Finally, use of demineralisation methods would help better understand the interaction between the organic

and inorganic phases. The demineralised bone may have allowed individual collagen fibrils to be identified more clearly, for example with TEM.

3.6 Conclusions

To conclude, in this study, zebrafish served as a readily accessible model for studying bone development. Here, this study has shown how the ultrastructure, composition of zebrafish bone changes from adolescence to early adulthood and mid-life. Wall thickness in the vertebral column increased by 122 % from 6 to 14 months. This was associated with a 12 % increase in Ca/P and a 35 % increase in elastic modulus. Ca/P and elastic modulus were found to be closely correlated. These changes in bone properties with skeletal development are consistent with trends reported for mammals.

Furthermore, using the zebrafish model, a nanoscale approach in the characterisation of small-scale biological samples and structures and linking the structure-property-functional properties was developed in this study. This approach has the potential to be extended for other ageing studies and bone pathology investigations in zebrafish. PeakForce QNM as the key technique in relating the structure and mechanical properties of small-scale biological structures was optimised in terms of its sample preparation, calibration and testing procedures. This pioneering study paves the way to probe human IMA and investigate structural and biomechanical changes with arterial stiffening in the following chapters.

3.7 Relevance of work to arterial stiffening

By using zebrafish as an animal model, AFM based PeakForce QNM technique was successfully applied for probing small-scale biological structures. This work is relevant to the remainder of the thesis as follows:

a. The appropriate preparation procedure for AFM characterisation of small-scale biological structures was validated. To maintain the fine architecture and avoid ice crystal formation, the biological tissues were snap frozen and cryosectioned prior to the AFM testing. Due to the substrate effect, it was found the nanomechanical and structural mapping gives high-quality mapping when the thickness of the tissue cryosection is fixed at 5 μm;
b. The calibration procedure for quantitative mapping was optimised by using a custom-made reference sample with known modulus, which eliminated the errors caused by reference sample ageing or wears;
c. The collagen fibrils could be visualised and probed via PeakForce QNM, which promised a target for exploring structural changes and link structure-property-function in biological tissues. Furthermore, comparing with SEM and TEM, AFM is capable of characterising this protein and biological structures without extra preparation and fixation which is believed to not only complicate the measurement but also lead to abnormal assessment.

References

ÅKESSON, K., GRYNPAS, M., HANCOCK, R., ODSELIUS, R. & OBRANT, K. 1994. Energy-dispersive X-ray microanalysis of the bone mineral content in human trabecular bone: a comparison with ICPES and neutron activation analysis. *Calcified tissue international,* 55**,** 236-239.

AKKUS, O., POLYAKOVA-AKKUS, A., ADAR, F. & SCHAFFLER, M. B. 2003. Aging of microstructural compartments in human compact bone. *Journal of Bone and Mineral Research,* 18**,** 1012-1019.

ARMSTRONG, T. 2007. *The human odyssey: Navigating the twelve stages of life*, Sterling Publishing Company.

ASHARANI, P., KEUPP, K., SEMLER, O., WANG, W., LI, Y., THIELE, H., YIGIT, G., POHL, E., BECKER, J. & FROMMOLT, P. 2012. Attenuated BMP1 function compromises osteogenesis, leading to bone fragility in humans and zebrafish. *The American Journal of Human Genetics,* 90**,** 661-674.

BARUT, B. A. & ZON, L. I. 2000. Realizing the potential of zebrafish as a model for human disease. *Physiological genomics,* 2**,** 49-51.

BENJAMINI, Y. & HOCHBERG, Y. 1995. Controlling the false discovery rate: a practical and powerful approach to multiple testing. *Journal of the royal statistical society. Series B (Methodological)***,** 289-300.

BRITTIJN, S. A., DUIVESTEIJN, S. J., BELMAMOUNE, M., BERTENS, L. F., BITTER, W., DEBRUIJN, J. D., CHAMPAGNE, D. L., CUPPEN, E., FLIK, G. & VANDENBROUCKE-GRAULS, C. M. 2009. Zebrafish development and regeneration: new tools for biomedical research. *International Journal of Developmental Biology,* 53**,** 835-850.

BUSHBY, A., FERGUSON, V. & BOYDE, A. 2004. Nanoindentation of bone: Comparison of specimens tested in liquid and embedded in polymethylmethacrylate. *Journal of Materials Research,* 19**,** 249-259.

CARDIFF, R. D., MILLER, C. H. & MUNN, R. J. 2014. Manual hematoxylin and eosin staining of mouse tissue sections. *Cold Spring Harbor protocols,* 2014**,** pdb. prot073411.

CASSELLA, J., GARRINGTON, N., STAMP, T. & ALI, S. 1995. An electron probe X-ray microanalytical study of bone mineral in osteogenesis imperfecta. *Calcified tissue international,* 56**,** 118-122.

CHILDS, S., CHEN, J.-N., GARRITY, D. M. & FISHMAN, M. C. 2002. Patterning of angiogenesis in the zebrafish embryo. *Development,* 129**,** 973-982.

CHITTENDEN, M., NAJAFI, A. R., LI, J. & JASIUK, I. 2015. Nanoindentation and ash content study of age dependent changes in porcine cortical bone. *Journal of Mechanics in Medicine and Biology,* 15**,** 1550074.

CUI, F.-Z., LI, Y. & GE, J. 2007. Self-assembly of mineralized collagen composites. *Materials Science and Engineering: R: Reports,* 57**,** 1-27.

DAS, M. 1994. Age determination and longevity in fishes. *Gerontology,* 40**,** 70-96.

DING, M., DALSTRA, M., DANIELSEN, C. C., KABEL, J., HVID, I. & LINDE, F. 1997. Age variations in the properties of human tibial trabecular bone. *J Bone Joint Surg Br,* 79**,** 995-1002.

ENSRUD, K. E. 2013. Epidemiology of fracture risk with advancing age. *Journals of Gerontology Series A: Biomedical Sciences and Medical Sciences,* 68**,** 1236-1242.

ESWARAN, S. K., GUPTA, A., ADAMS, M. F. & KEAVENY, T. M. 2006. Cortical and trabecular load sharing in the human vertebral body. *Journal of Bone and Mineral Research,* 21**,** 307-314.

FIAZ, A. W., LéON-KLOOSTERZIEL, K. M., GORT, G., SCHULTE-MERKER, S., VAN LEEUWEN, J. L. & KRANENBARG, S. 2012. Swim-training changes the spatio-temporal dynamics of skeletogenesis in zebrafish larvae (Danio rerio). *PloS one,* 7**,** e34072.

GE, J., WANG, X. & CUI, F. 2006. Microstructural characteristics and nanomechanical properties across the thickness of the wild-type zebrafish skeletal bone. *Materials Science and Engineering: C,* 26**,** 710-715.

GERHARD, G. S. 2003. Comparative aspects of zebrafish (Danio rerio) as a model for aging research. *Experimental gerontology,* 38**,** 1333-1341.

GERHARD, G. S., KAUFFMAN, E. J., WANG, X., STEWART, R., MOORE, J. L., KASALES, C. J., DEMIDENKO, E. & CHENG, K. C. 2002. Life spans and senescent phenotypes in two strains of Zebrafish (Danio rerio). *Experimental gerontology,* 37**,** 1055-1068.

GERULL, B., GRAMLICH, M., ATHERTON, J., MCNABB, M., TROMBITáS, K., SASSE-KLAASSEN, S., SEIDMAN, J., SEIDMAN, C., GRANZIER, H. & LABEIT, S. 2002. Mutations of TTN, encoding the giant muscle filament titin, cause familial dilated cardiomyopathy. *Nature genetics,* 30**,** 201.

GEURTZEN, K., VERNET, A., FREIDIN, A., RAUNER, M., HOFBAUER, L. C., SCHNEIDER, J. E., BRAND, M. & KNOPF, F. 2017. Immune suppressive and bone inhibitory effects of prednisolone in growing and regenerating zebrafish tissues. *Journal of Bone and Mineral Research*.

GILBERT, M. J., ZERULLA, T. C. & TIERNEY, K. B. 2014. Zebrafish (Danio rerio) as a model for the study of aging and exercise: physical ability and trainability decrease with age. *Experimental gerontology,* 50**,** 106-113.

GORE, A. V., MONZO, K., CHA, Y. R., PAN, W. & WEINSTEIN, B. M. 2012. Vascular development in the zebrafish. *Cold Spring Harbor perspectives in medicine,* 2**,** a006684.

GREGORY, M., HANUMANTHAIAH, R. & JAGADEESWARAN, P. 2002. Genetic analysis of hemostasis and thrombosis using vascular occlusion. *Blood Cells, Molecules, and Diseases,* 29**,** 286-295.

GRIZZLE, W. E., BELL, W. C. & SEXTON, K. C. 2011. Issues in collecting, processing and storing human tissues and associated information to support biomedical research. *Cancer Biomarkers,* 9**,** 531-549.

ISOGAI, S., HORIGUCHI, M. & WEINSTEIN, B. M. 2001. The vascular anatomy of the developing zebrafish: an atlas of embryonic and early larval development. *Developmental biology,* 230**,** 278-301.

ISOGAI, S., LAWSON, N. D., TORREALDAY, S., HORIGUCHI, M. & WEINSTEIN, B. M. 2003. Angiogenic network formation in the developing vertebrate trunk. *Development,* 130**,** 5281-5290.

JAGADEESWARAN, P., GREGORY, M., DAY, K., CYKOWSKI, M. & THATTALIYATH, B. 2005. Zebrafish: a genetic model for hemostasis and thrombosis. *Journal of Thrombosis and Haemostasis,* 3**,** 46-53.

KISHI, S., UCHIYAMA, J., BAUGHMAN, A. M., GOTO, T., LIN, M. C. & TSAI, S. B. 2003. The zebrafish as a vertebrate model of functional aging and very gradual senescence. *Experimental gerontology,* 38**,** 777-786.

KNöLL, R., POSTEL, R., WANG, J., KRäTZNER, R., HENNECKE, G., VACARU, A. M., VAKEEL, P., SCHUBERT, C., MURTHY, K. & RANA, B. K. 2007. Laminin-α4 and integrin-linked kinase mutations cause human cardiomyopathy via simultaneous defects in cardiomyocytes and endothelial cells. *Circulation,* 116**,** 515-525.

KNOPF, F., HAMMOND, C., CHEKURU, A., KURTH, T., HANS, S., WEBER, C. W., MAHATMA, G., FISHER, S., BRAND, M. & SCHULTE-MERKER, S. 2011. Bone regenerates via dedifferentiation of osteoblasts in the zebrafish fin. *Developmental cell,* 20**,** 713-724.

KOURKOUMELIS, N., BALATSOUKAS, I. & TZAPHLIDOU, M. 2012. Ca/P concentration ratio at different sites of normal and osteoporotic rabbit bones evaluated by Auger and energy dispersive X-ray spectroscopy. *Journal of biological physics,* 38**,** 279-291.

KOURKOUMELIS, N. & TZAPHLIDOU, M. 2010. Spectroscopic assessment of normal cortical bone: differences in relation to bone site and sex. *The Scientific World Journal,* 10**,** 402-412.

LAIZé, V., GAVAIA, P. J. & CANCELA, M. L. 2014. Fish: a suitable system to model human bone disorders and discover drugs with osteogenic or osteotoxic activities. *Drug Discovery Today: Disease Models,* 13**,** 29-37.

LAMBRECHTS, D. & CARMELIET, P. 2004. Genetics in zebrafish, mice, and humans to dissect congenital heart disease: insights in the role of VEGF. *Current topics in developmental biology*. Elsevier.

LEGRAND, E., CHAPPARD, D., PASCARETTI, C., DUQUENNE, M., KREBS, S., ROHMER, V., BASLE, M. F. & AUDRAN, M. 2000. Trabecular bone microarchitecture, bone mineral density, and vertebral fractures in male osteoporosis. *Journal of Bone and Mineral Research,* 15**,** 13-19.

LIESCHKE, G. J. & CURRIE, P. D. 2007. Animal models of human disease: zebrafish swim into view. *Nature Reviews Genetics,* 8**,** 353.

LOCHMüLLER, E.-M., KREFTING, N., BüRKLEIN, D. & ECKSTEIN, F. 2001. Effect of fixation, soft-tissues, and scan projection on bone mineral measurements with dual energy X-ray absorptiometry (DXA). *Calcified tissue international,* 68**,** 140-145.

MACKAY, E. W., APSCHNER, A. & SCHULTE-MERKER, S. 2013. A bone to pick with zebrafish. *BoneKEy reports,* 2.

MAHAMID, J., SHARIR, A., ADDADI, L. & WEINER, S. 2008. Amorphous calcium phosphate is a major component of the forming fin bones of zebrafish: Indications for an amorphous precursor phase. *Proceedings of the National Academy of Sciences,* 105**,** 12748-12753.

MIANO, J. M., GEORGER, M. A., RICH, A. & BENTLEY, K. L. D. M. 2006. Ultrastructure of zebrafish dorsal aortic cells. *Zebrafish,* 3**,** 455-463.

MIRZAALI, M. J., SCHWIEDRZIK, J. J., THAIWICHAI, S., BEST, J. P., MICHLER, J., ZYSSET, P. K. & WOLFRAM, U. 2016. Mechanical properties of cortical bone and their relationships with age, gender, composition and microindentation properties in the elderly. *Bone,* 93**,** 196-211.

NASIADKA, A. & CLARK, M. D. 2012. Zebrafish breeding in the laboratory environment. *ILAR journal,* 53**,** 161-168.

O'FLAHERTY, E. J. 2000. Modeling normal aging bone loss, with consideration of bone loss in osteoporosis. *Toxicological Sciences,* 55**,** 171-188.

RAGHAVAN, M., SAHAR, N. D., KOHN, D. H. & MORRIS, M. D. 2012. Age-specific profiles of tissue-level composition and mechanical properties in murine cortical bone. *Bone,* 50**,** 942-953.

RENSHAW, S. A., LOYNES, C. A., TRUSHELL, D. M., ELWORTHY, S., INGHAM, P. W. & WHYTE, M. K. 2006. A transgenic zebrafish model of neutrophilic inflammation. *Blood,* 108**,** 3976-3978.

RHO, J. Y., ZIOUPOS, P., CURREY, J. D. & PHARR, G. M. 2002. Microstructural elasticity and regional heterogeneity in human femoral bone of various ages examined by nano-indentation. *Journal of biomechanics,* 35**,** 189-198.

SARATHCHANDRA, P., KAYSER, M. & ALI, S. 1999. Abnormal mineral composition of osteogenesis imperfecta bone as determined by electron probe X-ray microanalysis on conventional and cryosections. *Calcified tissue international,* 65**,** 11-15.

SCHIFF, R. & GENNARO, J. 1979. The role of the buffer in the fixation of biological specimens for transmission and scanning electron microscopy. *Scanning,* 2**,** 135-148.

SHAPIRO, R. & HEANEY, R. 2003. Co-dependence of calcium and phosphorus for growth and bone development under conditions of varying deficiency. *Bone,* 32**,** 532-540.

SHIN, J. T. & FISHMAN, M. C. 2002. From zebrafish to human: modular medical models. *Annual Review of Genomics and Human Genetics,* 3**,** 311-340.

SPOORENDONK, K. M., HAMMOND, C. L., HUITEMA, L. F., VANOEVELEN, J. & SCHULTE-MERKER, S. 2010. Zebrafish as a unique model system in bone research: the power of genetics and in vivo imaging. *Journal of Applied Ichthyology,* 26**,** 219-224.

STAINIER, D., FOUQUET, B., CHEN, J.-N., WARREN, K. S., WEINSTEIN, B. M., MEILER, S. E., MOHIDEEN, M., NEUHAUSS, S., SOLNICA-KREZEL, L. & SCHIER, A. F. 1996. Mutations affecting the formation and function of the cardiovascular system in the zebrafish embryo. *Development,* 123**,** 285-292.

STAINIER, D. Y. & FISHMAN, M. C. 1994. The zebrafish as a model system to study cardiovascular development. *Trends in cardiovascular medicine,* 4**,** 207-212.

TU, S. & CHI, N. C. 2012. Zebrafish models in cardiac development and congenital heart birth defects. *Differentiation,* 84**,** 4-16.

TZAPHLIDOU, M. & ZAICHICK, V. 2003. Calcium, phosphorus, calcium-phosphorus ratio in rib bone of healthy humans. *Biological trace element research,* 93**,** 63-74.

VLIEGENTHART, A., TUCKER, C. S., DEL POZO, J. & DEAR, J. W. 2014. Zebrafish as model organisms for studying drug-induced liver injury. *British journal of clinical pharmacology,* 78**,** 1217-1227.

WALL, J., CHATTERJI, S. & JEFFERY, J. 1979. Age-related changes in the density and tensile strength of human femoral cortical bone. *Calcified tissue international,* 27**,** 105-108.

WANG, X.-M., CUI, F.-Z., GE, J. & MA, C. 2003. Alterations in mineral properties of zebrafish skeletal bone induced by liliput dtc232 gene mutation. *Journal of crystal growth,* 258**,** 394-401.

WANG, X., CUI, F., GE, J. & WANG, Y. 2004. Hierarchical structural comparisons of bones from wild-type and liliput dtc232 gene-mutated Zebrafish. *Journal of structural biology,* 145**,** 236-245.

WANG, X., CUI, F., GE, J., ZHANG, Y. & MA, C. 2002. Variation of nanomechanical properties of bone by gene mutation in the zebrafish. *Biomaterials,* 23**,** 4557-4563.

WEIGELE, J. & FRANZ-ODENDAAL, T. A. 2016. Functional bone histology of zebrafish reveals two types of endochondral ossification, different types of osteoblast clusters and a new bone type. *Journal of anatomy,* 229**,** 92-103.

WEIGELE, J. & FRANZ-ODENDAAL, T. A. 2016. Functional bone histology of zebrafish reveals two types of endochondral ossification, different types of osteoblast clusters and a new bone type. *Journal of anatomy,* 229**,** 92-103.

WESTERFIELD, M. 1995. *The zebrafish book: a guide for the laboratory use of zebrafish (Brachydanio rerio),* University of Oregon Press.

WITTEN, P. E., HANSEN, A. & HALL, B. K. 2001. Features of mono-and multinucleated bone resorbing cells of the zebrafish Danio rerio and their contribution to skeletal development, remodeling, and growth. *Journal of Morphology,* 250**,** 197-207.

YOU, M.-S., JIANG, Y.-J., YUH, C.-H., WANG, C.-M., TANG, C.-H., CHUANG, Y.-J., LIN, B.-H., WU, J.-L. & HWANG, S.-P. L. 2016. A Sketch of the Taiwan Zebrafish Core Facility. *Zebrafish,* 13**,** S-24-S-29.

YOUNG, T., MONCLUS, M., BURNETT, T., BROUGHTON, W., OGIN, S. & SMITH, P. 2011. The use of the PeakForceTM quantitative nanomechanical mapping AFM-based method for high-resolution Young's modulus measurement of polymers. *Measurement Science and Technology,* 22**,** 125703.

ZAICHICK, V. & TZAPHLIDOU, M. 2002. Determination of calcium, phosphorus, and the calcium/phosphorus ratio in cortical bone from the human femoral neck by neutron activation analysis. *Applied Radiation and Isotopes,* 56**,** 781-786.

ZHANG, Y., CUI, F., WANG, X., FENG, Q. & ZHU, X. 2002. Mechanical properties of skeletal bone in gene-mutated stöpsel dtl28d and wild-type zebrafish (Danio rerio) measured by atomic force microscopy-based nanoindentation. *Bone,* 30**,** 541-546.

Chapter 4

Nanomechanics and ultrastructure of the IMA adventitia in patients with low and high PWV

This chapter focusses on structural and biomechanical changes in the tunica adventitia of human IMA from patients with low and high degree of arterial stiffness. The PeakForce QNM technique that was comprehensively assessed and optimised in Chapter 3 is utilised to test the soft human tissue. The nanomechanical and structural properties of the collagen-rich tunica adventitia are characterised in ambient conditions. The morphology of adventitial collagen fibrils were subsequently analysed using a custom-made routine. Moreover, the relationship between the ultrastructural properties and the degree of arterial stiffness was assessed. Through integrating with the quantitative proteomic data, this chapter seeks to understand the underlying pathogenesis of arterial stiffening at the nano- and the molecule-level.

Abstract

The collagen-rich adventitia is the outermost arterial layer and plays an important biomechanical and physiological role in normal vessel function. While there has been a lot of effort to understand the role of the medial layer on arterial biomechanics, the adventitia has received less attention. This study hypothesised that different ultrastructural and nanomechanical properties would be exhibited in the adventitia of the IMA in patients with a low degree of arterial stiffening as compared to those with a high degree of arterial stiffening. Human IMA biopsies were obtained from a cohort of patients with arterial stiffening assessed via carotid-femoral PWV. Patients were grouped as low PWV (8.5±0.7 ms-1, n=8) and high PWV (13.4±3.0 ms-1, n=9). PeakForce QNM was used to determine the nanomechanical and morphological properties of the IMA. The nano-scale elastic modulus was found to correlate with PWV. This study shows for the first time that nano-scale alterations in adventitial collagen fibrils in the IMA are evident in patients with high PWV, even though the IMA is not involved in the carotid-femoral pathway. The approach in this study provides new insight into systematic structure-property changes in the vasculature, and also provides a method of characterising small biopsy samples to predict the development of arterial stiffening.

4.1 Introduction

Arteries are composite structures composed of three distinct layers, an inner intimal layer composed of endothelial cells, an elastin-rich medial layer and a collagen-rich external adventitial layer. Arteries stiffen as part of the natural ageing process and *in vivo* assessment of the arterial stiffening is important for clinical diagnosis. The most commonly used technique is PWV. PWV is based on recording the transit time of blood across two points in the vascular system and is considered a reliable method to determine arterial stiffness in routine clinical assessment (Laurent *et al*., 2006). Although PWV is a powerful predictor of risk of morbidity and mortality in a general population (Meaume *et al*., 2001), it does not capture the intricate and complex structural and biomechanical processes that occur in the ageing artery. Stiffness measurements derived from PWV assume that arteries are homogenous conduits, due to the inherent assumptions in the Moens-Korteweg equation on which the concept of PWV is based, although they are highly heterogeneous (Akhtar and Derby, 2015).

Arterial stiffening is associated with distinct changes across the individual layers. For example, age-related arterial stiffening is largely attributed to changes in the intima due to atherosclerosis, and degeneration of the media (Sawabe, 2010). Furthermore, within these layers, alterations can be localised to individual components at the nano- and micro- scale (Akhtar *et al*., 2016, Akhtar, 2014). Hence, to understand the mechanisms driving arterial stiffening, the nanostructure and mechanical properties of individual layers within the artery need to be considered.

Most studies which are concerned with vascular pathology or ageing have focused on the intima and medial layers of the artery whilst the adventitia has received less attention (Schulze-Bauer *et al*., 2002). The medial layer has an important biomechanical role because

during circumferential tension it bears approximately 60 % of the load (Kohn *et al*., 2015). However, the mechanical role of the adventitia in normal arterial function cannot be ignored. The adventitia is dominated by circumferentially arranged, wavy collagen fibrils (Kohn *et al*., 2015). Due to its high collagen content, the adventitia is the stiffest layer of the artery and is thought to bear around 75% of the load during longitudinal tension (Lu *et al*., 2004, Kohn *et al*., 2015). It becomes the mechanically dominant layer during high-pressure loading (Schulze-Bauer *et al*., 2002). The adventitia has also been found to exhibit differing nanomechanical and viscoelastic responses in different arteries, which is related to their *in vivo* physiological environment (Grant and Twigg, 2013). The adventitia is not only an essential structural and load-bearing layer of arteries, it also plays an important physiological role in several vascular processes including atherosclerosis (Hu *et al*., 2004) and pulmonary hypertension (El Kasmi *et al*., 2014). The adventitia also has properties of a stem/progenitor cell niche (Majesky *et al*., 2012). It has been hypothesised that the adventitia may have an important role in the ageing process due to a loss of function of niche-dependent signalling (Majesky *et al*., 2012).

Here, the PeakForce QNM (Young *et al*., 2011) was employed to investigate nano-scale properties of the adventitia in the human IMA. PeakForce QNM enables the co-localisation of ultrastructural and mechanical properties with a high resolution. This technique has been previously shown to allow detection of regional variations in the nanomechanical properties of collagen-rich tissue (Papi *et al*., 2014). This study presents both nanomechanical and ultrastructural data from the adventitia in a group of patients with known low or high PWV. The IMA can be collected during coronary by-pass operations and has already been established as a suitable model artery for generalised nonatherosclerotic arterial investigations because its matrix composition and biochemistry reflect alterations that occur in both the coronary and carotid arteries (Faarvang *et al*., 2016, Cangemi *et al*., 2011, Preil *et*

al., 2015). This study also relates the measured data to the expression of SLRPs which are involved in collagen fibril formation and have recently been found to be molecular targets for arterial stiffening (Hansen *et al*., 2015). This fundamental study offers new insight into how nano-scale changes in the adventitia are manifested in patients with a high degree of arterial stiffening. A number of studies have previously examined the specific contribution of the adventitia to the overall biomechanical properties of arteries (Hoffman *et al*., 2017, Schulze-Bauer *et al*., 2002, Holzapfel *et al*., 2005). However, there have been no previous studies which have studied the contribution of the adventitia in relation to high PWV in humans. Furthermore, there are still very limited studies on the mechanical properties of the adventitia at the nano-level (Grant and Twigg, 2013).

4.2 Materials and Methods

4.2.1 Clinical characterisation

The left IMA was collected from 17 patients during CABG operations and provided by the Centre of Individualized Medicine in Arterial Diseases (CIMA) (Odense University Hospital, Odense, Denmark), as part of a project approved by the Local Ethical Committee in Region Southern Denmark (S-2010044). The IMA is the repair artery for CABG operations. This study has made use of non-utilised IMA after the surgical procedure.

Prior to CABG, patients were assessed by carotid-femoral PWV by using the Sphygmocor system under standardised conditions as previously described in (Hansen *et al*., 2015). Clinical data, including age, gender, BMI, diabetes and hypertension were recorded before the surgery. The raw clinical data from all of the patients were kindly provided by Professor Lars Rasmussen (Odense University Hospital, Denmark). The included patients were taken

from a larger cohort (Hansen *et al*., 2015) to form two groups; low PWV (8.5 ± 0.7 ms^{-1}, n = 8 patients) and high PWV (13.4 ± 3.0 ms^{-1}, n = 9 patients), as summarised in Table 4.1. The categorisation of these patients as having 'low' and 'high' PWV are based on accepted reference and normal values for carotid-femoral PWV (Reference Values for Arterial Stiffness, 2010).

Table 4.1 Clinical parameters for IMA biopsy donors for the low (n=8) and high PWV groups (n=9). Mean and SD or percentage are provided for each parameter. Student's T-test was conducted for statistical analysis of the data. Additional data on smoking history is provided in Figure 4.11. The clinical parameter of each patient was summarised in Appendix B.

Clinical parameters	Low PWV		High PWV		*P* Value
	Mean	SD	Mean	SD	
Age, y	67.9	10.7	69.9	7	NS
BMI	26.5	4.7	28.4	4.6	NS
PWV, ms^{-1}	8.5	0.7	13.4	3	<0.001
Systolic blood pressure, mm Hg	131.3	18.7	154.1	28.6	NS
Diastolic blood pressure, mm Hg	77	10.7	79.4	12.3	NS
Male, sex, %	87.5		100		NS
Diabetes, %	12.5		0		NS
Hypertension, %	50		66.7		NS
Smoking, %	62.5		88.9		NS
Total cholesterol, $mmolL^{-1}$	4.1	0.5	4.9	1.5	NS
P-Cholesterol LDL, $mmolL^{-1}$	2.1	0.5	3.1	1.3	NS
P-Cholesterol HDL, $mmolL^{-1}$	1.2	0.1	1.1	0.3	NS
P-Triglyceride, $mmolL^{-1}$	1.6	0.6	1.6	0.5	NS
P-creatinin, $mmolL^{-1}$	89.8	19.9	91.6	20.4	NS
HbA1c	0.06	0.007	0.06	0.002	NS

4.2.2 PeakForce QNM characterisation

Immediately after surgery the IMA vessels were embedded in OCT compound (Tissue-Tek Sakura Finetek, The Netherlands) and immediately frozen at -80°C after snap freezing. The

unfixed, frozen samples were then cryosectioned to a nominal thickness of 5 μm using a Leica CM1850 cryostat (Leica Microsystems (UK) Ltd, Milton Keynes) and adhered onto glass coverslips. All the cryosections were stored in a -80°C freezer until testing. AFM imaging was conducted using the PeakForce QNM method with a MultiMode 8 AFM (NanoScope VIII MultiMode AFM, Bruker Nano Inc., Nano Surface Division, Santa Barbara, CA). Before measurement, the coverslips were mounted on metal stubs. The tissue sections were de-thawed at room temperature for 15 minutes and then washed with ultrapure water for 10 minutes to remove any excess OCT compound. Once the sample was fully dehydrated, the adventitia was imaged with AFM. All measurements were carried out at room temperature (21°C) with Bruker RTESPA-150 etched silicon probes. These probes have a nominal radius of 8 nm and a cantilever with a nominal spring constant of 5 Nm^{-1} and resonant frequency of 150 kHz. The spring constant and tip radius of the probe were calibrated prior to sample measurement. In addition, a PS1 reference sample (Vishay Precision Group, Heilbronn, Germany) with known elastic modulus was used to calibrate the elastic modulus measurements (see Chapter 3, Section 3.2.6) (Young *et al*., 2011).

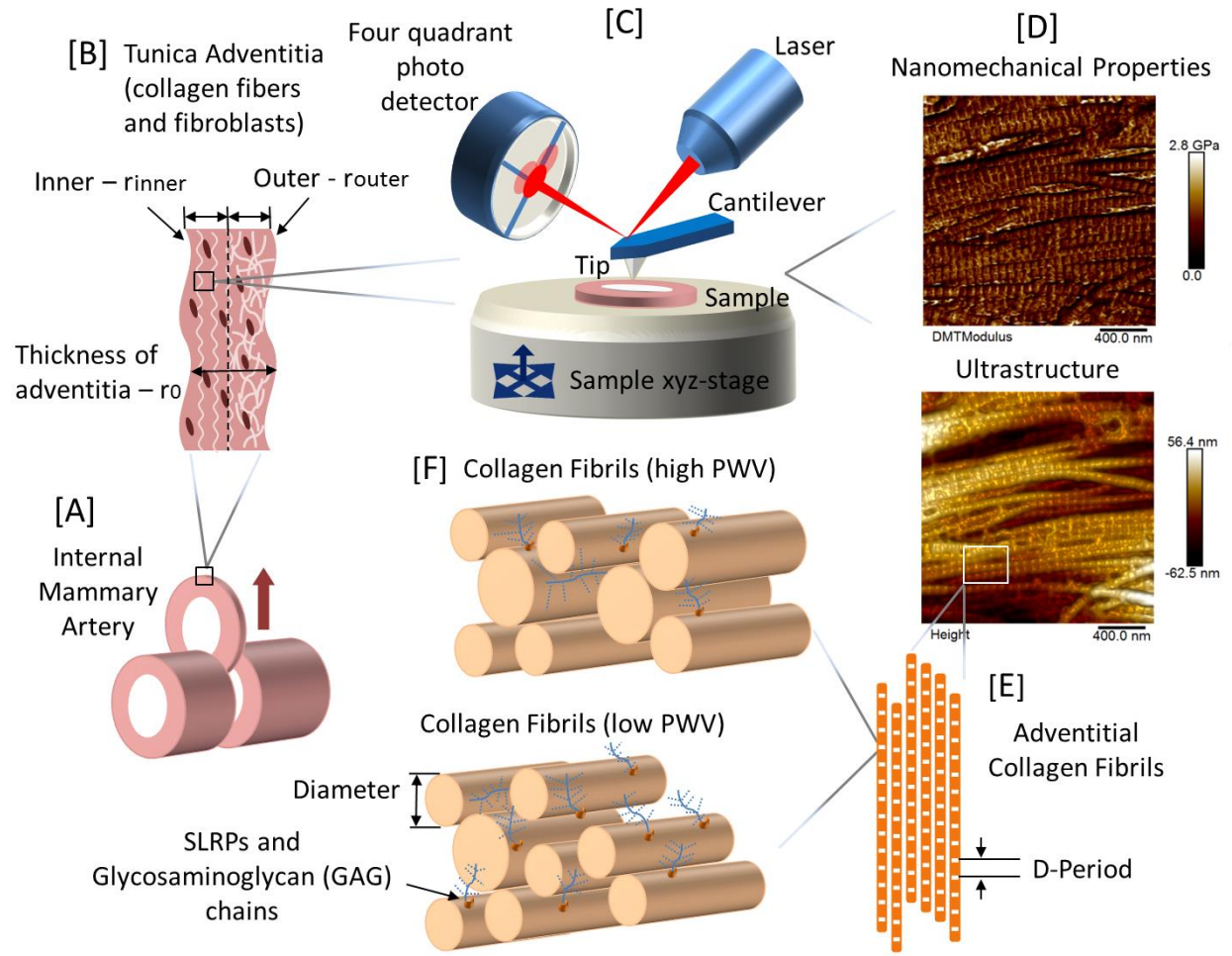

Figure 4.1 Schematic representation of the experimental approach (A) IMA sections (B) Location of adventitia for testing. Image analysis routine: (C) AFM imaging (D) Nanomechanical property measurement with PeakForce QNM (E) and (F) Collagen fibril characterisation.

Using the optical microscope integrated with the AFM setup, the inner adventitia (Figure 4.1) was identified, and the probe was placed over it prior to any testing. All testing was conducted with a scan rate of 0.93 Hz, a resolution of 256 pixels per line and with two fixed scan sizes (2 × 2 μm for mechanical and collagen morphological measurements and 5 × 5 μm for topographical observation). Along with topographical images, the PeakForce QNM method produced elastic modulus maps as described earlier. Thus, each image was composed of 65,536 measurements for mechanical property comparisons (256 × 256 independent force

curves). The indentation depth of the AFM tip into the IMA samples for all the force curves in this study was fixed around 5 nm that the ratio of the indentation depth relative to the thickness of the IMA tissue section was 0.1%. For each patient, 2 tissue sections were imaged and 3 random images were collected from each section for analysis, resulting in 6 images per patient. This added to a total of 48 and 54 images analysed for low and high PWV groups respectively. All of the raw AFM files were processed and analysed to yield the mean elastic modulus for each image with NanoScope Analysis version 1.5 (Bruker, Santa Barbara, CA). The force curves were fitted using the DMT analytical model as outlined by Young *et al.* (Young *et al.*, 2011).

4.2.3 Collagen fibril analysis

Collagen fibril diameters and D-periods were analysed using a custom routine for Image SXM (Appendix F) (Heilbronner and Barrett, 2013). Following image capture, the raw image (Figure 4.3A) was opened with Image SXM (Figure 4.3B) and a convolution filter was applied with appropriated threshold adjustment, by which the AFM image was converted to a binary black and white image. In the image, individual collagen fibril can be considered as consisting of contiguous rectangular objects in which the width and length are equivalent to the diameter and D-period of the fibril. Subsequently, several pixels were added or removed from the edges of these rectangles in the binary image to seal or dilate these rectangles for more accurate measurement, and then pixels from the edges of these rectangles were removed until they were reduced to one pixel wide skeletons (Figure 4.3C). This procedure was used to analyse over 3000 rectangles for each group (Figure 4.3D), to obtain collagen fibril diameter and D-periods. In total, 102 and 148 images were analysed in this manner for 7 patients with low PWV and 9 patients with high PWV. Images from 1 patient (patient 559) were composed of loosely packed fibrils and hence were unsuitable for the image analysis

routine which considered the fibrils as contiguous rectangular objects (see Figure 4.2). Thus, fibril morphology measurements for this patient were discarded.

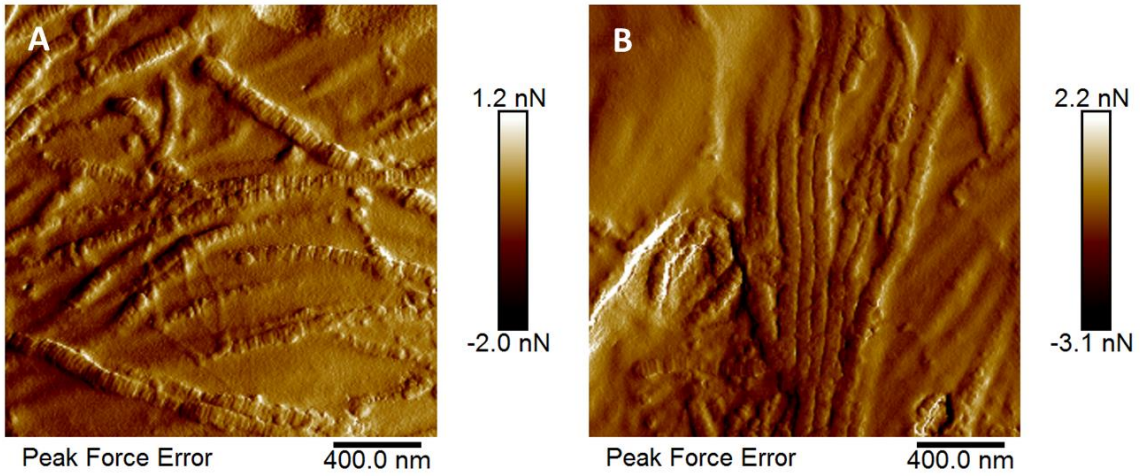

Figure 4.2 Peak Force Error AFM images (2 µm × 2 µm) of the adventitial layer of patient 559. The images were composed of loosely packed collagen fibrils and hence were unsuitable for the image analysis routine which considered the fibrils as contiguous rectangular objects.

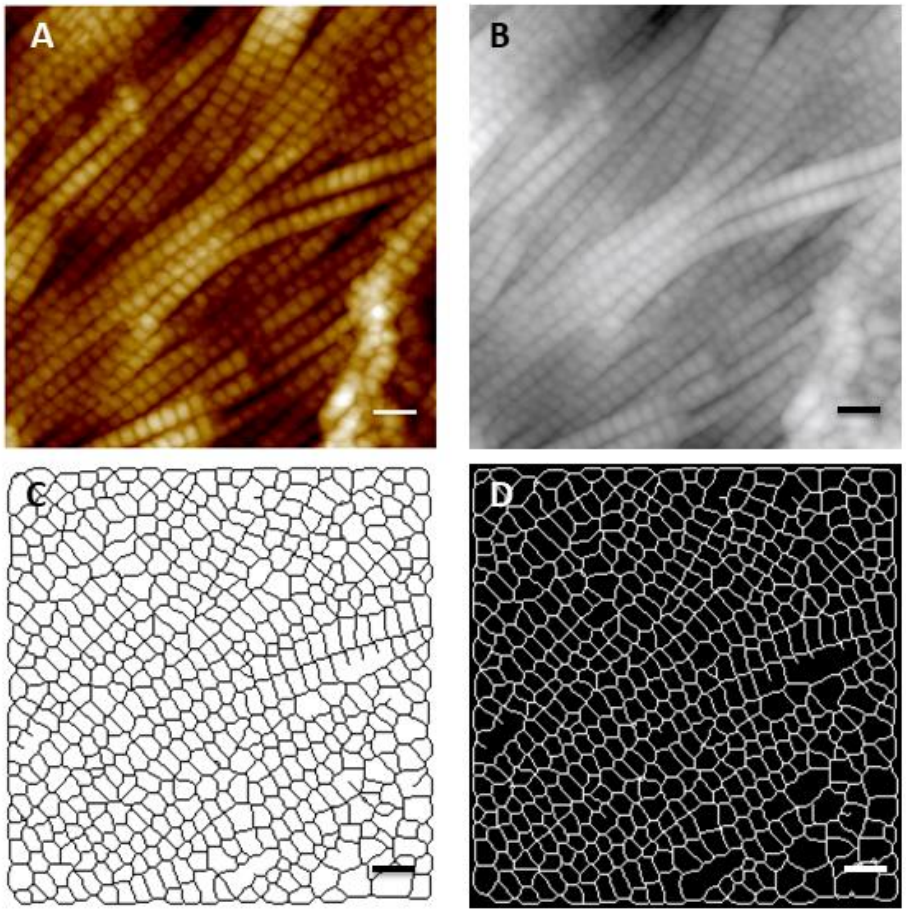

Figure 4.3 Image analysis routine: (A) Original 2 x 2 µm AFM topography image; (B) Loaded images in Image SXM; (C) Thresholded and skeletonised image; (D) Valid rectangles in the image. Scale bar represents 200 nm.

4.2.4 Histology

To ensure that the vessel did not contain atherosclerosis or other pathologies and to judge the location of the external elastic membrane and the media-adventitia border, standard histological staining was performed on frozen sections with Mason Trichrome (connective tissue stain) and Weigert's elastin staining as previously described (Preil *et al*., 2015b) (see Appendix C). The intima-media thickness was assessed from the Weigert's elastin stained images by calculating the circumference of the medial and intima rings, and then determining the difference in the radius of the two rings. These measurements were made in ImageJ (Schneider *et al*., 2012) for all 8 and 9 patients in the low and high PWV groups respectively.

4.2.5 Integration of quantitative proteomics, nanomechanical data and patient metadata

Quantitative proteomics data for some of the patient cohort analysed in this study were available from a larger cohort study published by Hansen *et al.* (Hansen *et al*., 2015). The raw data from this study were kindly provided by Professor Lars Rasmussen (Odense University Hospital, Denmark) for analysis. Full methodological data for these measurements can be found in their paper. The data available was for the 7 SLRP proteins that were found to be downregulated in the high PWV patients, namely decorin, biglycan, mimecan, lumican, prolargin, podocan and asporin. (Hansen *et al*., 2015). With the aim of integrating the nanomechanical and structural data acquired in this project with both proteomics data and patient metadata, a multivariate transformation called PCA had been used.

4.2.6 Statistical methods

All of the data are presented as mean ± SD and showed as mean ± SEM on all of the bar charts. The majority of the statistical analyses were tested using OriginPro, version 9 (OriginLab, Northampton, MA). All patient measurements were averaged prior to statistical analysis. Group differences were assessed via suitable 2-sample independent tests selected after appraisal of data normality and homoscedasticity. Patient clinical characteristics in the 2 groups were analysed with the Student's t-test. Mann-Whitney U Test was used to compare the nanomechanical properties and the morphology of adventitial collagen fibrils in low and high PWV groups. To assess for statistical significance in distributions of D-period and diameter of adventitial collagen fibrils and nanomechanical properties between the low and high PWV groups, Kolmogorov-Smirnov (K-S) tests were applied to the data. Spearman's Rank Order Correlation was used to obtain the correlation coefficient for the elastic modulus-

PWV relationship and a correlation test was used to test its significance. All statistical analyses were corrected for false discovery rate via Benjamini and Hoghberg method (Benjamini and Hochberg, 1995). Proteomics data were analysed in junction with nanomechanical variables and quantitative metadata variables (i.e. age, BMI, cholesterol and HbA1c) of all the patients via the unsupervised data transformation PCA. Patients with any missing values (reported in Table 4.2) were not included in the analysis. Data were mean centred and scaled prior to PCA analysis. The PCA analysis was performed in the statistical software R (Team, 2016).

Table 4.2 Summary of the patient numbers and subsequent tests that were conducted on tissue from each patient (n=8 and n=9 for the low and high PWV group). Nanomechanical analysis was conducted on tissue sections for each patient. Of these patients, collagen fibril diameter and D-period was determined for every patient except for 559 due to unreliable data obtained from the image analysis routine. Hence, there were 16 patients included in the collagen fibril morphology analysis (n=7 and n=9 for the low and high PWV group). The proteomics data was based on a previous study by Hansen *et al*. (2015). Hansen *et al*. collected proteomics data to determine SLRP expression for 12 of the patients included in this study (n= 6 in both the low and high PWV groups).

Patient No.	Number on PCA	Nanomechanical properties	Collagen fibril morphology	SLRPs expression
Low PWV				
522	1	Y	Y	Y
549	2	Y	Y	N
552	3	Y	Y	N
559	4	Y	N	Y
565	5	Y	Y	Y
631	6	Y	Y	Y
656	7	Y	Y	Y
693	8	Y	Y	Y
HighPWV				
524	9	Y	Y	Y
534	10	Y	Y	Y
573	11	Y	Y	N
603	12	Y	Y	Y
606	13	Y	Y	Y
620	14	Y	Y	N
627	15	Y	Y	Y
643	16	Y	Y	N
1202	17	Y	Y	Y

4.3 Results

4.3.1 Histological analysis

A histological study was undertaken on IMA vessels to assess the integrity of all tissue layers and to evaluate the presence of collagen and elastin. Representative histological sections of IMA vessels for both low and high PWV groups are shown in Figure 4.5. Collagen and elastin were present in the histological sections of both groups and the border between the media and adventitia could clearly be identified classifying these sample vessels as normal. It should be noted that the IMA is a transition artery which is typically muscular with little or no elastin, but it can have high elastin content in some individuals (Borovic *et al*., 2010a). Each of the IMA samples was characterised from the histology images and were all found to be muscular with low elastin content except for one patient in each group which had a moderate amount of elastin (see Appendix D). Example images from these two patients (patient 559 and patient 620) are presented in Figure 4.4. All histology images with Masson's collagen staining and Weigert's elastin staining for all the patients were available in Appendix C. As this study focusses on adventitial collagen, elastin content in the media was not consider a factor of influence in this study.

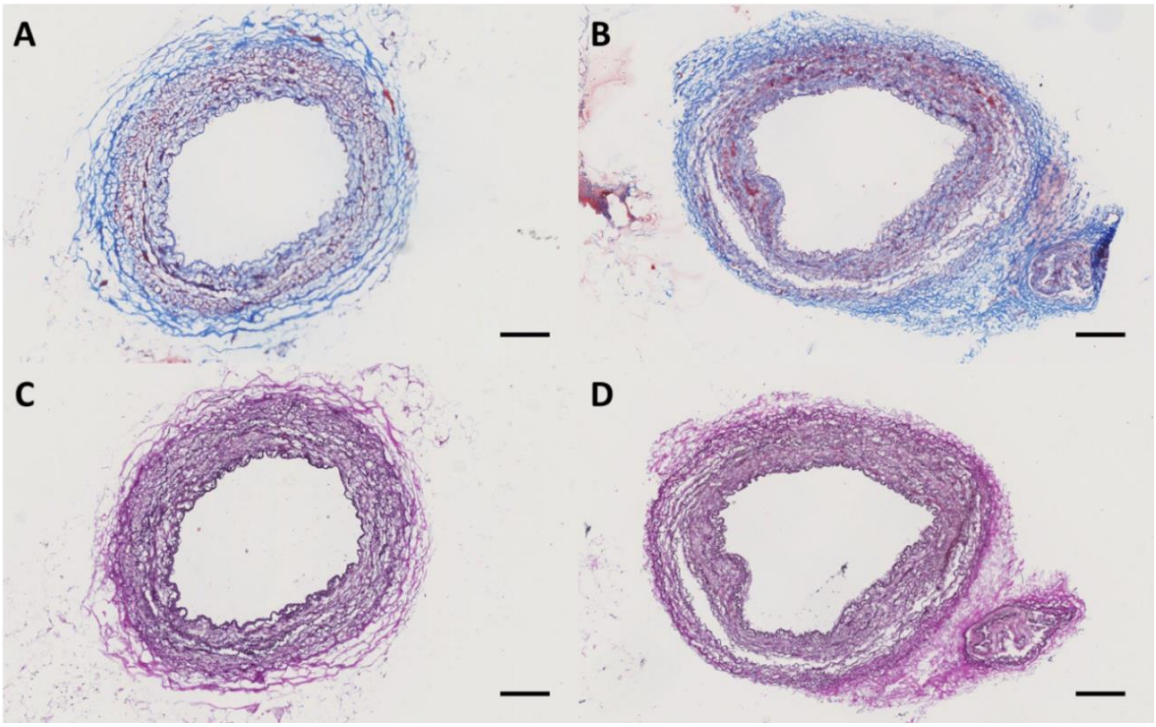

Figure 4.4 Masson's staining for collagen (A) Patient 559 and (B) Patient 620. Weigert's stain for elastin (C) Patient 559 (D) Patient 620. Both of these patients had higher levels of elastin than the others in the study. Scale bar indicated 200 µm.

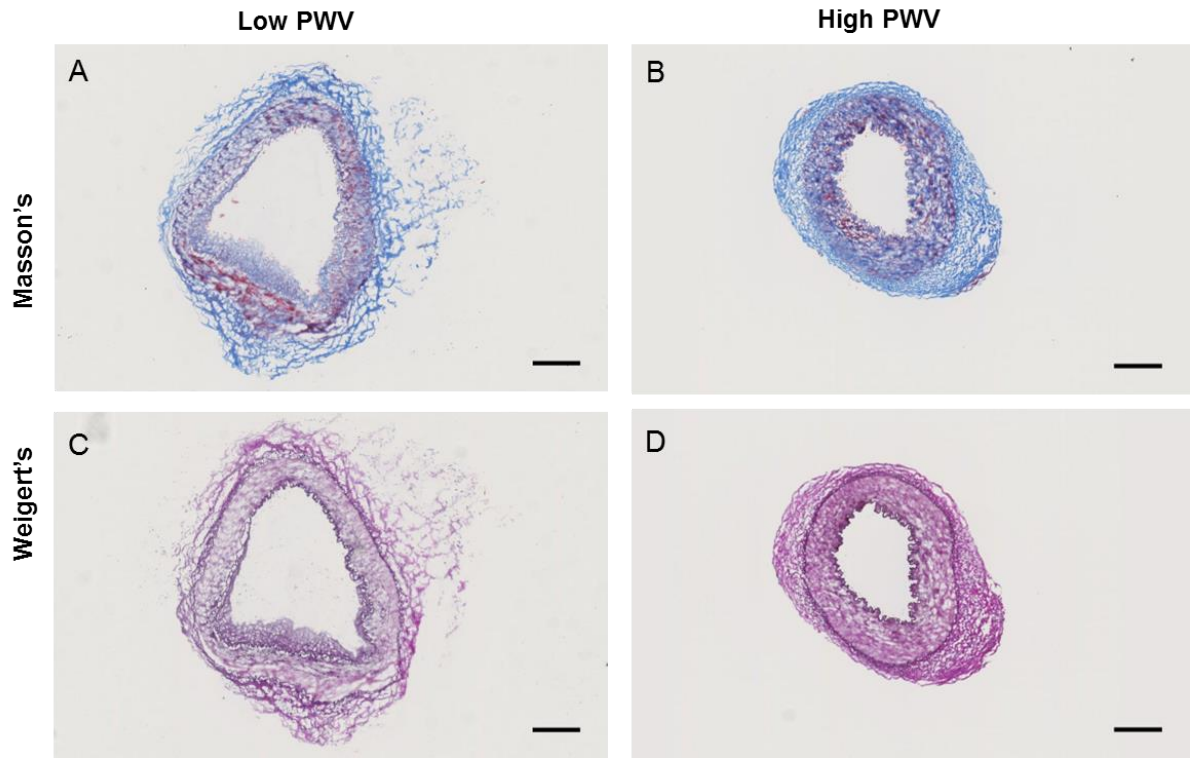

Figure 4.5 Histological sections for the IMA (A) and (B) Masson's staining for collagen in low (A) and high PWV (B) groups (C) and (D) Wiegert's staining for elastin in low (C) and high PWV (D) groups. Scale bar indicates 200 μm.

The intima-media thickness, as determined from the histology images, was 162.10 ± 78.3 μm and 209.3 ± 76.6 μm in the low and high PWV. The non-parametric Mann-Whitney U test demonstrated that there was no statistically significant difference between the two groups (p-value = 0.19).

4.3.2 Nanomechanical properties

The PeakForce QNM was used to capture high-resolution mechanical property maps along with collagen fibril morphology in the adventitia. These nano-scale measurements were compared to the clinical assessment of 'arterial stiffness' via carotid-femoral PWV. A total of 17 patients were analysed and 6 measurements were obtained for each. These were further averaged and statistical tests calculated.

The differences in elastic modulus between both groups of patients, i.e. low and high PWV (see Figures 4.6A), was tested via the non-parametric Mann-Whitney U test that resulted in a significant test (see details in Table 4.3). The different distribution of the elastic modulus measurements is shown in Figure 4.6B. A Kolmogorov-Smirnov test was performed resulting in a significant difference (p-value < 0.001) regarding elastic modulus distributions for both low and high PWV groups, indicating the significant heterogeneity at the sub-micron range for this variable. Furthermore, as shown in Figure 4.6C, Spearman's correlation between PWV and elastic modulus was calculated to be 0.56 and tested and shown to be significant (p-value = 0.02).

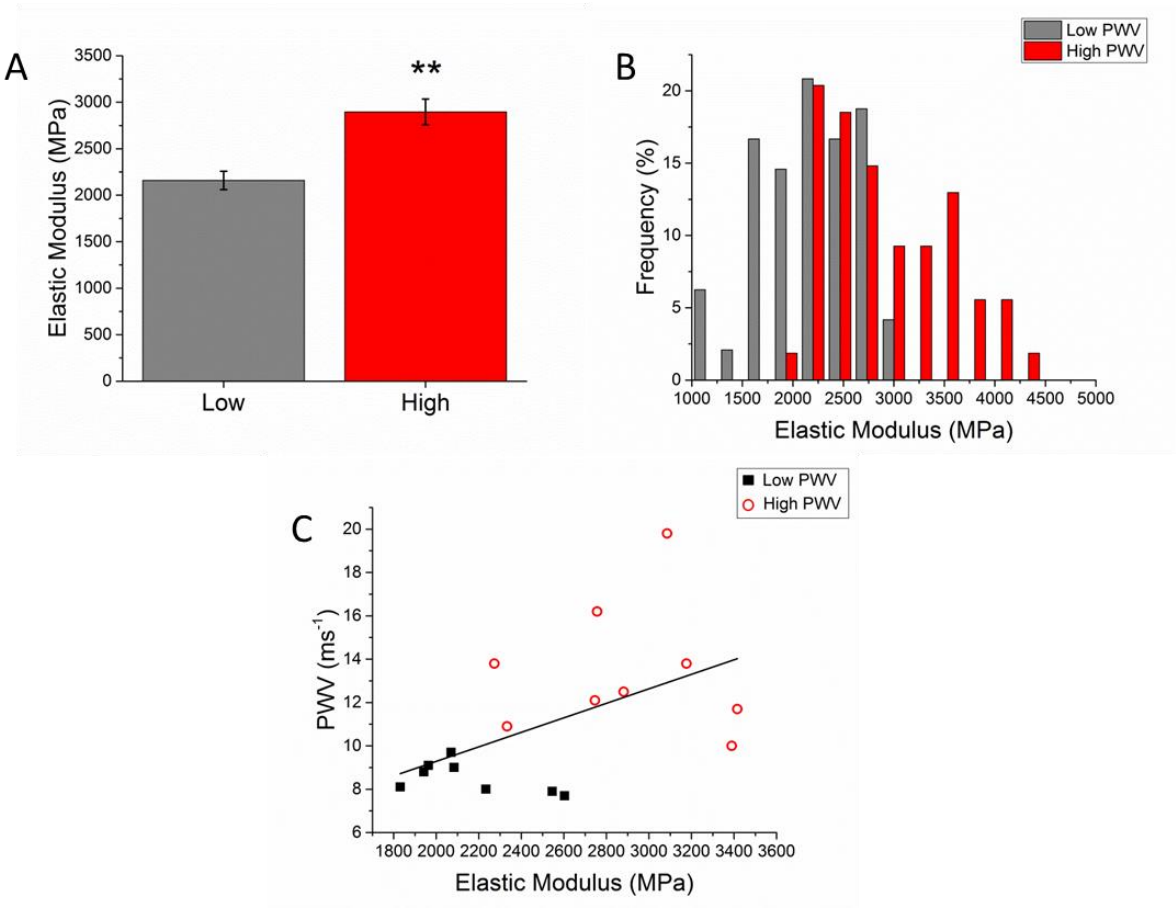

Figure 4.6 Nanomechanical properties of the adventitia for the low and high PWV group. (A) Bar graph showing mean ± SEM (n=8 and n=9 patients in the low and high group). Asterisks represent a significant difference between both groups with p-value<0.01 (B) Elastic modulus distribution in each group (n =48 and 54 measurements in the low and high PWV groups Kolmogorov-Smirnov, p<0.001). (C) A positive correlation of 0.56 between PWV and elastic modulus was found when data from both groups were pooled together (Spearman's Rank Order Correlation, p-value=0.02).

Table 4.3 Elastic modulus summary statistics. Median, mean, SD and sample size (n) for each cohort are provided for the low and high PWV groups. Results from the non-parametric Mann-Whitney U test are summarised.

Group	Elastic Modulus (MPa)			Statistical test	95% CI	p-value	Adjusted p-value
	n	Median	Mean				
Low PWV	8	2055	2159.3	Mann-Whitney	(-1154.8, -309.8)	9.8×10^{-4}	0.003
High PWV	9	2866.4	2895.2				

4.3.3 Morphology of adventitial collagen fibrils

Subsequently, the collagen fibril morphology in the adventitia for the low and high PWV groups was compared**.** Abundant collagen fibrils were observed in the adventitial layer with AFM in both groups (Figure 4.7). The collagen fibrils were found to be tightly packed and highly aligned (Figure 4.7A and 4.7B). In some instances, the fibrils were orientated transverse to the principal direction. In the smaller scan sizes (2 µm × 2 µm), the D-period and diameter of individual collagen fibrils could clearly be seen (Figure 4.7C and 4.7D). The example AFM topographical image of collagen fibrils in each patient was summarised in Appendix E.

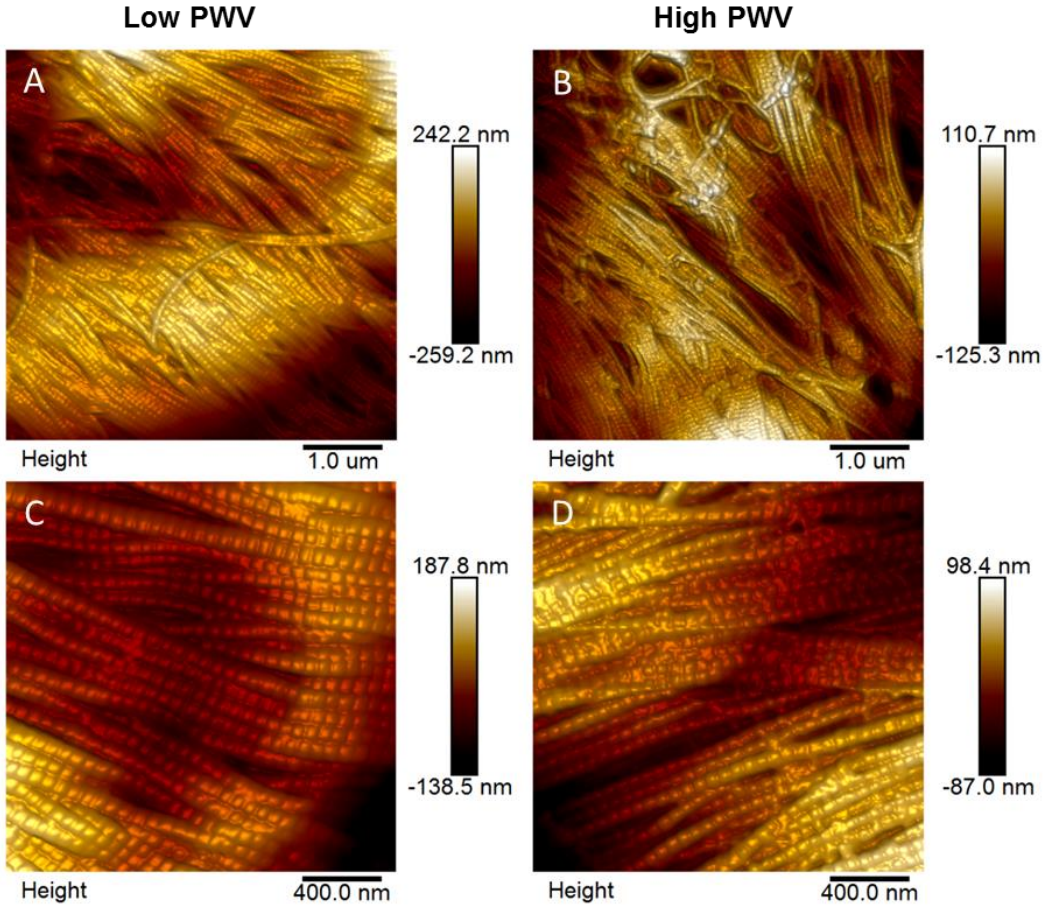

Figure 4.7 AFM topography images showing collagen fibrils in the adventitia. Example images are shown for the low (A) and high (B) PWV groups at 5 x 5 µm. Typical 2 x 2 µm images are also shown for the low (C) and high (D) PWV groups. At this scan size, individual collagen fibrils were clearly visible with their characteristic D-period.

For each of the patients, an average of 460 and 450 measurements were taken from the AFM images for collagen fibril diameter and D-period respectively. All measurement data obtained for each patient were averaged.

Collagen fibril diameters are shown in Figure 4.8. Differences in collagen fibril diameter between both groups of patients, i.e. low and high PWV (see Figures 4.8A), were tested via the non-parametric Mann-Whitney U test that resulted in a non-significant p-value (p-value = 0.8). Summary statistics are shown in Table 4.4. Despite not finding overall mean differences the low PWV patients presented a larger number of small diameter fibres than high PWV patients, e.g. 55.6 % of fibrils were < 120 nm in the low PWV group as compared to 51.4 % in the high PWV group. Consequently, the fibril size distributions were tested via a Kolmogorov-Smirnov test and a statistically significantly different was found (p-value = 0.0015). The distributions are shown in Figure 4.8B. Due to these differing distributions, the fibril diameters were further analysed by splitting the diameters into three size groups as shown in Figures 4.8C - 4.8E. The significance was determined with the Mann-Whitney test between both groups at these diameter interval: 70 - 120 nm, 120 - 150 nm and 150 - 200 nm. These subgroups were chosen as they are in agreement with previous studies focusing on collagen fibril ranges (Merrilees *et al*., 1987, Parry *et al*., 1978). The Mann-Whitney U test yielded a statistically significant difference for the 70 - 120 nm group, with the mean diameter being higher for the high PWV group (adjusted p-value = 0.049). Full details for the statistical tests can be found in Table 4.4.

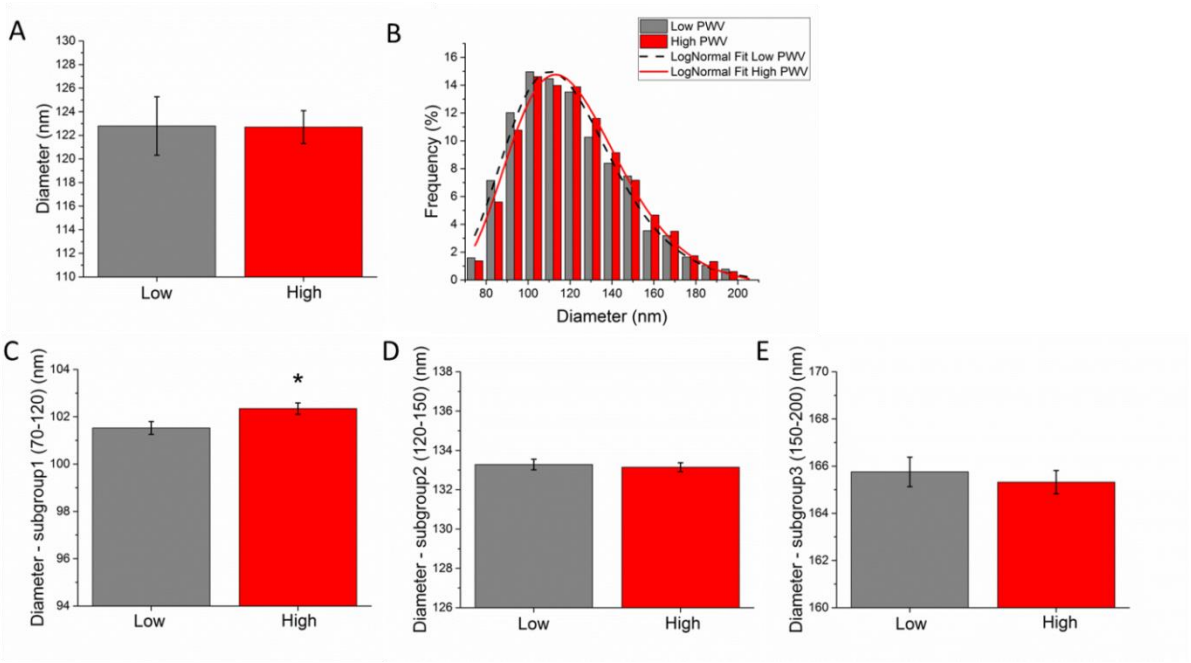

Figure 4.8 Collagen fibril diameter in the low and high PWV groups (A) Bar graph showing mean ± SEM (n=7 and n=9 patients in the low and high group) (B) Distribution of diameters in the two groups (n= 3228 and 4141 measurements in the low and high PWV groups respectively). The distributions were statistically different. (C) - (E) Diameter values shown in 3 sub-groups; 70-120 nm (C), 120-150 nm (D) and 150-200 nm. There was a statistically significant difference in the low sub-group, 70-120 nm (non-parametric Mann-Whitney U test, adj p-value=0.049).

Collagen fibril D-period data are shown in Figure 4.9 and summarised in Table 4.4. Similar to the diameter analysis, differences in collagen fibril D-period between both groups of patients, i.e. low and high PWV (Figure 4.9), were tested via the non-parametric Mann-Whitney U test that resulted in a non-significant p-value (p-value = 0.8). However, a statistically significant difference via Kolmogorov-Smirnov test was found in the D-period distribution between the two groups (p-value < 0.0001), as shown in Figure 4.9B. In the high PWV group, 36.9 % fibrils had a reduced D-period (< 59 nm) as compared to 31.8 % in the low PWV group. Furthermore, in the high PWV group, there were less fibrils with D-periods in the expected range of 59 - 70 nm (low PWV = 50.3%; high PWV = 43.3%). The expected ranges were determined from other studies (Tonniges *et al*., 2016, Fang *et al*., 2012). These differences are further highlighted in Figures 4.9C-4.9E where the D-period ranges are split

into 3 groups; 45 - 59 nm, 59 - 70 nm and 70 - 80 nm. The centre group, 59 - 70 nm covered the 'expected range' whereas the two tail groups (45 - 59 nm and 70 - 80 nm) represented those D-period values which are far from the expected values. The Mann-Whitney U Test revealed that there were statistically significant differences in the 45 - 59 nm (adjusted p-value < 0.0001) and 70 - 80 nm groups (adjusted p-value = 0.046).

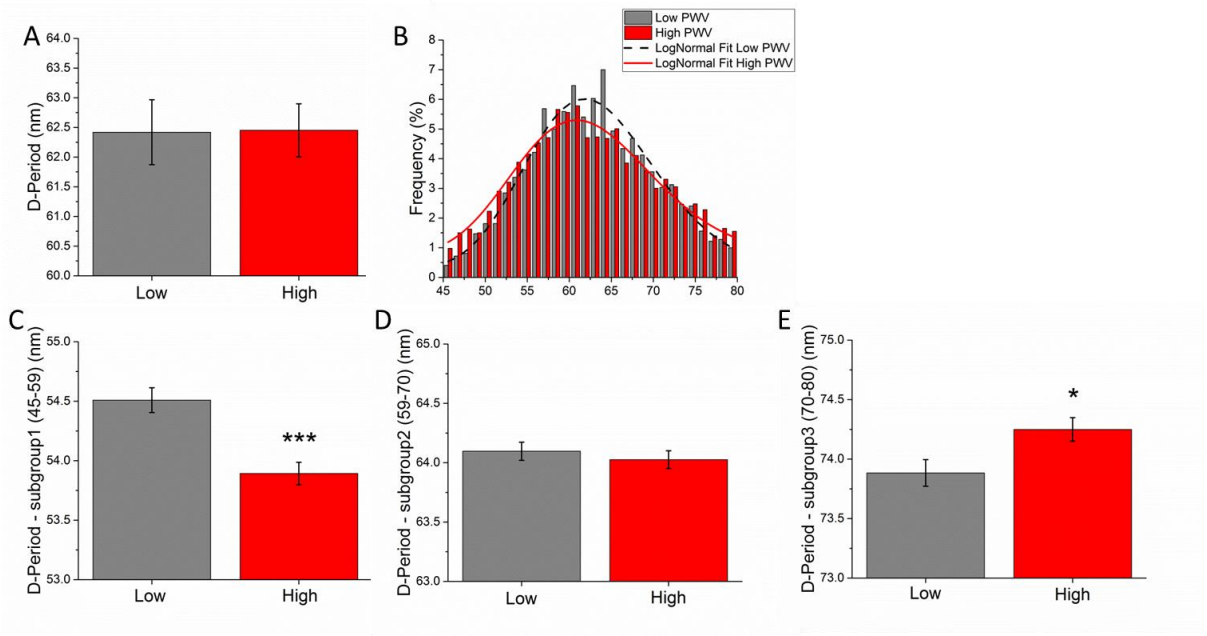

Figure 4. 9 Collagen fibril D-period in the low and high PWV groups. (A) Bar graph showing mean ± SEM (n = 7 and n = 9 patients in the low and high group) (Mann-Whitney U test, p-value = 0.8) (B) Distribution of diameters in the two groups (n = 3201 and 3994 measurements in the low and high PWV groups respectively). The distributions were statistically different (Kolmogorov-Smirnov, p-value < 0.0001). (C) - (E) D-period values shown in 3 sub-groups. There was a statistically significant difference in the low sub-group, 45 - 59 nm (Mann-Whitney U test, adj p-value < 0.0001) and also in the high sub-group, 70 - 80 nm (Mann-Whitney U test, adj p-value = 0.046).

Table 4.4 Collagen fibril diameter and D-period summary for the low and high PWV groups. Mean and SD and sample size are provided together with the results of the Mann-Whitney test for each variable.

Collagen fibril diameter							
		n	**mean**	**SD**	**95%CI**	**p-value**	**Adjusted p-value**
All	Low	7	122.8	6.6			
	High	9	122.7	4.2	(-6.41,6.81)	0.84	0.840
Subgroups (nm)		**Percentage (%)**	**mean**	**SD**			
70-120	Low	55.6	101.5	11.5	(-1.50, -0.05)	0.03	0.049
	High	51.4	102.3	11.1			
120-150	Low	30.9	133.3	8.5	(-0.55,0.82)	0.72	0.860
	High	33.7	133.1	8.5			
150-200	Low	13.5	165.7	13	(-1.16,1.28)	0.94	0.940
	High	14.9	165.3	12.2			
Collagen fibril D-period							
		n	**mean**	**SD**	**95%CI**	**p-value**	**Adjusted p-value**
All	Low	7	62.4	1.4			
	High	9	62.5	1.3	(-1.66,1.62)	0.76	0.840
Subgroups (nm)		**Percentage (%)**	**mean**	**SD**			
45-59	Low	31.8	54.5	3.3	(0.25,0.77)	$9.31x10^{-5}$	$5.58x10^{-4}$
	High	36.9	53.9	3.6			
59-70	Low	50.3	64.1	3.1	(-0.13,0.29)	0.47	0.71
	High	43.3	64	3.1			
70-80	Low	17.9	73.9	2.7	(-0.63,-0.06)	0.01	0.046
	High	19.8	74.2	2.8			

4.3.4 Principal component analysis

With the aim of studying the relations between the proteins published in Hansen *et al*. (2015) and the variables measured in this study were summarised and integrated in the multivariate transformation PCA to assess data structure as described in the methods. The score plot for this transformation is shown in Figure 4.10A where it can be appreciated that there is a difference between high and low PWV patients. The variables contributing the most to this

separation are shown in the loading plot (Figure 4.10B) where not surprisingly it can be seen that how PWV is one of the major contributors to the separation of the patients. Interestingly and in agreement with assessed data in this study, it is closely correlated with the elastic modulus. Furthermore, PCA on the data without the PWV variable shows similar separation between both high and low PWV patients and exhibits elastic modulus as one of the key variables to the separation (Figures 4.10C and 4.10D). Interestingly, D-period and collagen fibril diameter were also found to be negatively correlated. Most SLRPs were closed grouped in the PCA analysis with some differences in mimecan and biglycan. Mimecan was found to be one of the most contributing variables to the separation observed between groups. Biglycan was found closely related to collagen diameter. Additional data on smoking history is provided in Figure 4.11

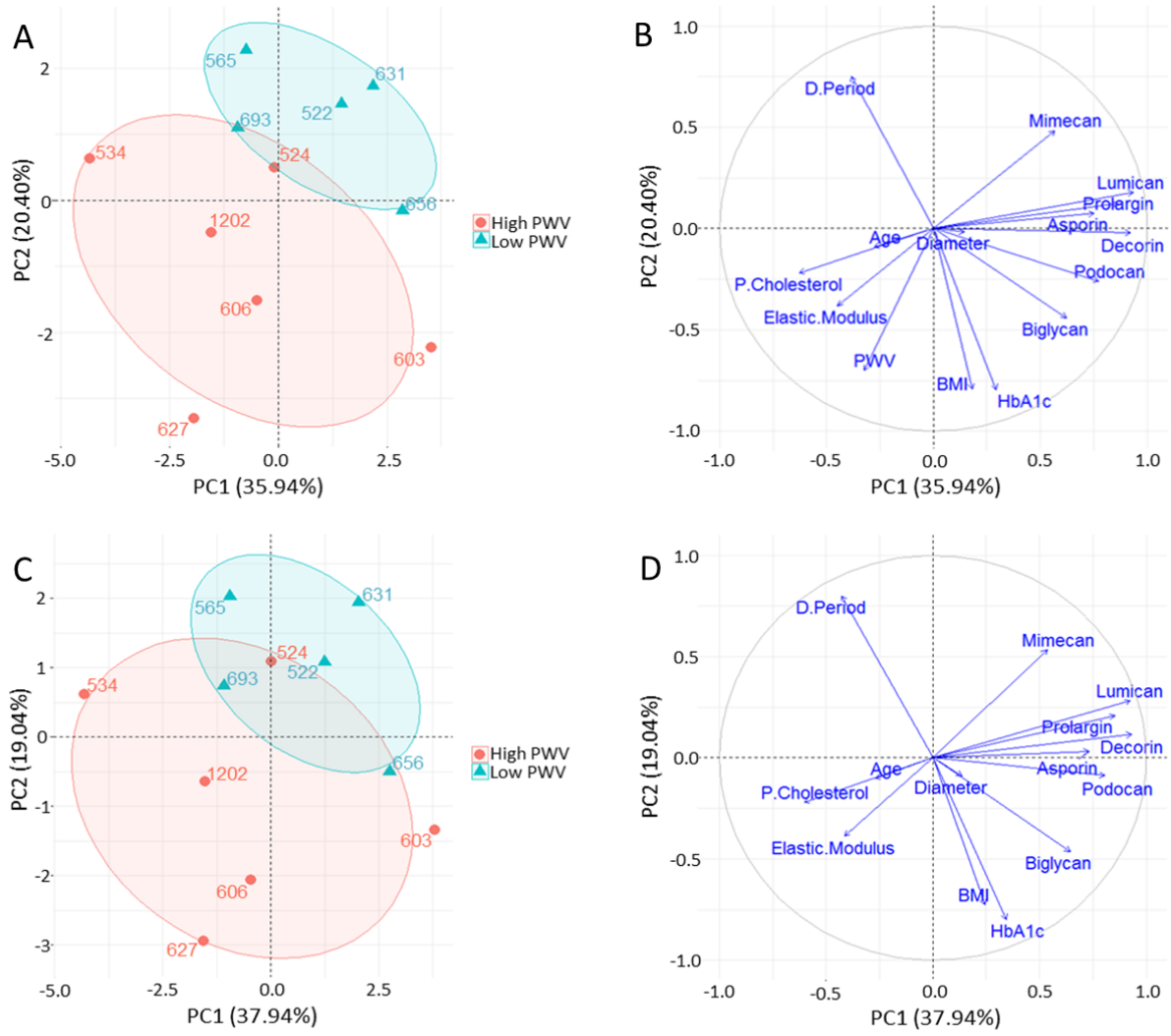

Figure 4.10 PCA of patient proteomics, quantitative metadata and nanomechanical variables. (A) Score plot of the two first principal components. Each dot represents a patient. Patients coloured by group, ellipses represent the 67% region around the mean of the points of each group. (B) Loading plot of (A) showing the variables that contribute the most to the structured observed in (A); PWV and Elastic modulus are two of the most contributing variables to the separation between both groups. (C) Score plot of the two principal components of patient data without the PWV variable. Similar separation between both groups can be observed. (D) Loading plot of (C) shows how elastic modulus is one of the most contributing variables to the separation observed. Of the SLRPs, mimecan presents the most contribution to the separation between groups observed.

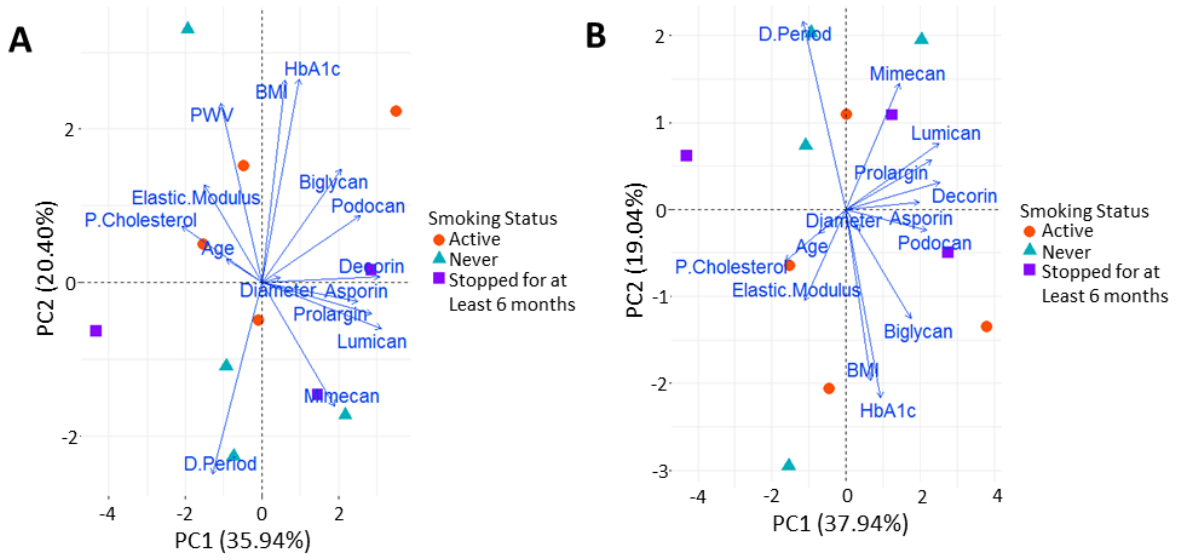

Figure 4.11 PCA plot with smoking history overlaid to the plot for each patient; (A) with PWV variable and (B) without PWV variable.

4.4 Discussion

In this study, the IMA was used as a model vessel to understand how the adventitia is altered in patients with a high degree of arterial stiffening. It is difficult to obtain aortic biopsies from arterial stiffening patients hence the IMA is essential. It is a suitable artery for *in vitro* arterial stiffening studies, since it is readily accessible as the repair artery during coronary artery bypass operations and hence it was available for this study from a well-characterised group of patients. The measure of 'arterial stiffening' used to characterise patients in this study was carotid-femoral PWV. Carotid-femoral PWV is an established measure of arterial stiffness *in vivo* and is determined from the time taken for the arterial pulse to propagate from the carotid to the femoral artery (Millasseau *et al.*, 2005). Although the stiffness of the IMA does not contribute to the carotid-femoral PWV measurement itself, it has already been shown to be a model vessel for arterial stiffening studies and reflects more systemic changes in the vasculature (Hansen *et al.*, 2015). This has also been highlighted by other studies. For

example, MMP-2 activity in the IMA has been found to be associated with age, hypertension and diabetes (Chung *et al*., 2008, Ergul *et al*., 2004). Furthermore, Fibulin-1, an important ECM protein involved in matrix organisation, has been found to accumulate in the wall of the IMA of patients with type 2 diabetes (Cangemi *et al*., 2011). Hence, each of these studies demonstrates that ECM changes in the IMA reflect generalised arterial alterations related to vascular stiffness, diabetes and other risk factors.

4.4.1 Nanomechanics of the adventitia

All previous studies that have utilised the IMA as a target to understand systemic changes associated with CVDs have reported global data for the IMAs e.g. with the use of destructive biochemical methods that do not discriminate across the different layers of the vessel (Hansen *et al*., 2015) or with measurements across the intima-media layers (Cangemi *et al*., 2011). Given that the IMA is now an established model for vascular disease, this study sought to focus on the role of the IMA adventitia in arterial stiffening. Grant and Twigg (Grant and Twigg, 2013) demonstrated that the nanomechanical and viscoelastic properties of the adventitia of the porcine aorta and pulmonary artery exhibit distinct differences which are in line with their functional properties. This study now demonstrates that the nanomechanical properties of the IMA adventitia can help discriminate between distinct patient cohorts. Specifically, the nanomechanical data demonstrate that the IMA adventitia exhibits different mechanical properties at the level of individual collagen fibrils in patients with low PWV as compared to those with elevated PWV. The changes are manifested as localised stiffness increases in the adventitia in high PWV patients, as determined with AFM, and by ultrastructural changes (see 4.2 and 4.3). Downregulation of certain SLRPs has been previously found in the IMA occurs in patients with high PWV (Hansen *et al*., 2015). Downregulation of SLRPs is particularly relevant for the adventitia because SLRPs are

involved collagen fibril formation (Chen and Birk, 2013, Kalamajski and Oldberg, 2010). Collagen fibril morphology is discussed further in the following sections.

4.4.2 Collagen fibril diameter

This study focused on the inner adventitia and the resulting fibril diameters are in agreement with the work of Merrilees *et al*. (Merrilees *et al*., 1987) in which they report the mean-fibril diameter ranges from 50 to 100 nm in the adventitia of arteries from human, pig and rat. Merrilees *et al*. observed that artery collagen fibril diameters were inversely correlated with GAG levels. Furthermore, they suggested that fibril diameters serve as excellent markers for determining GAG levels in samples which are too small to sample biochemically. Fibril/proteoglycan interactions are responsible for stress transfer within the ECM and are altered with changes in fibril diameters (Goh *et al*., 2012). Our PCA analysis hints at a complex interaction between collagen diameter and SLRPs. Biglycan and collagen diameter are relatively correlated but they have a different direction in space with respect to lumican, prolargin, decorin, asporin and podocan. The important role of biglycan and decorin in governing collagen fibril structure has been highlighted in a study on a compound knockout model of mouse tendon (i.e. both biglycan and decorin) where there was a shift to larger diameter fibrils and also a shift in the diameter distribution (Robinson *et al*., 2017).

The main difference in fibril diameter between low and high PWV groups that observed in this study was a different distribution of the collagen fibril diameters with high PWV patients showing less fibrils with small diameters (70 - 120 nm). Although there have been previous studies that have reported collagen fibril diameters in arteries (Merrilees *et al*., 1987, Tzaphlidou and Berillis, 2004), little is known about how collagen fibril diameters change in vascular tissue with ageing or with vascular stiffening. Current most developed understanding of the role of collagen fibril diameter in tissue biomechanics arises from studies on rat tail

tendon. An important study in this area is the work by Goh *et al*. (Goh *et al*., 2012). They developed a strain energy modelling approach to understand how collagen fibril diameter contributes to tendon resilience and resistance to failure. They suggested that their findings may have broader applicability to other connective tissues including vascular tissues. The Goh *et al*. model demonstrates that fibril size is related to strain energy density and that failure of the ECM is more likely to occur with smaller fibril diameters. This is because fracture is easier due to lower strain energy being absorbed; an increase in large diameter fibrils with a decrease in smaller diameter fibrils contributes to an increase in strain energy density. This is the trend that was found in the high PWV group. Hence, it was speculated that this change in fibril distribution, especially in small diameter collagen fibrils (< 120 nm), serves as a protective mechanism i.e. this provides resilience and resistance to the vessel as a response to wider pulse pressure and higher cardiac load associated with arterial stiffening.

The limitations of the Goh *et al*. model for tendon work are that the rat tail tendon is not weight-bearing and may be influenced by systemic effects of ageing (Goh *et al*., 2012). However, these are not limitations when applied to the IMA due to the reasons stated earlier; the IMA does not contribute to carotid-femoral PWV, and it is also affected by systemic effects in the vasculature.

4.4.3 Collagen fibril D-period

Collagen fibril D-period is typically reported during *in situ* loading for soft tissues e.g. (Inamdar *et al*., 2017) where the D-period provides an indication of collagen fibril strain during loading. Very small changes in D-period provide an essential indication of the internal stress state within a tissue. For example, a decrease of approximately 1 nm has been associated with enzymatic degradation of cartilage tissue, and a decrease of 0.2 nm (Inamdar

et al., 2017) was related to significant internal stress *in vivo* on the collagen network in corneal tissue (Bell *et al*., 2018).

D-period measurements have also been reported in the literature to compare different tissue types. For example, AFM has been used to characterise differences in D-period in the cornea and sclera for both mouse (Miyagawa *et al*., 2000) and human (Miyagawa *et al*., 2001) tissues. In these studies, the D-period in the sclera was found to be 3.3 nm and 2.4 nm lower than the cornea for the mouse and human respectively. These differences are thought to be related to differing ECM arrangements in the two types of tissue, for example, related to differences in proteoglycans and GAGs surrounding the collagen fibrils.

More recently, a number of studies have shown that collagen D-period distributions change as a function of disease, as reviewed by Chen *et al*. (Chen *et al*., 2017). This study also indicated statistically significant differences in the D-period distribution in the low and high PWV groups. This motivated us to analyse the data further by splitting the D-period measurements into three groups hence allowing us to clearly identify the trends in D-period beyond the expected range (59 - 70 nm) (Tonniges *et al*., 2016, Fang *et al*., 2012). It can be noticed that the most significant difference between the low and high PWV groups was found in the low D-period range (45 - 59 nm) and the high D-period range (70-80 nm), as shown in Figure 4.9C and 4.9E. Although it is now clear from this study and others (Chen *et al*., 2017) that heterogeneity present in the collagen D-period appears to be important for understanding tissue properties and function, there is still a gap in the understanding about why these changes occur.

To date, there are limited studies on collagen fibril D-period in vascular tissues. However, a recent study on a mouse model of abdominal aortic aneurysms used D-period measurements from AFM and TEM to investigate whether there was a difference in collagen fibril ‘quality’

in AAA tissue relative to controls (Tonniges *et al*., 2016). AFM revealed much more variability in the AAA tissue and TEM revealed statistically significant differences relative to controls. Hence, the collagen D-period serves as a good indicator of changes within the tissue's local environment.

It should be noted that the AFM image analysis routine in this study enabled a large dataset for D-period to be determined whereas previous studies utilising AFM have been limited by manual measurements on a small number of images e.g. (Miyagawa *et al*., 2001).

4.5 Limitations

This study provides valuable insight into the utility of the IMA for arterial stiffening investigations, however there are a number of limitations which should be addressed. Firstly, although this study compares the mechanical properties of the IMA with carotid-femoral PWV it has to be acknowledged that the IMA is not involved in carotid-femoral PWV pathway and this work does not provide a mechanistic link between the two. Secondly, due to the number of different tests that were conducted on the IMA samples in parallel studies it was not possible to compare the AFM data with established functional biomechanical tests such as wire or pressure myography. Thirdly, the study only focusses on adventitial collagen, whilst other studies on the IMA (including the prior proteomics work) are based on measurements across the entire vessel i.e. intima-adventitia. Future studies would benefit from accompanying data on the medial layer. Fourthly, this study was not able to provide any histological quantification of collagen content which would have complemented the AFM work. Fifthly, alterations in other molecular components of the adventitia may be contributing to elastic modulus differences that this study found. However, such studies are beyond the scope of the present work. Finally, this study was limited by a sample size of

seventeen patients. However, it is still a larger sample size than other relevant adventitial biomechanics studies where samples sizes of six (Hoffman *et al*., 2017), eleven (Schulze-Bauer *et al*., 2002) and thirteen (Holzapfel *et al*., 2005) have been reported for example.

4.6 Conclusions

The adventitia is an important layer of arteries in terms of both biomechanics and physiology of blood vessels, but in terms of arterial stiffening it has received little attention relative to the medial layer. This study on adventitial nanomechanics in the IMA compares patients with low and high PWV. This chapter has shown that the IMA is an ideal vessel for nano-scale *in vitro* experimentation because it is readily accessible during coronary artery bypass operations, and appears to reflect changes across the vasculature although it is not an elastic vessel and hence does not contribute to PWV measurements. This study found that the nanomechanical properties of the adventitia correlated with clinical assessment of arterial stiffness (via carotid-femoral PWV) and also downregulation of extracellular proteins that have already been shown to be associated with arterial stiffness. Interestingly, these extracellular proteins (SLRPs) are known to be involved in collagen fibrillogenesis (Hansen *et al*., 2015) and the ultrastructural properties of the adventitial collagen fibrils differed in the low and high PWV groups. In this work, the extensive dataset on collagen fibril diameter and D-period served as a suitable method for detecting alterations in the local adventitial environment. The findings obtained from this study highlight the important role of the adventitia in arterial stiffening and the suitability of the IMA as a target vessel for biomechanical studies. This study suggests that measurements of collagen fibril diameter and D-period are excellent nano-scale markers for assessing collagen fibril and adventitial ‘quality’ in pathology. The approach in this study provides a method of characterising small

biopsy samples to predict the development of arterial stiffening. This will be an invaluable approach for future studies developing new therapeutic targets for tackling arterial stiffening.

References

AKHTAR, R. 2014. In vitro characterisation of arterial stiffening: From the macro-to the nano-scale. *Artery Research,* 8**,** 1-8.

AKHTAR, R. & DERBY, B. 2015. *Mechanical Properties of Aging Soft Tissues*.

AKHTAR, R., GRAHAM, H. K., DERBY, B., SHERRATT, M. J., TRAFFORD, A. W., CHADWICK, R. S. & GAVARA, N. 2016. Frequency-modulated atomic force microscopy localises viscoelastic remodelling in the ageing sheep aorta. *Journal of the Mechanical Behavior of Biomedical Materials,* 64**,** 10-17.

BELL, J. S., HAYES, S., WHITFORD, C., SANCHEZ-WEATHERBY, J., SHEBANOVA, O., VERGARI, C., WINLOVE, C. P., TERRILL, N., SORENSEN, T., ELSHEIKH, A. & MEEK, K. M. 2018. The hierarchical response of human corneal collagen to load. *Acta Biomater,* 65**,** 216-225.

BENJAMINI, Y. & HOCHBERG, Y. 1995. Controlling the False Discovery Rate - a Practical and Powerful Approach to Multiple Testing. *Journal of the Royal Statistical Society Series B-Methodological,* 57**,** 289-300.

BOROVIC, M. L., BOROVIC, S., PERIC, M., VUKOVIC, P., MARINKOVIC, J., TODOROVIC, V., RADAK, D. & LACKOVIC, V. 2010. The internal thoracic artery as a transitional type of artery: a morphological and morphometric study. *Histol Histopathol,* 25**,** 561-76.

CANGEMI, C., SKOV, V., POULSEN, M. K., FUNDER, J., TWAL, W. O., GALL, M.-A., HJORTDAL, V., JESPERSEN, M. L., KRUSE, T. A., AAGARD, J., PARVING, H.-H., KNUDSEN, S., HøILUND-CARLSEN, P.-F., ROSSING, P., HENRIKSEN, J. E., ARGRAVES, W. S. & RASMUSSEN, L. M. 2011. Fibulin-1 is a marker for arterial extracellular matrix alterations in type 2 diabetes. *Clinical chemistry,* 57**,** 1556-65.

CHEN, J., AHN, T., COLON-BERNAL, I. D., KIM, J. & BANASZAK HOLL, M. M. 2017. The Relationship of Collagen Structural and Compositional Heterogeneity to Tissue Mechanical Properties: A Chemical Perspective. *ACS Nano,* 11**,** 10665-10671.

CHEN, S. & BIRK, D. E. 2013. The regulatory roles of small leucine-rich proteoglycans in extracellular matrix assembly. *The FEBS journal,* 280**,** 2120-2137.

CHUNG, A. W., BOOTH, A. D., ROSE, C., THOMPSON, C. R., LEVIN, A. & VAN BREEMEN, C. 2008. Increased matrix metalloproteinase 2 activity in the human internal mammary artery is associated with ageing, hypertension, diabetes and kidney dysfunction. *Journal of Vascular Research,* 45**,** 357-362.

EL KASMI, K. C., PUGLIESE, S. C., RIDDLE, S. R., POTH, J. M., ANDERSON, A. L., FRID, M. G., LI, M., PULLAMSETTI, S. S., SAVAI, R. & NAGEL, M. A. 2014. Adventitial fibroblasts induce a distinct proinflammatory/profibrotic macrophage phenotype in pulmonary hypertension. *The Journal of Immunology,* 193**,** 597-609.

ERGUL, A., PORTIK-DOBOS, V., HUTCHINSON, J., FRANCO, J. & ANSTADT, M. P. 2004. Downregulation of vascular matrix metalloproteinase inducer and activator proteins in hypertensive patients. *American Journal of Hypertension,* 17**,** 775-782.

FAARVANG, A. S. A., RøRDAM PREIL, S. A., NIELSEN, P. S., BECK, H. C., KRISTENSEN, L. P. & RASMUSSEN, L. M. 2016. Smoking is associated with lower amounts of arterial type I collagen and decorin. *Atherosclerosis,* 247**,** 201-206.

FANG, M., GOLDSTEIN, E. L., TURNER, A. S., LES, C. M., ORR, B. G., FISHER, G. J., WELCH, K. B., ROTHMAN, E. D. & BANASZAK HOLL, M. M. 2012. Type I collagen D-spacing in fibril bundles of dermis, tendon, and bone: bridging between nano- and micro-level tissue hierarchy. *ACS Nano,* 6**,** 9503-14.

GOH, K. L., HOLMES, D., LU, Y., PURSLOW, P. P., KADLER, K., BéCHET, D. & WESS, T. J. 2012. Bimodal collagen fibril diameter distributions direct age-related variations

in tendon resilience and resistance to rupture. *Journal of applied physiology,* 113**,** 878-888.

GRANT, C. A. & TWIGG, P. C. 2013. Pseudostatic and dynamic nanomechanics of the tunica adventitia in elastic arteries using atomic force microscopy. *ACS nano,* 7**,** 456-64.

HANSEN, M. L., BECK, H. C., IRMUKHAMEDOV, A., JENSEN, P. S., OLSEN, M. H. & RASMUSSEN, L. M. 2015. Proteome analysis of human arterial tissue discloses associations between the vascular content of small leucine-rich repeat proteoglycans and pulse wave velocity. *Arteriosclerosis, thrombosis, and vascular biology***,** ATVBAHA. 114.304706.

HEILBRONNER, R. & BARRETT, S. 2013. *Image Analysis in Earth Sciences: Microstructures and Textures of Earth Materials*, Springer Science & Business Media.

HOFFMAN, A. H., TENG, Z., ZHENG, J., WU, Z., WOODARD, P. K., BILLIAR, K. L., WANG, L. & TANG, D. 2017. Stiffness Properties of Adventitia, Media, and Full Thickness Human Atherosclerotic Carotid Arteries in the Axial and Circumferential Directions. *Journal of biomechanical engineering,* 139**,** 124501.

HOLZAPFEL, G. A., SOMMER, G., GASSER, C. T. & REGITNIG, P. 2005. Determination of layer-specific mechanical properties of human coronary arteries with nonatherosclerotic intimal thickening and related constitutive modeling. *American Journal of Physiology-Heart and Circulatory Physiology*, 289**,** H2048-H2058.

HU, Y., ZHANG, Z., TORSNEY, E., AFZAL, A. R., DAVISON, F., METZLER, B. & XU, Q. 2004. Abundant progenitor cells in the adventitia contribute to atherosclerosis of vein grafts in ApoE-deficient mice. *Journal of Clinical Investigation,* 113**,** 1258.

INAMDAR, S. R., KNIGHT, D. P., TERRILL, N. J., KARUNARATNE, A., CACHO-NERIN, F., KNIGHT, M. M. & GUPTA, H. S. 2017. The Secret Life of Collagen:

Temporal Changes in Nanoscale Fibrillar Pre-Strain and Molecular Organization During Physiological Loading of Cartilage. *ACS nano*.

KALAMAJSKI, S. & OLDBERG, Å. 2010. The role of small leucine-rich proteoglycans in collagen fibrillogenesis. *Matrix Biology,* 29**,** 248-253.

KOHN, J. C., LAMPI, M. C. & REINHART-KING, C. A. 2015. Age-related vascular stiffening: causes and consequences. *Frontiers in genetics,* 6.

LAURENT, S., COCKCROFT, J., VAN BORTEL, L., BOUTOUYRIE, P., GIANNATTASIO, C., HAYOZ, D., PANNIER, B., VLACHOPOULOS, C., WILKINSON, I. & STRUIJKER-BOUDIER, H. 2006. Expert consensus document on arterial stiffness: Methodological issues and clinical applications. *European Heart Journal,* 27**,** 2588-2605.

LU, X., PANDIT, A. & KASSAB, G. S. 2004. Biaxial incremental homeostatic elastic moduli of coronary artery: two-layer model. *American Journal of Physiology-Heart and Circulatory Physiology,* 287**,** H1663-H1669.

MAJESKY, M. W., DONG, X. R., HOGLUND, V., DAUM, G. & MAHONEY JR, W. M. 2012. The adventitia: a progenitor cell niche for the vessel wall. *Cells Tissues Organs,* 195**,** 73-81.

MEAUME, S., BENETOS, A., HENRY, O. F., RUDNICHI, A. & SAFAR, M. E. 2001. Aortic Pulse Wave Velocity Predicts Cardiovascular Mortality in Subjects >70 Years of Age. *Arteriosclerosis, Thrombosis, and Vascular Biology,* 21**,** 2046-2050.

MERRILEES, M. J., TIANG, K. M. & SCOTT, L. 1987. Changes in Collagen Fibril Diameters Across Artery Walls Including a Correlation with Glycosaminoglycan Content. *Connective tissue research,* 16**,** 237-257.

MILLASSEAU, S. C., STEWART, A. D., PATEL, S. J., REDWOOD, S. R. & CHOWIENCZYK, P. J. 2005. Evaluation of Carotid-Femoral Pulse Wave Velocity. *Hypertension,* 45**,** 222-226.

MIYAGAWA, A., KOBAYASHI, M., FUJITA, Y., HAMDY, O., HIRANO, K., NAKAMURA, M. & MIYAKE, Y. 2001. Surface ultrastructure of collagen fibrils and their association with proteoglycans in human cornea and sclera by atomic force microscopy and energy-filtering transmission electron microscopy. *Cornea,* 20**,** 651-656.

MIYAGAWA, A., KOBAYASHI, M., FUJITA, Y., NAKAMURA, M., HIRANO, K., KOBAYASHI, K. & MIYAKE, Y. 2000. Surface topology of collagen fibrils associated with proteoglycans in mouse cornea and sclera. *Japanese journal of ophthalmology,* 44**,** 591-595.

PAPI, M., PAOLETTI, P., GERAGHTY, B. & AKHTAR, R. 2014. Nanoscale characterization of the biomechanical properties of collagen fibrils in the sclera. *Applied Physics Letters,* 104.

PARRY, D. A., BARNES, G. R. & CRAIG, A. S. 1978. A comparison of the size distribution of collagen fibrils in connective tissues as a function of age and a possible relation between fibril size distribution and mechanical properties. *Proc R Soc Lond B Biol Sci,* 203**,** 305-21.

PREIL, S. A. R., KRISTENSEN, L. P., BECK, H. C., JENSEN, P. S., NIELSEN, P. S., STEINICHE, T., BJ??RLING-POULSEN, M., LARSEN, M. R., HANSEN, M. L. & RASMUSSEN, L. M. 2015. Quantitative Proteome Analysis Reveals Increased Content of Basement Membrane Proteins in Arteries from Patients with Type 2 Diabetes Mellitus and Lower Levels among Metformin Users. *Circulation: Cardiovascular Genetics,* 8**,** 727-735.

REFERENCE VALUES FOR ARTERIAL STIFFNESS, C. 2010. Determinants of pulse wave velocity in healthy people and in the presence of cardiovascular risk factors: 'establishing normal and reference values'. *Eur Heart J,* 31**,** 2338-50.

ROBINSON, K. A., SUN, M., BARNUM, C. E., WEISS, S. N., HUEGEL, J., SHETYE, S. S., LIN, L., SAEZ, D., ADAMS, S. M., IOZZO, R. V., SOSLOWSKY, L. J. & BIRK, D. E. 2017. Decorin and biglycan are necessary for maintaining collagen fibril structure, fiber realignment, and mechanical properties of mature tendons. *Matrix Biol,* 64**,** 81-93.

SAWABE, M. 2010. Vascular aging: from molecular mechanism to clinical significance. *Geriatrics & gerontology international,* 10.

SCHNEIDER, C. A., RASBAND, W. S. & ELICEIRI, K. W. 2012. NIH Image to ImageJ: 25 years of image analysis. *Nat Methods,* 9**,** 671-5.

SCHULZE-BAUER, C. A., REGITNIG, P. & HOLZAPFEL, G. A. 2002. Mechanics of the human femoral adventitia including the high-pressure response. *American Journal of Physiology-Heart and Circulatory Physiology,* 282**,** H2427-H2440.

TEAM, R. C. 2016. R: A language and environment for statistical computing. R Foundation for Statistical Computing, Vienna, Austria. 2014.

TONNIGES, J. R., ALBERT, B., CALOMENI, E., HANS, C. & AGARWAL, G. 2016. Ultrastructural Imaging of Collagen Fibrils in Mouse Model of Abdominal Aortic Aneurysm. *Microscopy and Microanalysis,* 22**,** 1196.

TZAPHLIDOU, M. & BERILLIS, P. 2004. Effect of lithium administration on collagen and breaking pressure of the rat thoracic descending aorta. *The Journal of Trace Elements in Experimental Medicine,* 17**,** 151-160.

YOUNG, T. J., MONCLUS, M. A., BURNETT, T. L., BROUGHTON, W. R., OGIN, S. L. & SMITH, P. A. 2011. The use of the PeakForce TM quantitative nanomechanical

mapping AFM-based method for high-resolution Young's modulus measurement of polymers. *Measurement Science and Technology,* 22**,** 125703-125703.

Chapter 5

Characterisation of ultrastructural changes in the medial layer of the IMA in patients with arterial stiffening

---

This chapter builds on the work presented in Chapter 4. In this chapter, the tunica media of the IMA is tested with PeakForce QNM for the same samples that were used for the adventitial work presented in Chapter 4. This chapter compares the tunica media in hydrated and dehydrated conditions. As in Chapter 4, the mechanical property data are also compared with SLRP expression in the low and high PWV groups. Finally, the adventitia data (Chapter 4) is compared with the medial data for assessing the best approach for determining arterial stiffness from the IMA samples.

Abstract

In Chapter 4, PeakForce QNM was used to investigate the relationship between collagen fibril morphology, nanomechanical properties, and PWV in the IMA adventitia. Using the same specimens and techniques, this chapter explores the nanoscale elastic modulus and ultrastructure of the tunica media in hydrated and dehydrated conditions from the same patients described in Chapter 4. In both hydrated and dehydrated conditions, the tunica media samples in the high PWV group were significantly stiffer than samples in the low PWV group. The elastic modulus of the hydrated and dehydrated tunica media was significantly correlated with the standard clinical assessment of arterial stiffness (carotid-femoral PWV). Unlike in the adventitial collagen fibrils, there was no change in medial collagen fibril size in patients with high PWV. Medial collagen fibrils are dramatically smaller than the adventitial collagen fibrils. Interestingly, only in the hydrated condition was the expression activity of several SLRPs found to be negatively related to the medial elastic modulus. Both the hydrated media and dehydrated adventitia are suitable for reflecting the development of arterial stiffening and SLRPs expression. The comprehensive study of the collagen fibrils and nanomechanical properties integrating with the proteomic analysis in the IMAs demonstrated the possibility of linking property, mechanics, and function in biological samples. The study also identified targets for predicting arterial stiffening and CVDs.

5.1 Introduction

As arterial pulsation increases with age, the tunica media becomes progressively stiffer, driven by a comprehensive consequence of alterations in the arterial ECM (Brüel and Oxlund, 1996). This alteration involves medial degeneration; fragmentation, calcification, and MMP degradation. It also includes disrupting muscular attachments, stiffening of SMCs (Qiu *et al*., 2010), increased collagen deposition, and decreased elastin expression (Fleenor *et al*., 2010). Alteration also sees the accumulation of advanced glycation end-products (AGEs) (Bakris *et al*., 2004, McNulty *et al*., 2007).

Stiffening-related changes in the tunica media have been studied from a macro-scale (Weisbecker *et al*., 2013), micro-scale (Graham *et al*., 2011, Akhtar *et al*., 2016), at a cellular level (Qiu *et al*., 2010), as well as the molecular level (Cecelja and Chowienczyk, 2016, Lacolley *et al*., 2017, Sims *et al*., 1996, Wallace *et al*., 2005). However, information about alterations in the medial ultrastructure and ECM components is largely unknown. It has been widely acknowledged that altered ECM microstructure and components in the artery occur together with changes in their mechanical behaviour, which are likely to contribute to fundamental arterial stiffening. However, the assessment of the ultrastructural properties is highly dependent on length-scale, which significantly limits our understanding of the pathology of arterial stiffening and CVDs.

In Chapter 4, the PeakForce QNM technique was utilised and successfully determined ultrastructural changes in the tunica adventitia from patients with arterial stiffening. In this chapter, the tunica media of the same specimens from the same patients are probed using the same technique. This chapter focusses on nanomechanical properties and collagen fibril morphology of tunica media in patients with a low and high degree of arterial stiffness.

More importantly, to the author's best knowledge, there is no one use this technique for vascular tissue. This study develops an *in situ* nanomechanical mapping approach for the hydrated specimen in a fluid environment using PeakForce QNM. The measured data was also related to the expression activity of SLRPs, which are not only involved in collagen formation and organisation (Kalamajski and Oldberg, 2010) but also play essential roles in the biology of elastic fibres (Schaefer *et al*., 2007, Hwang *et al*., 2008), SMC-associated intima thickening (Onda *et al*., 2002), atherosclerosis (Zhang *et al*., 2015), and atherosclerotic plaques (Fischer *et al*., 2004). Thus, the SLRPs are relevant for studies on the media as well as the adventitia. This chapter further highlights how the changes in localised ultrastructural properties are associated with global arterial stiffness. This study further validates the utility of PeakForce QNM for assessing nanoscale mechanical changes in small-scale biological structures in ambient and fluid conditions.

5.2 Materials and Methods

5.2.1 PeakForce QNM study in ambient condition

All the samples were tested by PeakForce QNM as described in Chapter 4, Section 4.2.2. Quantitative measurement was carried out using the same probe (RTESPA-150), calibration procedure, and analytical model (DMT). For comparison, the scan size, scan rate, and resolution were also consistent with the tunica adventitial study. All AFM raw files were processed with the same software (Bruker, NanoScope Analysis, version 1.5). To identify the IEL and EEL for localised measurement, optical microscopy integrated with the AFM setup was utilised. Three random localised areas were probed in the media of each tissue section. Two sections were studied for each patient. Thus, six measurements were conducted in total for each patient for biomechanical comparison.

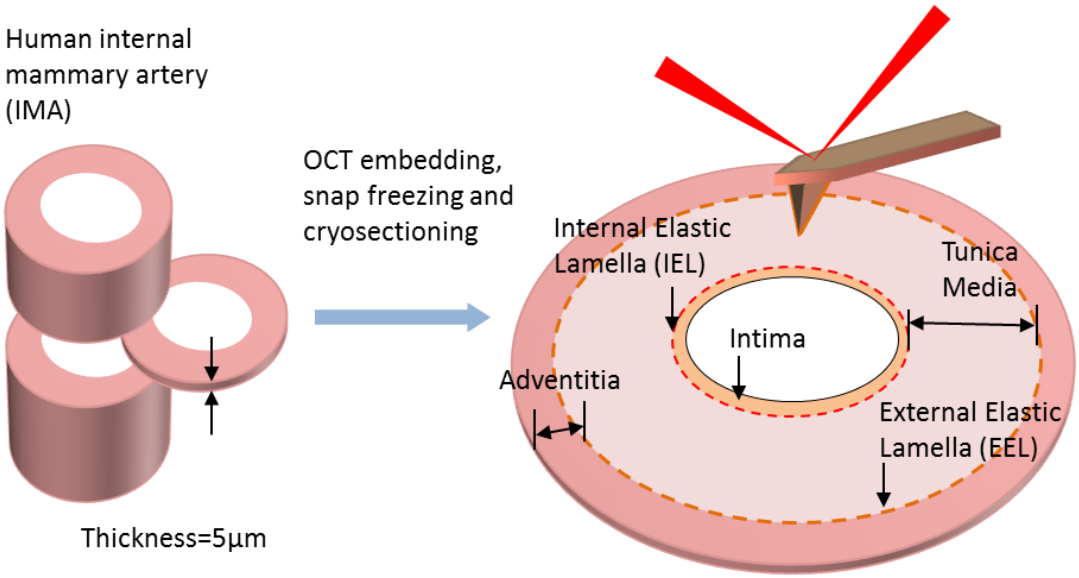

Figure 5.1 The approach for localised nanomechanical mapping of the tunica media in human IMA. The IEL and EEL distinctly separate the tunica intima, tunica media, and tunica adventitia in the IMA.

5.2.2 PeakForce QNM study in a fluid environment

By using the same AFM setup, a Bruker SCANASYST-FLUID probe with an intentionally blunt tip (nominal tip radius = 20 nm) and extremely low spring constant (nominal spring constant = 0.7 Nm^{-1}, resonant frequency = 150 kHz) was applied to map the delicate hydrated tissue section in distilled water. All of the liquid measurements were conducted in a fluid cell (MTFEML, Bruker).

After conducting the same procedure to calibrate tip radius and spring constant of the probe, a polydimethylsiloxane (PDMS) sample was used as the reference sample for modulus measurement calibration. The elastic modulus of PDMS was determined independently via nanoindentation (Nanoindenter G200 with a DCM-II Head, KLA-Tencor, Milpitas, CA, USA) utilising a 100 µm flat punch prior to the calibration. The testing was conducted at 110 Hz

using an oscillatory nanoindentation method (Akhtar *et al*., 2018). The nanoindentation data yielded an average elastic modulus of 5.1 ± 0.36 MPa.

For liquid environment testing, the scan rate was fixed at 0.5 Hz, and the resolution was set at 384 pixels/line. The scan size was consistent with the dehydrated sample testing (2 × 2 μm) for comparison. Thus 147,456 (384 × 384 independent force curves) were obtained in each image to yield the mean elastic modulus. The indentation depth of the sharp tip into the hydrated artery sections for all the force curves was fixed around 20 nm. Thus, the indentation depth/tissue thickness ratio was 0.4% for the hydrated artery samples in this study. In the fluid environment, three random locations per tissue section and two sections per patient were tested for each patient, with a total of six positions studied in each patient. However, samples from three patients (ID: 552 in low PWV, and 620 and 643 in high PWV) were unintentionally damaged during the hydration process and could not be studied. Thus, in total, seven patients in the low and high PWV groups were examined in the fluid environment.

5.2.3 Characterisation of collagen fibril size

For each patient, there were two PeakForce error images with distinct collagen fibrils selected from the dehydrated tunica media. There were also three complete fibrils assessed for the collagen fibril assessment in each image. Thus, in total, there were six fibrils analysed in each patient. Examples of PeakForce error images of each patient for collagen fibril analysis are summarised in Appendix G.

5.2.4 Integration of quantitative proteomics, nanomechanical data and patient metadata

As described in Chapter 4 Section 4.2.5, the 7 SLRPs proteins were integrated with the nanomechanical and structural data obtained in this study and patient metadata using PCA.

5.2.5 Statistical methods

Patient characteristics were presented as mean ± SD and all the bar charts were presented as mean ± SEM. All patient measurements were averaged prior to statistical analysis. All patient measurements were averaged before statistical analysis. Group differences were assessed via a suitable 2-sample independent test selected after appraisal of data normality and homoscedasticity. Differences between nanomechanical properties of hydrated and dehydrated media and medial collagen fibril diameter of the low and high PWV group were tested with the Mann-Whitney U test. Kolmogorov-Smirnov (K-S) tests were applied to assess the statistical significance in distribution of media collagen fibril diameter and nanomechanical properties of hydrated and dehydrated media between the low and high PWV groups. As the non-parametric version in this study, Spearman's correlation coefficient was used to test relationships between the measured elastic modulus of hydrated and dehydrated media and the PWV as well as with the SLRP's expression activity. Proteomics data were analysed in junction with nanomechanical variables and quantitative metadata variables (i.e. age, BMI, cholesterol and HbA1c) of all the patients via the unsupervised data transformation PCA. All statistical analyses were tested using OriginPro version 9 (OriginLab, Northampton, MA).

5.3. Results

5.3.1 Collagen fibrils in the hydrated and dehydrated medial layer

All of the AFM PeakForce Error images of dehydrated tunica media from the 17 patients were examined. For each patient, there was at least one AFM PeakForce Error image that showed randomly organised collagen fibrils (see Appendix G). In the present study, the medial collagen fibrils appeared to be dispersed and embedded into the ground ECM substrate in both groups (Figure 5.2A and 5.2B). At a higher magnification (2 μm × 2 μm), fine individual collagen fibrils could be seen, and most of them formed laterally associated bundles in the media. However, the 67 nm D-period of these fibrils were poorly visible (Figure 5.2A – 5.2D). These findings were different as compared with the adventitial results in Chapter 4, where the collagen fibrils were highly arranged along one direction with distinct fibril edges.

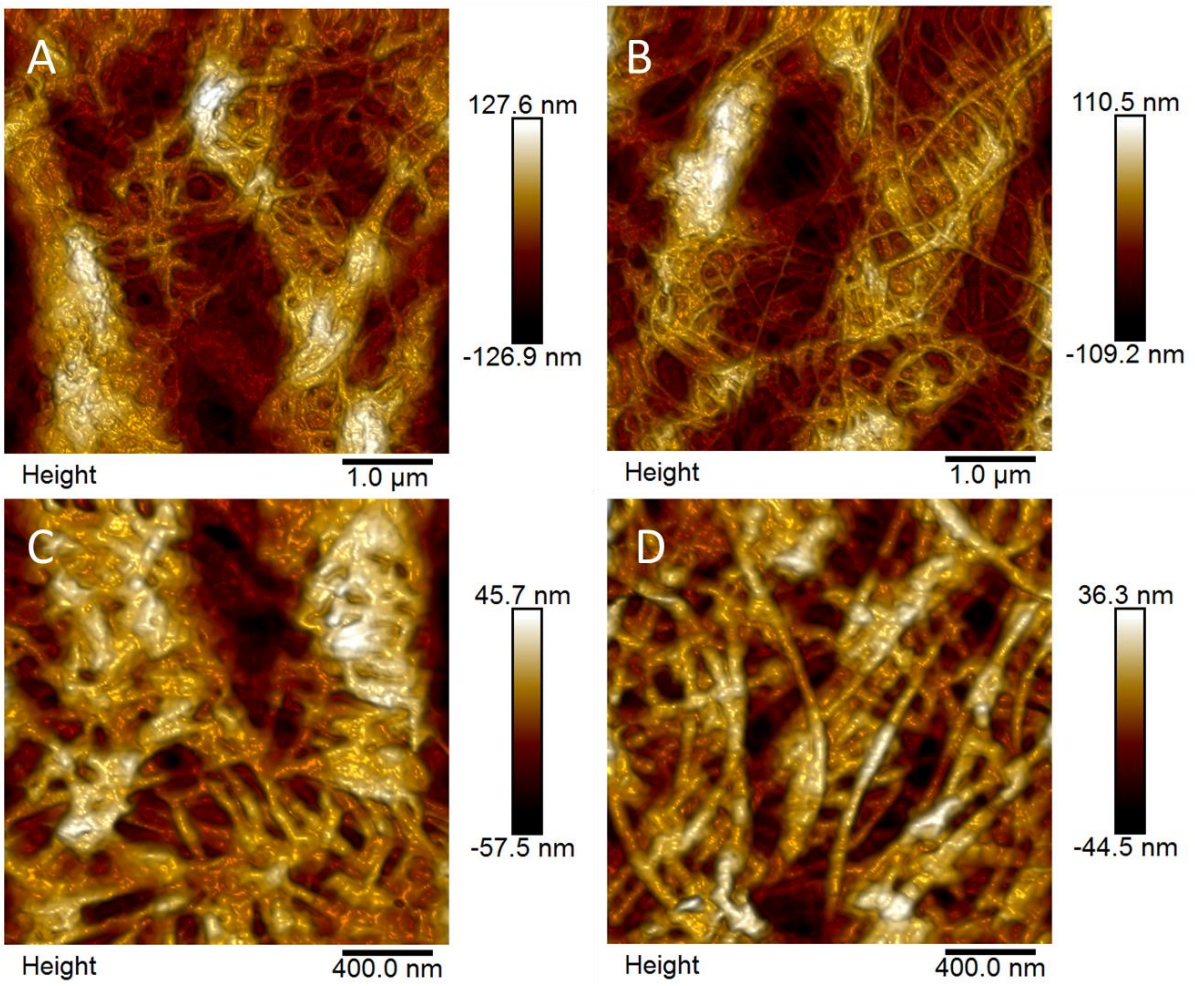

Figure 5.2 AFM topography images of the collagen fibrils in the dehydrated tunica media from patients with (A & C) low and (B & D) high PWV. Dispersed medial collagen fibrils were distinct in (A) low and (B) high PWV groups in 5 ×5 µm^2 AFM height images. High magnification AFM height images (2 ×2 µm^2) of collagen fibrils were interwoven with each other in the tunica media from the (C) low and (D) high PWV group.

In hydrated tissue sections, the medial collagen fibrils were poorly recognisable (Figure 5.3), which may be attributed to the decreased height differences between gap and overlap regions accompanied with collagen swelling in the fluid, as previously reported (Spitzner *et al*., 2015). Thus, collagen fibril imaging of hydrated tissue sections in a fluid environment often leads to degraded image resolution and quality, so that is impossible for fibril size assessment.

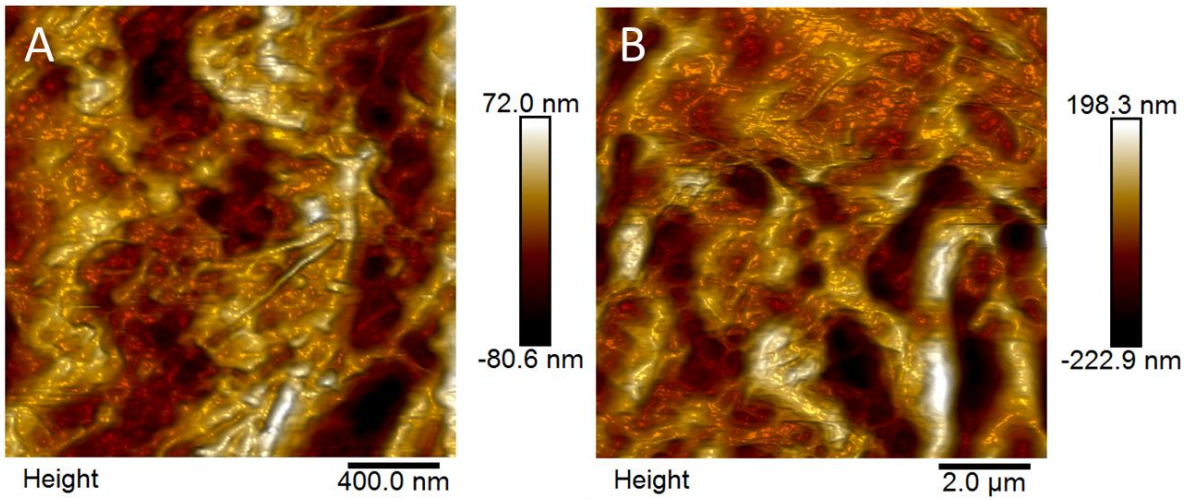

Figure 5.3 AFM topography images of the collagen fibrils in the hydrated tunica media from patients with (A) low and (B) high PWV. Image size was (A) 2 ×2 µm^2 and (B) 10 ×10 µm^2.

Subsequently, the collagen fibril size in the dehydrated media for the low and high PWV groups was manually assessed and compared. Collagen fibril diameters in the dehydrated media of each patient are shown in Table 5.1. Overall, differences in collagen fibril diameter between both groups of patients, i.e. low and high PWV (Figure 5.4) were tested using a non-parametric Mann-Whitney U test and resulted in a non-significant p-value ($p = 0.47$). There was also no statistical difference in the distribution of fibril diameter in the low and high PWV groups (Kolmogorov-Smirnov test, $p = 0.17$).

For each of the patients, the diameter of adventitial collagen fibril was larger than that of medial collagen fibril (Table 5.1). Overall, a significant increase in fibril diameter was found from the media to adventitia in both low and high PWV groups (Mann-Whitney U test, low PWV: $p = 0.00146$; high PWV: $p = 0.00041$). In each group, the distribution of collagen fibril diameter of the media and adventitia was also found to be dramatically different (Kolmogorov-Smirnov test, $p < 0.0001$) (Figure 5.4). This increasing trend in collagen fibril diameter from the media to adventitia was consistent with previous studies (Merrilees *et al*., 1987, Buck, 1987, Dingemans *et al*., 2000).

Table 5.1 Collagen fibril diameters in the tunica media and custom routine measured adventitial fibril size of each patient. Three fibrils in each image and two images for each patient were measured in the tunica media. More than 40 fibrils were measured in adventitia for each patient.

	Patient ID	Media	Adventitia
Low PWV (n = 6 fibrils in the media)	522	98.65 ± 22.76	131.36 ± 23.81
	549	88.47 ± 32.29	131.46 ± 29.74
	552	77.20 ± 6.02	119.85 ± 23.41
	559	85.52 ± 4.87	N
	565	70.25 ± 3.65	123.74 ± 25.63
	631	77.78 ± 7.56	118.52 ± 24.66
	656	78.60 ± 10.14	120.58 ± 25.82
	693	79.65 ± 5.15	114.02 ± 22.16
Overall (n = number of patients)		82.01 ± 8.68	122.79 ± 6.56
High PWV (n = 6 fibrils in the media)	524	89.91 ± 8.45	122.99 ± 24.04
	534	83.32 ± 27.50	120.07 ± 25.70
	573	69.80 ± 4.90	126.26 ± 23.42
	603	85.43 ± 10.02	120.69 ± 25.20
	606	113.54 ± 10.69	130.56 ± 26.16
	620	77.81 ± 9.45	125.92 ± 31.36
	627	87.48 ± 11.62	120.90 ± 25.64
	643	79.15 ± 8.11	120.03 ± 22.36
	1202	85.69 ± 8.60	116.93 ± 23.97
Overall(n = number of patients)		85.79 ± 12.04	122.70 ± 4.18
p		0.47	0.84

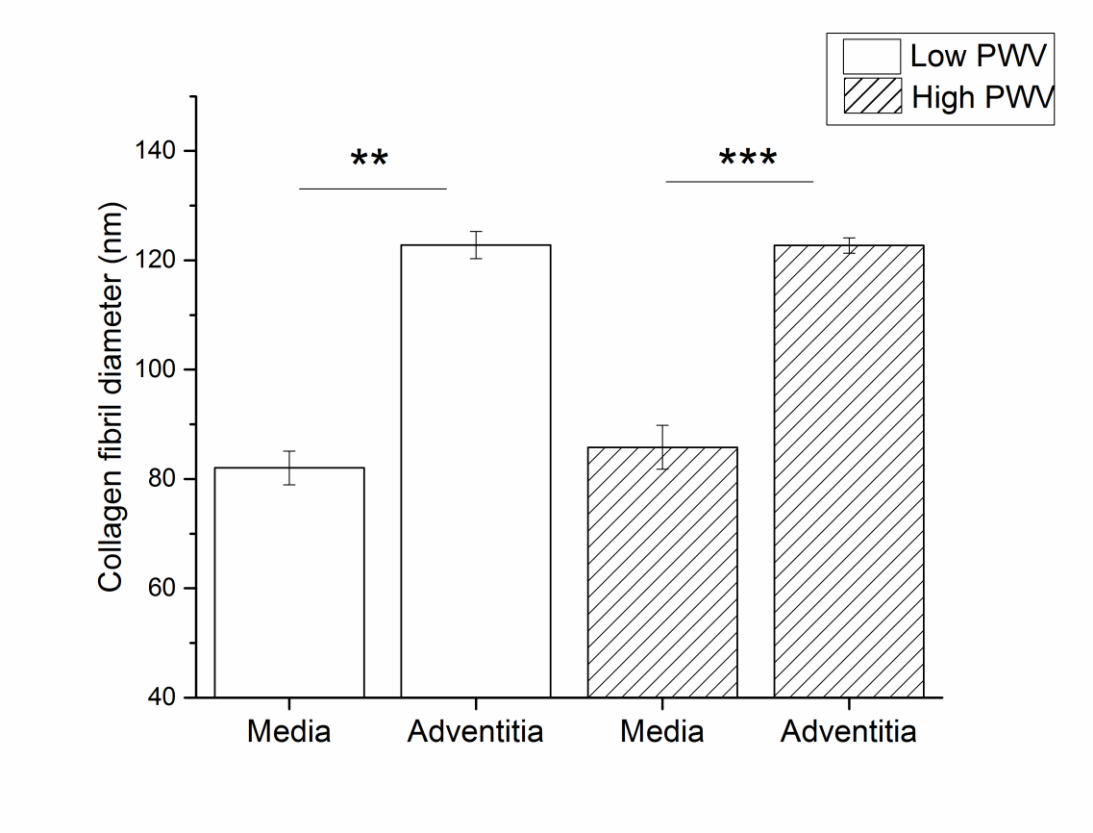

Figure 5.4 Collagen fibril diameter in tunica media and adventitia of patients with low and high PWV. Bar chart represents mean with SEM. Significant increases in fibril diameters from the media to adventitia were found in the low and high PWV group, respectively.

5.3.3 Nanomechanical properties of dehydrated media in ambient condition

In ambient condition, patients with high PWV had a stiffer media than the low PWV group (low PWV = 2116.2 ± 523.1 MPa; high PWV = 3163.6 ± 548.7 MPa, Mann-Whitney U test, $p = 0.003$) (Figure 5.5A). The elastic modulus ranged from 1325.5 to 2770.7 MPa and 2520.3 to 4030.0 MPa in the low and high PWV groups, respectively. Modulus distribution between these two groups was also found to be significantly different (Kolmogorov–Smirnov test, $p < 0.0001$) (Figure 5.5B).

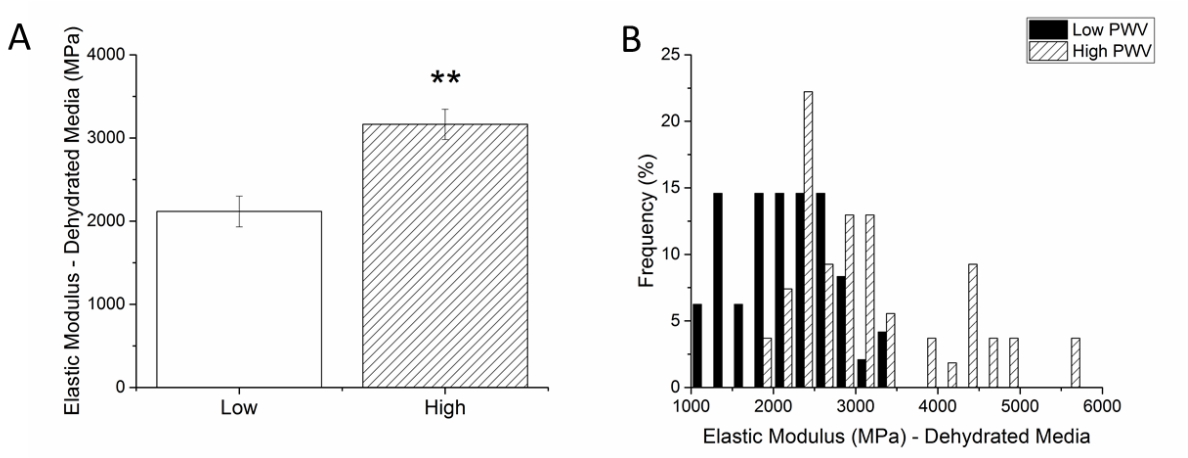

Figure 5.5 Nanomechanical properties of the dehydrated media in both groups in ambient condition. (A) Bar graph showing a significant difference in elastic modulus of patients as mean ± SEM (n = 8 patients in low PWV group; n = 9 patients in high PWV group). (B) Distribution of measured elastic modulus for both groups, significant differences were found between modulus distributions of two groups overall in the dehydrated media (Kolmogorov–Smirnov test, $p < 0.0001$).

The mechanical data of dehydrated media was compared with the adventitial data in the same patients (Table 5.2). Overall, the two layers in patients with high PWV were significantly stiffer than those in the low PWV group (low PWV: n = 8 patients; high PWV: n = 9 patients). Although there was no statistical difference in the measured elastic modulus between the dehydrated media and adventitia in each group (Mann-Whitney U test, $p > 0.05$), the dehydrated media was slightly stiffer than the dehydrated adventitia in the high PWV group. In addition, in patients with high PWV, the ultrastructural stiffness increased by 49.5% and 34.1% in the dehydrated media and adventitia, respectively. The coefficient of variation of the measured elastic modulus was also decreased in dehydrated media in high PWV. Taken together, these findings imply that the dehydrated media might undergo more mechanical related alterations in the ultrastructure during arterial stiffening.

Table 5.2 Nanomechanical properties of individual layers in dehydrated IMA in ambient condition. Mann-Whitney U test is used to test the statistical difference between each layer of the low and high PWV groups.

	Low PWV	
	Media	**Adventitia**
n	8	8
Median (MPa)	2114.3	2055
Mean (MPa)	2116.2	2159.3
SD (MPa)	523.1	282.5
Coefficient of variation (%)	24.7	13.1
	High PWV	
	Media	**Adventitia**
n	9	9
Median (MPa)	2921.4	2866.4
Mean (MPa)	3163.6	2895.2
SD (MPa)	548.7	414.4
Coefficient of variation (%)	17.3	14.3
p	0.003	0.002

5.3.4 Nanomechanical properties of hydrated media in a fluid environment

In the fluid environment, the hydrated media in the high PWV group was approximately three times stiffer than that in low PWV group (low PWV group = 250.6 ± 39.0 kPa; high PWV group = 721.7 ± 291.9 kPa, Mann-Whitney test, $p = 0.005$) (Figure 5.6A). The median of measured elastic modulus of the hydrated media was 248.1 kPa and 654.7 kPa for the low and high PWV groups respectively. The measured elastic modulus of the patients ranged from 180.1 to 292.7 kPa, and 286.6 to 1114.7 kPa in the low and high PWV groups. A significant difference was found between modulus distributions in the two groups (Kolmogorov–Smirnov test, $p < 0.0001$) (Figure 5.6B). Furthermore, variation in the elastic

modulus between the low and high groups was more significant in the hydrated media than in dehydrated media. The stiffness of the dehydrated media increased 52% in the high PWV group relative to that of low PWV, while the elastic modulus of the hydrated tunica media in high PWV group was raised 188% compared to the low PWV group. After dehydration in ambient condition, the mechanical properties of these dry tissue sections were three times more stiffer than that of hydrated samples.

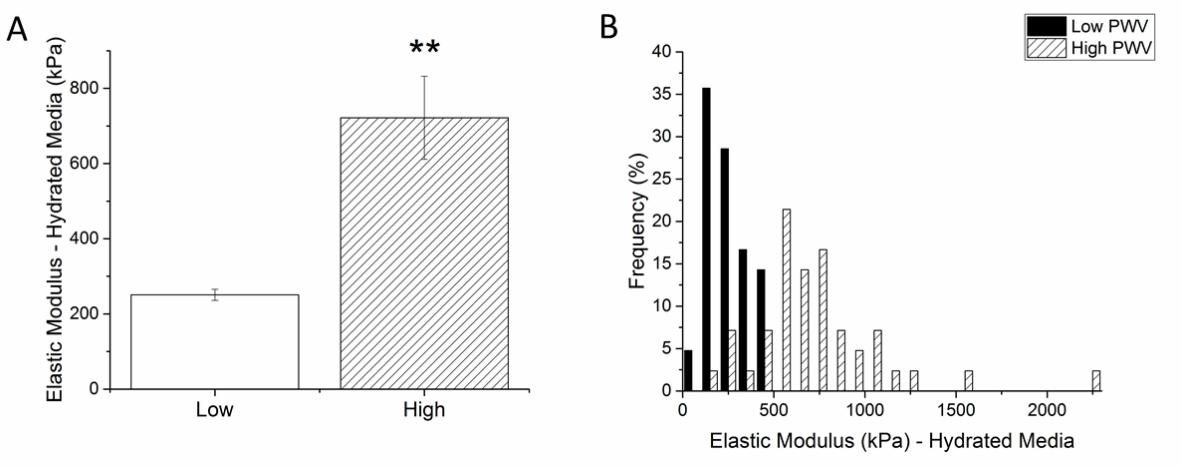

Figure 5.6 Nanomechanical properties of the hydrated media in the fluid environment in all available patients. (A) The elastic modulus of hydrated media in each patient (n = 7 patients per group, Mann-Whitney test, p = 0.005). (B) Modulus distribution of tunica media in low and high PWV groups (n = 42 measurements per group, Kolmogorov–Smirnov test, p < 0.0001).

5.3.5 Correlation analysis

To assess the relationship between nanomechanical properties (PWV) and SLRP expression activity, Spearman's rank-order correlation was used to calculate the correlation coefficient for the relationships to test their significance (Table 5.3). There were 17 available patients assessed in ambient condition and 14 available patients in a fluid environment. Overall, the nanomechanical properties of hydrated and dehydrated media were significantly and positively correlated with the patient's PWV value, which was similar to the dehydrated

adventitia. These findings suggest that all of the dehydrated media and adventitia, as well as the hydrated media, can be used for reflecting clinical arterial stiffness.

For correlations between SLRP expression and nanomechanical properties of different layers in all the available patients (n = 12 patients for both conditions), 4 of 7 SLRPs showed significant and negative correlation with measured elastic modulus of hydrated media. This corresponds to a previous study (Hansen *et al*., 2015) where 5 of 7 SLRPs (lumican, mimecan, prolargin, asporin and decorin) were downregulated in patients with high PWV. Nevertheless, the measured elastic modulus of dehydrated layers was not related to SLRP expression.

Table 5.3 Spearman's rank-order correlation for assessing correlations of nanomechanical properties of different layers - PWV and SLRP expressions.

IMA layers and testing conditions	**PWV**		**SLRP expression**						
			Lumican	Mimecan	Prolargin	Asporin	Podocan	Decorin	Biglycan
Hydrated Media	r	0.63	-0.71	-0.54	-0.72	-0.62	-0.48	-0.63	-0.15
	p	0.017*	0.01**	0.07	0.008**	0.033*	0.11	0.028*	0.63
Dehydrated Media	r	0.62	-0.20	-0.02	-0.48	-0.51	-0.27	-0.22	-0.12
	p	0.008**	0.54	0.95	0.12	0.09	0.39	0.48	0.71
Dehydrated Adventitia	r	0.56	-0.50	-0.45	-0.52	-0.39	-0.34	-0.34	-0.20
	p	0.02*	0.10	0.15	0.09	0.21	0.28	0.29	0.53

5.3.6 Principle component analysis

The variables measured in this study were summarised and integrated with the SLRPs data by PCA. The score plot for this transformation is shown in Figure 5.7A where it can be appreciated that there is a difference between high and low PWV patients. The variables contributing the most to this separation are shown in the loading plot (Figure 5.7B) where, not surprisingly, it can be seen that how PWV is one of the major contributors to the separation of the patients. Interestingly and in agreement with assessed data in this study, it is closely correlated with the elastic modulus of dehydrated layers. Furthermore, PCA on the data without the PWV variable shows similar separation between both high and low PWV patients and exhibits elastic modulus of the hydrated and dehydrated layers as three of the key variables to the separation (Figures 5.7C and 5.7D). The elastic modulus of hydrated media was closely related to the age. In addition, the nanomechanical properties of dehydrated media and adventitia were closely correlated. Most SLRPs were closed grouped in the PCA analysis with some differences in mimecan and biglycan, which was similar to the PCA data of the adventitia (Chapter 4 Section 4.3.4).

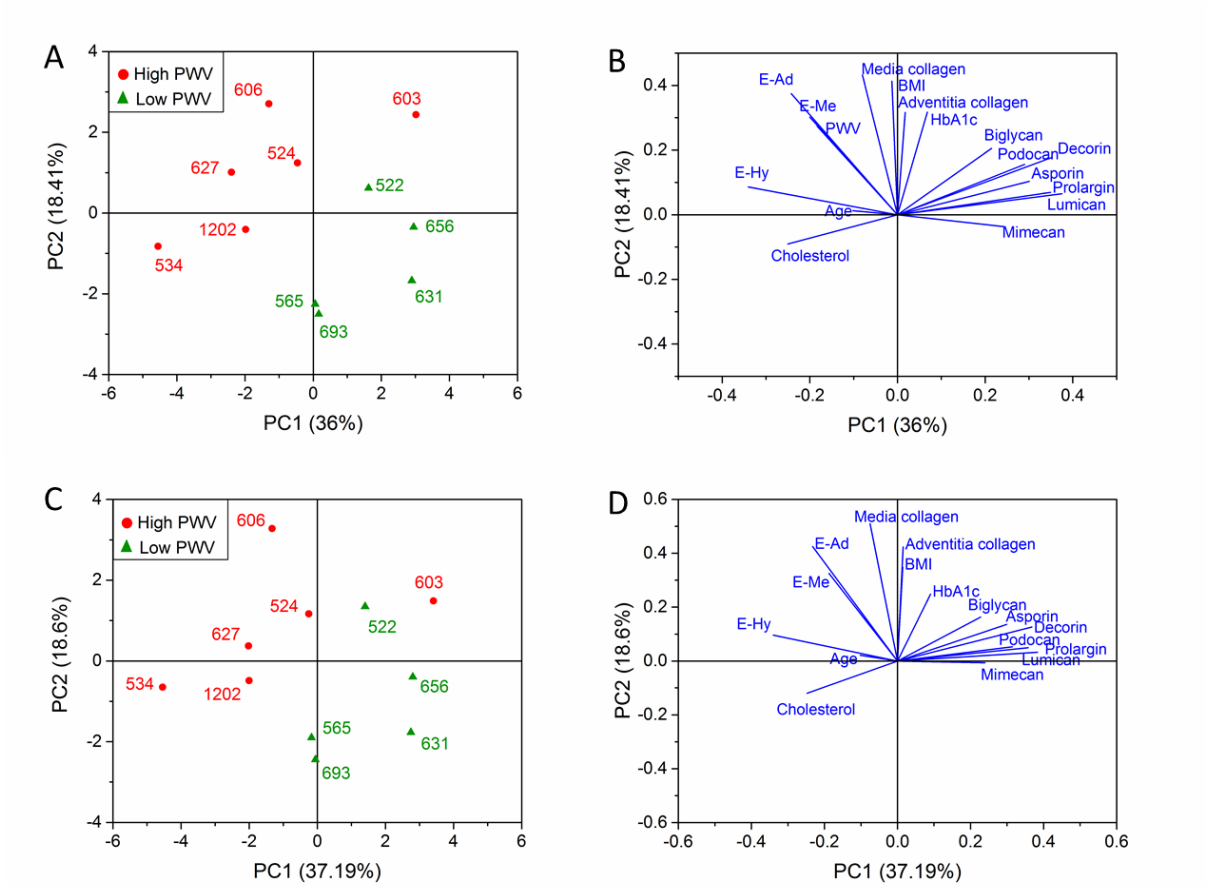

Figure 5.7 PCA of patient proteomics, quantitative metadata and nanomechanical variables. (A) Scope plot of the two first components. Each dot represents a patient. Each dot represents a patient. Patients coloured by group. (B) Loading plot of (A) showing the variables that contribute the most of the structured observed in (A); PWV and elastic modulus of hydrated media (E-Hy), dehydrated media (E-Me) and adventitia (E-Ad) are four of the most contributing variables to the separation between both groups. (C) Score plot of the two principal components of patient data without the PWV variable. Similar separation between both groups can be observed. (D) Loading plot of (C) shows the E - Hy, E - Me and E - Ad are three of the most contributing variables to the separation observed. Elastic modulus of dehydrated media (E-Me) and adventitia (E-Ad) were highly correlated. Of the SLRPs, mimecan presents the most contribution to the separation between groups observed.

5.4 Discussion

In this study, the tunica media of human IMA was characterised building on the adventitial work presented in Chapter 4. The nanomechanical and ultrastructural properties of hydrated and dehydrated media were assessed to understand how the media is changed in patients with

a high degree of arterial stiffening. The structural features of media and adventitia were compared and evaluated by correlation analysis to assess the best approach for determining arterial stiffness from the IMA samples. Human IMA has been histologically well-characterised as a transitional type of artery due to its low number of elastic lamellae (Borovic *et al*., 2010). Herein, the types of the IMAs from all of the 17 patients were assessed by Prof. Rasmussen that most of the IMAs are the muscular type (15 of 17) except for two patients (patient 559 and 620) (see Appendix D).

Weigert's elastic stain shows that there is little or no elastin in all the measured samples, and that predominant SMCs can constitute circumferentially continuous fibrous helix in the media (Borovic *et al*., 2010). These medial SMCs drive constriction or dilation of the artery to maintain tone and regulate blood flow to the peripheral regions of the body (Shirwany and Zou, 2010). Therefore, they contribute profoundly to the mechanical properties of the IMA, allowing for viscoelastic behaviour with hysteresis (Holzapfel *et al*., 2002). Although the IMA is mechanically negligible for global stiffness (O'Rourke *et al*., 2002) and PWV measurement (Cameron *et al*., 2003), it has recently been suggested as a promising target for disclosing the pathogenesis of arterial stiffening, especially at the molecular level (Chung *et al*., 2008, Engler *et al*., 2004, Faarvang *et al*., 2016, Preil *et al*., 2015, Hansen *et al*., 2015).

5.4.1 Collagen fibrils in the IMA

In this study, medial collagen was characterised by dispersed collagen fibrils, while adventitial collagen fibrils were found to be highly organised (Chapter 4, Section 4.3.3). These findings were consistent with those of a previous study (Beenakker, 2012). These different morphologies and architectures appear optimal for achieving layer-specific functionalities, i.e. media is mechanically predominant under the physiological condition allowing for vasoconstriction with the blood pulse, while the adventitial layer is crucial for

preventing the artery from overstretching and rupturing at high pressure and strain. Subsequently, the collagen fibril size was determined and a significant increase was found in collagen fibril diameter from the media to the adventitia. The fibril diameter was 69.78-113.54 nm with an average of 84.01 nm in the tunica media. This was smaller than the diameter in the adventitia. The progressive increase in fibril diameter from the media to the adventitia is in agreement with findings from previous studies (Merrilees *et al*., 1987, Buck, 1987, Dingemans *et al*., 2000). The presence of larger collagen fibrils has been speculated as an adaptation to the high mechanical requirement of the external media and adventitia (Dingemans *et al*., 2000).

However, the measured fibril sizes in previous studies were relatively small than those determined in this study. Buck (1987) studied the fibril size across the entire rat carotid artery and found the largest fibrils in the adventitia (mean = 66.1 nm) compared to fibrils in different regions of the media (innermost media: 29.7 nm; middle media: 30.7 nm; outermost media: 37.4 nm). Buck (1987) also found that the fibrils in the outer interlamellar space have a larger size relative to the other fibrils in the media, which may arise due to either the higher mechanical requirement in the external media or the effects of adventitial fibroblasts. Merrilees *et al*. (1987) studied collagen fibril size across the arterial wall from a variety of mammal arteries. They found the size of the intimal and innermost medial collagen fibrils were similar, ranging from 30 to 40 nm, while the adventitial collagen fibrils were relatively larger in the aorta and femoral artery (mean fibril diameter: 60 – 80 nm) from humans and pigs than that in coronary arteries (fibril diameter: 50 – 60 nm). Dingemans *et al*. (2000) also discovered that the fibrils in the human aorta were larger in the external media (mean = 46.58 nm) than that in the inner media (mean = 37.36 nm). These results may be due to the arteries being tested from different sites in different species of mammals, which could lead to different fibril sizes. Moreover, all of the fibril size measurements were conducted at the

longitudinal outer surface of the IMA fibrils from selected AFM images, whereas previous studies performed analyses of cross-sectioned collagen fibrils (Goh *et al*., 2012, Wood *et al*., 2011, Goh *et al*., 2008). In addition, all IMA samples were not fixed or chemically treated before AFM imaging. However, for other imaging methods, the arterial tissue needed advance fixation or treatment.

Previous quantitative proteomic tests (Hansen *et al*., 2015) distinguished five downregulated SLRPs in the IMAs from patients with high PWV and speculated on the possible effects of SLRPs in arterial stiffening, as well as on regulating collagen fibril assembly and architecture. Alterations in the adventitial collagen fibrils have been characterised to reveal the relation of SLRP expression-collagen fibril morphology-biomechanics in the IMA adventitia (see Chapter 4). However, in this study, there was no significant change in the collagen fibril size of the tunica media in patients with high PWV. Our PCA analysis also indicates that there are no correlations between the media collagen diameter and elastic modulus of the hydrated and dehydrated layers, as well as the SLRPs. Thus, it is suggested that the downregulated SLRPs exhibited more influence in the adventitial collagen fibril assembly and formation rather than collagen fibrils in the tunica media.

5.4.2 Mechanical properties of the hydrated and dehydrated IMAs

Although the PeakForce QNM has been recently used to probe biological samples under physiological conditions, information concerning how PeakForce QNM assess the nanomechanical properties of vascular tissue and arterial stiffening is scant. This study developed the PeakForce QNM mechanical mapping in the fluid condition for investigating the hydrated IMAs and the development of arterial stiffening for the first time. By using the

hydrated and dehydrated IMA tissue sections, the possibility of using the ultrastructural mechanics to reflect the degree of arterial stiffness was proved. This study demonstrated that both the hydrated and dehydrated tunica media showed an elevated stiffness at the ultrastructural level in the high PWV group.

The literature on the layer-specific biomechanical properties of the human artery is sparse. The most relevant nanoindentation and AFM mechanical studies of arterial tissues in different species of mammals are summarised in Table 5.4. All of the studies reported data for hydrated arterial tissues. The stiffness of hydrated tunica media in the present study (mean elastic modulus: 250 kPa for low PWV, 722 kPa for high PWV, overall range 180 - 1115 kPa) is much higher than that of isolated medial SMCs (< 30 kPa) (Qiu *et al*., 2010, Engler *et al*., 2004), which could occur due to the heterogeneity of biological tissues. Nevertheless, localised mechanical properties of the aortic media were much stiffer and exhibited considerable variability (kPa to GPa) (Beenakker *et al*., 2012) than the hydrated IMA media. The reduced stiffness and minor mechanical variation in the IMA media may occur because of the absence of elastic lamella, which has been proven to dramatically increase local stiffness (Kermani *et al*., 2017). On the other hand, the hydrated IMA media were slightly stiffer compared to those of the porcine aorta (60 - 130 kPa), determined by a custom-made nanoindentation test setup (Kermani *et al*., 2017, Hemmasizadeh *et al*., 2012). The relatively higher stiffness in this study may result from the different experimental parameters. For example, Hemmasizadeh *et al*. (2012) and Kermani *et al*. (2017) used a conical indenter with a much bigger tip radius (10 μm) relative to the probe used in this study (tip radius = 20 nm), which is believed to significantly reduce the measured stiffness (Sicard *et al*., 2017). In addition, Hemmasizadeh *et al*. (2012) and Kermani *et al*. (2017) determined the mechanical data by fitting the quasilinear viscoelastic model (QLV) rather than the DMT mode we used in this study.

The nanomechanical properties of dehydrated tissue sections in ambient condition were more than three orders of magnitude stiffer than that of hydrated samples in the fluid environment. This suggests the importance of water content in affecting the mechanical properties of soft biological tissues.

In an arterial wall, collagen, elastin and SMCs are primarily responsible for the load-bearing functionality and variable stiffness across the arterial wall. This is mainly due to the arterial wall morphological quantities, including the elastic lamellae density, the total protein content, and the elastin circumferential percentage of fibres (Hemmasizadeh *et al*., 2015). In the present study, the staining and AFM topographical data were carefully checked to confirm that there was little or no elastin and elastic fibre in the IMA media. Meanwhile, all of the mechanical measurements were conducted on the areas without elastic fibres. Therefore, it is reasonable to speculate that the mechanical data in this study reflects nanoscale mechanical properties of the IMA medial ultrastructure which mainly attribute to the SMCs, collagen, proteoglycans and other ECM, except for elastin and elastic fibres.

More importantly, the nanomechanical data suggests that the dehydrated medial layer experienced greater degree stiffening in its ultrastructure compared to the adventitia in patients with high PWV, which may indicate that stiffening-related changes may accumulate more frequently in the media.

In an artery, SMCs are essential in regulating the synthesis and organising the arterial ECM, including collagen, elastin, and proteoglycans, which are highly responsible for arterial biomechanics (Lacolley *et al*., 2017). Mechanical connection and signalling between the SMCs and arterial ECM can also contribute to the arterial mechanical behaviour observed (Qiu *et al*., 2010). SMC dysfunction is highly related to not only elevated proliferation and migration ability of SMCs, but also to increased ECM synthesis and signalling. These factors

collectively result in impaired vasodilation and the ability to regulate blood pressure and subsequent arterial stiffening. Hansen *et al*. (2015) have identified a variety of altered network-forming collagens (type VIII and type IV) and actin cytoskeletal components in the IMAs from patients with a high PWV. These abnormal components have been discovered to regulate SMC migration, differentiation and morphogenesis (Sibinga *et al*., 1997, MacBeath *et al*., 1996, Lopes *et al*., 2013) while acting as connections between SMCs and the ECM (Gorenne *et al*., 2003). This can further increase medial tissue remodelling and stiffening, as well as global tissue stiffness.

Table 5.4 Summary of the mechanical properties of different layers across the arterial wall from mammals by nanoindentation and AFM studies. Dulbeco's Modified Eagle Medium (DMEM).

Vessel type	Tip/Indenter	Analytical Mode	Condition	Elastic modulus of layers			References
				Intima	Media	Adventitia	
Porcine aorta	R=10μm	QLV	PBS		Innermost:124 ± 37 Inner:114 ± 38 Outer: 124 ± 43 kPa	95 ± 28 kPa	(Kermani *et al.*, 2017)
Porcine aorta	R=10μm	QLV	PBS	Inner half:60 ± 2 Outer half:70 ± 2 kPa			(Hemmasizadeh *et al.*, 2012)
Human femoral artery	R= 0.17mm	Sneddon	Saline solution	34.3 kPa			(Lundkvist *et al.*, 1996)
Porcine aorta	R=20 nm k=0.58N/m	Hertz	PBS 25℃/37℃		25℃ 100kPa - 1GPa 37℃ 100kPa - 100MPa	25℃ 100kPa -100MPa 37℃ 50kPa - 10MPa	(Beenakker *et al.*, 2012)
Ferret aorta and vena cava	R=10 μm	Modified Oliver-Pharr method	Dehydrated	Aorta:8 MPa Vena:44 MPa	Aorta:21 Vena:28 MPa	Aorta:35 Vena:43 MPa	(Akhtar *et al.*, 2009)

Porcine aorta and pulmonary artery	R=10 µm k=0.32N/m	Hertz	Ultrapure water, 37℃			Aorta: 0.7- 391 and 15.8kPa/Pulmonary artery: 2.3 - 1130 and 88.9 kPa	(Grant and Twigg, 2012)
Bovine carotid artery	R= 4.5µm k=0.12N/m	Hertz	PBS		Subendothelial matrix: 2.5 ± 1.9 kPa		(Peloquin *et al*., 2011)
Porcine carotid artery	Tip radius 2.5µm		DMEM		5 - 8 kPa		(Engler *et al*., 2007)
Monkey thoracic aorta			PBS/ 20℃	VSMC young(~ 6.4 year) = 13.7 ± 2.4 kPa old (~ 25 year) = 23.3 ± 3.0 kPa			(Qiu *et al*., 2010)
Porcine carotid artery	R=2µm k=60pN/nm	Hertz	DMEM	SMC: 5 - 8kPa			(Engler *et al*., 2004)
Rat aorta	R 20-40 nm k=0.32N/m	Hertz	Growth medium 37 ℃	0.35 - 0.55 MPa			(Mao *et al*., 2009)

5.4.3 Role of SLRPs in the IMA mechanical properties

Proteoglycans are a family of complex and diverse macromolecules that are fundamentally associated with functionality and mechanics of the arterial wall. Although they are a minor component of the arterial wall (2 - 5% by dry weight) (Wight, 1989), proteoglycans - especially SLRPs - play an essential role in arteriogenesis (Kampmann *et al*., 2009), atherosclerosis (Talusan *et al*., 2005), and arterial ECM remodelling (Barallobre-Barreiro *et al*., 2012). The quantitative proteomics data collected in this study from the entire IMA tissue have further integrated the nanomechanical data in the 12 available patients (6 patients per group) to explain the underlying factors associated with arterial stiffening. This study indicated that only the nanomechanical properties of the hydrated media are related to the expression activity of SLRPs. Based on the correlation analysis, it is reasonable to speculate that the hydrated media is a better layer to study stiffening related tissue remodelling. In the physiological environment, testing can reveal the tissue's structure and mechanics that closely resemble features *in vivo*.

SLRPs are essential in the structural integrity and functionality of the arterial wall by modulating synthesis, assembly and remodelling of arterial ECM components such as collagen, elastin, and SMCs. Expect for controlling collagen fibrillogenesis and collagen organisation, studies have revealed the importance of SLRPs in regulating proliferation and migration of SMCs that is predominant in the media of muscular arteries. Accumulated lumican, which is expressed in the SMCs, is located in the fibrous thickened intima and media where it associates with intimal thickening and is capable of maintaining adventitial mechanical properties in patients with atherosclerosis (Onda *et al*., 2002). Highly expressed mimecan found in human SMCs is shown to accelerate cell proliferation, migration and death, thereby regulating atherosclerosis (Zhang *et al*., 2015) and atherosclerotic plaques (Fernández

et al., 2003). Biglycan promotes SMC proliferation and migration in arteriosclerotic lesions related to arterial repair and pathogenesis of vascular injury (Shimizu-Hirota *et al*., 2004). Upregulated decorin is discovered in calcified regions in human atherosclerotic lesions, where it accelerates SMC calcification (Fischer *et al*., 2004).

5.5. Conclusions

This study probed the nanoscale stiffening-related ultrastructural changes in the tunica media of human IMAs in ambient and fluid conditions (ultrapure water) in patients with a high PWV. This study built on the adventitial study presented in Chapter 4. It is worth noting that the mechanical properties of the medial ultrastructure in both environments correlated well with the carotid-femoral PWV. Moreover, the tunica media was likely to experience more stiffening-related changes in the ultrastructure that mainly consists of SMCs, collagen, and proteoglycans. In addition, the correlation analysis suggested that the nanomechanical properties of both the hydrated and dehydrated tissue are suitable for reflecting the degree of arterial stiffness. Both the hydrated media and dehydrated adventitia were useful markers for indicating SLRP expression, revealed to be related to arterial stiffness. Unlike the adventitial fibrils, there were no distinct alterations in the medial collagen fibril diameter in patients with high PWV, although a trend of increased fibril size was found from the media to the adventitia. Nanomechanical mapping of hydrated vascular tissue conducted by the PeakForce QNM was developed in the fluid condition, which will be a significant approach for understanding the development of arterial stiffening and CVDs.

References

AKHTAR, R., DRAPER, E. R., ADAMS, D. J. & HAY, J. 2018. Oscillatory nanoindentation of highly compliant hydrogels: A critical comparative analysis with rheometry. *Journal of Materials Research,* 33**,** 873-883.

AKHTAR, R., GRAHAM, H., DERBY, B., SHERRATT, M., TRAFFORD, A., CHADWICK, R. & GAVARA, N. 2016. Frequency-modulated atomic force microscopy localises viscoelastic remodelling in the ageing sheep aorta. *Journal of the mechanical behavior of biomedical materials,* 64**,** 10-17.

AKHTAR, R., SCHWARZER, N., SHERRATT, M., WATSON, R., GRAHAM, H., TRAFFORD, A., MUMMERY, P. & DERBY, B. 2009. Nanoindentation of histological specimens: mapping the elastic properties of soft tissues. *Journal of materials research,* 24**,** 638-646.

BAKRIS, G. L., BANK, A. J., KASS, D. A., NEUTEL, J. M., PRESTON, R. A. & OPARIL, S. 2004. Advanced glycation end-product cross-link breakers: a novel approach to cardiovascular pathologies related to the aging process. *American journal of hypertension,* 17**,** 23S-30S.

BARALLOBRE-BARREIRO, J., DIDANGELOS, A., SCHOENDUBE, F. A., DROZDOV, I., YIN, X., FERNáNDEZ-CAGGIANO, M., WILLEIT, P., PUNTMANN, V. O., ALDAMA-LóPEZ, G. & SHAH, A. M. 2012. Proteomics analysis of cardiac extracellular matrix remodeling in a porcine model of ischemia-reperfusion injury. *Circulation***,** CIRCULATIONAHA. 111.056952.

BEENAKKER, J.-W. M., ASHCROFT, B. A., LINDEMAN, J. H. & OOSTERKAMP, T. H. 2012. Mechanical properties of the extracellular matrix of the aorta studied by enzymatic treatments. *Biophysical journal,* 102**,** 1731-1737.

BEENAKKER, J. W. M. 2012. *Unravelling the collagen network of the arterial wall*, Huygens Laboratory, Institute of Physics, Faculty of Science, Leiden University.

BOROVIC, M. L., BOROVIC, S., PERIC, M., VUKOVIC, P., MARINKOVIC, J., TODOROVIC, V., RADAK, D. & LAČKOVIC, V. 2010. The internal thoracic artery as a transitional type of artery: a morphological and morphometric study. *Histology and histopathology,* 25**,** 561.

BRüEL, A. & OXLUND, H. 1996. Changes in biomechanical properties, composition of collagen and elastin, and advanced glycation endproducts of the rat aorta in relation to age. *Atherosclerosis,* 127**,** 155-165.

BUCK, R. C. 1987. Collagen fibril diameter in the common carotid artery of the rat. *Connective tissue research,* 16**,** 121-129.

CAMERON, J. D., BULPITT, C. J., PINTO, E. S. & RAJKUMAR, C. 2003. The aging of elastic and muscular arteries: a comparison of diabetic and nondiabetic subjects. *Diabetes care,* 26**,** 2133-2138.

CECELJA, M. & CHOWIENCZYK, P. 2016. Molecular mechanisms of arterial stiffening. *Pulse,* 4**,** 43-48.

CHUNG, A., BOOTH, A., ROSE, C., THOMPSON, C., LEVIN, A. & VAN BREEMEN, C. 2008. Increased matrix metalloproteinase 2 activity in the human internal mammary artery is associated with ageing, hypertension, diabetes and kidney dysfunction. *Journal of vascular research,* 45**,** 357-362.

DINGEMANS, K. P., TEELING, P., LAGENDIJK, J. H. & BECKER, A. E. 2000. Extracellular matrix of the human aortic media: an ultrastructural histochemical and immunohistochemical study of the adult aortic media. *The Anatomical Record,* 258**,** 1-14.

ENGLER, A. J., REHFELDT, F., SEN, S. & DISCHER, D. E. 2007. Microtissue elasticity: measurements by atomic force microscopy and its influence on cell differentiation. *Methods in cell biology,* 83**,** 521-545.

ENGLER, A. J., RICHERT, L., WONG, J. Y., PICART, C. & DISCHER, D. E. 2004. Surface probe measurements of the elasticity of sectioned tissue, thin gels and polyelectrolyte multilayer films: correlations between substrate stiffness and cell adhesion. *Surface Science,* 570**,** 142-154.

FAARVANG, A.-S. A., PREIL, S. A. R., NIELSEN, P. S., BECK, H. C., KRISTENSEN, L. P. & RASMUSSEN, L. M. 2016. Smoking is associated with lower amounts of arterial type I collagen and decorin. *Atherosclerosis,* 247**,** 201-206.

FERNáNDEZ, B., KAMPMANN, A., PIPP, F., ZIMMERMANN, R. & SCHAPER, W. 2003. Osteoglycin expression and localization in rabbit tissues and atherosclerotic plaques. *Vascular Biochemistry.* Springer.

FISCHER, J. W., STEITZ, S. A., JOHNSON, P. Y., BURKE, A., KOLODGIE, F., VIRMANI, R., GIACHELLI, C. & WIGHT, T. N. 2004. Decorin promotes aortic smooth muscle cell calcification and colocalizes to calcified regions in human atherosclerotic lesions. *Arteriosclerosis, thrombosis, and vascular biology,* 24**,** 2391-2396.

FLEENOR, B. S., MARSHALL, K. D., DURRANT, J. R., LESNIEWSKI, L. A. & SEALS, D. R. 2010. Arterial stiffening with ageing is associated with transforming growth factor-β1-related changes in adventitial collagen: reversal by aerobic exercise. *The Journal of physiology,* 588**,** 3971-3982.

GOH, K., HOLMES, D., LU, H.-Y., RICHARDSON, S., KADLER, K., PURSLOW, P. & WESS, T. J. 2008. Ageing changes in the tensile properties of tendons: influence of collagen fibril volume fraction. *Journal of biomechanical engineering,* 130**,** 021011.

GOH, K. L., HOLMES, D., LU, Y., PURSLOW, P. P., KADLER, K., BéCHET, D. & WESS, T. J. 2012. Bimodal collagen fibril diameter distributions direct age-related variations in tendon resilience and resistance to rupture. *Journal of applied physiology,* 113**,** 878-888.

GORENNE, I., NAKAMOTO, R. K., PHELPS, C. P., BECKERLE, M. C., SOMLYO, A. V. & SOMLYO, A. P. 2003. LPP, a LIM protein highly expressed in smooth muscle. *American Journal of Physiology-Cell Physiology,* 285**,** C674-C685.

GRAHAM, H. K., AKHTAR, R., KRIDIOTIS, C., DERBY, B., KUNDU, T., TRAFFORD, A. W. & SHERRATT, M. J. 2011. Localised micro-mechanical stiffening in the ageing aorta. *Mechanisms of ageing and development,* 132**,** 459-467.

GRANT, C. A. & TWIGG, P. C. 2012. Pseudostatic and dynamic nanomechanics of the tunica adventitia in elastic arteries using atomic force microscopy. *ACS nano,* 7**,** 456-464.

HANSEN, M. L., BECK, H. C., IRMUKHAMEDOV, A., JENSEN, P. S., OLSEN, M. H. & RASMUSSEN, L. M. 2015. Proteome analysis of human arterial tissue discloses associations between the vascular content of small leucine-rich repeat proteoglycans and pulse wave velocity. *Arteriosclerosis, thrombosis, and vascular biology***,** ATVBAHA. 114.304706.

HEMMASIZADEH, A., AUTIERI, M. & DARVISH, K. 2012. Multilayer material properties of aorta determined from nanoindentation tests. *Journal of the mechanical behavior of biomedical materials,* 15**,** 199-207.

HEMMASIZADEH, A., TSAMIS, A., CHEHELTANI, R., ASSARI, S., D'AMORE, A., AUTIERI, M., KIANI, M. F., PLESHKO, N., WAGNER, W. R. & WATKINS, S. C. 2015. Correlations between transmural mechanical and morphological properties in

porcine thoracic descending aorta. *journal of the mechanical behavior of biomedical materials,* 47**,** 12-20.

HOLZAPFEL, G. A., GASSER, T. C. & STADLER, M. 2002. A structural model for the viscoelastic behavior of arterial walls: continuum formulation and finite element analysis. *European Journal of Mechanics-A/Solids,* 21**,** 441-463.

HWANG, J.-Y., JOHNSON, P. Y., BRAUN, K. R., HINEK, A., FISCHER, J. W., O'BRIEN, K. D., STARCHER, B., CLOWES, A. W., MERRILEES, M. J. & WIGHT, T. N. 2008. Retrovirally mediated overexpression of glycosaminoglycan-deficient biglycan in arterial smooth muscle cells induces tropoelastin synthesis and elastic fiber formation in vitro and in neointimae after vascular injury. *The American journal of pathology,* 173**,** 1919-1928.

KALAMAJSKI, S. & OLDBERG, Å. 2010. The role of small leucine-rich proteoglycans in collagen fibrillogenesis. *Matrix Biology,* 29**,** 248-253.

KAMPMANN, A., FERNáNDEZ, B., DEINDL, E., KUBIN, T., PIPP, F., EITENMüLLER, I., HOEFER, I. E., SCHAPER, W. & ZIMMERMANN, R. 2009. The proteoglycan osteoglycin/mimecan is correlated with arteriogenesis. *Molecular and cellular biochemistry,* 322**,** 15-23.

KERMANI, G., HEMMASIZADEH, A., ASSARI, S., AUTIERI, M. & DARVISH, K. 2017. Investigation of inhomogeneous and anisotropic material behavior of porcine thoracic aorta using nano-indentation tests. *Journal of the mechanical behavior of biomedical materials,* 69**,** 50-56.

LACOLLEY, P., REGNAULT, V., SEGERS, P. & LAURENT, S. 2017. Vascular Smooth Muscle Cells and Arterial Stiffening: Relevance in Development, Aging, and Disease. *Physiological reviews,* 97**,** 1555-1617.

LOPES, J., ADIGUZEL, E., GU, S., LIU, S.-L., HOU, G., HEXIMER, S., ASSOIAN, R. K. & BENDECK, M. P. 2013. Type VIII collagen mediates vessel wall remodeling after arterial injury and fibrous cap formation in atherosclerosis. *The American journal of pathology,* 182**,** 2241-2253.

LUNDKVIST, A., LILLEODDEN, E., SIEKHAUS, W., KINNEY, J., PRUITT, L. & BALOOCH, M. 1996. Viscoelastic properties of healthy human artery measured in saline solution by AFM-based indentation technique. *MRS Online Proceedings Library Archive,* 436.

MACBEATH, J., KIELTY, C. M. & SHUTTLEWORTH, C. A. 1996. Type VIII collagen is a product of vascular smooth-muscle cells in development and disease. *Biochemical Journal,* 319**,** 993.

MAO, Y., SUN, Q., WANG, X., OUYANG, Q., HAN, L., JIANG, L. & HAN, D. 2009. In vivo nanomechanical imaging of blood-vessel tissues directly in living mammals using atomic force microscopy. *Applied Physics Letters,* 95**,** 013704.

MCNULTY, M., MAHMUD, A. & FEELY, J. 2007. Advanced glycation end-products and arterial stiffness in hypertension. *American journal of hypertension,* 20**,** 242-247.

MERRILEES, M. J., TIANG, K. M. & SCOTT, L. 1987. Changes in collagen fibril diameters across artery walls including a correlation with glycosaminoglycan content. *Connective tissue research,* 16**,** 237-257.

O'ROURKE, M. F., STAESSEN, J. A., VLACHOPOULOS, C. & DUPREZ, D. 2002. Clinical applications of arterial stiffness; definitions and reference values. *American journal of hypertension,* 15**,** 426-444.

ONDA, M., ISHIWATA, T., KAWAHARA, K., WANG, R., NAITO, Z. & SUGISAKI, Y. 2002. Expression of lumican in thickened intima and smooth muscle cells in human coronary atherosclerosis. *Experimental and molecular pathology,* 72**,** 142-149.

PELOQUIN, J., HUYNH, J., WILLIAMS, R. M. & REINHART-KING, C. A. 2011. Indentation measurements of the subendothelial matrix in bovine carotid arteries. *Journal of biomechanics,* 44**,** 815-821.

PREIL, S. A., KRISTENSEN, L. P., BECK, H. C., JENSEN, P. S., NIELSEN, P. S., STEINICHE, T., BJøRLING-POULSEN, M., LARSEN, M. R., HANSEN, M. L. & RASMUSSEN, L. M. 2015. Quantitative proteome analysis reveals increased content of basement membrane proteins in arteries from patients with type 2 diabetes and lower levels among metformin users. *Circulation: Genomic and Precision Medicine***,** CIRCGENETICS. 115.001165.

QIU, H., ZHU, Y., SUN, Z., TRZECIAKOWSKI, J. P., GANSNER, M., DEPRE, C., RESUELLO, R. R., NATIVIDAD, F. F., HUNTER, W. C. & GENIN, G. M. 2010. Vascular smooth muscle cell stiffness as a mechanism for increased aortic stiffness with agingnovelty and significance. *Circulation research,* 107**,** 615-619.

SCHAEFER, L., TSALASTRA, W., BABELOVA, A., BALIOVA, M., MINNERUP, J., SOROKIN, L., GRöNE, H.-J., REINHARDT, D. P., PFEILSCHIFTER, J. & IOZZO, R. V. 2007. Decorin-mediated regulation of fibrillin-1 in the kidney involves the insulin-like growth factor-I receptor and Mammalian target of rapamycin. *The American journal of pathology,* 170**,** 301-315.

SHIMIZU-HIROTA, R., SASAMURA, H., KURODA, M., KOBAYASHI, E., HAYASHI, M. & SARUTA, T. 2004. Extracellular matrix glycoprotein biglycan enhances vascular smooth muscle cell proliferation and migration. *Circulation research,* 94**,** 1067-1074.

SHIRWANY, N. A. & ZOU, M.-H. 2010. Arterial stiffness: a brief review. *Acta Pharmacologica Sinica,* 31**,** 1267.

SIBINGA, N. E., FOSTER, L. C., HSIEH, C.-M., PERRELLA, M. A., LEE, W.-S., ENDEGE, W. O., SAGE, E. H., LEE, M.-E. & HABER, E. 1997. Collagen VIII is expressed by vascular smooth muscle cells in response to vascular injury. *Circulation research,* 80**,** 532-541.

SICARD, D., FREDENBURGH, L. E. & TSCHUMPERLIN, D. J. 2017. Measured pulmonary arterial tissue stiffness is highly sensitive to AFM indenter dimensions. *Journal of the mechanical behavior of biomedical materials,* 74**,** 118-127.

SIMS, T., RASMUSSEN, L., OXLUND, H. & BAILEY, A. 1996. The role of glycation cross-links in diabetic vascular stiffening. *Diabetologia,* 39**,** 946.

SPITZNER, E.-C., RÖPER, S., ZERSON, M., BERNSTEIN, A. & MAGERLE, R. 2015. Nanoscale swelling heterogeneities in type I collagen fibrils. *ACS nano,* 9**,** 5683-5694.

TALUSAN, P., BEDRI, S., YANG, S., KATTAPURAM, T., SILVA, N., ROUGHLEY, P. J. & STONE, J. R. 2005. Analysis of intimal proteoglycans in atherosclerosis-prone and atherosclerosis-resistant human arteries by mass spectrometry. *Molecular & Cellular Proteomics,* 4**,** 1350-1357.

WALLACE, S., MCENIERY, C. M., DAKHAM, Z., PUSALKAR, P., MAKI-PETAJA, K., ASHBY, M. J., COCKCROFT, J. R. & WILKINSON, I. B. 2005. Matrix metalloproteinase-9 (MMP-9), MMP-2, and serum elastase activity are associated with systolic hypertension and arterial stiffness. *Arteriosclerosis, thrombosis, and vascular biology,* 25**,** 372-378.

WEISBECKER, H., VIERTLER, C., PIERCE, D. M. & HOLZAPFEL, G. A. 2013. The role of elastin and collagen in the softening behavior of the human thoracic aortic media. *Journal of biomechanics,* 46**,** 1859-1865.

WIGHT, T. N. 1989. Cell biology of arterial proteoglycans. *Arteriosclerosis, Thrombosis, and Vascular Biology,* 9**,** 1-20.

WOOD, L. K., ARRUDA, E. M. & BROOKS, S. V. 2011. Regional stiffening with aging in tibialis anterior tendons of mice occurs independent of changes in collagen fibril morphology. *Journal of applied physiology,* 111**,** 999-1006.

ZHANG, H. J., WANG, J., LIU, H. F., ZHANG, X. N., ZHAN, M. & CHEN, F. L. 2015. Overexpression of mimecan in human aortic smooth muscle cells inhibits cell proliferation and enhances apoptosis and migration. *Experimental and therapeutic medicine,* 10**,** 187-192.

Chapter 6

Discussion and Limitations

This chapter discusses the main findings of this thesis and compares them with similar research in the literature to highlights the implications of this research. The limitations of this work are also described.

6.1 Discussion

6.1.1 Nanomechanical mapping by AFM PeakForce QNM

In this thesis, the author developed the AFM PeakForce QNM technique to characterise the small-scale biological structures in air and fluid environments. The mechanical properties of these tissues and ECM components are important in normal function and in the progressions of diseases and ageing. To gain insight into changes in the biomechanics of tissue structure with the development of diseases and ageing, it is essential to accurately assess the nanomechanical properties of tissue structure and ECM components. Nevertheless, the accuracy of the nanomechanical mapping highly depends on various factors such as probe parameters, calibration and operation procedures. In particular, the influence of AFM tip geometry and diameter on the mechanical assessment is considerable. The measured Young's modulus is significantly increased when using a sharp AFM tip, compared to larger tips (Sicard *et al*., 2017). In this study, two different shape tips were used in air (RTESPA-150: tip radius = 8 nm) and fluid (SCANASYST-FLUID: tip radius = 20 nm) conditions respectively. Such probes are much smaller than the indenters/probes used in previous arterial nanoindentation (Kermani *et al*., 2017, Hemmasizadeh *et al*., 2012, Akhtar *et al*., 2009) and AFM nanoindentation (Lundkvist *et al*., 1996, Grant and Twigg, 2012, Peloquin *et al*., 2011, Engler *et al*., 2007, Engler *et al*., 2004) measurements and the measured elastic modulus significantly vary. Only a few other researchers (Beenakker *et al*., 2012, Mao *et al*., 2009) used the similar tip sizes as in this work. Thus, the tip geometry and radius can be a critical parameter when compared with literature values for arterial tissues mechanical characterisation by AFM or nanoindentation methods. Moreover, the measured elastic modulus from a sharp tip is capable of reflecting the interaction of the AFM tip with the nanoscale arterial structure and ECM compounds. The advantages of using sharp tips are

theoretically attractive, including a better resolution for probing smaller cellular and ECM features. The DMT analytical model used in this study assumed the sharp tip to be spherical which can minimise the strain and fulfil the assumption of small strains in Hertz's mode (Sicard *et al*., 2017).

Tissue section thickness is also a key parameter that significantly associates with the measured elastic modulus. Generally, the measured elastic modulus increases as the section thickness decreases. The relatively high measured elastic modulus on thin sections can be attributed to the influence of the underlying hard substrate (Gavara and Chadwick, 2012), the large indentation depth-to-section thickness ratio (> 10 %) and the finite section effect (Dimitriadis *et al*., 2002). Moreover, the variability of elastic modulus determined on thick section is much higher than that on the thin section (Sicard *et al*., 2017). This significant variation of measured elastic modulus in AFM measurement can reflect the heterogeneity of the sample (Rico *et al*., 2005). It is also noteworthy that the Hertz/DMT model assumes homogeneity and isotropy of samples. However, biological tissues like arteries and bones are anisotropic, hence the inherent tissue anisotropy may contribute to the thickness associated variation of the measured elastic modulus. In addition, the elastic modulus of thin tissue sections (thickness ≤ 10 μm) is not influenced by the applied force, while for the thick section the measured modulus can be significantly increased with more load applied onto the tip (Sicard *et al*., 2017). Taken together, to gain accurate mechanical mapping, it is, therefore, reasonable to section the zebrafish vertical column and human IMA to 10 μm and 5 μm thickness respectively in this study. More importantly, the maximum indentation depth is precisely controlled under 10 nm in this study through controlling the applied force on the AFM tip that the section thickness-to-tip radius ratios far exceeded the accepted value and avoids the non-linear strain-stiffening properties and substrate effect (Karduna *et al*., 1997).

The range of the working force applied to the sample plays an important role in the mechanical testing of soft biological tissues. Small applied forces can cause serious errors resulting from high experimental noise and misidentification of the contact point, whilst high loading forces can damage the tissue and even fracture the probe (Sicard *et al*., 2017). In this study, PeakForce QNM is capable of controlling the applied force around nN, thus allows for a relatively accurate mechanical measurement on the delicate soft tissue.

6.1.2 Characterisation of small-scale biological structures and tissue ECM components

Although the functionalities of biological samples are highly dependent on the tissue structure, the fundamental mechanical and structural properties of localised microstructure and tissue ECM components remain poorly understood. This is mainly because of the disparity between the measurable length scale of conventional mechanical testing techniques (10^{-3} to 10^{-1} m) and the size of biological tissue components (10^{-6} to 10^{-4} m) (Akhtar *et al*., 2011). In this study, the average size of the zebrafish vertebral column is less than 200 μm in diameter. This corresponds to the dimensions of most tissue components and cells (Akhtar *et al*., 2011), as well as the human IMAs. PeakForce QNM promises an exciting potential to directly link the properties of fine tissue microstructure and even ECM components to their *in situ* nanomechanical properties, which drive a comprehensive understanding into how the tissue ultrastructural properties affect the overall tissue properties and the pathology of numerous diseases and ageing process.

To date, there lacks a standard predictor that can be widely targeted to explore changes in biological tissue structure in the progress of diseases and ageing. Given the ubiquitous distribution throughout the body and characteristic banding pattern, collagen fibrils are

regarded as a perfect nanoscale marker to reflect the tissue ultrastructural properties and link tissue structure and mechanics at the nanoscale. The collagen fibril morphology and organisation in numerous tissues have been well documented to associate with the pathological progression of various diseases and ageing (Kotova *et al*., 2015, Wood *et al*., 2011, Wallace *et al*., 2010, Danielson *et al*., 1997, Daxer *et al*., 1998, Sáez *et al*., 2016). However, due to its small size (diameter ranges from approximately 20 nm in the corneal (Daxer *et al*., 1998) to 500 nm in the tendon (Goh *et al*., 2012)), conventional mechanical testing methods cannot directly probe its mechanical properties. This research examined the bone and arterial tissues by using the AFM based PeakForce QNM and demonstrated the utility of this technique for characterising the morphological and mechanical properties of collagen fibrils simultaneously in both soft and hard biological tissues. Furthermore, this study developed a custom collagen fibril analysis routine (Chapter 4) that significantly improved the utility of collagen fibril as a tissue quality marker compared to the previous 2D fast Fourier transform image analysis method (Wallace *et al*., 2010, Wallace *et al*., 2011, Fang *et al*., 2012). Using PeakForce QNM, this study demonstrated that collagen promises an excellent target to illuminate age- and disease-related changes and link structure-mechanics-function in biological tissues.

6.1.3 Stiffening of the human IMA

In this study, the ultrastructural stiffness of the hydrated media and dehydrated media and adventitia in the IMA from low and high PWV group were characterised for understanding the development of arterial stiffening at the nanoscale. Meanwhile, the topography of the corresponding ultrastructure was also mapped.

All of the hydrated and dehydrated IMA individual layers exhibit high structural stiffness at the nanoscale in patients with high PWV, which demonstrates that the tissue ultrastructural

mechanical behaviour of the IMA in hydrated or dehydrated condition severs as a powerful predictor for distinguishing patient cohort. Moreover, the localised elastic modulus of the hydrated media and dehydrated adventitia associated with the degree of arterial stiffness assessed by PWV. Given the various tissue constitutions of each arterial layer, the ultrastructural properties combined with the proteome analysis data are utilised to investigate the localised ultrastructural stiffening in different layers with the development of arterial stiffening.

Given the no or little elastin content in the media in this study, most of the IMAs are muscular arteries. Thus, the IMA media mainly consists of collagen, SMCs and other ECM components and the IMA adventitia is primarily composed of collagen and fibroblasts. However, the *in situ* ultrastructural imaging of the IMA only revealed distinct fibrillary collagen (type I and type III) (O'Connell *et al*., 2008) in the dehydrated media and adventitia, while the other tissue components were not distinguishable. This is because the fibrillar collagen fibrils possess the characteristic 67 nm banding structure and are abundant across the IMA, especially in the adventitia. Thus, the morphology of these arterial collagen fibrils serves as an excellent nanoscale marker for exposing the ultrastructural changes with arterial stiffening. In the human IMA, medial collagen fibrils were significantly smaller than the adventitial collagen fibrils. This finding is consistent with the previous studies (Buck, 1987, Dingemans *et al*., 2000, Merrilees *et al*., 1987). Although there was no statistically significant difference in the medial collagen fibril diameter in patients with high PWV, the diameter and D-period of adventitial collagen fibrils showed profound alterations in the high PWV group. The main differences were the distributions of the collagen fibril sizes and D-periods. In particular, there are less collagen fibrils with small diameters (70 - 120 nm) in the IMA adventitia from high PWV group, which is presumed to be a protective mechanism for withstanding high blood pressure and wider pulse pressure with arterial stiffening. On the

other hand, for the adventitial collagen fibrils in the IMA with high PWV, there were more fibrils with the low D-period (45 - 59 nm) and also more fibrils with the high D-period (70 - 80 nm). Although the underlying reasons of the altered D-period are still unknown, the heterogeneity in the collagen D-period is important for understanding tissue properties and functions (Chen *et al*., 2017). Collectively, both the collagen diameter and D-period serve as good nanoscale predictor for reflecting changes within the arterial tissue's local ultrastructure.

In the IMAs, the PeakForce QNM data was integrated with the proteome analysis data for understanding the associations between the ECM remodelling and ultrastructural alterations with arterial stiffening. The subgroup of ECM proteins called SLRPs was almost all significantly regulated in patients with high PWV (Hansen *et al*., 2015). In the present study, within the dehydrated adventitia, previous identified arterial stiffening associated SLRPs were found to contribute to the separation of the patients with low and high PWV. Biglycan was found closely related to adventitia collagen diameter. More importantly, in hydrated media, these SLRPs were negatively correlated with the ultrastructural stiffness. The SLRPs are essential in the tissue ECM remodelling since they are capable of regulating the critical tissue components. In particular, SLRPs are involved in collagen fibril formation (Chen and Birk, 2013, Kalamajski and Oldberg, 2010) that result in abnormal fibril diameter and distribution (Robinson *et al*., 2017) and even tissue failure and dysfunction (Danielson *et al*., 1997, Heegaard *et al*., 2007, Chen and Birk, 2013, Corsi *et al*., 2002). Thus, it is reasonable to speculate that the ultrastructural stiffening in the collagen-rich IMA adventitia is associated with the altered collagen morphology that may attribute to the downregulated SLRPs. Furthermore, the arterial SLRPs highly expressed in the SMCs are important in regulating the proliferation and migration of SMCs which is predominant in the IMA media (Onda *et al*., 2002, Zhang *et al*., 2015). Although the SMC is mechanically insignificant for the arterial wall, it is crucial to controlling the synthesis and organising of the arterial ECM, including

collagen, elastin, and proteoglycans, which are highly responsible for arterial mechanics (Lacolley *et al*., 2017). Therefore, it is tempting to speculate that the downregulated certain SLRPs may lead to disordered proliferation and migration of the medial SMCs and thus increase the medial ultrastructural stiffness with the development of arterial stiffening. In addition, there were some other abnormal ECM proteins (e.g. network-forming collagens and actin cytoskeletal components) observed in patients with high degree of arterial stiffness. These proteins are also important in the SMC migration, differentiation and morphogenesis (Sibinga *et al*., 1997, MacBeath *et al*., 1996, Lopes *et al*., 2013). These structural proteins serve as critical connections between the SMCs and ECM (Gorenne *et al*., 2003) in the arterial wall. Collectively, the IMA medial remodelling profoundly associates with the expression activity of SLRPs and several other specific ECM proteins with the progression of arterial stiffening.

6.2 Limitations

6.2.1 PeakForce QNM technique limitations

In this study, it has been shown that PeakForce QNM promises to be an exciting approach for characterising small-scale biological structures and the ECM components at the nanoscale. This approach significantly improves the understanding of how the altered tissue properties associated with the development of diseases and ageing. Nevertheless, there are still several limitations with this nanoscale technique that must be considered. Firstly, the main limitation of this technique is itself invasive and requires tissue isolation and cutting to expose the surface which is to be probed (Sicard *et al*., 2017). The nanomechanical and ultrastructural mapping is also profoundly influenced by the tissue section thickness, probe size and applied force. Secondly, the piezo actuators of the AFM have a limited range in the z-direction,

which significantly limits the sample thickness or depth (10 - 20 μm). Also, since the probe needs to be scanned across the sample surface during the AFM testing, it is possible that the shape of the probe is convoluted into the resulting image and the imaging error can be worse when the tip is dulled or damaged. Thus, the sample surface must be relatively flat, and the tissue section thickness cannot exceed the testing limitation. Thirdly, due to the considerable heterogeneity and soft behaviour, the AFM scanning area for biological structure generally cannot exceeds 50 × 50 μm^2 and the AFM can only characterise the localised mechanical properties instead of across the whole tissue. Finally, although PeakForce QNM has dramatically improved the scanning speed, a tradeoff between the image quality and testing time need to be addressed.

6.2.3 Sample limitations

6.2.3.1 Zebrafish model

When the zebrafish are used as a model for understanding bone development, differences in the bone structure and remodelling process between the zebrafish and the human need to be addressed, though the zebrafish skeleton possesses numerous similarities compared to human bone. The loading environment on the zebrafish skeleton system is also different to that of humans. Due to the small dimension of the zebrafish and its skeleton, it is challenging to conduct conventional mechanical testing methods, which is similar to the issues with the human IMA.

6.2.3.2 Human IMA

In this study, the human IMA is used as a model vessel for understanding the development of arterial stiffening. However, there also have a number of limitations which should be addressed. The IMA is not involved in the carotid-femoral PWV pathway, meaning the

stiffness of the IMA does not contribute to the carotid-femoral PWV measurement itself. This study also does not demonstrate a mechanistic relationship between the elastic modulus of the IMA and the PWV assessment. Secondly, although the IMA is a transitional type of artery, most of the measured IMAs are muscular arteries where the elastin and elastic fibres are absent. However, the medial elastic fibres and lamellae are essential for the mechanics and function of the arterial tissue. Finally, due to the limit amount of tissue available per patient and various parallel studies conducted in this study, it is not possible to compare the AFM data with established functional biomechanical tests such as wire or pressure myography.

6.2.4 Limitations with the experimental approach

6.2.4.1 Zebrafish vertebral column study

For the zebrafish skeleton study, only the posterior of the precaudal vertebral column was characterised. However, it is important to examine the entire vertebral column from the precaudal to the caudal vertebrae for a better understanding of the regional variations in the bone structure with the progression of diseases or ageing. Moreover, PeakForce QNM only determines the nanoscale elastic modulus which cannot comprehensively characterise the mechanical properties of bone. Although the collagen fibrils were observed in the zebrafish skeleton, it is difficult to directly analyse these bone collagen due to the interfibrillar mineralisation.

6.2.4.2 Human IMA study

In the arterial stiffening study, firstly, the nano-level structural and mechanical alterations across the arterial wall with arterial stiffening have been examined. However, it was not possible to test the tunica intima due to its thin thickness. Secondly, although the diameter and D-period of adventitial collagen fibrils and medial collagen fibril size have been analysed,

the organisation of the arterial collagen fibrils is not studied. This is essential for assessing the global biomechanics of the biological tissue. Thirdly, this study did not conduct any quantitative measurement of the collagen and elastin content in the individual layers which would complement the AFM work for explaining the progression of arterial stiffening. Finally, except for the certain identified proteins from the quantitative proteomic analysis, there still have numerous stiffening related proteins and molecules in the arteries that to be further identified.

6.2.4.3 Nanomechanical data analysis

For each patient, there were 6 random localised images captured. This entailed 65,536 and 147,456 measurements in each mechanical mapping in ambient and liquid conditions respectively. This study used the mean as metric for each image because the nanomechanical measurements of most images were normally distributed (see example in Figure 6 panels A&B). However, there were some images that have different distributions with the most common a positively skewed normal distribution (see example Figure 6 panels C&D), which is normal in biological tissue nanomechanics. Thus, it is better to use median instead of the mean to represent those images. To avoid the invalidation of the nanomechanical measurements, the mechanical mapping of the low and high PWV patients were conducted at the same time with the same AFM probe. In addition, the non-parametric statistical methods (Mann-Whitney, Kruskal-Wallis and Kolmogorov–Smirnov tests) were used in this study to analyse the nanomechanical data between the two groups.

In this study, the author followed the same method for all samples to compare two groups of patients. Thus, it is expected that there should be not major bias introduced due to the limitation above and so the overall results should not change.

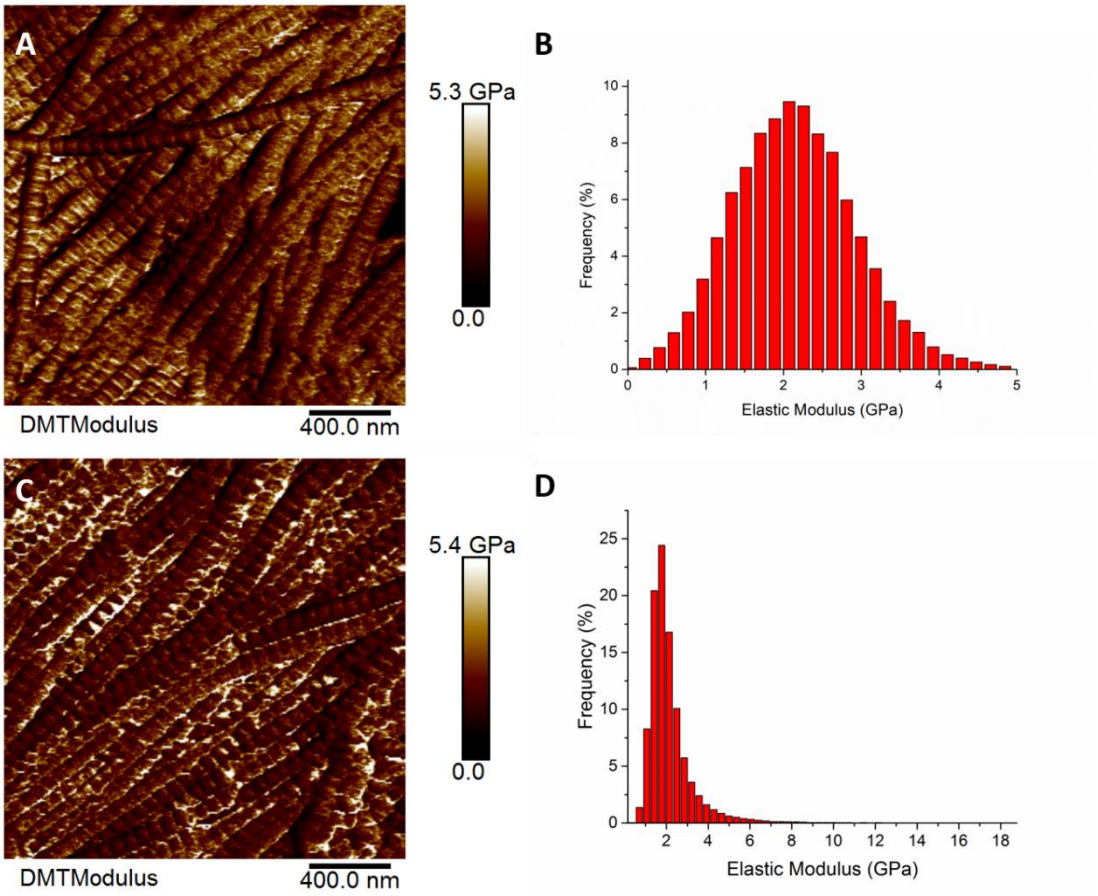

Figure 6. Example DMT modulus images of the nanomechanical properties and the corresponding modulus distribution of the dehydrated adventitia from patient No. 534 (A and B) and No. 693 (C and D). There were 65,536 measurements in each image.

In this study, the author followed the same method for all samples to compare two groups of patients. Thus, it is expected that there should be not major bias introduced due to the limitation above and so the overall results should not change.

References

AKHTAR, R., SCHWARZER, N., SHERRATT, M., WATSON, R., GRAHAM, H., TRAFFORD, A., MUMMERY, P. & DERBY, B. 2009. Nanoindentation of

histological specimens: mapping the elastic properties of soft tissues. *Journal of materials research,* 24**,** 638-646.

AKHTAR, R., SHERRATT, M. J., CRUICKSHANK, J. K. & DERBY, B. 2011. Characterizing the elastic properties of tissues. *Materials Today,* 14**,** 96-105.

BEENAKKER, J.-W. M., ASHCROFT, B. A., LINDEMAN, J. H. & OOSTERKAMP, T. H. 2012. Mechanical properties of the extracellular matrix of the aorta studied by enzymatic treatments. *Biophysical journal,* 102**,** 1731-1737.

BUCK, R. C. 1987. Collagen fibril diameter in the common carotid artery of the rat. *Connective tissue research,* 16**,** 121-129.

CHEN, J., AHN, T., COLON-BERNAL, I. D., KIM, J. & BANASZAK HOLL, M. M. 2017. The Relationship of Collagen Structural and Compositional Heterogeneity to Tissue Mechanical Properties: A Chemical Perspective. *ACS Nano,* 11**,** 10665-10671.

CHEN, S. & BIRK, D. E. 2013. The regulatory roles of small leucine-rich proteoglycans in extracellular matrix assembly. *The FEBS journal,* 280**,** 2120-2137.

CORSI, A., XU, T., CHEN, X. D., BOYDE, A., LIANG, J., MANKANI, M., SOMMER, B., IOZZO, R., EICHSTETTER, I. & ROBEY, P. G. 2002. Phenotypic effects of biglycan deficiency are linked to collagen fibril abnormalities, are synergized by decorin deficiency, and mimic Ehlers-Danlos-like changes in bone and other connective tissues. *Journal of Bone and Mineral Research,* 17**,** 1180-1189.

DANIELSON, K. G., BARIBAULT, H., HOLMES, D. F., GRAHAM, H., KADLER, K. E. & IOZZO, R. V. 1997. Targeted disruption of decorin leads to abnormal collagen fibril morphology and skin fragility. *The Journal of cell biology,* 136**,** 729-743.

DAXER, A., MISOF, K., GRABNER, B., ETTL, A. & FRATZL, P. 1998. Collagen fibrils in the human corneal stroma: structure and aging. *Investigative ophthalmology & visual science,* 39**,** 644-648.

DIMITRIADIS, E. K., HORKAY, F., MARESCA, J., KACHAR, B. & CHADWICK, R. S. 2002. Determination of elastic moduli of thin layers of soft material using the atomic force microscope. *Biophysical journal,* 82**,** 2798-2810.

DINGEMANS, K. P., TEELING, P., LAGENDIJK, J. H. & BECKER, A. E. 2000. Extracellular matrix of the human aortic media: an ultrastructural histochemical and immunohistochemical study of the adult aortic media. *The Anatomical Record,* 258**,** 1-14.

ENGLER, A. J., REHFELDT, F., SEN, S. & DISCHER, D. E. 2007. Microtissue elasticity: measurements by atomic force microscopy and its influence on cell differentiation. *Methods in cell biology,* 83**,** 521-545.

ENGLER, A. J., RICHERT, L., WONG, J. Y., PICART, C. & DISCHER, D. E. 2004. Surface probe measurements of the elasticity of sectioned tissue, thin gels and polyelectrolyte multilayer films: correlations between substrate stiffness and cell adhesion. *Surface Science,* 570**,** 142-154.

FANG, M., GOLDSTEIN, E. L., TURNER, A. S., LES, C. M., ORR, B. G., FISHER, G. J., WELCH, K. B., ROTHMAN, E. D. & BANASZAK HOLL, M. M. 2012. Type I collagen D-spacing in fibril bundles of dermis, tendon, and bone: bridging between nano-and micro-level tissue hierarchy. *ACS nano,* 6**,** 9503-9514.

GAVARA, N. & CHADWICK, R. S. 2012. Determination of the elastic moduli of thin samples and adherent cells using conical atomic force microscope tips. *Nature nanotechnology,* 7**,** 733.

GOH, K. L., HOLMES, D., LU, Y., PURSLOW, P. P., KADLER, K., BéCHET, D. & WESS, T. J. 2012. Bimodal collagen fibril diameter distributions direct age-related variations in tendon resilience and resistance to rupture. *Journal of applied physiology,* 113**,** 878-888.

GORENNE, I., NAKAMOTO, R. K., PHELPS, C. P., BECKERLE, M. C., SOMLYO, A. V. & SOMLYO, A. P. 2003. LPP, a LIM protein highly expressed in smooth muscle. *American Journal of Physiology-Cell Physiology,* 285**,** C674-C685.

GRANT, C. A. & TWIGG, P. C. 2012. Pseudostatic and dynamic nanomechanics of the tunica adventitia in elastic arteries using atomic force microscopy. *ACS nano,* 7**,** 456-464.

HANSEN, M. L., BECK, H. C., IRMUKHAMEDOV, A., JENSEN, P. S., OLSEN, M. H. & RASMUSSEN, L. M. 2015. Proteome analysis of human arterial tissue discloses associations between the vascular content of small leucine-rich repeat proteoglycans and pulse wave velocity. *Arteriosclerosis, thrombosis, and vascular biology***,** ATVBAHA. 114.304706.

HEEGAARD, A.-M., CORSI, A., DANIELSEN, C. C., NIELSEN, K. L., JORGENSEN, H. L., RIMINUCCI, M., YOUNG, M. F. & BIANCO, P. 2007. Biglycan deficiency causes spontaneous aortic dissection and rupture in mice. *Circulation,* 115**,** 2731-2738.

HEMMASIZADEH, A., AUTIERI, M. & DARVISH, K. 2012. Multilayer material properties of aorta determined from nanoindentation tests. *Journal of the mechanical behavior of biomedical materials,* 15**,** 199-207.

KALAMAJSKI, S. & OLDBERG, Å. 2010. The role of small leucine-rich proteoglycans in collagen fibrillogenesis. *Matrix Biology,* 29**,** 248-253.

KARDUNA, A. R., HALPERIN, H. R. & YIN, F. C. 1997. Experimental and numerical analyses of indentation in finite-sized isotropic and anisotropic rubber-like materials. *Annals of biomedical engineering,* 25**,** 1009-1016.

KERMANI, G., HEMMASIZADEH, A., ASSARI, S., AUTIERI, M. & DARVISH, K. 2017. Investigation of inhomogeneous and anisotropic material behavior of porcine thoracic

aorta using nano-indentation tests. *Journal of the mechanical behavior of biomedical materials,* 69**,** 50-56.

KOTOVA, S. L., TIMASHEV, P. S., GULLER, A. E., SHEKHTER, A. B., MISURKIN, P. I., BAGRATASHVILI, V. N. & SOLOVIEVA, A. B. 2015. Collagen structure deterioration in the skin of patients with pelvic organ prolapse determined by atomic force microscopy. *Microscopy and Microanalysis,* 21**,** 324-333.

LACOLLEY, P., REGNAULT, V., SEGERS, P. & LAURENT, S. 2017. Vascular Smooth Muscle Cells and Arterial Stiffening: Relevance in Development, Aging, and Disease. *Physiological reviews,* 97**,** 1555-1617.

LOPES, J., ADIGUZEL, E., GU, S., LIU, S.-L., HOU, G., HEXIMER, S., ASSOIAN, R. K. & BENDECK, M. P. 2013. Type VIII collagen mediates vessel wall remodeling after arterial injury and fibrous cap formation in atherosclerosis. *The American journal of pathology,* 182**,** 2241-2253.

LUNDKVIST, A., LILLEODDEN, E., SIEKHAUS, W., KINNEY, J., PRUITT, L. & BALOOCH, M. 1996. Viscoelastic properties of healthy human artery measured in saline solution by AFM-based indentation technique. *MRS Online Proceedings Library Archive,* 436.

MACBEATH, J., KIELTY, C. M. & SHUTTLEWORTH, C. A. 1996. Type VIII collagen is a product of vascular smooth-muscle cells in development and disease. *Biochemical Journal,* 319**,** 993.

MAO, Y., SUN, Q., WANG, X., OUYANG, Q., HAN, L., JIANG, L. & HAN, D. 2009. In vivo nanomechanical imaging of blood-vessel tissues directly in living mammals using atomic force microscopy. *Applied Physics Letters,* 95**,** 013704.

MERRILEES, M. J., TIANG, K. M. & SCOTT, L. 1987. Changes in collagen fibril diameters across artery walls including a correlation with glycosaminoglycan content. *Connective tissue research,* 16**,** 237-257.

O'CONNELL, M. K., MURTHY, S., PHAN, S., XU, C., BUCHANAN, J., SPILKER, R., DALMAN, R. L., ZARINS, C. K., DENK, W. & TAYLOR, C. A. 2008. The three-dimensional micro-and nanostructure of the aortic medial lamellar unit measured using 3D confocal and electron microscopy imaging. *Matrix Biology,* 27**,** 171-181.

ONDA, M., ISHIWATA, T., KAWAHARA, K., WANG, R., NAITO, Z. & SUGISAKI, Y. 2002. Expression of lumican in thickened intima and smooth muscle cells in human coronary atherosclerosis. *Experimental and molecular pathology,* 72**,** 142-149.

PELOQUIN, J., HUYNH, J., WILLIAMS, R. M. & REINHART-KING, C. A. 2011. Indentation measurements of the subendothelial matrix in bovine carotid arteries. *Journal of biomechanics,* 44**,** 815-821.

RICO, F., ROCA-CUSACHS, P., GAVARA, N., FARRé, R., ROTGER, M. & NAVAJAS, D. 2005. Probing mechanical properties of living cells by atomic force microscopy with blunted pyramidal cantilever tips. *Physical Review E,* 72**,** 021914.

ROBINSON, K. A., SUN, M., BARNUM, C. E., WEISS, S. N., HUEGEL, J., SHETYE, S. S., LIN, L., SAEZ, D., ADAMS, S. M., IOZZO, R. V., SOSLOWSKY, L. J. & BIRK, D. E. 2017. Decorin and biglycan are necessary for maintaining collagen fibril structure, fiber realignment, and mechanical properties of mature tendons. *Matrix Biol,* 64**,** 81-93.

SáEZ, P., GARCíA, A., PEñA, E., GASSER, T. C. & MARTíNEZ, M. 2016. Microstructural quantification of collagen fiber orientations and its integration in constitutive modeling of the porcine carotid artery. *Acta biomaterialia,* 33**,** 183-193.

SIBINGA, N. E., FOSTER, L. C., HSIEH, C.-M., PERRELLA, M. A., LEE, W.-S., ENDEGE, W. O., SAGE, E. H., LEE, M.-E. & HABER, E. 1997. Collagen VIII is expressed by vascular smooth muscle cells in response to vascular injury. *Circulation research,* 80**,** 532-541.

SICARD, D., FREDENBURGH, L. E. & TSCHUMPERLIN, D. J. 2017. Measured pulmonary arterial tissue stiffness is highly sensitive to AFM indenter dimensions. *Journal of the mechanical behavior of biomedical materials,* 74**,** 118-127.

WALLACE, J. M., ERICKSON, B., LES, C. M., ORR, B. G. & HOLL, M. M. B. 2010. Distribution of type I collagen morphologies in bone: relation to estrogen depletion. *Bone,* 46**,** 1349-1354.

WALLACE, J. M., ORR, B. G., MARINI, J. C. & HOLL, M. M. B. 2011. Nanoscale morphology of Type I collagen is altered in the Brtl mouse model of Osteogenesis Imperfecta. *Journal of structural biology,* 173**,** 146-152.

WOOD, L. K., ARRUDA, E. M. & BROOKS, S. V. 2011. Regional stiffening with aging in tibialis anterior tendons of mice occurs independent of changes in collagen fibril morphology. *Journal of applied physiology,* 111**,** 999-1006.

ZHANG, H. J., WANG, J., LIU, H. F., ZHANG, X. N., ZHAN, M. & CHEN, F. L. 2015. Overexpression of mimecan in human aortic smooth muscle cells inhibits cell proliferation and enhances apoptosis and migration. *Experimental and therapeutic medicine,* 10**,** 187-192.

Chapter 7

Conclusions and Future work

This chapter summarises the key findings and contributions of the research work. In addition, suggestions for continuing the current work are also made.

7.1 Conclusions

A zebrafish animal model and its vertebral column have been used to validate the utility of using the AFM Peakforce QNM for characterising small-scale biological structures. The human IMA has shown to be a model vessel for arterial stiffening and reflects more systemic changes in the vasculature. The nanomechanical mapping approach has been optimised and developed in the fluid and air environments for assessing hydrated and dehydrated tissues. The alterations in the mechanical properties of the medial and adventitial ultrastructure in patients with high arterial stiffness have been examined and found to associate with the clinical arterial stiffness assessment (PWV). The changes in the morphology of collagen fibrils across the IMA from patients with low and high PWV have also been determined to explain the nanomechanical data. The quantitative proteomics data has been integrated with the PeakForce QNM nanomechanical and morphological data for investigating the underlying changes and the structure-mechanics-function relation in vessels with arterial stiffening. Based on the objectives of this thesis, the key findings can be concluded in the following section.

The first objective of this thesis was to explore the utility of the AFM PeakForce QNM for probing localised nanomechanical and structural properties of small biological samples using a zebrafish model. The vertebral column of the zebrafish was studied at a range of ages. This was the first study to show how the ultrastructural and mechanical properties of the zebrafish bone change with advancing age. PeakForce QNM was validated with a range of complementary techniques including SEM and EDX. This allowed the sample preparation, nanomechanical mapping calibration and ultrastructural characterisation to be optimised for the subsequent work.

Having validated the utility of the PeakForce QNM for characterising small-scale biological structures, the next objective of the thesis was to assess the alterations in the IMA adventitia with the development of arterial stiffening. Given the difficulty in obtaining an aortic biopsy from patients with arterial stiffening and the readily accessible and ability of human IMA to reflecting changes across the vasculature, the IMA is seen as an ideal vessel for nano-scale *in vitro* characterisation of the development of arterial stiffening and CVDs. Here, the nanomechanical properties of the IMA dehydrated adventitia were determined using PeakForce QNM, and the measured elastic modulus of adventitia was associated with the clinical assessment of arterial stiffness (via carotid-femoral PWV) and certain SLRPs that have already found to be correlated with arterial stiffness (Hansen *et al*., 2015). Using a custom routine for Image SXM, the diameter and D-period of adventitial collagen fibrils were assessed, and both morphological parameters served as suitable nano-scale predictors for detecting changes in the local adventitial property and evaluating collagen fibril and adventitial 'quality' in pathology. The altered mechanical and morphological properties of IMA adventitia highlight the important role of the adventitia in arterial stiffening.

The third objective of this thesis was to assess the ultrastructural alterations in the IMA media in high PWV group, which is built on the second objective. The nanomechanical properties of the dehydrated media were also associated with the PWV assessed arterial stiffness. Given the different degree of increase in the nanomechanical properties and the different coefficient of variation of the measured modulus, the SMC-dominated media experienced more severe stiffening-related changes compared to the collagen-rich adventitia. However, there were no significant changes in the medial collagen diameter in patients with high PWV, which suggest the media collagen might not be a useful marker for assessing the alterations in the media with arterial stiffening, and hence highlights the relevance of the adventitia work covered with the previous objective. Compared to the adventitial collagen, the medial

collagen fibrils were smaller and randomly distributed that attribute to the different physiological functions of the media and adventitia. Although the nanomechanical properties of dehydrated media and adventitia were closely correlated and both played a role in the separation observed between both high and low PWV patients, the medial collagen diameter was not associated with the SLRPs. Hence, the dehydrated adventitia is a more powerful target for arterial stiffening study.

To the best of the author's knowledge, PeakForce QNM has never been used to assess hydrated vascular tissue under physiological condition. Here, the fourth objective of this thesis was to develop the PeakForce QNM conducted nanomechanical mapping in a fluid condition for characterising alterations in the IMA with arterial stiffening. The characterisation of hydrated biological samples in a fluid condition is no doubt a better environment for modelling the *in vivo* physiological environment. The PeakForce QNM nanomechanical mapping calibration in ambient condition was found to be accessible in the fluid conditions. A Spearman's rank correlation confirmed a statistically significant correlation ($p < 0.05$) between the nanomechanical properties of hydrated media and the clinical assessed arterial stiffness, as well as the certain SLRPs expression that has been proved to downregulated in high PWV group. Thus, in a physiological environment, the hydrated arterial tissue better reflects the changes in the certain SLRPs and thus associates with the ECM remodelling and pathology of arterial stiffening. This will be an invaluable approach for future studies exploring localised nano-scale alterations in vascular tissue with arterial stiffness and even CVDs.

Collectively, in the thesis, the Spearman's rank correlation revealed the positive correlations between the nanoscale mechanical properties of the hydrated and dehydrated individual IMA layers and the clinical assessment of arterial stiffness (via carotid-femoral PWV), which

demonstrates the possibility of characterising small biopsy samples for predicting the development of arterial stiffening.

Having assessed the localised nanomechanical alterations in the hydrated and dehydrated IMA individual layer and collagen fibril morphology across the IMA, the final objective of the thesis was to link the localised ultrastructural properties across the human IMA with the expression of arterial ECM proteins that have associated with high degree of arterial stiffness. The quantitative proteomics data of the IMAs were combined with the findings in this thesis to explain the localised arterial tissue remodelling with the development of arterial stiffening via the Spearman's rank correlation and PCA analysis. Due to the multi-functionality of the SLRPs in the key arterial tissue components including collagen, elastin and SMCs, the expression activity of certain SLRPs was relevant to the structure of collagen-rich IMA adventitia, and negatively correlated with the nanomechanical properties of the hydrated SMCs dominant IMA media. Therefore, the nanoscale localised characterisation of the individual hydrated and dehydrated arterial layers integrating by the certain arterial ECM proteins comprehensively disclosed the associations between the stiffening-related alterations at the molecular-level and that at the tissue ultrastructural-level in the artery for understanding the development of arterial stiffening.

7.2 Overall summary

In conclusion, based on the AFM Peakforce QNM technique, a systematic approach has been developed for assessing localised nanoscale mechanical and structural properties of small-scale biological samples and structures in hydrated and dehydrated conditions. Collagen fibrils serve as a nanoscale maker for reflecting the disease- or ageing-related changes in biological tissue. Alterations in the nanomechanical properties and collagen fibril

morphology across the human IMA have been characterised and associated with the degree of arterial stiffness. Finally, when combined with the quantitative proteomic data, the localised nanoscale characterisation of arterial structure bridges the gap between the understanding of the molecular-level pathological alterations and the apparent-level tissue dysfunction.

7.3 Future work

7.3.1 Nanomechanical mapping in a physiological environment

This study proves that it is more representative when the hydrated tissue is studied in a fluid environment. Therefore, for better modelling the disease- and ageing-related changes, it is recommended to characterise the *in situ* ultrastructural properties of hydrated arterial tissue section in a physiological environment. The approach for assessing hydrated biological tissue needs to be further developed to probe the localised mechanical and structural properties at the nano-scale.

7.3.2 Demineralisation for revealing the collagen fibrils in zebrafish skeleton

The collagen fibril has been proved to be an excellent nanoscale marker to explore the changes in tissue ultrastructure and mechanics with the development of diseases and ageing. To better assess the bone collagen fibril morphology, it is necessary to remove the minerals prior to the AFM testing. It has been established that the ethylenediaminetetraacetic acid (EDTA) (Sasaki *et al*., 2002) is an appropriate acid to demineralise and reveal the collagen fibrils in bone structure.

7.3.3 Characterisation of IMA tunica intima

The IMA tunica intima is highly associated with the development of hyperplasia and atherosclerosis (Ruengsakulrach *et al*., 1999). Thus, it is recommended to characterise the changes in the intimal ultrastructure in the future. Although the IMA intima is too thin to be accurately mapped in the tissue section in the present study, it is possible to cut the IMA tube longitudinally and expose the intima for AFM testing without tissue sectioning. This approach has been established *in vivo* in a rat aorta (Mao *et al*., 2009).

7.3.4 Quantitative assessment of the collagen and elastin content in different layers

Since both the collagen and elastin are key components to the mechanical and structural properties of arterial wall, it would be worth quantifying the changes in collagen and elastin concentrations of the different layers with arterial stiffening. This would complement the AFM work.

7.3.5 Layer-specific distribution of the SLRPs and other ECM remodelling associated proteins

Although the proteome analysis of the IMA has revealed the altered expression activity of certain SLRPs and several other ECM proteins, these proteins are collected from the overall IMA tissue that is not possible to reflect the layer-specific distribution. Given the localised characterisation of ultrastructural properties realised in this study, for the better association between the alterations at the molecule-level and the ultrastructure-level, it is critical to determine the layer-specific distribution of the SLRPs in the future.

Reference

HANSEN, M. L., BECK, H. C., IRMUKHAMEDOV, A., JENSEN, P. S., OLSEN, M. H. & RASMUSSEN, L. M. 2015. Proteome analysis of human arterial tissue discloses associations between the vascular content of small leucine-rich repeat proteoglycans and pulse wave velocity. *Arteriosclerosis, thrombosis, and vascular biology***,** ATVBAHA. 114.304706.

MAO, Y., SUN, Q., WANG, X., OUYANG, Q., HAN, L., JIANG, L. & HAN, D. 2009. In vivo nanomechanical imaging of blood-vessel tissues directly in living mammals using atomic force microscopy. *Applied Physics Letters,* 95**,** 013704.

RUENGSAKULRACH, P., SINCLAIR, R., KOMEDA, M., RAMAN, J., GORDON, I. & BUXTON, B. 1999. Comparative histopathology of radial artery versus internal thoracic artery and risk factors for development of intimal hyperplasia and atherosclerosis. *Circulation,* 100**,** II-139-Ii-144.

SASAKI, N., TAGAMI, A., GOTO, T., TANIGUCHI, M., NAKATA, M. & HIKICHI, K. 2002. Atomic force microscopic studies on the structure of bovine femoral cortical bone at the collagen fibril-mineral level. *Journal of Materials Science: Materials in Medicine,* 13**,** 333-337.

Appendix A

PeakForce QNM Calibration

To avoid accumulated errors that can cause errors in modulus measurements, the relative calibration method was conducted using a reference sample of known modulus prior to the PeakForce QNM mechanical measurement.

I. After choosing a probe that can cause enough deformation in the sample and still retain high force sensitivity, the deflection sensitivity was calibrated as the PeakForce QNM mode ramps the Z piezo and acquires force curves. A cantilever that is not thermally equilibrated tends to bend during the scanning process. This leads to movement of the laser spot which causes a sudden change of DMT modulus. To avoid this drift, it is notable that the probe needs to be maintained in the fluid environment at least 30 minutes for equilibration prior to any calibration.

a. The scan size was set to 0 nm and the probe was engaged onto a clean sapphire.
b. Then the ramp mode was active that the system scanning can be stopped and the probe can be located above the centre of the previous images.
c. After entering the parameter settings and selecting ramp single, the force-z position curve was obtained and the deflection sensitivity around the contact (steepest) portion of the approach was calculated.

II. Substantially, the spring constant of the probe was calibrated using thermal tuning method.

a. The probe was adequately withdrawn from the sample surface to ensure the probe could not interact with the sample during its self-excitation in the thermal tune.

b. A frequency range that includes the resonant frequency of the cantilever and active the thermal tune was selected to acquire the Power-Frequency curve.
c. Finally, the spring constant (K) of the cantilever can be obtained.

III. With regard to the relative calibration method, photostress coating polymer (PS1, Vishay Precision Group, Heilbronn, Germany) and custom made polydimethylsiloxane (PDMS) was used for mechanical measurement calibration in ambient and fluid conditions respectively. After inputting the nominal tip radius, the reference sample was loaded and conducted the mechanical measurement in small scan size (< 1 μm^2).

a. For ambient condition calibration, the 'ScanAsyst Auto Control' needed to be turned off and the Peak Force setpoint was adjusted accordingly until the deformation was around 1-3 nm and the measured DMT modulus was consistent with the known elastic modulus.
b. For fluid environment calibration, the 'ScanAsyst Auto Control' mode was applied to reduce the feedback gain and lower the noise.
c. In the PeakForce QNM measurements, it is essential to adjust the Peak Force setpoint to keep the deformation consistent with both reference and measured samples.

Appendix B

Clinical characteristics of all the patients. Former in smoking status means stopped smoking for at least 6 months.

Patient ID	Age,y	BMI	PWV, ms^{-1}	HbA1c	Cholesterol, $mmolL^{-1}$	LDL, $mmolL^{-1}$	HDL, $mmolL^{-1}$	Triglycerid, $mmolL^{-1}$	Creatinine, $mmolL^{-1}$	BP, mm Hg	Hypertension	Diabetes	Smoking
522	73.2	26	7.9	0.056	3.5	1.6	1.3	1.3	106	144/82	no	no	Former
549	57.9	26	7.7	0.061	3.7	1.6	1.3	1.7	69	156/79	no	no	Active
552	69.7	35	8	0.058	3.9	2.1	0.9	2	100	155/95	yes	no	Former
559	84.4	25	9.7	0.075	4.2	2.6	1.1	1.1	66	120/65	yes	yes	Former
565	66.3	24	9.1	0.054	4.8	2.9	1.1	1.8	87	115/75	yes	no	Never
631	67.7	26	8.8	0.053	4.1	1.7	1.1	2.8	125	115/80	no	no	Never
656	49.1	31	8.1	0.058	4.6	2.7	1.3	1.3	77	135/80	yes	no	Former
693	74.6	19	9	0.058	3.6	1.9	1.3	0.8	88	110/60	no	no	Never
524	64.4	26	13.8	0.055	3.8	1.9	1	2	91	128/72	no	no	Active
534	61.9	30	12.5	0.054	6.5	4.6	1.3	1.3	130	158/83	yes	no	Former
573	74.8	25	19.8	0.055	4.8	3	1.3	1.2	82	154/69	yes	no	Former
603	67.4	36	13.8	0.061	3.4	1.9	0.5	2.3	82	215/104	yes	no	Active
606	69.6	31	10	0.058	3.8	1.9	1.3	1.4	68	137/85	yes	no	Active
620	82.5	21	12.1	0.055	3.9	2.4	1.2	0.7	73	140/70	no	no	Former
627	72.6	33	16.2	0.059	6.5	4.5	1.1	1.9	92	184/76	no	no	Never
643	60.8	25	11.7	0.056	7.3	5.3	1.1	1.9	87	130/90	yes	no	Former
1202	74.8	29	10.9	0.057	3.8	2.3	0.9	1.4	119	141/66	yes	no	Active

Appendix C

Weigert's stain for elastin (left) and Masson's stain for collagen (right) for in all the patients. Scale Bar indicated 200 µm.

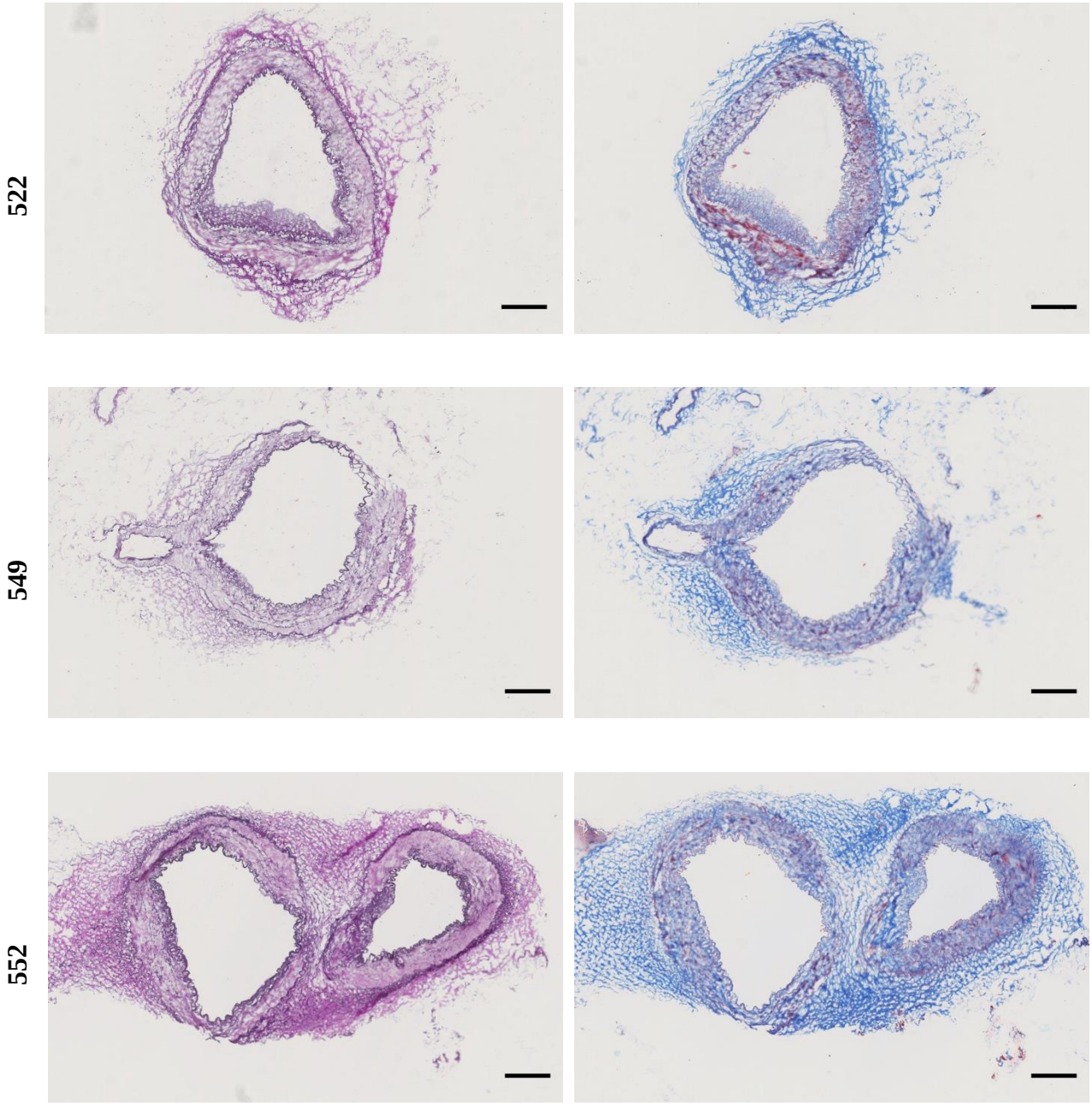

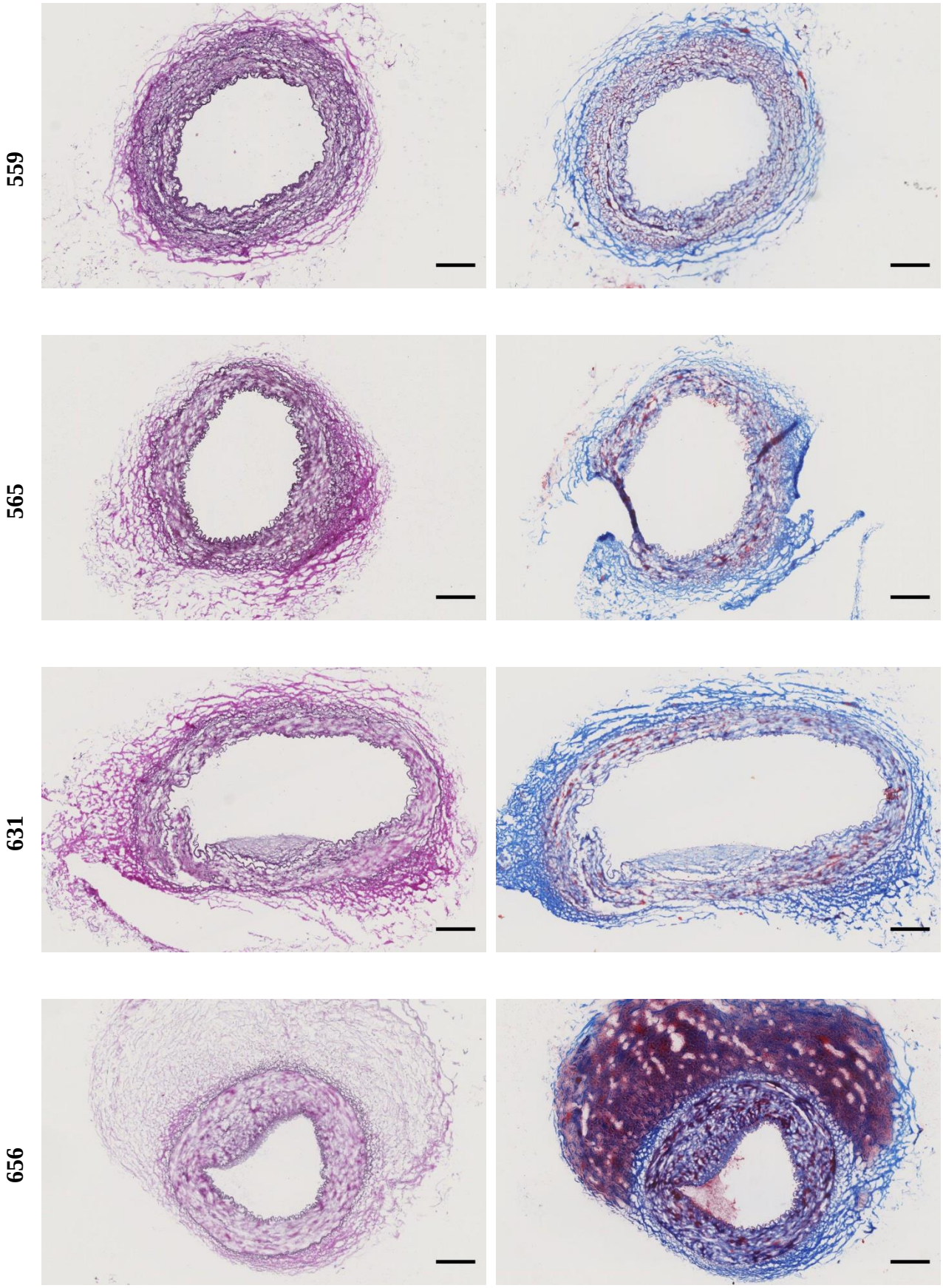
559
565
631
656

693

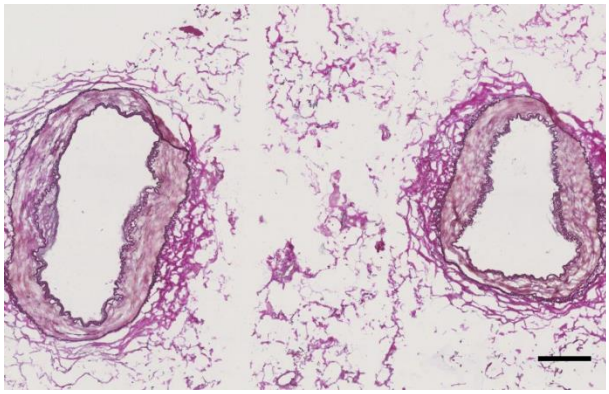

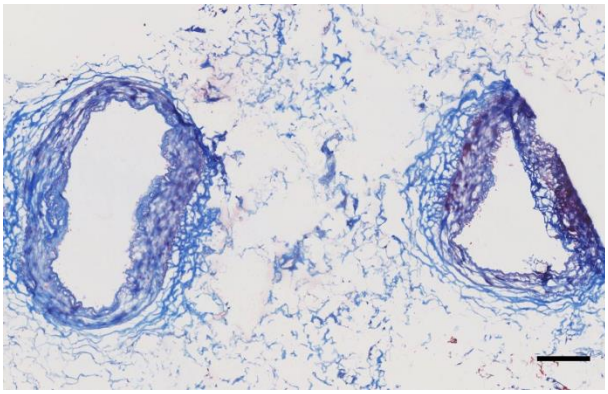

524

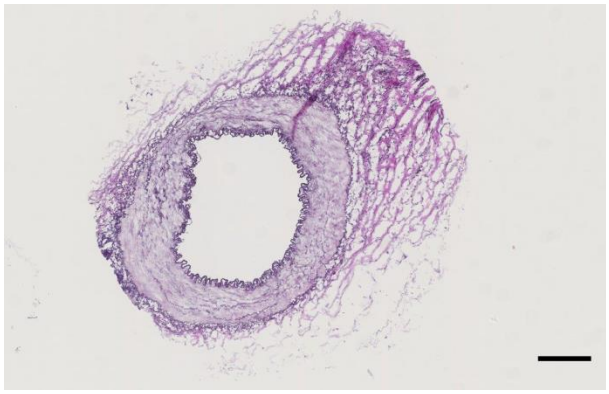

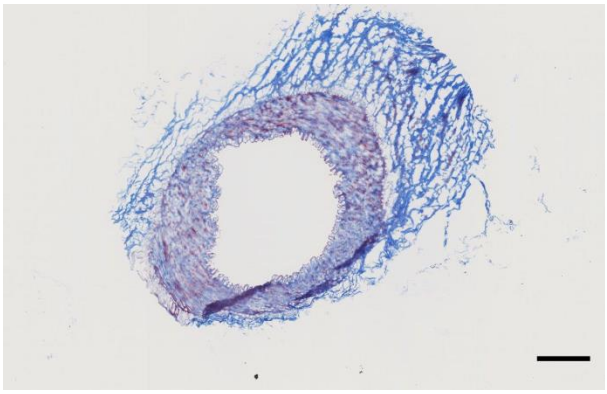

534

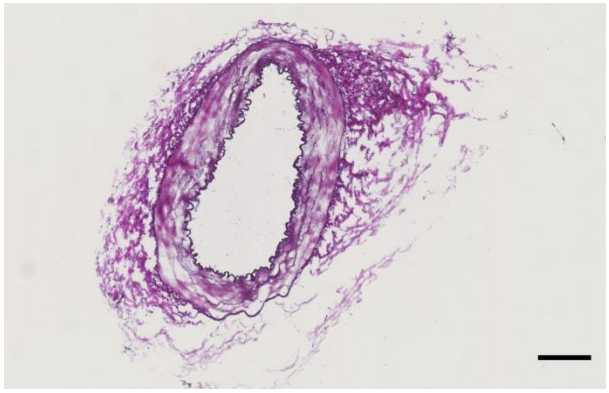

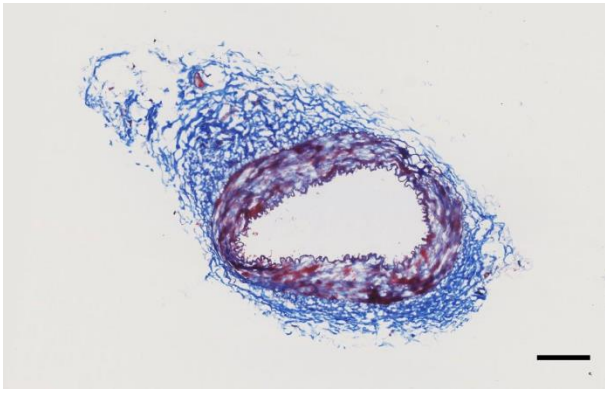

573

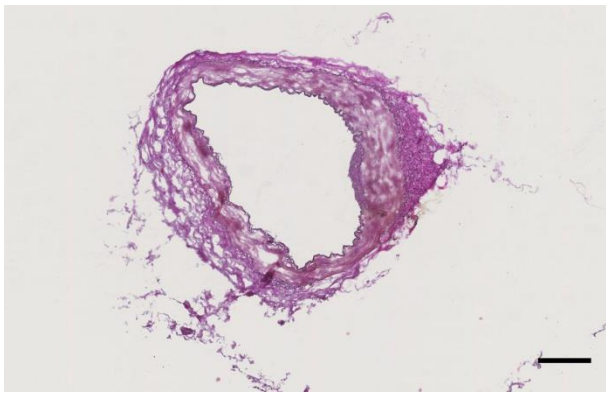

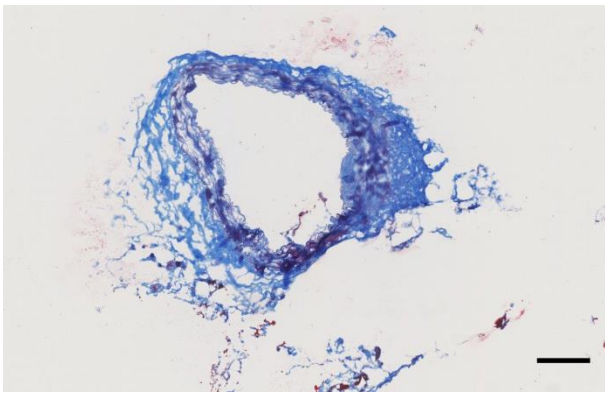

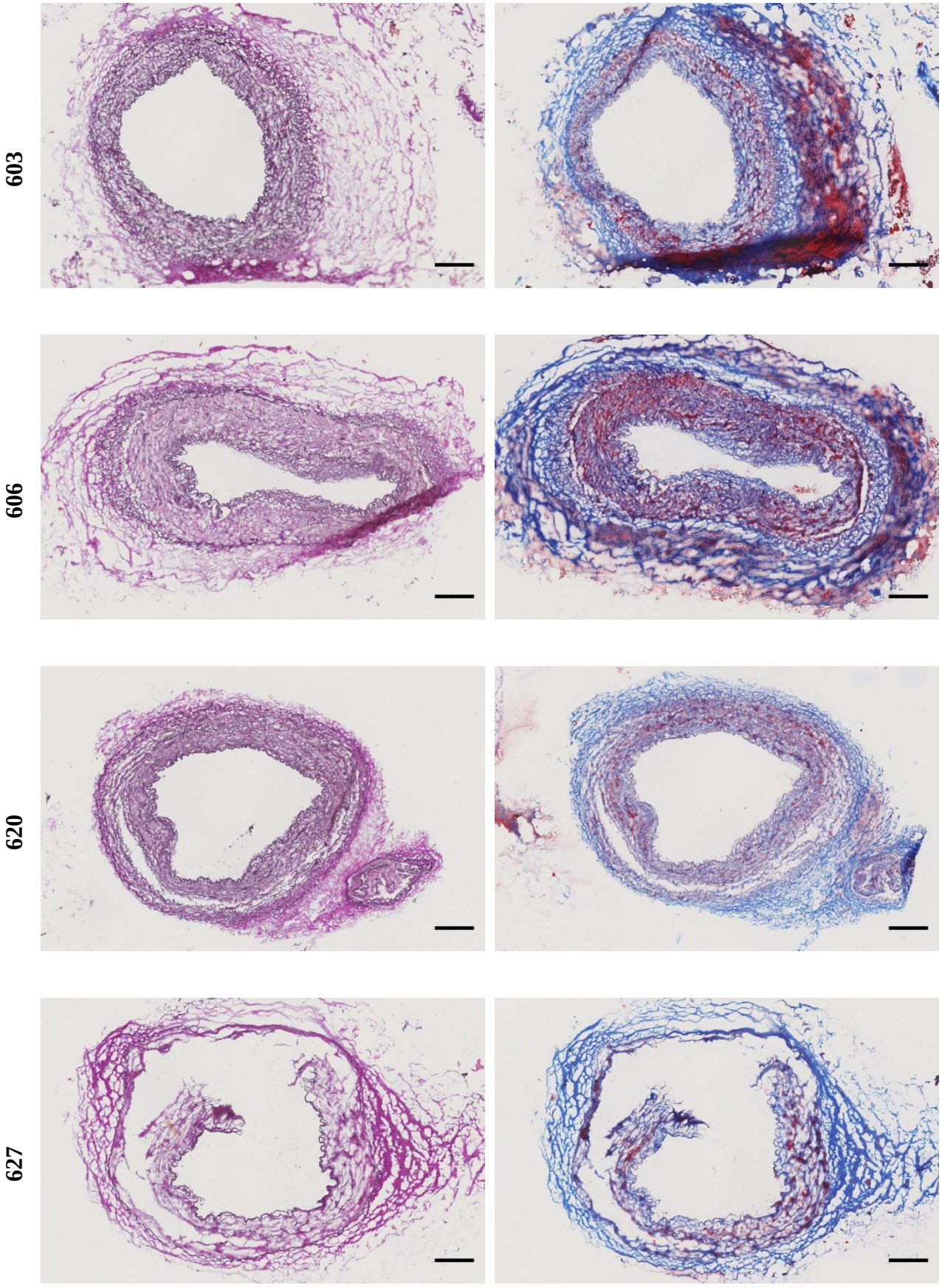
603
606
620
627

643

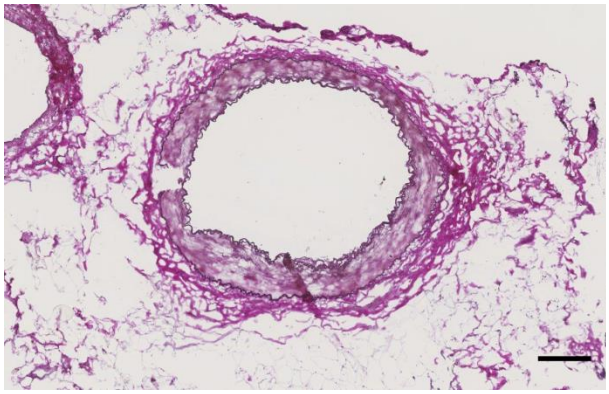

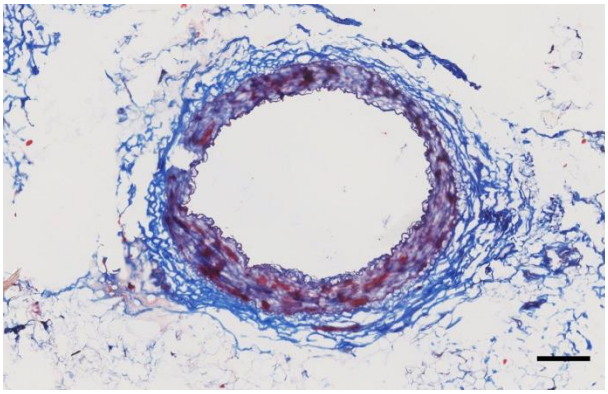

1202

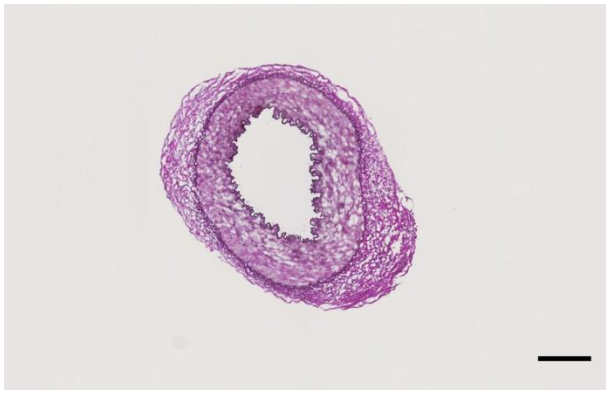

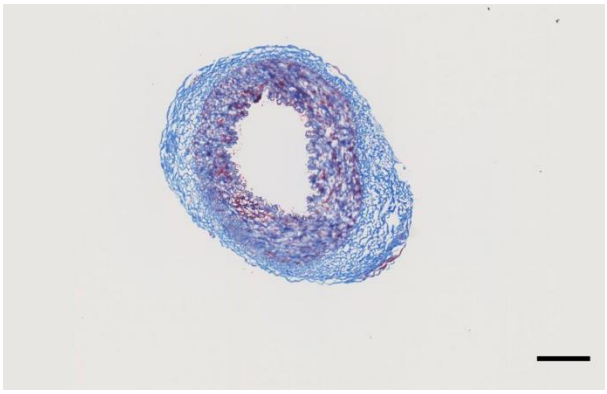

Appendix D

Elastin content of the IMAs. This data were conducted and assessed by Prof Lars Melholt Rasmussen who is expert in cardiovascular research.

Low PWV Group:

522: Muscular, no elastin

549: Muscular, low elastin content

552: Muscular, low elastin, strong external elastic membrane

559: Elastic/muscular, moderate elastin content

565: Muscular, but with elastic fragments in the media/adventitial border

631: Muscular/elastic artery, some elastin fibrils in media

656: Muscular

693: Muscular

High PWV Group:

524: Muscular, low elastin content

534: Muscular, low elastin content

573: Muscular

603: Muscular, low elastin stain in media, elastin fragment in the adventitia

606: Muscular, elastic fragments in adventitia

620: Elastic artery (maybe in between elastic/muscular)

627: Probably muscular. Quality not good

643: Muscular

1202: Muscular, strong external elastic membrane

Appendix E

PeakForce height images of adventitial collagen fibrils of the IMAs.

Low PWV

522

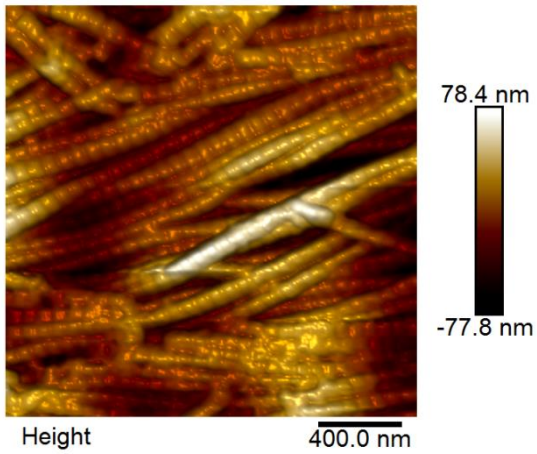

549

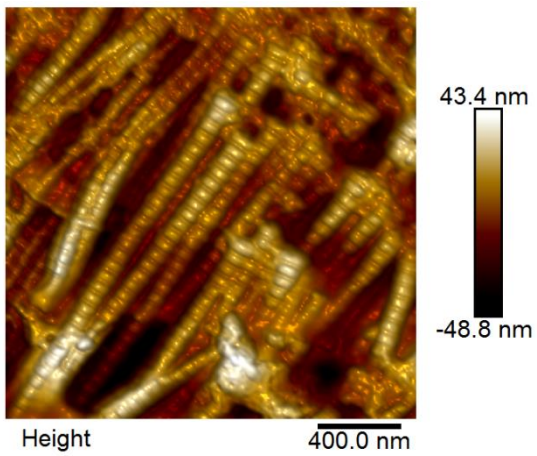

High PWV

524

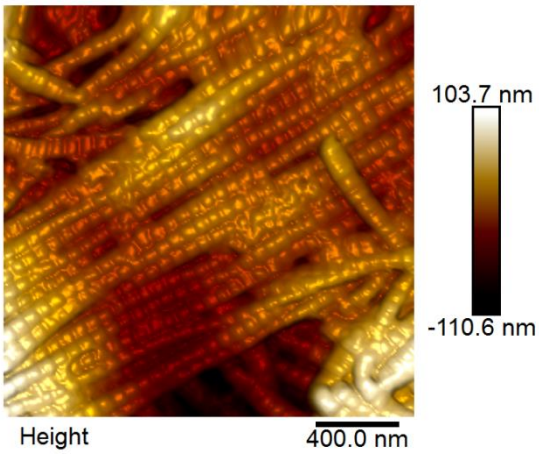

534

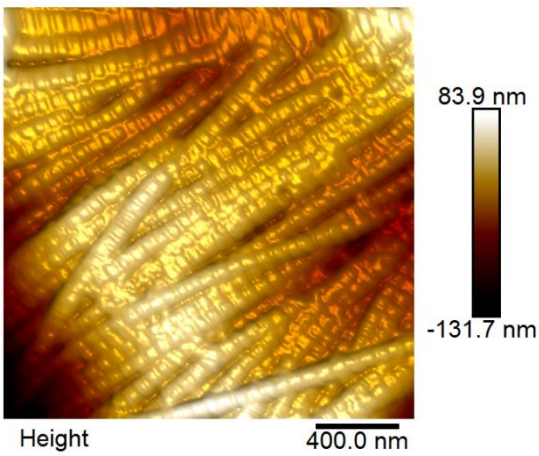

552

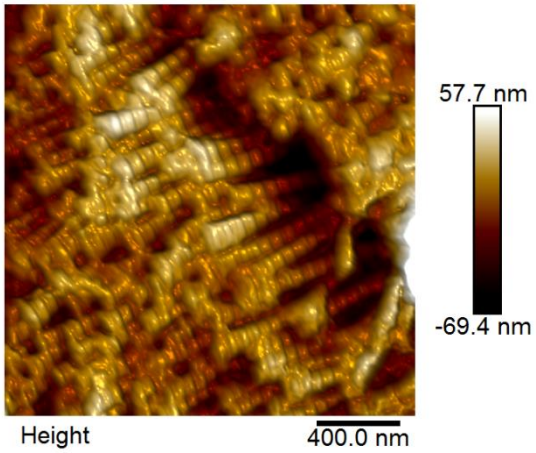

573

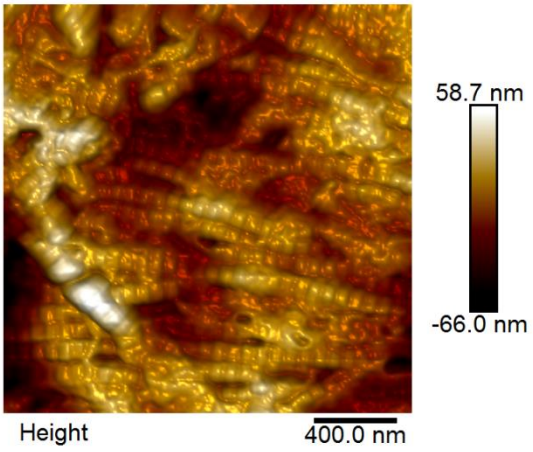

559

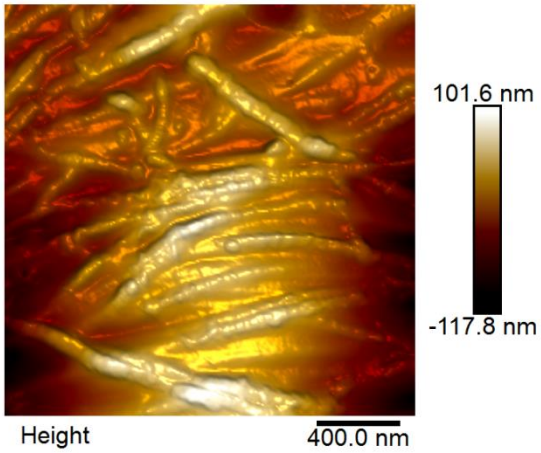

603

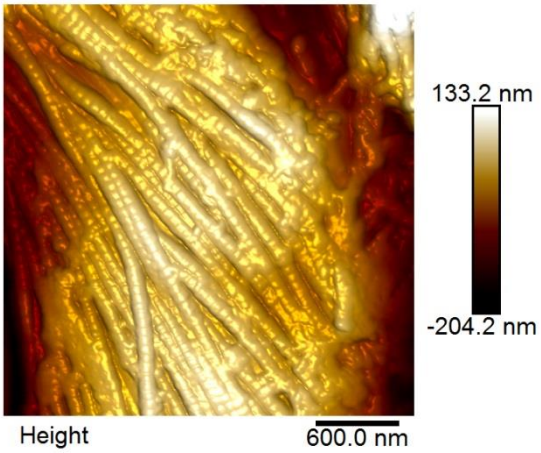

565

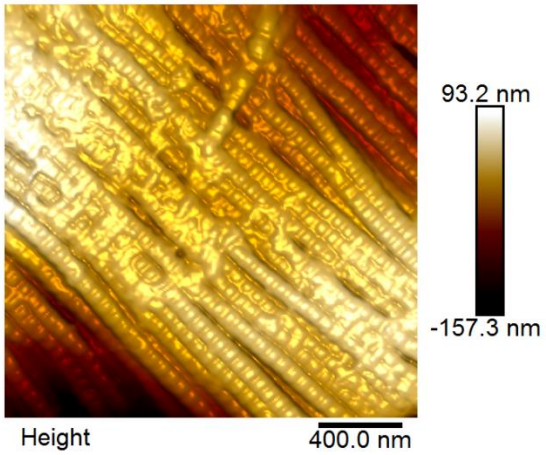

606

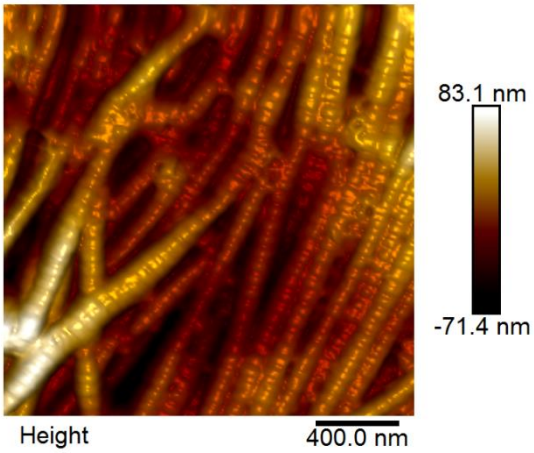

631

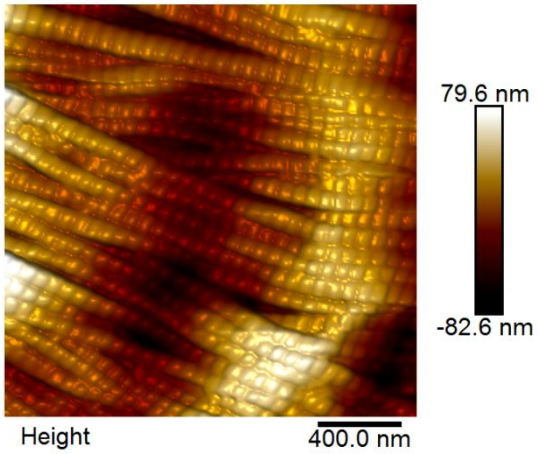

620

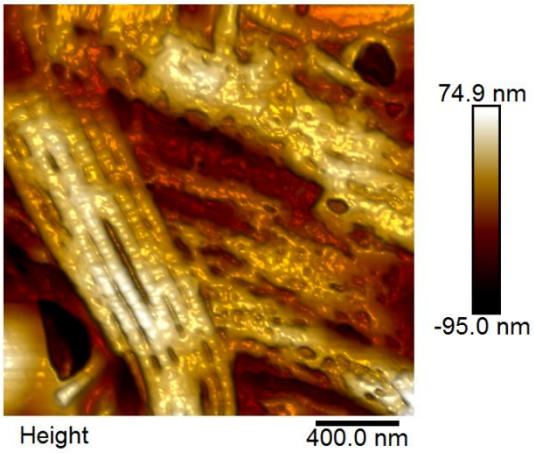

656

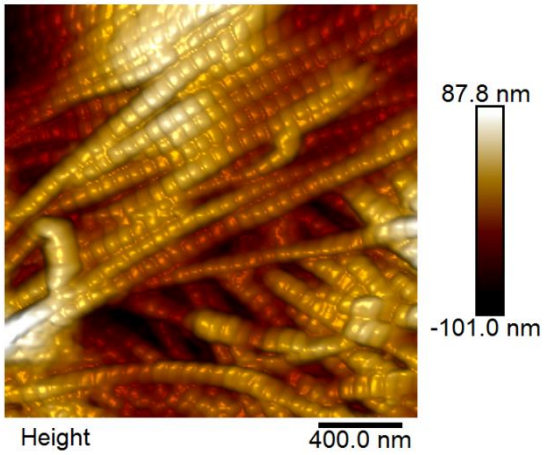

627

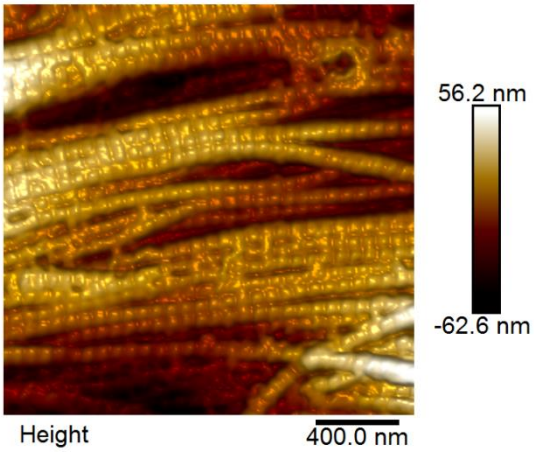

693

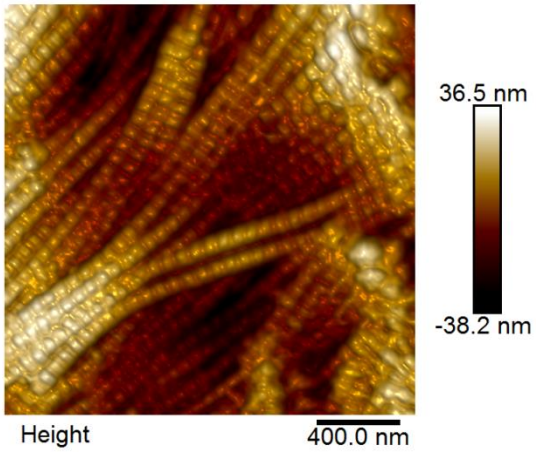

643

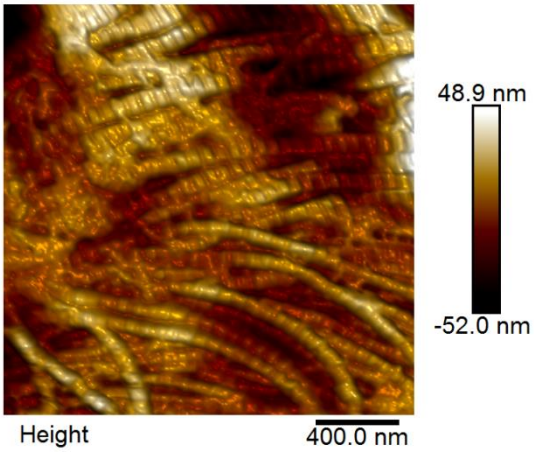

1202

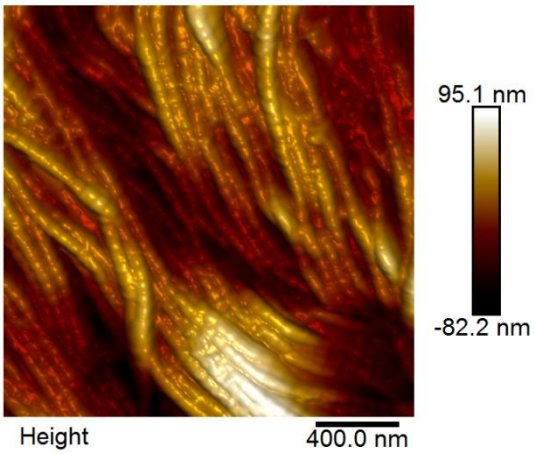

Appendix F

Macro for the collagen fibril analysis in Image SXM

{01}var

{02}x,mode,mean,min, max, ThisPic: real;

{03} name: string;

{04} n: integer;

{05} begin

{06}UnsharpMask('11x11');

{07}Measure;

{08}GetResults(n, mean, mode, min ,max);

{09}SetThreshold(mode);

{10}MakeBinary;

{11}SetBinaryCount(2);

{12}Dilate;

{13}Erode;

{14}Dilate;

{15}Erode;

{16}Dilate;

{17}Erode;

{18}Dilate;

{19}Erode;

{20}Dilate;

{21}Erode;

{22}Skeletonize;

{23}Dilate;

{24}Invert;

{25}SetForegroundColor(255); { Make border black so that it touches}

{26}SetLineWidth(6); { all objects truncated by the border}

{27}DrawBoundary;

SetForegroundColor(0);

MakeRoi(0, 0, 32, 8);

Fill;

KillRoi;

SetParticleSize(6, 92);

{28}AnalyzeParticles('label','reset','ignore');

{29}ShowResults;

{30} end;

Appendix G

Peak Force Error images (2 µm × 2 µm) of the medial collagen fibrils from all the patients.

Low PWV

522

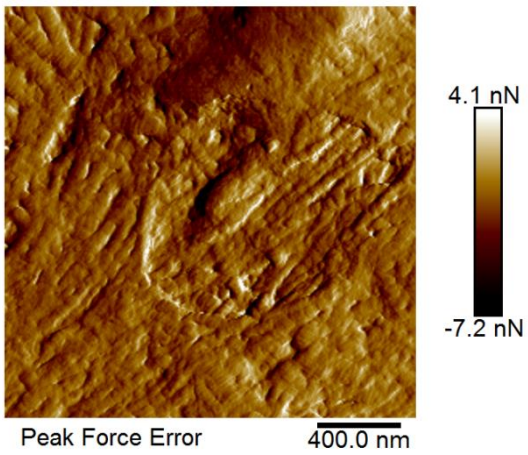

549

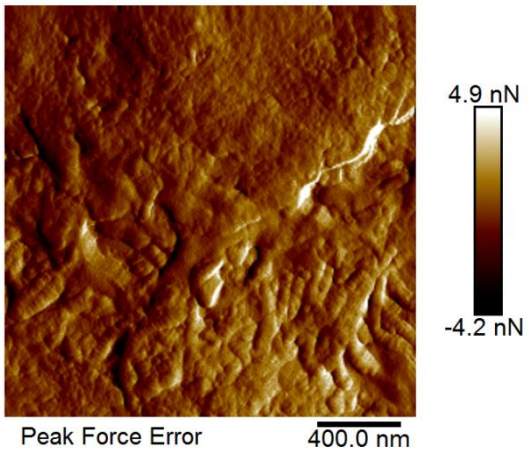

High PWV

524

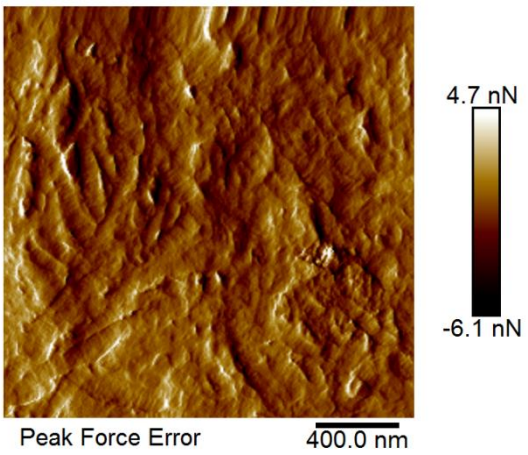

534

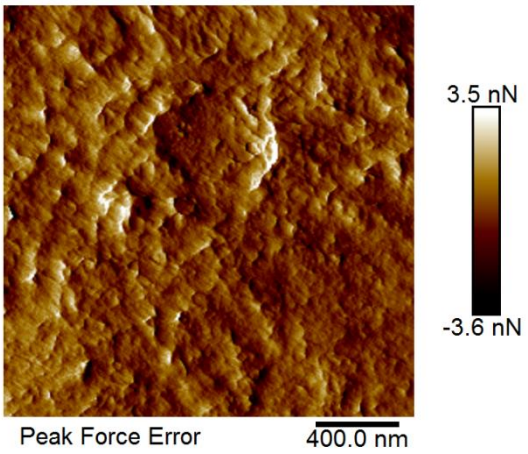

552

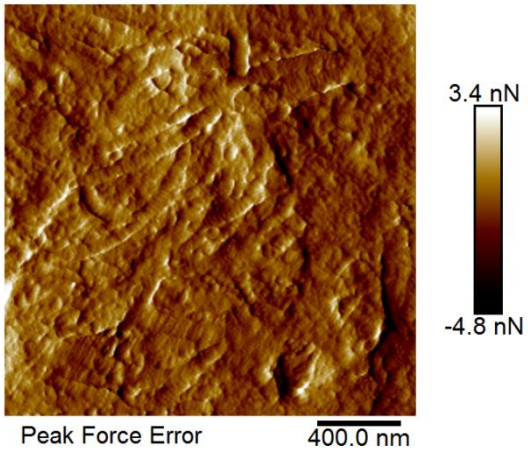

573

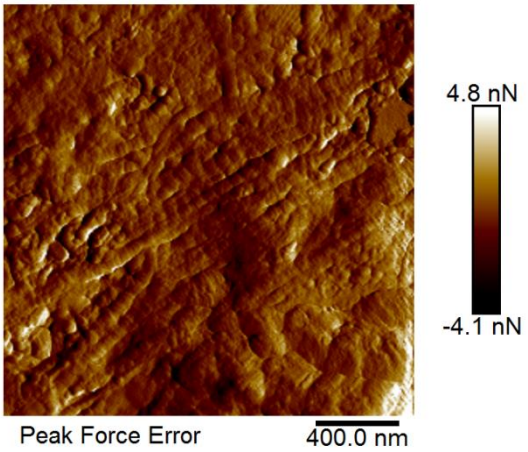

559

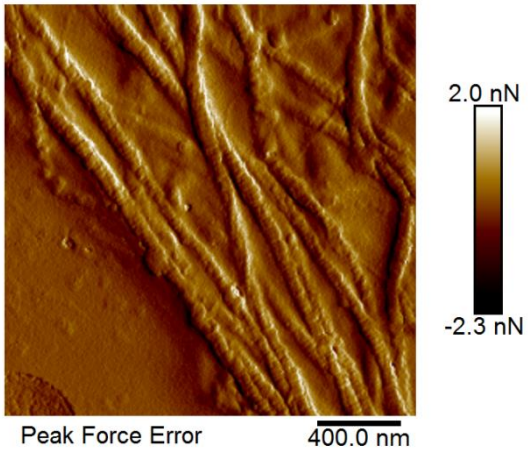

603

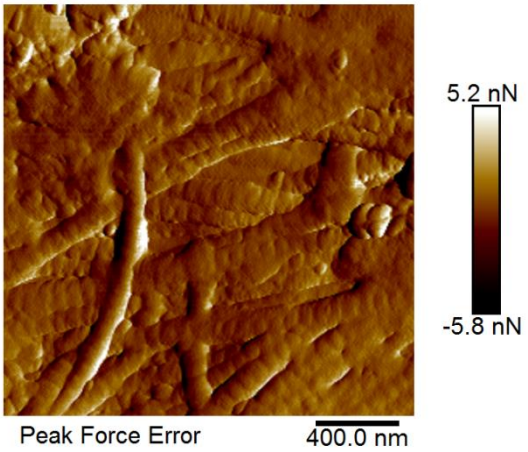

565

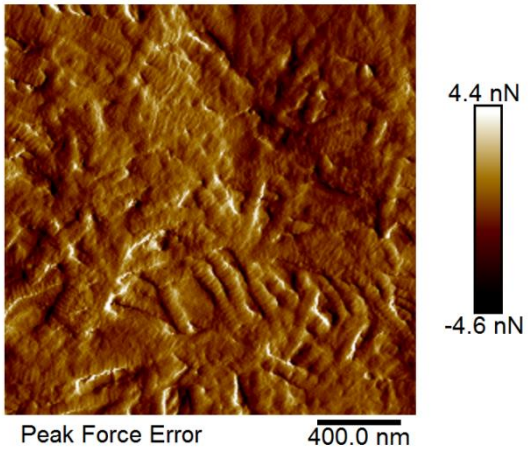

606

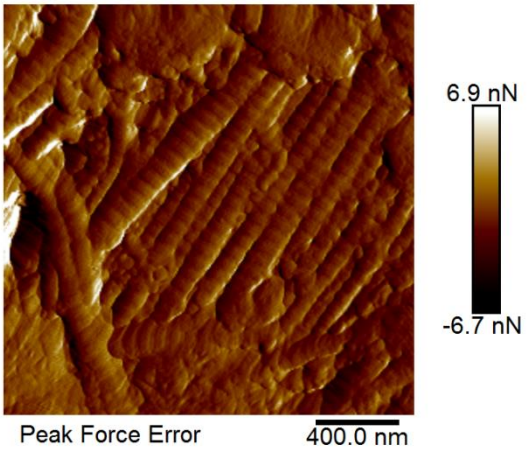

631

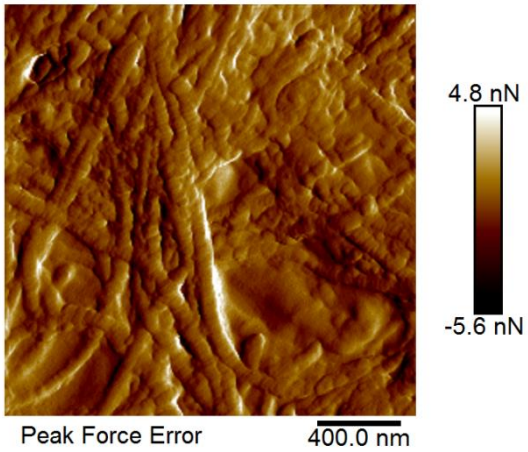

620

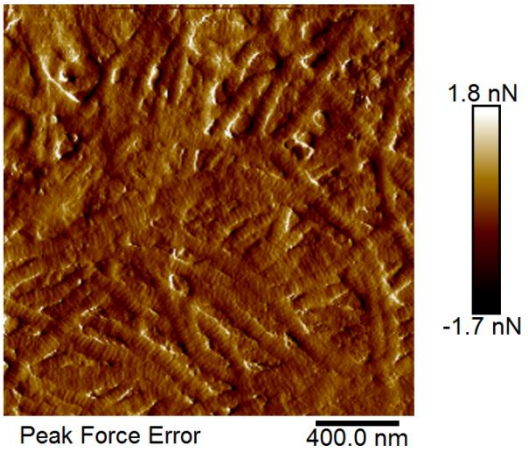

656

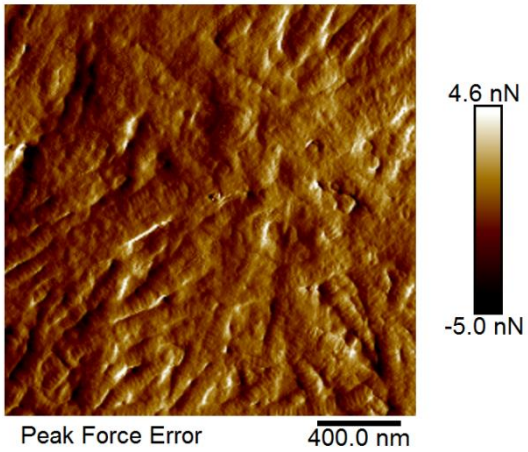

627

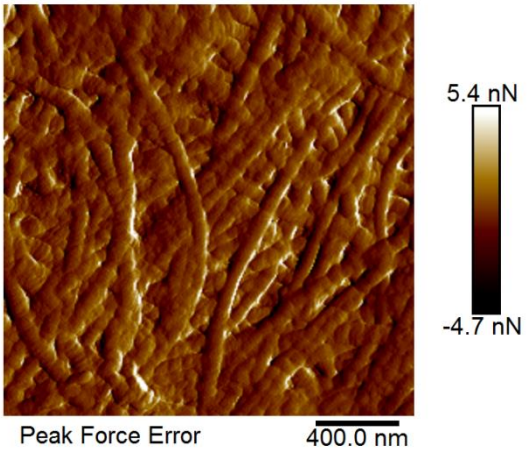

693

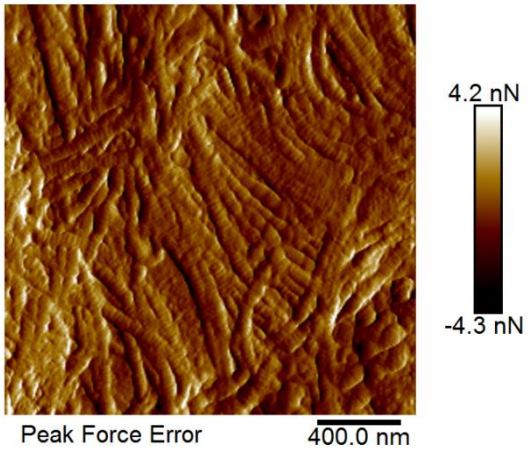

643

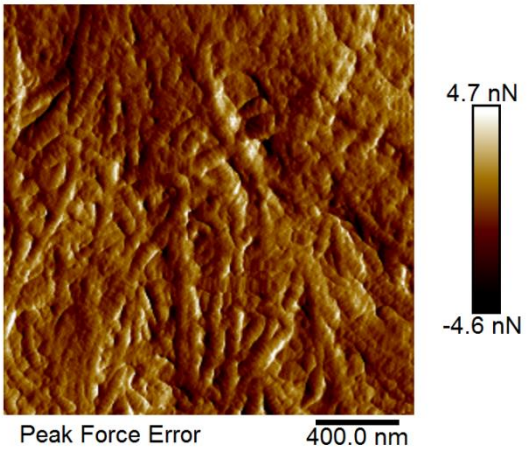

1202